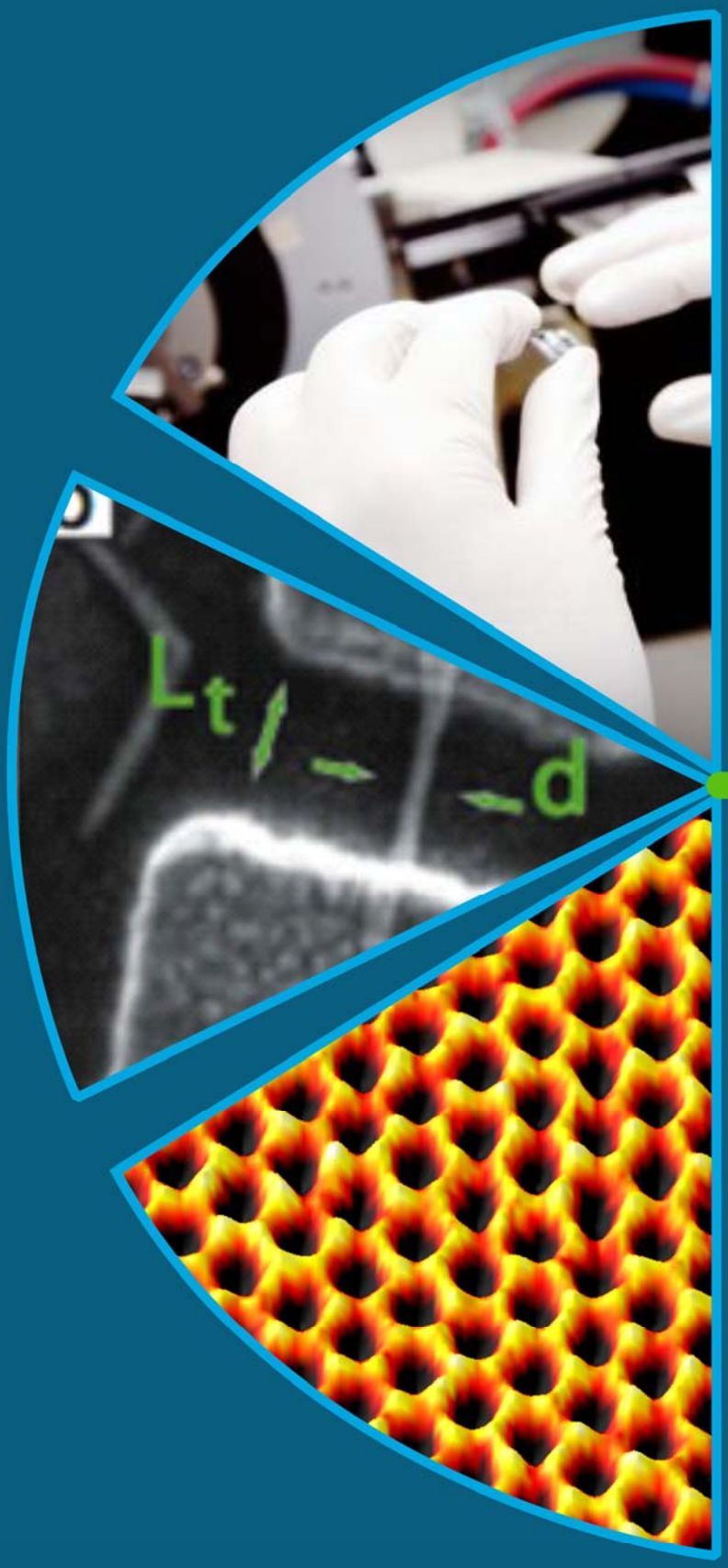

V. FOCUSED FUNDAMENTAL RESEARCH

Introduction

Cathode Development

Anode Development

Electrolyte Development

Cell Analysis and Modeling

V. FOCUSED FUNDAMENTAL RESEARCH

V.A Introduction

The focused fundamental research program, also called the Batteries for Advanced Transportation Technologies (BATT) program, is supported by the DOE's Vehicle Technologies program (DOE-VT) to research and analyze new materials for high-performance, next generation, rechargeable batteries for use in HEVs, PHEVs, and EVs. The effort in 2011 continued the increased emphasis on high-energy materials for PHEV and EV applications and expanded efforts into technologies for enabling the use of Li metal anodes.

Background and Program Context

The BATT Program addresses the fundamental problems of chemical and mechanical instabilities that have slowed the development of automotive batteries with acceptable cost, performance, life, and safety. The aim is to develop and test new materials and to use traditional and novel diagnostics and modeling methods to better understand cell and material performance and lifetime limitations before initiating battery scale-up and development,. Emphasis is placed on the synthesis of components into cells with determination of failure modes, while continuing with materials synthesis and evaluation, advanced diagnostics, and improved model development. Battery chemistries are monitored continuously with timely substitution of more promising components. This is done with advice from within the BATT Program and from outside experts, including consultation with automotive companies and DOE. Also factored into the BATT Program direction is the monitoring of world-wide battery R&D activities. The Program not only supports research that leads to improvements to existing materials, but also into high-risk "leap-frog" technologies that might have a tremendous impact in the marketplace. An overview of the activities and focus of the program is shown in Figure V - 1.

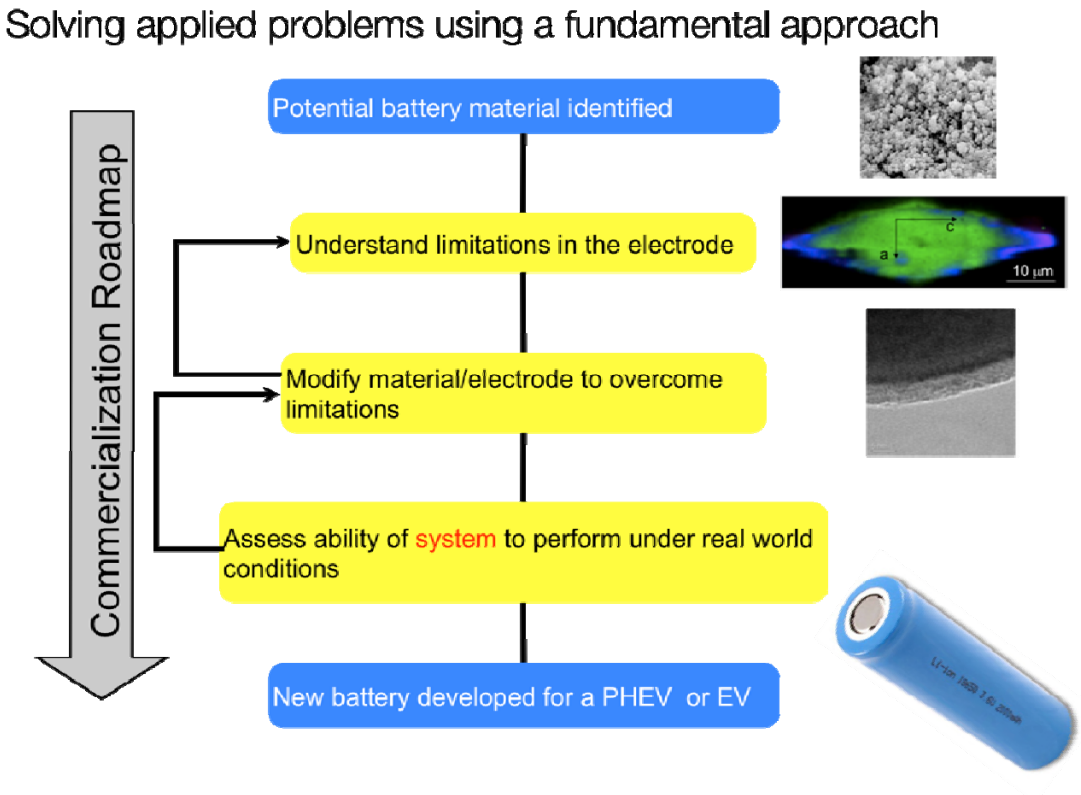

Figure V - 1: BATT Overview

The work is administered by the Lawrence Berkeley National Laboratory (LBNL), with principal researchers from LBNL, five additional national laboratories, fourteen universities, and two commercial companies. The program is organized into the following areas:

- New Cathode Systems, Performance and Limitations
- New Anode Materials
- Novel Electrolytes and their Characterization,
- Li-ion Modeling, Diagnostics, and Cell Analysis

The BATT program has an enviable team of principle investigators, many of them world renowned, who push the battery field forward in each of these areas. The interaction among the four main focus areas is shown in Figure V - 2.

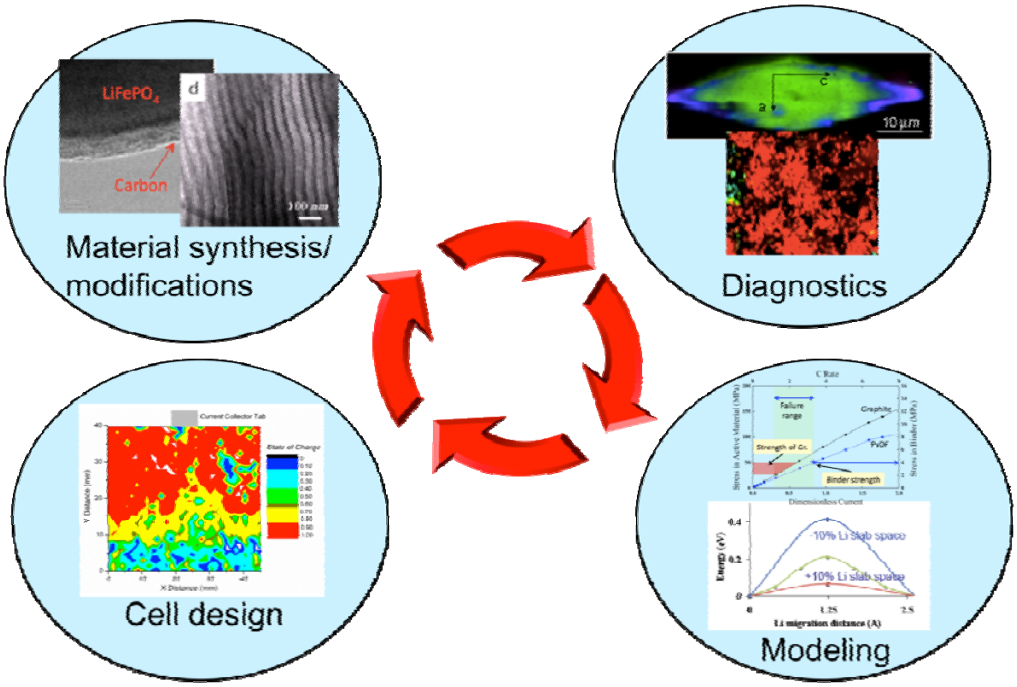

Figure V - 2: BATT Focus Areas

This section summarizes the research activities of this program in FY 2011. The website for the BATT Program is found at http://batt.lbl.gov. Brief descriptions of each research area are as follows.

The ***New Cathode Materials*** task aims to find improved cathode materials that offer significant improvements in volumetric and specific energy and/or power over current state of the art materials, like $LiCoO_2$. A request for proposals for new cathode materials was issued in late 2010 and four new projects have been selected. The new projects include work on the high voltage, high-energy layered/layered or Li rich cathode materials, a project investigating Li bearing mixed polyanion glasses, and project investigating polyanions that may cycle more than one Li ion per transition metal ion such as the silicates, and one project that will develop *in situ* reactors designed to investigate solvothermal synthesis reactions in real-time using synchrotron. These new projects have only recently begun and have not generated any new results, but abstracts for each are provided below.

The ***New Anode Materials*** task involves a significant focus on silicon, which offers ten times the capacity of currently used graphite anodes. Researchers are investigating several forms of Si, including nanowires, nanoparticles, clathrate structures, and others. They are also investigating methods for stabilizing Si and Sn composite negative electrodes, including the use of Cu foam current collectors, atomic layer deposition to stabilize alloy electrodes, and a number of Si/carbon nanocomposite materials.

The ***Novel Electrolyte Materials*** task continues projects that began in 2009 following a BATT solicitation posted in 2008. These five research efforts focus on expanding the temperature range of cells, additives to stabilize the negative and

positive interfaces, development of new overcharge shuttles to further stabilize Li-ion cells, new ionic liquids to enable higher voltage windows, and first principles modeling to understand and eventually to construct a more stable SEI.

The ***Modeling, Diagnostics, and Cell Analysis*** tasks involve the use of advanced diagnostics techniques, such as FTIR, X-ray absorption fine structure (XAFS), X-ray diffraction (XRD), nuclear magnetic resonance (NMR) and other techniques to investigate interfacial and other properties in Li-ion batteries. Several modeling approaches are used to understand cell and fundamental material properties, including *ab-initio* calculations, macroscopic cell calculations, and finite element simulations. Finally, standard cell making and testing techniques are developed and applied to provide a common evaluation process for new materials.

The BATT program regularly solicits new proposals in each of the above four areas. The 2012 RFP will bein the Modeling, Diagnostics, and Cell Analysis task area. In addition, BATT program management always accepts unsolicited proposals on any advanced energy storage technology that significantly advances the state of the art is is appropriate for the R&D focus of the BATT program. Unsolicited proposals are reviewed in concert with the solicited proposals.

V.B Cathode Development

V.B.1 First Principles Calculations and NMR Spectroscopy of Electrode Materials (MIT, SUNY)

Gerbrand Ceder (Principal Investigator)
Department of Materials Science and Engineering
Massachusetts Institute of Technology
77 Massachusetts Avenue
Cambridge, MA 02139-4307

Clare P. Grey (Co-Principal Investigator)
Chemistry Departments
University of Cambridge / Stony Brook University
Phone: (+44) 1223 336509; Fax: (+44) 1223 336017
E-mail: cpg27@cam.ac.uk

Start Date: May 2006
Projected End Date: February 2012

Objectives

- Determine the effect of structure on stability and rate capability of cathodes and anodes.
- Explore relationships between electro-chemistry and particle size and shape.
- Develop new materials.

Technical Barriers

Low rate capabilities, high cost, poor stability of electrode materials, low energy density.

Technical Targets

- Specific power 300 W/kg, 10 year life, <20% capacity fade. Low cost.

Accomplishments

- Understood Li diffusion limits in nano versus micron olivine, and broadened insight to many other 1D intercalation materials.
- Investigated Li diffusion in graphite (with Kostecki and Persson) and $Li(Ni_{0.5}Mn_{1.5})O_4$ spinel and established high rate capability of both. NMR used (with Cabana and Chen) to investigate local structures in spinel.
- Investigated shape, size and processing effects on rate in a series of cathode materials
- Several novel intercalation cathodes proposed by high-throughput computing and tested. NMR methods employed to investigate the structure of new phosphocarbonates.
- Developed and used ^{29}Si NMR methods to study lithiated silicon anodes.
- Used *in situ* NMR and SEM to investigate Li dendrite formation.

✧ ✧ ✧ ✧ ✧

Introduction

Achieving DOE goals in this field requires both an understanding of how current materials function – with a view to improving rate, capacity and long term cycling performance – and the discovery of new materials and new mechanisms by which these materials function. This joint theoretical and experimental program attacks these issues by developing new experimental (and theoretical) tools to investigate battery materials both *in* and *ex situ*, and then applies these to understand relationships between structure and function. One aim is to use these findings to optimize material function and/or develop new materials.

Approach

Use solid state NMR and diffraction/TEM to characterize local and long range structure as a function of particle size, sample preparation method, state of charge and number of charge cycles (cathodes). Use electrochemistry to correlate particle size with rate performance. Continue to develop the use of *in situ* NMR methods to identify structural changes and reactivity in oxides and intermetallics. Use first principles calculations (density functional theory) to identify redox-active metals, relative stability of different structures, the effect of structure and particle size on cell voltages and rate capability, and to identify promising cathode materials for BATT applications.

Results

Particle size and morphology studies: Materials with poor electronic conductivity often require nano-sizing and/or carbon coatings to improve their performance.

Systematic experimental and theoretical studies have been performed to explore the effect of size and shape on electrochemical performance. In the 1st experimental study, $LiFePO_4$ was synthesized hydrothermally in the presence of NH_4^+ and citric acid (CA), resulting in some unusual morphologies (Figure V - 3). The mechanisms for their formation were investigated by XRD, FTIR, NMR and electron microscopy. The electrochemical performance was optimized for the hollow morphologies prepared at intermediate times, even though the particle sizes are approximately 1 micron. Presumably, the hollowed structures reduce the diffusion lengths for Li^+. Unusual morphologies are observed (e.g., see Fig. 1, for 5 and 52h), the complexing ability of CA allowing ready dissolution and reprecipitation of Fe^{2+} and the NH_4^+ ions which appear to control growth along certain directions. (Collaboration with Prof. Jonathan C.Y. Chung, City University of Hong Kong). In a second study, molten salts were used to grow novel morphologies (e.g., almost perfect concave cuboctahedra) of layered materials such as $LiCoO_2$ and its doped variants. Effects of morphologies on rate were explored, the results highlighting the effect that nano-sizing has on the rate of side reactions with the electrolyte for electrodes operating above approx. 4.2 V.

In parallel studies, the effect on ball-milling – a typical method used to reduce particle size - was explored on local structure, this time focusing on the α and β-polytypes of $Li_3Fe_2(PO_4)_3$. We used NMR to show that the ball-milling reduces particle size while also increasing the number of defects; a noticeable increase in Li mobility is observed. Both effects (size and mobility) are important in improving the electrochemical performance of these materials.

Rate and Particle Size Effects. Following on our study of particle size effects on the rate performance of $LiFePO_4$, we have successfully investigated the rate limits of $LiNi_{0.5}Mn_{1.5}O_4$ using both first principles computations and experiments. Figure V - 4 shows the energy along the migration paths with lowest activation barrier. These computational results predict that Li can migrate ≈ 3μm in about 10 seconds indicating that no nanosizing would be needed to achieve high rate capability in this material. This is important as the high voltage of this cathode material makes it susceptible to surface reactions with the electrolyte. Hence, keeping the surface area low is paramount.

To test the rate capability of $LiNi_{0.5}Mn_{1.5}O_4$,, phase-pure ordered material with particle size about 3-5μm was prepared and assembled in both coin and swagelock cells. Figure V - 4 (bottom) shows excellent discharge capacities. At 0.2C 147mAh/g is obtained which is close to the theoretical capacity of this material. At 20C and 40C rate, the capacities are still high, respectively 134mAh/g and 110mAh/g. Excellent cyclability can also be achieved. The high rate capability observed is in agreement with the calculated low Li migration barrier. This $LiNi_{0.5}Mn_{1.5}O_4$ with 3-5μm particle size shows better rate capability than 50nm.

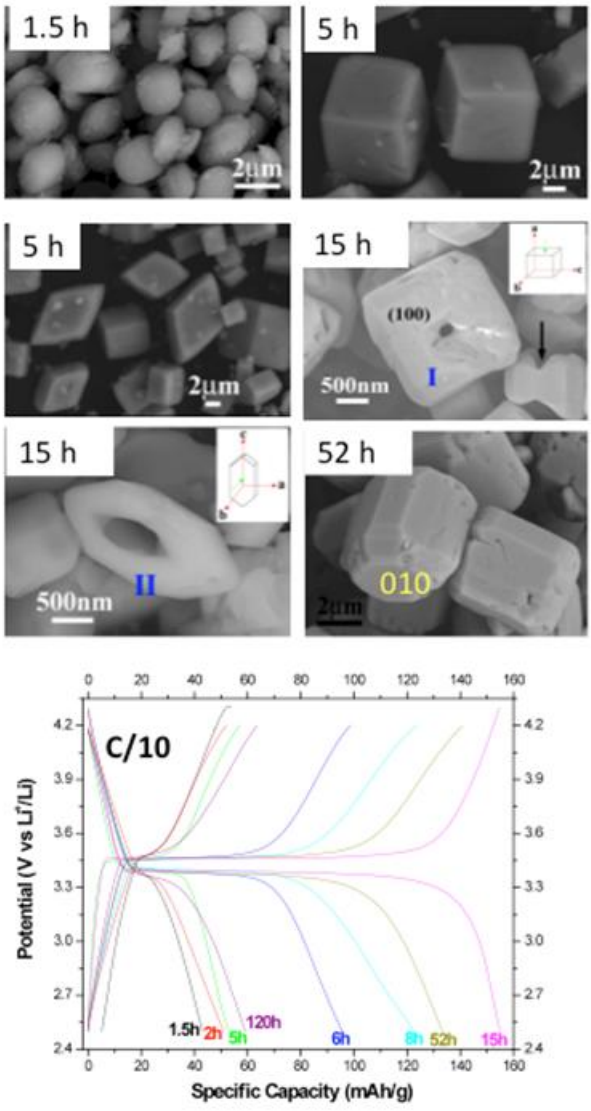

Figure V - 3: Morphologies of stoichiometric $LiFePO_4$ seen as a function of reaction time and their corresponding electrochemical performance.

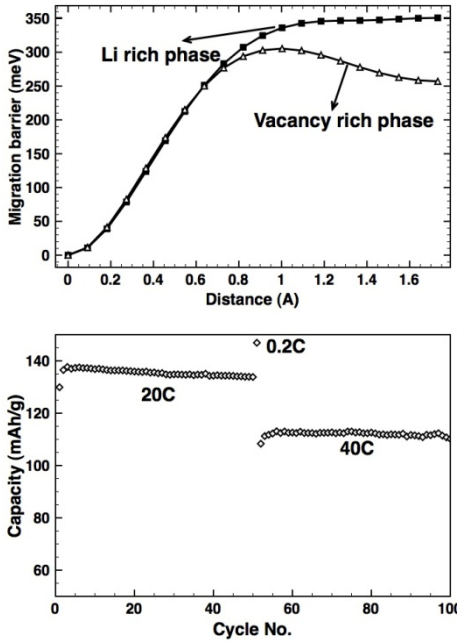

Figure V - 4: (top) Energy barriers for Li migration in $LiNi_{0.5}Mn_{1.5}O_4$. (bottom): Capacity at high rates for cathodes made with micron sized $LiNi_{0.5}Mn_{1.5}O_4$

Structure and Function of High Capacity Anodes: Silicon has attracted considerable interest as an anode material for high-energy lithium ion batteries due to its very high specific capacity (3579 mAh/g). Efforts in this reporting period have focused on developing methods to establish how Si's operating behavior is affected by the size and morphology of the Si particles, making use of new experiments involving ^{29}Si NMR spectroscopy. Unfortunately, analysis of the silicon substructure by the direct probe ^{29}Si, has been hampered by the low signal-noise ratio and the difficulty in interpreting the usually very broad and poorly resolved spectra of lithiated Si particles. Thus, we have developed a number of suitable NMR techniques for the determination of both Si-Si and Li-Si connectivities, which make use of covalent interactions between Si atoms (J-coupling), and through space (dipolar) interactions between nuclei. The approach is demonstrated with the crystalline lithium silicide $Li_{12}Si_7$. Its structure includes 5-membered Si rings which are stacked in one-dimensional chains, as well as 4-membered Si "Y" stars located in the planes between the Si_5 rings, as shown in Figure V - 5.

Figure V - 6 shows dimensional (2D) NMR experiment that investigates covalent interactions (bonds) between atoms (^{29}Si INADEQUATE NMR). In this spectrum, two bonded atoms giving rise to resonances with frequencies ν_1 and ν_2 result in a correlation at $\nu_1+\nu_2$ in the indirect dimension of the 2D spectrum. No correlations are seen for non-bonded atoms. Consistent with this, separate sets of connectivities are seen between the Si atoms in the rings (resonances b, c, d, e, and g) and the stars (a, f, h and i).

These experiments, along with NMR experiments designed to measure Li-Si connectivities are being employed to investigate structure in cycled ^{29}Si-enriched battery materials. In parallel to this method development, we have now (i) established a method to perform *in situ* NMR experiments of carboxymethyl-cellulose coated Si nanoparticles, so that we can now study this chemistry *in situ* and (ii) performed detailed *ex situ* NMR studies of Si nanoparticles.

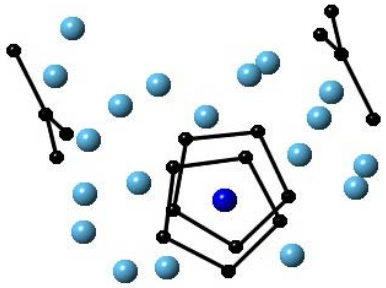

Figure V - 5: Fragment of the crystal structure of $Li_{12}Si_7$ showing the Si_4 stars and the Si_5 rings (black) and Li atoms in light/dark blue.

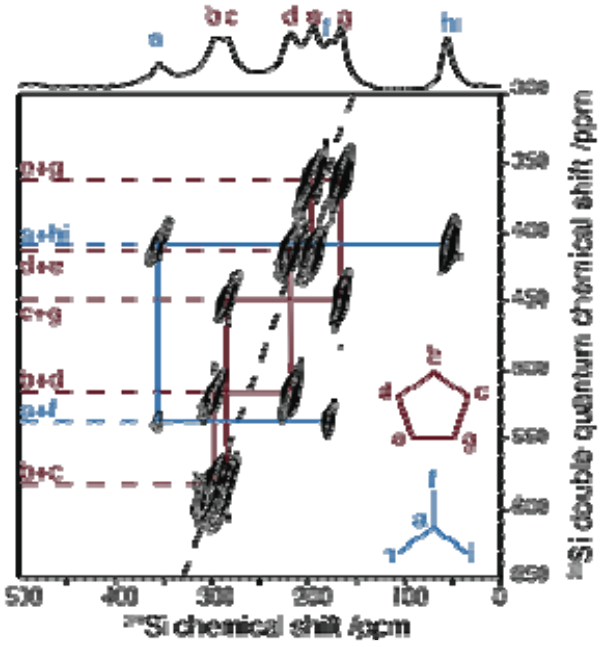

Figure V - 6: Experimental one-pulse spectrum (top) and ^{29}Si 2D INADEQUATE NMR spectrum of $Li_{12}Si_7$ at 233 K.

The dashed line represents the 2ν-ν line. Solid lines are added so as to follow the Si-Si connectivities.

Materials discovery: Using *ab initio* high-throughput computations, we performed a search for new Li-ion cathode materials with high specific energy, electrochemical activity in a voltage range compatible with current commercial electrolytes (< 4.5V) and good

lithium-ion diffusion. We have identified compounds based on the crystal structure of the sidorenkite (a rare mineral of formula $Na_3Mn(CO_3)(PO_4)$ to be of interest as cathode materials. Two-electron activity and high specific energies (> 800 Wh/kg) can be expected from this class of materials. We have also performed a further computational stability exploration, evaluating the stability of the generic $A_3M(YO_3)(XO_4)$ compositions (with A=Na, Li, M=a redox active element and Y=C, B) in the sidorenkite crystal structure. Figure V - 7 shows the result of this stability analysis. Each line represents a mixture of polyanions (e.g., SO_4-CO_3), and each column a specific metal cation. Experimental work on some of these materials has been initiated. Some of the materials predicted have now been successfully synthesized and their electrochemical properties are being tested as a potential cathode material for a Na-ion or Li-ion battery. Structural characterization, including time-resolved powder diffraction and ^{23}Na NMR spectrosopy, has been carried out to evaluate limitations to performance.

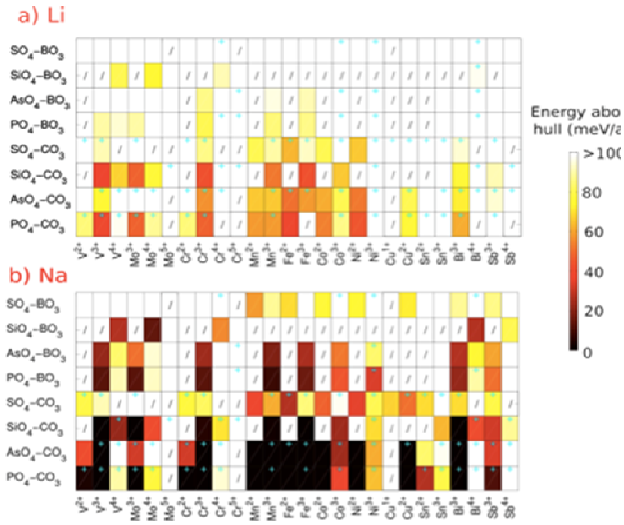

Figure V - 7: Stability of the generic $A_3M(YO_3)(XO_4)$ compositions (with A=Na,Li, M= and Y=C,B) in the sidorenkite crystal structure. The color is a measure of thermodynamic stability. Light (dark) colors indicate instability (stability)

Conclusions and Future Directions

In conclusion, relationships between morphology and electrochemical performance have been explored both theoretically and experimentally, highlighting the role that defects, ionic transport and the amount of active surface areas (for Li insertion/removal) play in controlling rate. New NMR *in* and *ex situ* methodologies to investigate local and microstructure have been developed. The approaches have been used to investigate silicon and Li dendrite formation.

FY 2011 Publications/Presentations

1. Presentation to the 2010 DOE Annual Peer Review Meeting.
2. "Pair Distribution Function Analysis and Solid State NMR Studies of Silicon Electrodes for Lithium Ion Batteries: Understanding the (De)lithiation Mechanisms," B. Key, M. Morcrette, J-M. Tarascon and C.P. Grey, *J. Am. Chem. Soc.,* **133**, 503-512 (2011).
3. "$LiCoO_2$ Concaved Cuboctahedrons from Symmetry-Controlled Topological Reactions," H.L. Chen, L.J. Wu, L.H. Zhang, Y.M. Zhu and C.P. Grey, *J. Am. Chem. Soc.*, 133, 262–270 (2011).
4. "Effect of Ball-Milling and Lithium Insertion on the Lithium Mobility and Structure of $Li_3Fe_2(PO_4)_3$," J. Cabana, J. Shirakawa, M. Nakayama, M. Wakihara and C.P. Grey, *J. Mater. Chem.,* 21, 10012-10020 (2011).
5. "C-13 Solid State NMR Suggests Unusual Breakdown Products in SEI Formation on Lithium Ion Electrodes," N. Leifer, M.C. Smart, G.K.S. Prakash, L. Gonzalez, L. Sanchez, K.A. Smith, P. Bhalla, C.P. Grey and S.G. Greenbaum, *J. Electrochem. Soc*., 158, A471-A480, (2011).
6. "Citric Acid- and Ammonium-Mediated Morphological Transformations of Olivine $LiFePO_4$ Particles," Z. Lu, H. Chen, R. Robert, B.Y.X. Zhu, J. Deng, L. Wu, C.Y. Chung and C.P. Grey, *Chem. Mat.,* 23, 2848-2859, (2011).
7. "Resolving the different silicon clusters in $Li_{12}Si_7$ by ^{29}Si and $^{6,7}Li$ Solid State Nuclear Magnetic Resonance Spectroscopy", T. K.-J. Köster, E. Salager, A. J. Morris, B. Key, V. Seznec, M. Morcrette, C. J. Pickard, C. P. Grey, *Angewandte*, in press (2011). Presentation to the 2010 DOE Annual Peer Review Meeting.
8. "Iron and Manganese Pyrophosphates as Cathodes for Lithium-Ion Batteries," H. Zhou, S. Upreti, N.A. Chernova, G. Hautier, G. Ceder, M.S. Whittingham, *Chem. Mater.*, 23 (2), 293-300 (2011).
9. "Recharging Lithium Battery Research With First-Principles Methods," G. Ceder, G. Hautier, A. Jain, S.P. Ong, *MRS Bulletin*, 36, pp. 185-191 (2011).
10. "Comparison of Small Polaron Migration and Phase Separation in Olivine LiMnPO4 and LiFePO4 Using Hybrid Density Functional Theory," S.P. Ong, V. Chevrier, G. Ceder, *Physical Review B*, 83, 075112 (2011).
11. "Challenges for Na-ion Negative Electrodes," V.L. Chevrier, G. Ceder, *Journal of the Electrochemical Society*, 158 (9), A1011-A1014 (2011).
12. "Voltage, Stability and Diffusion Barrier Differences Between Sodium-Ion and Lithium-Ion Intercalation Materials," S.P. Ong, V.L. Chevrier, G. Hautier, A.

Jain, C.J. Moore, S. Kim, X. Ma., G. Ceder, *Energy & Environmental Science*, 4 (9), 3680-3688 (2011).
13. "Novel Mixed Polyanions Lithium-Ion Battery Cathode Materials Predicted by High-Throughput Ab Initio Computations," G. Hautier, A. Jain, H. Chen, C. Moore, S.P. Ong, G. Ceder, *J. Mater. Chem.*, 21, 17147-17153 (2011).
14. "Synthesis and Electrochemical Properties of Monoclinic $LiMnB0_3$ as a Li Intercalation Material," *Journal of the Electrochemical Society*, 158 (3), A309-A315 (2011).

V.B.2 Cell Analysis, High-energy Density Cathodes and Anodes (LBNL)

Thomas Richardson
Lawrence Berkeley National Laboratory
Environmental Energy Technologies Division
Berkeley, CA 94720
Phone: (510) 486-8619; Fax: (510) 486-8609
E-mail: TJRichardson@lbl.gov

Start Date: October 1, 2004
Projected End Date: September 30, 2012

Objectives

- Synthesize and evaluate new electrode materials with improved energy density.
- Investigate the relationship of structure, morphology and performance of cathode and anode materials.
- Explore kinetic barriers, and utilize the knowledge gained to design and develop electrodes with improved energy density, rate performance and stability.

Technical Barriers

- Low energy density
- Poor cycle life

Technical Targets

- Available energy: 11.6 kWh
- Cycle life: 5,000 cycles

Accomplishments

- High voltage cathodes: Micron-sized, nanoporous, carbon-coated spheres of lithium cobalt phosphate, prepared by spray pyrolysis, were shown to have superior utilization and rate capability.
- Cell analysis: Focused ion beam (FIB) tomography was applied to composite electrodes to visualize the sizes and shapes of voids, cracks, and agglomerated particles, whose characteristics and distribution directly impact cell performance.

✧ ✧ ✧ ✧ ✧

Introduction

EV and PHEV batteries will have to have higher energy densities with good power capability, long cycle lives, and a high margin of safety. Advances in both anode and cathode chemistries are needed to achieve these goals. In addition, improving the design and construction of electrodes and reducing irreversible capacity losses are key routes to maximizing the utilization of theoretical capacities.

Approach

High energy density cathodes. High voltage olivine phosphates such as $LiNiPO_4$ and $LiCoPO_4$ have good theoretical capacities, but have performed poorly in the areas of utilization and rate. While the use of small particles improves both parameters, it can lead to poor packing densities and undesirable side reactions. Our previous success with spray pyrolized $LiFePO_4$ suggested that $LiCoPO_4$ might also benefit from the porous sphere morphology.

Cell Analysis. The optimization of porous composite electrodes is a subject of great interest. We have shown using x-ray diffraction that the distribution of charge in porous electrodes is affected by both electronic resistances in the current collector and composite matrix and by electrolyte polarization. 3D imaging techniques, however, are needed to determine the internal structure of the electrodes and the distribution of solids and pores.

Results

High energy density cathodes. In collaboration with Marca Doeff, $LiCoPO_4$/C nanoporous spheres were prepared by ultrasonic spray pyrolysis from aqueous precursor solutions. This material, with two discharge plateaus of about equal capacity at 4.8 V and 4.7 V and a theoretical capacity of 167 mAh/g, has previously suffered from poor utilization, rate performance, and cycling stability. The porous microspheres (Figure V - 8) consisting of ~70 nm sized carbon coated $LiCoPO_4$ primary particles had a residual carbon content of 2.4 wt.%. Electrodes containing 10 wt % carbon black and 5 wt % PTFE exhibited excellent rate capability in lithium half-cells, delivering 123 mAh/g at C/10 and 80 mAh/g at 5C,. The capacity retention at C/10 was 95% after 20 cycles, with coulombic efficiencies of 97% after the first cycle. (Figure V - 9).

The method is fast, simple, scalable, and energy-efficient. While the energy density of electrodes containing these particles was not optimized, it exceeded those of electrodes made from conventional nanoparticles.

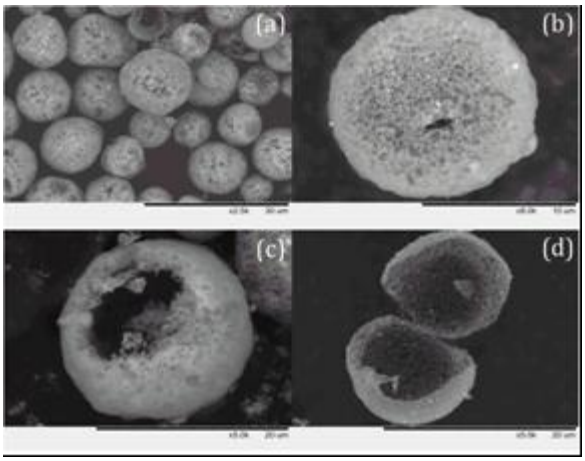

Figure V - 8: SEM images of (a) the nanoporous $LiCoPO_4$/C particles; (b) the surface of a single particle; (c, d) broken particles, showing the 3D interconnected pores.

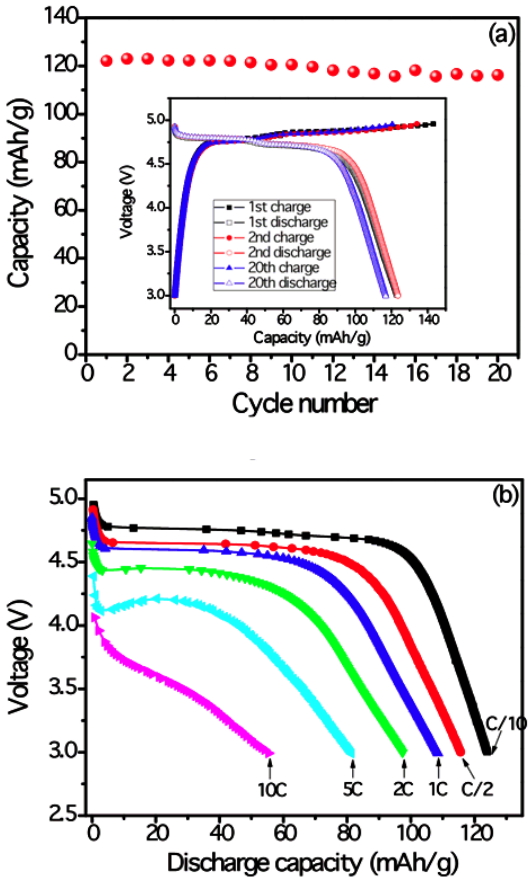

Figure V - 9: (a) Charge-discharge profiles at C/10, (inset) capacity retention and coulombic efficiency at C/10; (b) Discharge profiles at varying rates.

Cell Analysis. Composite electrodes are complex and non-uniform systems of active materials, conductive additives, binders, and pores of varying sizes. The conduction paths for electrons and ions depend on the individual characteristics of these components as well as on their spatial distributions. Due to the fragility of the electrodes, means of visualizing their internal structure must be chosen so as not to disturb the arrangement and connectivity of the particles and pores. X-ray tomography has been shown to be of great value in some cases, but is limited when the relative masses of the components are very different. We have applied ion beam milling to sequential "slicing" and imaging the exposed cross section surfaces of electrodes. Software reconstruction of these images gives an accurate picture of the sampled volume, including voids, cracks, and agglomerated particles.

An $LiFePO_4$ cathode (Figure V - 10) with a wide size range of primary and secondary particles, randomly distributed pores and numerous shallow cracks was subjected to Ga-ion beam milling. First, a u-shaped trench was cut (Figure V - 11) to a depth of about 10 μm to isolate a 6 μm x 8μm cuboidal region.

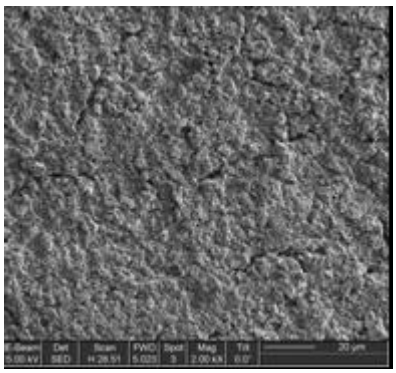

Figure V - 10: Surface of the fresh electrode.

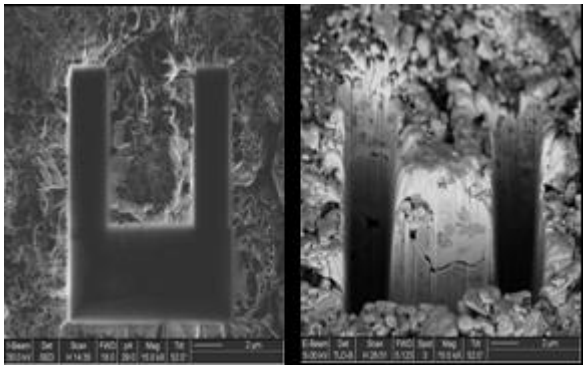

Figure V - 11: Top and side views of the trench.

Material was removed from the vertical face of the slab in 250 increments, 30 nm each in depth (Figure V - 12), revealing a network of large, connected pores surrounding dense, microporous agglomerates.

Figure V - 12: (a) Images of the cross section at depths of 1.5, 2.5, 4.0, 5.2, 7.5 μm.

Conclusions and Future Directions

Cathodes: While a small number of high capacity and high voltage cathode materials have become the focus of research on routes to increased energy density in lithium ion batteries, the spinels and layered oxides have not yet been commercialized due to excessive irreversible capacity losses and/or electrolyte instability. The high voltage phosphates may also be unstable, and serious rate limitations combined with incomplete utilization of the theoretical capacities have delayed their introduction as well. In the coming year, we will examine the surface chemistries of high-voltage cathodes to suggest guidelines for materials synthesis and component compatibility.

Cell Analysis. Mapping the structure of electrodes and the distributions of current and charge within them shines new light on electrode design parameters. We have begun an investigation of the influence of pore size and wall thickness in highly ordered nanoporous thin film electrodes, and will continue to collaborate with Venkat Srinivasan to improve the accuracy of our measurements and the utility of his models.

FY 2011 Publications/Presentations

1. "Spherical Nanoporous $LiCoPO_4$/C Composites as High Performance Cathode Materials for Rechargeable Lithium Batteries," J. Liu, T. E. Conry, X. Song, L. Yang, M. M. Doeff, and T. J. Richardson, Journal of Materials Chemistry, 21, 9984-9987 (2011). DOI: 10.1039/c1jm10793c
2. "Improved Kinetics and Stabilities in Mg-Substituted $LiMnPO_4$," G. Chen, A.K. Shukla, X. Song and T. J. Richardson, Journal of Materials Chemistry, 21, 10126-10133 (2011). DOI: 10.1039/C0JM04230G
3. "Nanoporous Spherical $LiFePO_4$ for High Performance Cathodes," J. Liu, T. E. Conry, X. Song, M. M. Doeff, and T. J. Richardson, Energy & Environmental Science, 4, 885 - 888 (2011).

V.B.3 Olivines and Substituted Layered Materials (LBNL)

Marca M. Doeff
Lawrence Berkeley National Laboratory
M/S 62R0100
Berkeley, CA 94720
Phone (510) 486-5821
Fax (510) 486-4881
E-mail mmdoeff@lbl.gov

Start Date: October 1, 2010
Projected End Date: September 30, 2011

Objectives

- Synthesize and characterize Al and Ti-substituted NMCs ($Li[Ni_xCo_{0.1-y}M_yMn_x]O_2$) cathode materials
- Demonstrate spray pyrolysis method for synthesis of oxide and olivine cathode materials.

Technical Barriers

The cost of vehicular batteries is too high and the energy density needs to be improved. The Co content of cathode materials needs to be decreased and processing of all cathode materials needs to be simplified to lower material costs. The performance of high voltage electrode materials like $LiNi_{0.5}Mn_{1.5}O_4$, which can potentially raise energy density, needs to be improved.

Technical Targets

- Reduce cobalt content in NMCs by substitution with low-cost metals such as Al or Ti, while maintaining good electrochemical performance.
- Design a spray pyrolysis system and demonstrate the synthesis of high performance electrode materials made by aqueous processing.

Accomplishments

- Demonstrated excellent electrochemical performance with $LiCoPO_4$/C cathode materials made by spray pyrolysis
- Demonstrated good morphological control of high voltage $LiNi_{0.5}Mn_{1.5}O_4$ spinel cathode material made by spray pyrolysis
- Determined origin of improved cycling with Al-substituted NMCs using synchrotron techniques

2. Identified reason for increased capacity with Ti-substituted NMCs

✧ ✧ ✧ ✧ ✧

Introduction

Achieving DOE cost and energy goals for vehicular batteries require improvement to the cathode materials. Cost reductions can be realized by reducing the fraction of expensive Co in layered NMC ($Li[Ni_xCo_yMn_x]O_2$) formulations and by adopting simpler processing methods for making materials. The challenge in both cases is to maintain or improve upon the physical and electrochemical characteristics of the conventional materials. NMCs with lower Co contents often have lower rate capability than the most commonly used $Li[Ni_{1/3}Co_{1/3}Mn_{1/3}]O_2$. We have, however, recently found that partial Ti-substitution increases practical capacities for some formulations, while Al-substitution can result in improved cycling and, in some cases, higher rate capabilities. Our work this past year has been directed towards understanding the origins of these improvements, using synchrotron and other characterization techniques. We are also developing a simple spray pyrolysis method for synthesis of olivine and oxide cathode materials, which reduces the steps needed for processing and the associated cost. To this end, we have successfully synthesized high-performance $LiCoPO_4$/C composites and $LiNi_{0.5}Mn_{1.5}O_4$ cathode materials. These high voltage materials have the potential of raising the energy density of vehicular batteries because fewer high voltage cells need to be connected into large battery packs. Less hardware is needed, so that weight and volume, as well as cost, decreases.

Approach

A precursor solution is sprayed through an ultrasonic nozzle into a heated furnace tube for the spray pyrolysis experiments. Particle characteristics such as size, size distribution, morphology, porosity, etc. can be controlled by varying experimental conditions including nozzle frequency, type and concentration of precursors in solution, the use of additives, temperature, and post-production thermal treatments. A variety of physical techniques are used to characterize materials including x-ray powder diffraction (XRD), scanning electron microscopy (SEM), and elemental analysis. Composite electrodes are tested in half-cell configurations. Pouch cells with lithium anodes and composite cathodes are assembled and cycled in the relevant SSRL beamline for *in situ* XAS and x-ray diffraction experiments. The Advanced Photon Source (APS) at Argonne National Lab is also used

for structural characterization of powders and electrodes *ex situ.*

Results

Substituted NMCs. We previously demonstrated that Al can be fully substituted for Co in the $Li[Ni_{0.45}Co_{0.1-y}Al_yMn_{0.45}]O_2$ system. The best electrochemical results are obtained with the $Li[Ni_{0.45}Co_{0.05}Al_{0.05}Mn_{0.45}]O_2$ compound, which cycles better than the unsubstituted variant (hereafter indicated as 992-NMC) with a similar initial capacity. The initial capacity of the fully substituted material, $Li[Ni_{0.45}Al_{0.1}Mn_{0.45}]O_2$, is lower, although similar cycling improvements are observed. High-resolution XRD patterns of the pristine powders are shown in Figure V - 13.

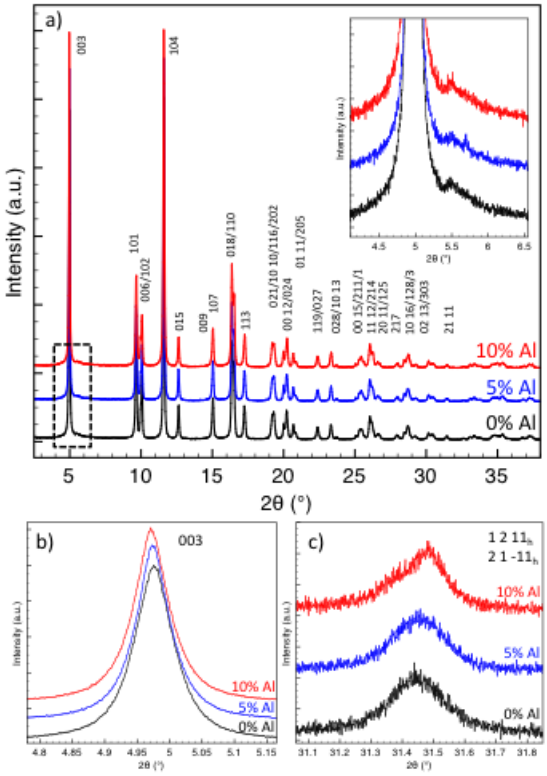

Figure V - 13: High resolution XRD patterns of $Li[Ni_{0.45}Co_{0.1-y}Al_yMn_{0.45}]O_2$ compounds: a) full patterns with inset showing superstructure peaks b) detail showing 003 peaks, and c) detail showing peak splitting in the 10% Al substituted sample, indicative of a monoclinic distortion.

All materials are phase-pure, and weak superstructure peaks appear near the 003 peak, arising from Li/Ni antisite mixing. Pattern refinement indicates that 9-10% of the Ni resides on Li (*3a*) sites, rising with the Al content. A close examination of the 1211 reflection (Figure V - 13c) in the 10% Al substituted material reveals peak splitting, indicative of a monoclinic distortion for this sample. X-ray absorption studies suggest that Al-substitution relieves some of the inherent strain within the edge-sharing octahedral layer caused by differing metal-oxygen bond distances, and is responsible for the monoclinic distortion.

Analysis of XRD patterns obtained *ex situ* on electrodes cycled 50 times and stopped in the discharged state indicate that the monoclinic distortion is retained for the 10% Al substituted material. Interestingly, the amount of Ni present on *3a* sites decreases by about 1% for all of the materials. While no new peaks indicating any secondary phase growth are observed with cycling for any of the cathodes, there is a relative expansion of all lattice parameters with cycle number, which cannot be explained solely by differing degrees of lithiation. This is indicative of structural changes induced by the cycling. Significantly, the relative changes in lattice parameters are minimized, and the decrease in antisite concentration is highest, in the y=0.05 sample, which also shows the best cycling performance.

We have previously observed higher discharge capacities and improved cycling for several Ti-substituted NMC ($Li_{1+x}[Ni_{0.33}Co_{0.33-y}Ti_yMn_{0.33}]_{1-x}O_2$ cathode materials, in which Ti is aliovalently substituted for Co. Either lithium-excess or lithium-stoichiometric compounds can by synthesized, although the solid solution range for both is very limited (on the order of a few atom percent). Figure V - 14 shows a typical first cycle in a lithium half-cell of the baseline 333-NMC and examples of the two types of titanium-substituted cathodes.

A decrease in the first cycle inefficiency is responsible for the improved practical capacities exhibited by the stoichiometric Ti-substituted cathodes. For the lithium-excess materials, a formation reaction, evident on a high voltage plateau during charge, in which both lithium and oxygen are lost irreversibly and the normally inert Mn is made electroactive also contributes capacity, but increases inefficiency somewhat. Further evidence for this is the slight inflection seen at the end of discharge, near 3V, consistent with electroactive Mn. First cycle coulombic inefficiencies are observed in NMC cathodes even when they are charged very conservatively. This phenomenon has been attributed to kinetic limitations near the end of discharge, which prevent full lithiation from occurring in the normal potential range. For a reason not yet understood, the presence of Ti in the NMC electrodes improves the kinetics and decreases this inefficiency, allowing higher capacities to be obtained upon subsequent discharges.

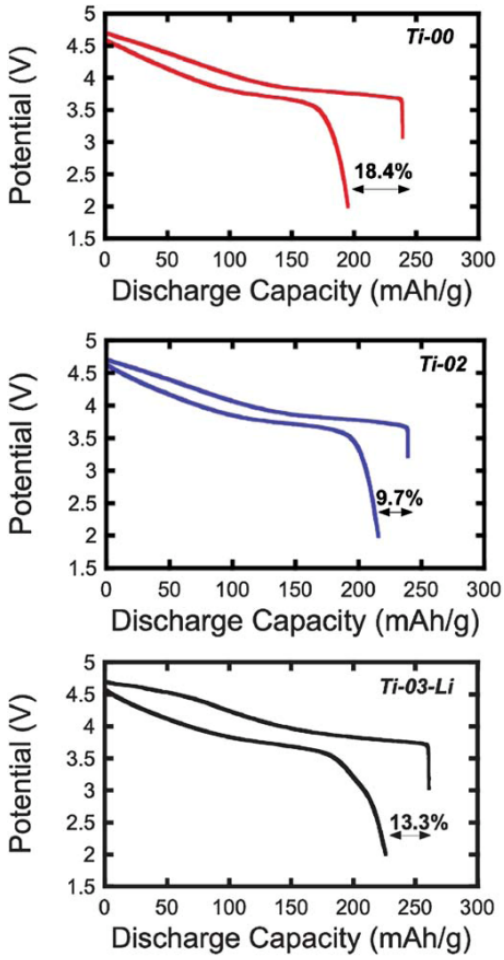

Figure V - 14: First cycles of lithium cells charged and discharged between 4.7-2.0V at 0.1 mA/cm^2 containing $Li_{1+x}[Ni_{0.33}Co_{0.33-y}Ti_yMn_{0.33}]_{1-x}O_2$ cathodes; (top) baseline material, $Li[Ni_{1/3}Co_{1/3}Mn_{1/3}]O_2$, (x=0, y=0) (middle) stoichiometric Ti-substituted material (x=0 and y=0.02) and (bottom) lithium-excess material (x=0.05 and y=0.03).

Spray Pyrolysis. Nanoporous $LiCoPO_4$/C composites were prepared via a spray pyrolysis technique from solutions containing a citric acid additive. The decomposition of the citric acid resulted in the deposition of a thin amorphous carbon layer on all surfaces of the spherical nanoporous particles (Figure V - 15 and Figure V - 16).

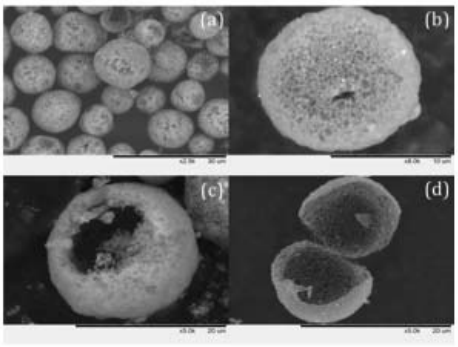

Figure V - 15: SEM images of (a) nanoporous $LiCoPO_4$/2.4%C composite particles; (b) the surface of a single particle; (c, d) particles broken open to show the 3D interconnected pores.

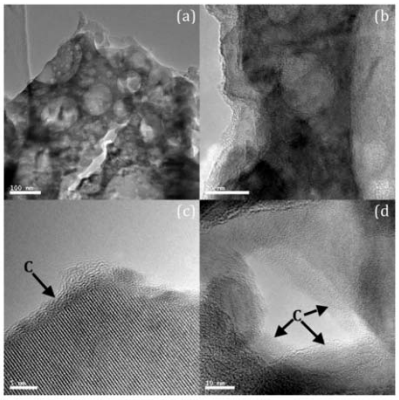

Figure V - 16: (a) TEM image of a fractured $LiCoPO_4$/C particle, showing the pore structure; and (b) the nanocrystalline character of the composites; (c, d) HRTEM images of the fracture edge and the inside of a nanopore, the amorphous carbon coating on both the outer surface and the inner pore walls.

The electrochemical performance of this material in lithium half-cells is among the best ever reported for a $LiCoPO_4$ electrode (Figure V - 17), due to the optimized nanostructure, which provides intimately connected pathways for ions and electrons to move. Although the primary particles are very small (about 70 nm), the secondary particles are large (~10 μm) and regularly shaped, allowing easy processing into composite electrodes. Unlike with irregularly shaped nanometric powders, there is no need to increase the amount of carbon additive, which further reduces practical specific energy, to ensure connectivity. In spite of the high operating voltage, good capacity retention is observed over twenty cycles with a reasonable coulombic efficiency of 97% after the first cycle (a LiBOB additive was used to minimize irreversible oxidation of electrolyte). These results clearly exhibit the advantages that hierarchical structuring conveys when applied to transport-limited polyanionic compounds.

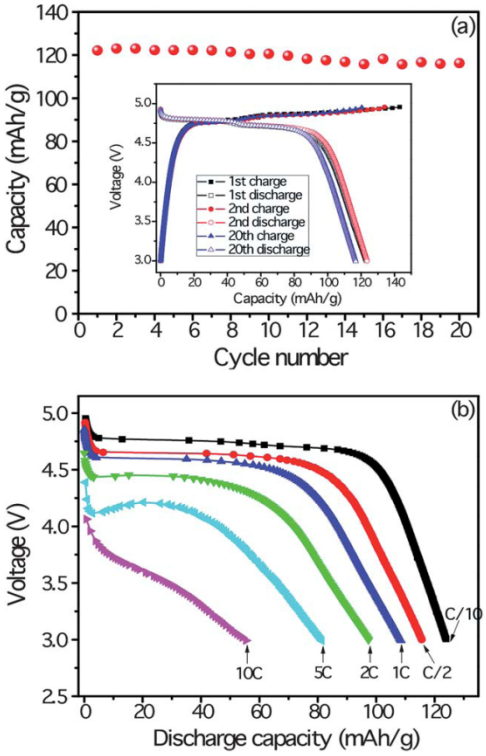

Figure V - 17: a) Cycling data for Li/1M $LiPF_6$ in 1:1 DEC/EC with 1 wt.% LiBOB/nanoporous $LiCoPO_4$ cells at C/10 rate, and, (b) discharges at rates varying from C/10 to 10C.

Spray pyrolysis has also been carried out under varying conditions to make the high voltage spinel $LiNi_{0.5}Mn_{1.5}O_4$. Figure V - 18 shows the variety of particle morphologies and sizes that can be synthesized by changing nozzle frequencies, thermal treatments and precursor concentrations. This good morphological control will allow us to study the effect of particle size and shape on the electrochemistry of $LiNi_{0.5}Mn_{1.5}O_4$.

Conclusions and Future Directions

We are currently working on several papers summarizing the characterization of the $Li[Ni_{0.45}Co_{0.1-y}Al_yMn_{0.45}]O_2$ cathodes, but no further experiments on this system are planned. Instead, we will concentrate on the Ti-substituted NMCs and the possibility of increasing energy density. We will characterize materials using a variety of techniques to understand the reason for the improved first cycle efficiencies and optimize compositions.

We will continue to work on the spray pyrolysis method for synthesis of high-energy cathode materials, including NMCs and the high voltage spinel, $LiNi_{0.5}Mn_{1.5}O_4$. We will study the effect of differing morphologies on the electrochemistry of the spinel in the upcoming year. In particular, it will be important to track the coulombic inefficiencies, which are correlated with side reactions that jeopardize the safety of the system and shorten cycle life. The presence of Mn^{3+} in $LiNi_{0.5}Mn_{1.5}O_4$ may also shorten cycle life due to its dissolution by acidic components in the electrolyte, so we will attempt to minimize its presence. Ti-substitution can ameliorate the dissolution, but may also decrease capacity. Finally we will explore methods for coating particles with alumina or zinc oxide *in situ* in the spray pyrolysis reactor to protect against side reactions associated with high voltage operation.

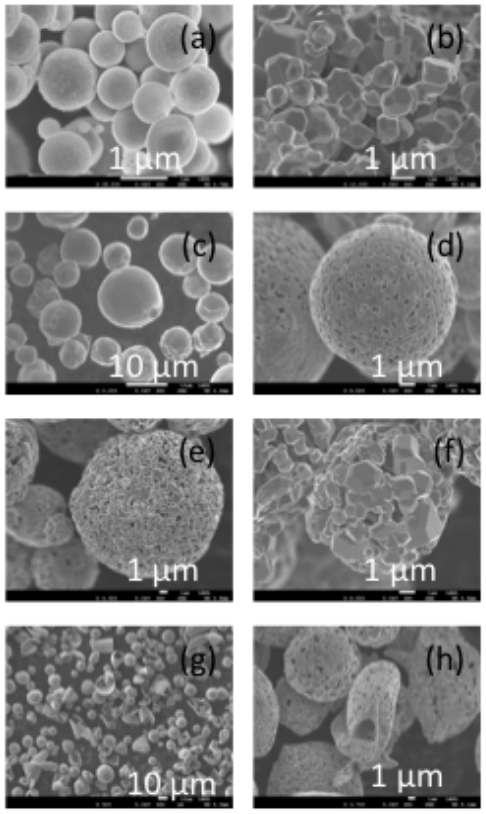

Figure V - 18: SEM images of spray pyrolyzed $LiNi_{0.5}Mn_{1.5}O_4$ samples: (a) 1 µm particles made using 2.4 MHz nozzle and 1M nitrate precursors at 700°C. (b) sample "a" heated to 900°C for fifteen minutes. (c) 10 µm particles made using 120 kHz nozzle and 1M nitrate precursors at 700°C. (d) sample "c" heated to 800°C for four hours. (e) sample "c" heated to 900°C for 15 minutes. (f) sample c heated to 900°C for four hours. (g) burst particles made using 2.4 MHz nozzle and 3M nitrate precursors at 700°C. (h) sample "g" heated to 900°C for fifteen minutes.

FY 2011 Publications/Presentations

1. 2011 DOE Annual Peer Review Meeting Presentation, May 2011.
2. "Spherical Nanoporous $LiCoPO_4$/C Composites as High Performance Cathode Materials for Rechargeable Lithium Batteries" Jun Liu, Thomas E. Conry, Xiangyun Song, Li Yang, Marca M. Doeff, and Thomas J. Richardson, **J. Mater. Chem.** 21, 9984 (2011).

3. "Aliovalent Titanium Substitution in Layered Mixed Li Ni-Mn-Co Oxides for Lithium Battery Applications" Kinson Kam and Marca M. Doeff, **J. Mater. Chem.** 21, 9991 (2011).
4. "Three Dimensional Nanoporous Spherical $LiFePO_4$ for High Performance Cathodes" Jun Liu, Thomas E. Conry, Xiangyun Song, Marca M. Doeff and Thomas J. Richardson, **Energy & Environmental Science,** 4, 885 (2011).
5. "Structural and Electrochemical Investigation of $Li[Ni_{0.4}Co_{0.15}Al_{0.05}Mn_{0.4}]O_2$ Cathode Material" C. Rumble, T.E. Conry, Marca Doeff, Elton J. Cairns, James E. Penner-Hahn, and Aniruddha Deb, **J. Electrochem. Soc.** 157, A1317 (2010).
6. "Aliovalent Substitution in Mixed Ni-Mn-Co Oxide Cathodes" Kinson C. Kam and Marca M. Doeff 2011 Materials Research Society Meeting, San Francisco, CA April 2011, Abstract M3.5.
7. "Finding Room for Improvement in Transition Metal Oxide Cathodes for Lithium-Ion Batteries" Kinson C. Kam and Marca Doeff, International Conference on Advanced Ceramics and Composites, January, 2011 Daytona Beach, FL, Abstract ICACC-S14-019-2011.
8. "The Effect of Al-Substitution in $LiNi_{0.45}Co_{0.1-x}Al_xMn_{0.45}O_2$ Layered Oxide Cathode Materials" T. Conry, J. Cabana, and M Doeff, 218th meeting of the Electrochemical Society, October 2010, Las Vegas Nevada, Abstract 1000.
9. "Lithium Ion Battery Cathodes for Traction Applications" Electrical Energy Storage Meeting, University of Michigan, Ann Arbor, MI, August 3, 2011. (invited)
10. "Lithium Ion Battery Cathodes for Traction Applications" ALS-CXRO seminar series, Lawrence Berkeley National Laboratory, Berkeley, CA, July 6, 2011. (invited)

V.B.4 Stabilized Spinels and Nano Olivines (U. Texas)

Arumugam Manthiram

University of Texas at Austin
Materials Science and Engineering Program
Austin, TX 78712
Phone: (512) 471-1791; Fax: (512) 471-7681
E-mail: rmanth@mail.utexas.edu

Subcontractor: None

Start Date: April 1, 2004
Projected End Date: December 31, 2011

Objectives

- Develop high-performance cathodes for lithium-ion batteries and a fundamental understanding of their structure-composition-performance relationships
- Develop low-cost spinel oxide cathodes that can offer high energy and power, long cycle life at elevated temperatures, good storage properties, and good safety
- Develop novel low-cost synthesis and manufacturing processes for polyanion-containing cathodes such as phosphates and silicates that can offer high energy, while exhibiting good thermal stability and safety

Technical Barriers

This project addresses the following technical barriers of the lithium-ion battery technology, especially focusing on the cathode materials:

- Battery cost
- Safety
- Cycle life
- Energy and power

Technical Targets

- Long cycle life for high-voltage spinel cathodes
- Low manufacturing cost for polyanion cathodes
- Increased energy and power with spinel and polyanion cathodes

Accomplishments

- Fundamental understanding of the factors that control the electrochemical performances (*e.g.*, cycle life, rate capability, and coulombic efficiency) of high-voltage (4.7 V) spinel cathodes
- Establishment of the segregation of certain cations to the surface and their benefits in providing a robust cathode-electrolyte interface and superior electrochemical performances
- Synthesis of high-voltage spinel cathodes with unique morphologies and high tap density
- Understanding the factors influencing the thermal stability of 4 V spinel oxide and oxyfluoride cathodes
- Synthesis of metastable $LiFe_{1-x}(VO)_xPO_4$ and various polymorphs of $LiVOPO_4$ cathodes by a novel microwave-assisted solvothermal process

✧ ✧ ✧ ✧ ✧

Introduction

Achieving the DOE targets for vehicle applications will require development of low-cost, safe cathode and anode materials with high energy and power and long life. Accordingly, this project focuses on improving the performance and/or lowering the manufacturing cost of high-voltage spinel and polyanion cathodes. The major issue in employing the high-voltage spinel is the aggressive reaction of the cathode surface with the electrolyte at the high operating voltage of 4.7 V and the consequent degradation of cycle life and rate capability. This project focuses on overcoming this difficulty and on improving the tap density and volumetric energy density. With the polyanion cathodes, novel synthesis approaches are pursued to access the metastable $LiFe_{1-x}(VO)_xPO_4$ and to stabilize the various polymorphic modifications of $LiVOPO_4$ that operate at slightly higher voltage than the olivine $LiFePO_4$.

Approach

To meet the DOE performance and cost targets for vehicle applications, our approach is to develop a firm scientific understanding of the factors that control/influence the electrochemical performances of the spinel oxide and polyanion-containing cathodes and utilize the knowledge gained to design and develop high performance cathode compositions. In this regard, cationic substitutions in the high-voltage spinels, surface modifications with self-surface segregation of certain cations during the synthesis process, and novel synthesis approaches for spinel and polyanion cathodes are being pursued. The materials synthesized by conventional solid-

state or solution-based synthesis approaches are characterized by a variety of chemical and physical techniques: wet-chemical analysis by inductively coupled plasma (ICP) analysis, X-ray diffraction (XRD), scanning electron microscopy (SEM), transmission electron microscopy (TEM), thermal analysis, Fourier transform infrared (FTIR) spectroscopy, Raman spectroscopy, and X-ray photoelectron spectroscopy (XPS). The electrochemical performances are evaluated with coin cells with charge-discharge, cyclability, rate capability, and impedance spectroscopic measurements. Based on the chemical, structural, morphological, and electrochemical data collected with the synthesized samples, an in-depth structure-property-performance relationship is established. The understanding gained is utilized to refine the compositions and develop new materials.

Results

Stabilized High-voltage Spinel Cathodes: We previously showed that the Fe-substituted high-voltage spinel cathodes exhibit much improved electrochemical performances (cyclability and rate capability) compared to the pristine $LiMn_{1.5}Ni_{0.5}O_4$. In order to develop further understanding, we have focused on investigating various cationic substitutions in $LiMn_{1.5}Ni_{0.5-y}M_yO_4$ (M = Al, Cr, Fe, Co, Zn, and Ga) and the self-surface segregation of cations by time-of-flight – secondary ion mass spectroscopy (TOF-SIMS).

The above cationic substitutions eliminate the $Li_xNi_{1-x}O$ impurity phase, increase the Mn^{3+} content, and suppress the ordering between Mn^{4+} and Ni^{2+}, resulting in improved electrochemical performance. Figure V - 19 compares the TOF-SIMS depth profiles of Mn, Ni, and Fe in $LiMn_{1.5}Ni_{0.42}Fe_{0.08}O_4$. The data show a much higher concentration of Fe on the surface compared to that in the bulk, indicating a segregation of Fe to the surface during the synthesis process. This observation is consistent with our earlier findings with XPS. The segregation of Fe to the surface seems to provide a more stable interface with the electrolyte, offering superior cycle life at 55°C and high rate capability. Similar TOF-SIMS investigations of other $LiMn_{1.5}Ni_{0.42}M_{0.08}O_4$ also reveals a segregation of M = Al, Cr, and Ga to the surface, but not M = Co and Zn.

With an aim to understand the origin of variations in the performance of undoped $LiMn_{1.5}Ni_{0.5}O_4$ and to increase the tap density of the high-voltage spinels, we have also focused on the synthesis of the undoped $LiMn_{1.5}Ni_{0.5}O_4$ by various methods such as a hydroxide precipitation, a carbonate precipitation, an ammonium bicarbonate-mediated process, and a urea-mediated process. These processes were used to prepare materials with varying morphologies.

Figure V - 20 shows the first charge-discharge profiles and the corresponding SEM images of the $LiMn_{1.5}Ni_{0.5}O_4$ samples prepared with various morphologies. The commercial and spherical 2 samples composed of relatively smaller particles (1 – 2 μm) with a lower tap density of 1.3 – 1.5 g/cm^3 show lower discharge capacities of ~ 120 mAh/g. On the other hand, the polyhedral 1, polyhedral 2, cubic, spherical 1, and spherical 3 samples with a larger particle size of 5 to 15 μm exhibit larger discharge capacities of ~ 130 mAh/g. The larger particle size also leads to a high tap density of 1.8 – 2.0 g/cm^3 for the polyhedral 1, cubic, and spherical 1 samples, which is beneficial to increase the volumetric energy density. Among the seven samples in Figure V - 20, the spherical 3 sample shows the lowest coulombic efficiency of 77 % due to the high surface area caused by the loosely packed, submicron-size crystallites, lowering the tap density to 1.6 g/cm^3, and the increased solid-electrolyte interfacial (SEI) layer formation. On the other hand, the cubic and spherical 1 samples show higher coulombic efficiencies of, respectively, 80 and 84 % due to a larger particle size and smaller surface area.

Figure V - 21 compares the cyclability of the various $LiMn_{1.5}Ni_{0.5}O_4$ samples. All the samples show better cyclability than the commercial sample. Among the six samples synthesized by us, the spherical 3 sample shows the largest capacity fade due to the larger surface area and increased reaction with the electrolyte. Also, the commercial and the spherical 3 samples show a smaller 4 V plateau, implying a lower Mn^{3+} content, compared to the cubic, polyhedral 2, spherical 1, and spherical 2 samples, so the better cyclability of the latter samples could be related to the higher Mn^{3+} content. However, the polyhedral 1 sample with a smaller 4 V plateau also exhibits better cyclability. Thus, particle size, surface area, morphology, Mn^{3+} content, and degree of cation disorder in the 16d octahedral site all seem to play a role in controlling the electrochemical properties and our future work will focus on developing a further understanding of the influence of these parameters.

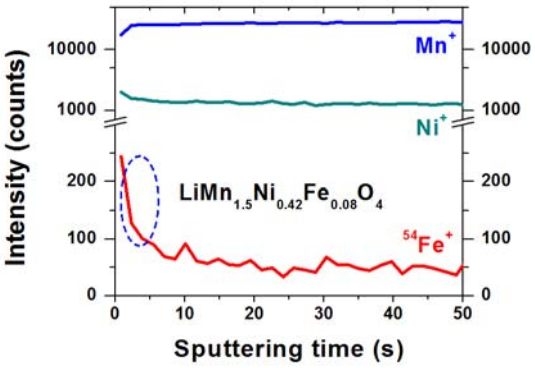

Figure V - 19: TOF-SIMS depth profile of the $LiMn_{1.5}Ni_{0.42}Fe_{0.08}O_4$ sample.

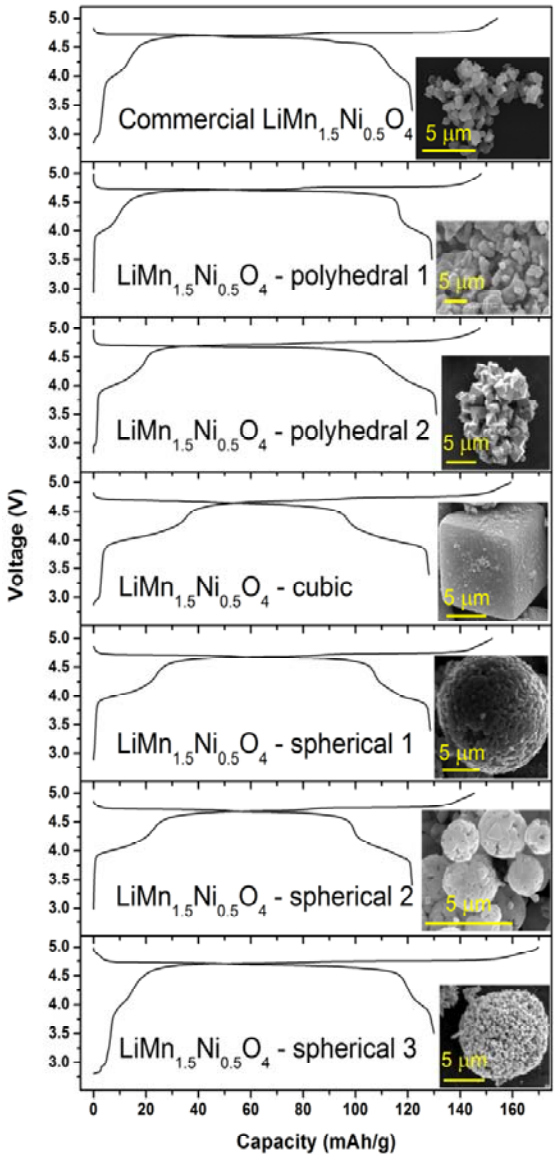

Figure V - 20: Charge-discharge profiles and SEM images of the $LiMn_{1.5}Ni_{0.5}O_4$ samples with different morphologies.

Thermal Stability of 4 V Spinel Cathodes: The 4 V spinel cathodes are now commercially employed for vehicle applications, but the variations in their thermal stability and safety are not fully explored. Accordingly, the thermal stability characteristics of the 4 V spinel oxide and oxyfluoride cathodes $Li_{1.1}Mn_{1.9-y}M_yO_{4-z}F_z$ (M = Ni and Al, $0 \le y \le 0.3$, and $0 \le z \le 0.2$) have been investigated systematically by monitoring the onset temperature and reaction enthalpy for the exothermic reaction with differential scanning calorimetry (DSC). The peak onset temperature increases and the reaction enthalpy decreases (*i.e.*, thermal stability increases) with decreasing lithium content in the cathode in the charged state or increasing specific capacity (*i.e.*, with increasing amount of lithium extraction). Also, the oxyfluorides are found to exhibit better thermal stability than the corresponding oxide analogs due to a stronger Mn-F bond.

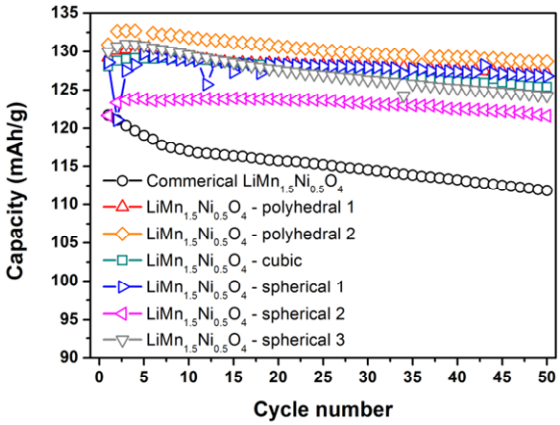

Figure V - 21: Cyclability of the various $LiMn_{1.5}Ni_{0.5}O_4$ samples with different morphologies.

Nanostructured Polyanion Cathodes: A novel microwave-assisted solvothermal process has been successfully used to obtain $LiFe_{1-x}(VO)_xPO_4$ for $0 \le x \le 0.25$. Characterization of the products reveals the formation of (i) Fe vacancies and an oxidation of some Fe^{2+} to Fe^{3+} to maintain charge neutrality and (ii) a suppression of the two-phase plateau behavior that is characteristic of $LiFePO_4$. The $LiFe_{1-x}(VO)_xPO_4$ phases disproportionate to more stable $LiFePO_4$ and $Li_3V_2(PO_4)_3$ when heated at 700°C in inert atmospheres, implying that they are metastable and cannot be accessed by conventional high-temperature synthesis.

$LiVOPO_4$ crystallizes in three polymorphic modifications (orthorhombic, triclinic, and tetragonal) with a theoretical capacity of 159 mAh/g and an operating voltage of 3.7 - 4.0 V (depending on the polymorph), leading to higher energy density than $LiFePO_4$. These polymorphs can be synthesized by various methods including sol-gel, hydrothermal, solvothermal, carbothermal reduction, and chemical lithiation of $VOPO_4$. As part of our ongoing activities in exploiting the microwave-assisted synthesis processes as they offer reaction products within a short reaction time with unique nanomorphologies, we have pursued the microwave-assisted solvothermal (MW-ST) synthesis of $LiVOPO_4$. We have been able to obtain all the three polymorphs of $LiVOPO_4$ within 30 minutes at < 230°C by conducting the MW-ST process in a novel mixed solvent (ethanol and water) medium. By varying the Li:V:P and the water:ethanol ratios, we have identified the conditions to obtain nearly phase-pure products of the three polymorphs.

The XRD patterns shown in Figure V - 22 reveal that highly crystalline phases of the three polymorphic modifications can be obtained by the MW-ST process. Inductively coupled plasma (ICP) analysis indicates slight deviations from the nominal contents due to the presence

of trace amounts of impurity phases. Further fine tuning of the conditions to eliminate the minor impurity phases and characterization of the samples by electron microscopy and electrochemical measurements are currently in progress.

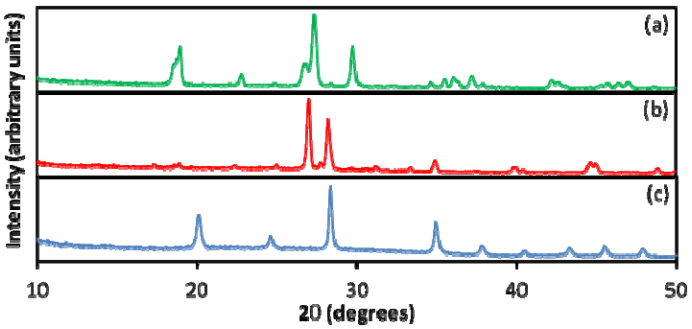

Figure V - 22: XRD patterns of (a) triclinic, (b) orthorhombic, and (c) tetragonal $LiVOPO_4$.

Conclusions and Future Directions

Substitution of M^{n+} in the high-voltage spinel cathodes $LiMn_{1.5}Ni_{0.42}M_{0.08}O_4$ (M = Al, Cr, Fe, Co, Zn, and Ga) eliminates the $Li_xNi_{1-x}O$ impurity phase, increases the Mn^{3+} content, and suppresses the ordering between Mn^{4+} and Ni^{2+}, resulting in improved cyclability and rate capability. Characterization of the samples by TOF-SIMS reveals a segregation of Al, Cr, Fe, and Ga to the surface, which leads to a robust cathode-electrolyte interface and superior cycle life at elevated temperatures due to the suppression of SEI layer formation. Also, synthesis of the undoped $LiMn_{1.5}Ni_{0.5}O_4$ in various morphologies by novel synthesis approaches and their characterization reveal that the variations in performance is due to the differences in the Mn^{3+} content. Samples with higher Mn^{3+} content show better performance. Our future work is focused on adopting the synthesis approaches developed to obtain the doped samples with high tap density and assessing the role of morphology on electrochemical performances.

With the 4 V spinels, the oxyfluorides exhibit better thermal stability than the corresponding oxides. Also, the cathodes with lower lithium content in the charged state or with higher capacity exhibit better thermal stability.

The metastable $LiFe_{1-x}(VO)_xPO_4$ ($0 \le x \le 0.25$) and the three crystallographic modifications of $LiVOPO_4$ have been obtained by a novel microwave-solvothermal process. Our future work is focused on comparing the properties of the three forms of $LiVOPO_4$ as well as exploring the microwave-solvothermal process for other polyanion cathodes based on silicates and Nasicon-type phosphates.

FY 2011 Publications/Presentations

Journal Articles

1. T. Muraliganth, K. R. Stroukoff, and A. Manthiram, "Microwave-Solvothermal Synthesis of Nanostructured Li_2MSiO_4/C (M = Mn and Fe) Cathodes for Lithium-Ion Batteries," *Chemistry of Materials*, **22**, 5754-5761 (2010).
2. S. Yoon and A. Manthiram, "Nanostructured Sn-Ti-C Composite Anodes for Lithium Ion Batteries," *Electrochimica Acta* **56**, 3029-3035 (2011).
3. A. Manthiram, "Materials Challenges and Opportunities of Lithium-ion Batteries," *Journal of Physical Chemistry Letters*, **2**, 176-184 (2011).
4. K. R. Stroukoff and A. Manthiram, "Thermal Stability of Spinel $Li_{1.1}Mn_{1.9-y}M_yO_{4-z}F_z$ (M = Ni, Al, and Li, $0 \le y \le 0.3$, and $0 \le z \le 0.2$) Cathodes for Lithium Ion Batteries," *Journal of Materials Chemistry* **21**, 10165-10170 (2011).
5. K. L. Harrison and A. Manthiram, "Microwave-assisted Solvothermal Synthesis and Characterization of Metastable $LiFe_{1-x}(VO)_xPO_4$ Cathodes," *Inorganic Chemistry* **50**, 3613-3620 (2011).
6. D.W. Shin and A. Manthiram, "Surface-segregated, high-voltage spinel $LiMn_{1.5}Ni_{0.42}Ga_{0.08}O_4$ cathodes with superior high-temperature cyclability for lithium-ion batteries," *Electrochemistry Communications* **13**, 1213-1216 (2011).

Presentations

1. A. Manthiram and T. Muraliganth, "Electrochemical Behavior and Shifts in the Redox Potentials of Olivine $LiM_{1-y}M_yPO_4$ (M = Fe, Mn, and Co) Solid Solutions," *218th Meeting of the Electrochemical Society Meeting,* Las Vegas, NV, October 10 – 15, 2010.
2. A. Manthiram, "Nanotechnology for Electrical Energy Storage," *Nano Monterey 2010: Applications of Nanotechnology to New Energy Sources*, Monterey, Mexico, November 18 – 19, 2010 (plenary talk).
3. A. Manthiram, T. Muraliganth, A. Vadivel Murugan, and K. L. Harrison, "Microwave-assisted Solvothermal Synthesis of Nanostructured Materials for Lithium-ion Batteries," *2010 Fall Meeting of the Materials Research Society,* Boston, MA, November 28 – December 3, 2010 (invited).

4. A. Manthiram, "Next Generation Lithium-ion Batteries," *10X Battery R&D Conference*, San Francisco, CA, January 10 – 12, 2011 (keynote talk).
5. A. Manthiram, "Materials Challenges and Opportunities of Lithium-ion Batteries for Electrical Energy Storage," *American Physical Society Meeting*, Dallas, TX, March 21 – 25, 2011 (invited).
6. A. Manthiram, "Next Generation of Electrode Materials for Lithium Ion Batteries," NAATBatt Annual Meeting and Conference, Louisville, KY, September 7-8, 2011.

V.B.5 The Synthesis and Characterization of Substituted Olivines and Manganese Oxides (SUNY)

M. Stanley Whittingham (Project Manager)
Binghamton University
Vestal Parkway East
Binghamton, NY 13902-6000
Phone: (607) 777-4623; Fax: (607) 777-4623
E-mail: stanwhit@binghamton.edu

Start Date: June 1, 2007
Projected End Date: December 31, 2011

Objectives

- Find lower-cost and higher-capacity cathodes, exceeding 200 Ah/kg (700-800 Wh/kg lab experimental)
- Find high-rate PHEV compatible cathodes
- Both of the above are to be based on environmentally benign materials.

Technical Barriers

This project addresses the following technical barriers:

(A) Lower cost materials and processing

(B) Higher power materials

(C) Higher capacity materials

(D) Abuse-tolerant safer cathodes

Technical Targets

- Identify $LiNi_yMn_yCo_{1-2y}O_2$ systems that can achieve 200 Ah/kg for PHEV applications.
- Identify and evaluate phosphate structures, containing Fe and/or Mn that have the potential of achieving an energy density exceeding 700 Wh/kg.
- Identify other materials, including those containing vanadium, that can undergo more than one electron transfer per redox center.

Accomplishments

- Shown for the stoichiometric layered oxides that the composition $LiMn_{0.4}Ni_{0.4}Co_{0.2}O_2$ is as good electrochemically as $LiMn_{0.33}Ni_{0.33}Co_{0.33}O_2$.
  - Lower cobalt contents have higher surface area and lower cost.
  - Capacities over 200 Ah/kg at the C rate in these Li/M=1 layered oxides will require charging voltages over 4.4 volts at room temperature (RT).
  - In collaboration with NREL showed that these layered oxides have inherent high rate capabilities
  - Shown that the Li-rich Mn-rich materials have inferior rate capability than the $LiNi_{1/3}Mn_{1/3}Co_{1/3}O_2$ materials at 2C and higher rates at RT.
  - The Li-rich Mn-rich materials have much inferior thermal stability than materials such as $LiNi_{0.4}Mn_{0.4}Co_{0.2}O_2$. Al substitution helps increase the thermal stability, but it remains lower than NMC.
- Identified the pyrophosphates, $Li_2MP_2O_7$, as candidate materials that can achieve an energy density exceeding 700 Wh/kg.
  - $Li_2FeP_2O_7$ cycles one lithium readily
  - $Li_2MnP_2O_7$ and $Li_2CoP_2O_7$ were inferior electrochemically.
  - Working with Primet, $Li_2FeP_2O_7$ was nano-scissored and more than one Li was cycled.
    - However, severe electrolyte decomposition occurs.
    - Calculations by G. Ceder at MIT concluded that electrolytes with stabilities over 5 volts are needed.
- Identified $VOPO_4$ and VPO_4, as well as vanadium oxides as viable candidates for > 1 electron transfer.
- Technology transfer accomplished
  - Working with several local battery companies (Primet on nano-scissored material), and many ex-students now in battery companies
  - Students now have positions at BNL, NREL, PNNL, Toyota (Ann Arbor), MIT, and Primet

✧ ✧ ✧ ✧ ✧

Introduction

Achieving the DOE energy and power targets for PHEV and EV batteries will require much higher capacity

materials. To meet the DOE cost targets, we are looking at reducing high-cost components and for power and energy targets at modifying the chemical composition and morphology of the cathode compounds.

Approach

Our cathode approach is to place emphasis on low cost materials, predominantly oxides and phosphates, both pure and modified with other transition metals, using a range of practical synthesis approaches. These materials will be synthesized, and characterized both structurally, including defects and morphology, and for thermal and chemical stability. All will be evaluated electrochemically in a range of cell configurations.

For the modified layered dioxides, we are determining the role of each of the transition metals, with the goal of minimizing expensive components such as cobalt. To that end, we are studying the layered compositions, $LiNi_yMn_yCo_{1-2y}O_2$, with a close to stoichiometric Li to transition metal ratio and comparing them to the Li-rich Mn-rich compounds.

We are also searching for new classes of materials that might react with more than one lithium ion per redox center. Phosphates are one area for our search and vanadium containing materials another area.

Results

Layered Transition Metal Oxides. We formed a range of transition metal oxides of formula $LiNi_yMn_yCo_{1-2y}O_2$ to determine the optimum composition for both energy density and power density. The voltage/capacity curves were determined and found to depend little on the chemical composition except at low values of the lithium content, when the redox of Co becomes involved and pushed the potential higher. The lower cobalt material with y = 0.4 showed as good electrochemical behavior as the commonly used $LiNi_{1/3}Mn_{1/3}Co_{1/3}O_2$ material, except at the highest discharge rates. In collaboration with C. Ban and A. Dillon at NREL, the rate behavior was determined and shown to be excellent as indicated in Figure V - 23. Full details are given in publication #3 listed below.

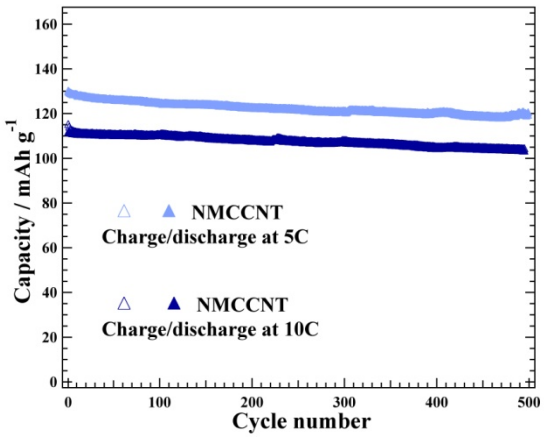

Figure V - 23: High-rate cycling of $LiNi_{0.4}Mn_{0.4}Co_{0.22}O_2$, using carbon nanotube mesh grid.

The results, shown in Figure V - 23, clearly show that the layered materials can deliver high rates when the electrode is configured optimally.

Our earlier work showed that a manganese content exceeding 0.5 in the formula $Li[Ni_{1-y-z}Mn_yCo_z]O_2$ is detrimental to the rate capability of these layered oxides with a Li/M ratio of unity. This year we expanded the study to the lithium-rich oxides described by the mixture $yLi_2MnO_3\bullet(1-y)LiNi_{0.4}Mn_{0.4}Co_{0.2}O_2$, where y=0.5 giving an overall composition of $Li_{1.2}Ni_{0.16}Mn_{0.56}Co_{0.08}O_2$. The results were somewhat surprising, with the rate capacities being worse than the Li/M stoichiometric material at higher rates, but this material also showed very poor thermal stability, no better than NCA. Although the thermal stability could be improved by substitution of some of the cobalt by aluminum, it is still much worse than $LiNi_{1/3}Mn_{1/3}Co_{1/3}O_2$ and $LiNi_{0.4}Mn_{0.4}Co_{0.4}O_2$ as shown in Figure V - 24. Aluminum contents above 5% do not seem to further stabilize the compound. As earlier work from Argonne National Lab has shown good stability for the Li-rich $Li_{1+y}[Ni_{1/3}Mn_{1/3}Co_{1/3}]_{1-y}O_2$ the instability is probably associated with the high manganese content. Thus, our conclusions of this layered oxide study are that the manganese content should probably be kept at less than 50% of the transition metal and also no higher than the nickel content in order to achieve high rates in a safe cathode.

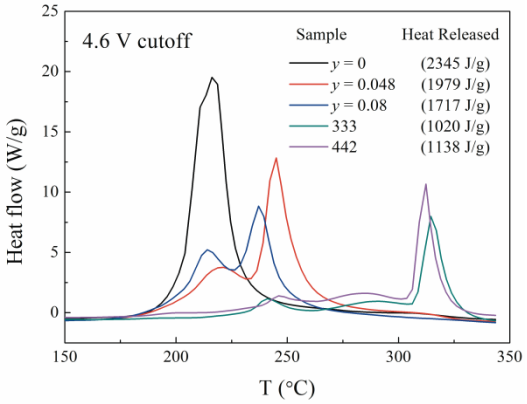

Figure V - 24: Differential scanning calorimetry at 10°/min of delithiated $Li_{1.2}Ni_{0.16}Mn_{0.56}Co_{0.08-y}Al_yO_2$ (y = 0, 0.048, 0.08) compared with the more stable NMC electrodes, $LiNi_{0.33}Mn_{0.33}Co_{0.33}O_2$ and $LiNi_{0.4}Mn_{0.4}Co_{0.2}O_2$.

Higher Capacity Electrodes – Pyrophosphates. The pyrophosphate, $Li_2FeP_2O_7$, can have a capacity well in excess of 200 Ah/kg. Working with Primet in Ithaca we have nanosized the compound, and tested a number of electrolytes. The results are shown in Figure V - 25. Although there is still a large amount of side-reactions above 5 volts, we are now achieving capacities that exceed one Li per iron (110 mAh/g). The maximum discharge capacity obtained is around 150 mAh/g, and we hope with still improved electrolyte to exceed 200 mAh/g and achieve 700 Wh/kg and at a higher volumetric energy density than $LiFePO_4$. The student has studied a number of ionic liquids at Monash University, but none have shown the required stability to date. We continue our collaboration with G. Ceder at MIT to determine the operating potentials of these systems.

Studies are continuing on vanadium based oxides and phosphates, as vanadium offers the opportunity for a two electron redox process between V^{5+} and V^{3+}. We have formed novel vanadium oxides and mixed phases of lithium vanadium phosphate. The Ceder group has also identified the $VOPO_4$ class of material as the most promising of the phosphates.

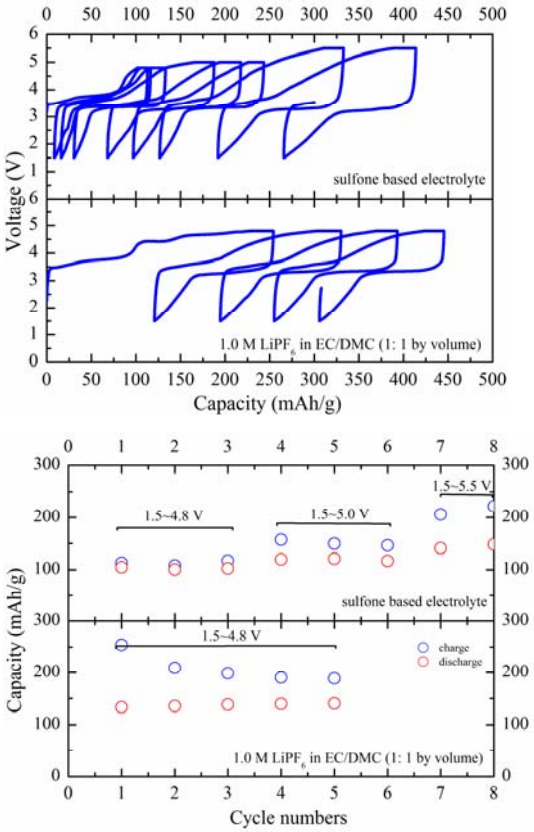

Figure V - 25: Comparison of the cycling performance for the C-coated $Li_2FeP_2O_7$ material nanosized by Primet using the EC/DMC electrolyte and the sulfone-based electrolyte from PNNL. The loading of the active material is around 4 mg for the EC/DMC and 5.3 mg for the sulfone with the electrode area of 1.2 cm^2. The cycling rate is C/20.

Conclusions and Future Directions

200 Ah/kg can only be obtained from the layered oxides at the C rate if charging is in excess of 4.4 volts, but more stable electrolytes will be needed. Collaborative work with NREL showed that $LiNi_{0.4}Mn_{0.4}Co_{0.2}O_2$ has an inherent high discharge rate. Increasing both the lithium and the manganese content did not lead to higher energy densities at the 2C rate. Moreover, these manganese-rich compounds show remarkably poor thermal stabilities, no better than NCA, which can be improved by the substitution of some of the cobalt by aluminum but are still much less stable than NMC. The pyrophosphate's electrochemical performance can be improved by nano-scissoring, but the stability limit of the electrolyte is being exceeded. Future work will complete the pyrophosphate project and get initial data on a range of vanadyl phosphates. The project is due to finish in December 2011.

FY 2011 Publications/Presentations

1. Presentation to the 2011 DOE Annual Peer Review Meeting, Washington, DC.

2. Hui Zhou, Shailesh Upreti, Natasha A. Chernova, Geoffroy Hautier, Gerbrand Ceder, and M. Stanley Whittingham "Iron and Manganese Pyrophosphates as Cathodes for Lithium Ion Batteries", Chemistry of Materials, 2011, 23: 293-300.
3. Chunmei Ban, Zheng Li, Zhuangchun Wu, Melanie J. Kirkham, Le Chen, Yoon Seok Jung, E. Andrew Payzant, Yanfa Yan, M. Stanley Whittingham, and Anne C. Dillon "Extremely Durable High-Rate Capability of a $LiNi_{0.4}Mn_{0.4}Co_{0.2}O_2$ Cathode Enabled by Single–Wall Carbon Nanotubes", Advanced Energy Materials, 2011, 1: 58-62.
4. Zheng Li, Natasha A. Chernova, Megan Roppolo, Shailesh Upreti, Cole Petersburg, Faisal M. Alamgir, and M. Stanley Whittingham, "Comparative study of the capacity and rate capability of $LiNi_yMn_yCo_{1-2y}O_2$ (y=0.5, 0.45, 0.4, 0.33)", J. Electrochem. Soc., 2011, 158: A516-A522.
5. Shailesh Upreti, Olga V. Yakubovich, Natasha A. Chernova and M. Stanley Whittingham, "A novel lithium copper iron phosphate with idealized formula$Li_5Cu_2^{2+}Fe^{3+}(PO_4)_4$: crystal structure and distribution of defects", Acta Cryst., 2011, E67: i29.
6. Hui Zhou, Shailesh Upreti, Natasha A. Chernova and M. Stanley Whittingham, "Lithium cobalt(II) pyrophosphate, $Li_{1.86}CoP_2O_7$, from synchrotron X-ray powder data", Acta Cryst. 2011, E67: i58–i59.
7. Many invited presentations, incl.:
   - Electrochemical Society, Materials Research Society, Pacific Power Sources Conf., IBA
   - U. C. San Diego, Stony Brook U., Wake Forest U., Michigan State U.
   - ORNL, Haldor Topsoe-Copenhagen
   - Local outreach

V.B.6 Cell Analysis-Interfacial Processes: SEI Formation and Stability on Cycling (HQ)

Karim Zaghib
Hydro-Quebec IREQ
1800 Lionel Boulet
Varennes, QC, Canada J3X 1S1

Phone: (450) 652 8019; Fax: (450) 652 8424
E-mail: Zaghib.Karim@ireq.ca
mailto:cashtiani@ENERDEL.com

Subcontractor:
Lawrence Berkeley National Laboratory, Berkeley, CA

Start Date: March 2010
Projected End Date: September 2011

Objectives

- Synthesis and evaluation of high-voltage cathode (spinel Mn-Ni) with improved electrochemical stability.
- Reduce the oxidation of the cathode composition, electrolyte, and separator. Find the appropriate alternative anode composition that meets the requirement for low cost and high energy.
- Continue development of *ex situ* and *in situ* SEM to increase our understanding of the failure mode of the cathode and anode materials.

Technical Barriers

Low energy density and poor cycle/calendar life

Technical Targets

- Identify a suitable technique to stabilize the interface reaction of the high-voltage oxide (Mn-Ni based, e.g., $LiMn_{1.5}Ni_{0.5}O_4$) cathode by surface coating with a more stable material such as an olivine. The emphasis is to improve electrochemical performance at high voltage
- Investigate the effect of the type of binder, electrolyte composition, and separator on performance at high voltage
- Develop high-capacity anodes based on Si composition.

Accomplishments

- Demonstration of the benefit of surface coating of high-voltage $LiMn_{1.5}Ni_{0.5}O_4$ cathode with $LiFePO_4$ olivine material
- Optimize a silicon-based composition as high-capacity anode material.
- Develop *ex situ* and *in situ* SEM tools for understanding the SEI layer and the failure mode in Si-based anode.

✧ ✧ ✧ ✧ ✧

Introduction

BATT is searching for the next-generation systems for high energy. In 2011, BATT program management recommended working with; (i) spinel high-voltage cathode based on Mn-Ni, (ii) Si-based alloy anode and (iii) studies on SEI layers on alloy anode and cathode.

Following the strategy to develop high-energy batteries, high-voltage cathodes based on Mn-Ni spinel will be studied. In the first part of the project, HQ plans to protect the surface of the cathode by a thin layer of olivine $LiFePO_4$. By this process, we expect to reduce the oxidation of the electrolyte and enhance the safety of the high-voltage cathode. Dry or wet processes will be explored to modify the surface of the cathode.

The HQ strategy related to the anode material is based on mixing particles of carbon-coated SiO_x with graphite powder to reduce the volume expansion and increase the first-cycle coulombic efficiency. To improve the capacity of the anode; we evaluated nano-Si particles mixed with graphite as one configuration and ternary compounds nano-Si-SiOx-graphite as a second configuration. Varying Si-nano:graphite:SiOx compositions will be investigated to determine the minimum content of graphite required in the anode. Due to the major effect of the binder on the performance of the anode, various types of binder were investigated

To further improve our comprehension on the SEI layer with the Si-based anodes and Mn-Ni cathodes, two analysis methods are adopted; *ex situ* SEM on cycled electrodes with liquid electrolyte and *in situ* SEM during anode cycling where the dry polymer was used as binder in the anode to avoid electrolyte evaporation.

Approach

Our approach is to develop an appropriate method to stabilize the interface reaction of the high-voltage oxide (Mn-Ni based like $LiMn_{1.5}Ni_{0.5}O_4$) by surface coating with a more stable material like olivine. The emphasis is to improve electrochemical performance at high voltage. The binder type, electrolyte composition and separator will be investigated. The high-capacity Si-based anode composition will be optimized by varying the graphite and SiOx content.

Results

Stabilize interface of LMNO. A promising result was observed with the spinel cathode coated with C-$LiFePO_4$ by a dry process, i.e., good cycle life (between 3 and 4.9V) in standard electrolyte EC-DEC-1M $LiPF_6$, compared to bare material. A comparison of the first few formations cycles shows a coulombic efficiency (CE) of 91% with a reversible capacity of 108 mAh/g of the bare cathode, and 85% with a reversible capacity of 123 mAh/g for the coated cathode (Figure V - 26).

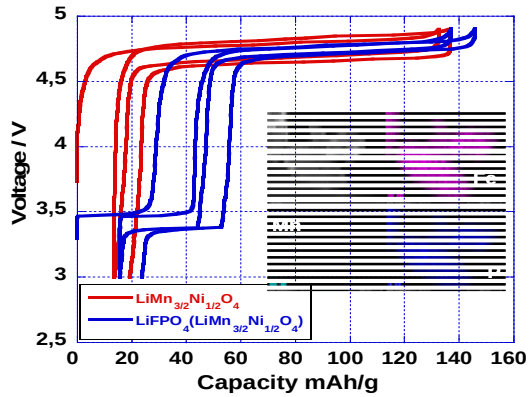

Figure V - 26: First few cycles of Li/EC-DEC 1M $LiPF_6$ / $LiFePO_4$(LMNO). Inset: elemental mapping of LFP-coated spinel LMNO.

In Figure V - 27, the Ragone plots show the discharge capacity as a function of rate. At low rate, a comparable capacity was obtained, but when the rate is higher than 10C, the C-LFP coated cathode differs from the bare one. At 15C, 60 mAh/g and 40 mAh/g were delivered by the cells, respectively, with and without the coated powder material. At 20C, no capacity was obtained with the spinel oxide cathode, however even at 40C rate, a low capacity of 20 mAh/g was still obtained with the coated cathode. The improved rate capability is due to the presence of facile Li-ions in LFP, which could serve as a buffer of high gradient ions when the rate is high.

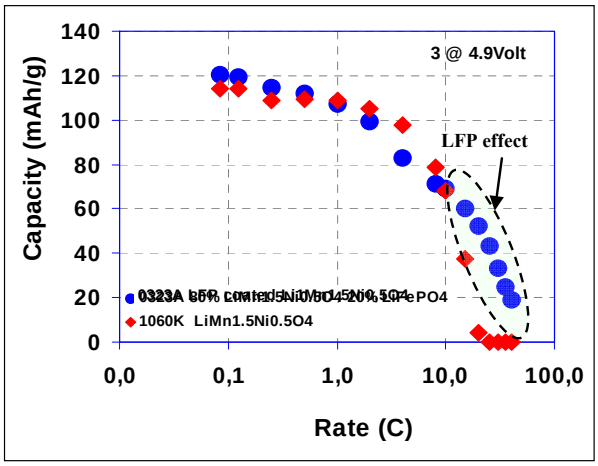

Figure V - 27: Rate capability of LMNO compared to $LiFePO_4$(LMNO) in EC-DEC-$LiPF_6$.

Si-anode. The SiO anode material was evaluated using a binder of poly(acrylonitrile butadiene). The first cycle showed a reversible capacity of 1000 mAh/g and coulombic efficiency of 80%, and 98% in the second cycle. The cycle life was determined at a cycling rate of C/6 between 2.5 and 0.010 V. The capacity dropped from 800 mAh/g to less than 400 mAh/g after the first 60 cycles. We found that 1-hour floating reduces the capacity fade, and it remains stable at 800 mAh/g during cycling (Figure V - 28).

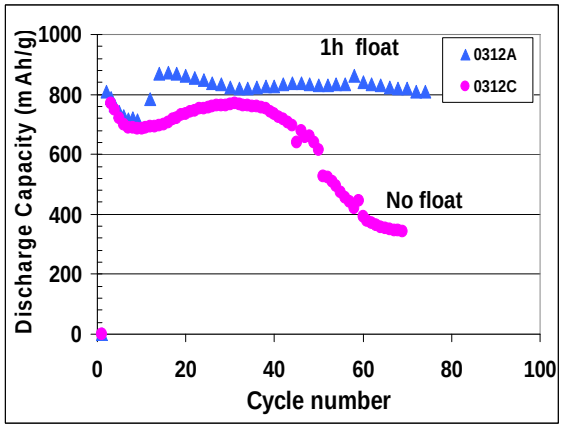

Figure V - 28: Cycling of Li/EC-DEC-1M $LiPF_6$/SiOx:Gr (1:1) cell at C/6.

Different anode compositions of C-SiOx/Si/graphite were evaluated to increase the CE and the reversible capacity. When the anode composition is 50%-50% (C-SiOx-graphite), the 3rd cycle CE was 81.6% with 996 mAh/g reversible capacity. When 25% Si-nano is introduced, replacing the SiOx (25/50/25), the discharge capacity is 2000 mAh/g, which drops to 50% in the second charge with low CE of 57%. On other hand, the composition without Si, shows the highest CE (98%). A small effect on the reversible capacity was noticed when the graphite content is reduced; 976 mAh/g and 1005

mAh/g with the compositions of SiOx:Gr (60:40) and (50:50), respectively.

***Ex Situ /In Situ* SEM.** For the *ex situ* analysis, a number of Li/SiOx-Graphite (1:1) cells with EC-DEC-1M $LiPF_6$ were discharged to different states: 0.5V, 0.1V, 0.05V, 0.005V and charged to 2.5V. The anodes from these cells were analyzed by SEM and compared to the baseline electrode. The cross section of these electrodes is shown in Figure V - 29; the baseline electrode shows good porosity (Figure V - 29a) to absorb the volume expansion of the anode during cycling. However this porosity is completely changed after the cell is fully discharged (5mV); the volume expansion caused densification of the electrode (Figure V - 29c), and bigger particles start to show cracks. The elemental chemical analysis showed a significant increase in the O content (most probably from Li_2O formation), particularly in the open porosity/binder region (Figure V - 29b). When the cell is charged to 2.5V, a decrease in the O content compared to a fully discharged cell was observed, but still higher than the baseline electrode. This indicates the presence of irreversible transformation. Also, the electrode reverts back to the porous state after densification when the electrode is discharged to 5mV.

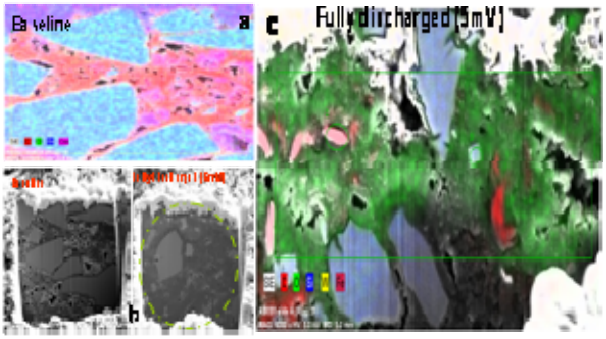

Figure V - 29: Reference electrode of SiO:Gr and fully discharged (5mV) in EC-DEC-1M $LiPF_6$

Conclusions and Future Directions

HQ succeeded to coat the surface of LMNO with C-LFP by using a dry process. The cycle life and high-rate performance were impoved compared to the bare material. Efforts will continue on improving the performance of stabilazed LMNO cathode material.

The high-capacity fade of the Si-based anode material is a major challenge, and volume expansion has limited progress. Different binders and anode compositions were evaluated, but performance still needs further improvement. The *in situ* and *ex situ* experiments have provided better understanding of the cycling mechanism of this anode and the failure mode associated with its capacity fade. These techniques have revealed that the bigger anode particles (ca. 13 µm) start to crack at around 0.1V. During the charging process, all of the cracks remained – however, some fissures in the smaller particles (< 2µ) did not crack.

The volume expansion caused densification of the electrode, and bigger particles start to show cracks. The elemental chemical analysis showed a significant increase in the O content (most probably from Li_2O formation), particularly in the open porosity/binder region. Further effort is needed to understand the limits of the particle size and porosity needed to make stable Si-based anode materials.

FY 2011 Publications/Presentations

1. 2011 DOE Annual Peer Review Meeting Presentation.
2. 219th ECS meeting, 1-6 May 2011, Montreal, Canada.
3. EV2011 conference, September 26-29, Toronto, Canada.

V.B.7 The Role of Surface Chemistry on the Cycling and Rate Capability of Lithium Positive Electrode Materials (MIT)

Yang Shao-Horn
Massachusetts Institute of Technology, 3-344
Mechanical Engineering and Materials Engineering
77 Massachusetts Avenue
Cambridge, MA 02139
Phone: (617) 253-2259; Fax: (617) 258-7018
E-mail: shaohorn@mit.edu

Subcontractor:
A.N. Mansour, NSWCCD, West Bethesda, MD

Start Date: June 1, 2010
Projected End Date: December 31, 2011

Objectives

- Develop a fundamental understanding of processes associated with the interfacial instability between active materials and electrolyte.
- Design low cost positive electrodes with stable electrode-electrolyte interface with improved cycling performance and rate capability over wider operating temperatures.
- Develop a fundamental understanding of the role of catalyst on performance parameters of Li-O_2 cells.

Technical Barriers

This project addresses the following technical barriers in relation to positive electrode materials for lithium-ion batteries:

(A) High Cost

(B) Poor cycle life

(C) Low specific energy

(D) Abuse tolerance

Technical Targets

- PHEV: Specific energy 56-96 Wh/kg; Specific power 316-750 W/kg; 15-year life (40°C); 3,000-5,000 cycles
- EV: Specific energy 200 Wh/kg; 1,000 cycles

Accomplishments

- Cycled bare $LiCoO_2$ and "$AlPO_4$"-coated $LiCoO_2$ electrodes in lithium cells with 1 M of $LiPF_6$ and 1M $LiClO_4$ in EC:DMC and characterized the surface chemistry by XPS using conventional Al X-rays (1487 eV) and monochromatic synchrotron X-rays (2555 eV) to increase the depth of the analyzed region.
- Characterized the discharge products of cathodes and the role of catalysts in Li-O_2 cells by conventional Al X-rays and monochromatic synchrotron X-rays.
- Evaluated the electrochemical activities of Li-rich $(Li_2O)_x.(MO_2)_y$ (where M = Mn, Co, Ni, etc.) system and improved the electrochemical activity by the application of non-precious Co_3O_4 nanoparticles.
- Characterized the atomic structure of layered-layered $0.5Li_2MnO_3+0.5LiNi_{0.44}Co_{0.25}Mn_{0.31}O_2$ composite materials by TEM (collaboration with M.M. Thackeray).

✧ ✧ ✧ ✧ ✧

Introduction

Achieving a fundamental understanding of the role of coatings and synthesis conditions on the surface chemistry and structural integrity of positive electrode materials is necessary to design stable surfaces and structures for Li-ion batteries. The design of chemically and structurally-stable surfaces of Li storage materials is key to the development of low cost, high-energy, high-power, long-life, and thermally-stable Li rechargeable batteries.

Approach

- Probe the surface chemistry of positive electrode materials before and after cycling using surface-sensitive electron microscopy, angle resolved X-ray photoelectron spectroscopy and electron-yield X-ray adsorption spectroscopy.
- Study the bulk structure of positive electrode materials before and after cycling using synchrotron X-ray diffraction and transmission X-ray absorption spectroscopy.
- Correlate surface chemistry and bulk structure information with electrochemical performance characteristics such as capacity retention and rate capability to determine the origin of surface instability.

Apply the fundamental understanding gained from the project to design stable surfaces to improve the cycle life and efficiency of Li rechargeable batteries.

Results

Interfacial stability of "$AlPO_4$"-Coated $LiCoO_2$. Our previous research has shown 1) that "$AlPO_4$" coating can induce fluoride formation in the cycled electrode with $LiPF_6$-containing electrolyte and reduce the growth of high-impedance organic layer during cycling. To determine the role of the salt contribution toward the formation of metal fluorides, bare and "$AlPO_4$"-coated $LiCoO_2$ electrodes were cycled 20 times in 1 M $LiPF_6$ or $LiClO_4$ in EC:DMC (1:1) at the C/5 rate between 2.0-4.6 V vs. Li (V_{Li}) with 4 hour hold at 4.6 V_{Li}. The coated electrodes cycled in $LiPF_6$ demonstrate higher capacity retention compared to electrodes cycled in $LiClO_4$, as shown in Figure V - 30. Hence, the coating does not provide an advantage when cycling was performed in $LiClO_4$ electrolyte, which supports the hypothesis that the promotion of metal fluoride on the coated electrode surface with $LiPF_6$ salt is responsible for the improved capacity retention observed previously. It is interesting to note that the bare electrode cycled in $LiClO_4$ has higher capacity retention than the bare electrode cycled in $LiPF_6$ or the coated electrode cycled in $LiClO_4$, as shown in Figure V - 31. The origin is currently not understood.

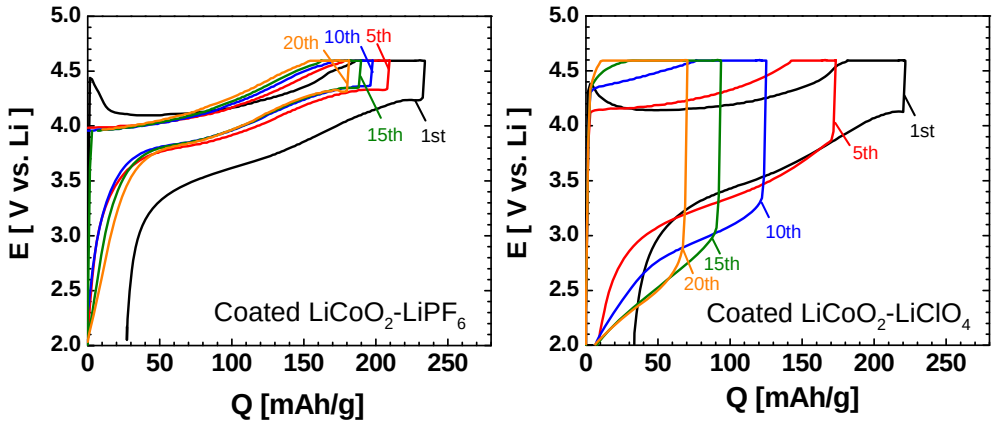

Figure V - 30: Voltage capacity profiles for "AlPO4" -coated LiCoO2 electrodes cycled in lithium cells with $LiPF_6$ and $LiClO_4$ in EC:DMC, C/5.

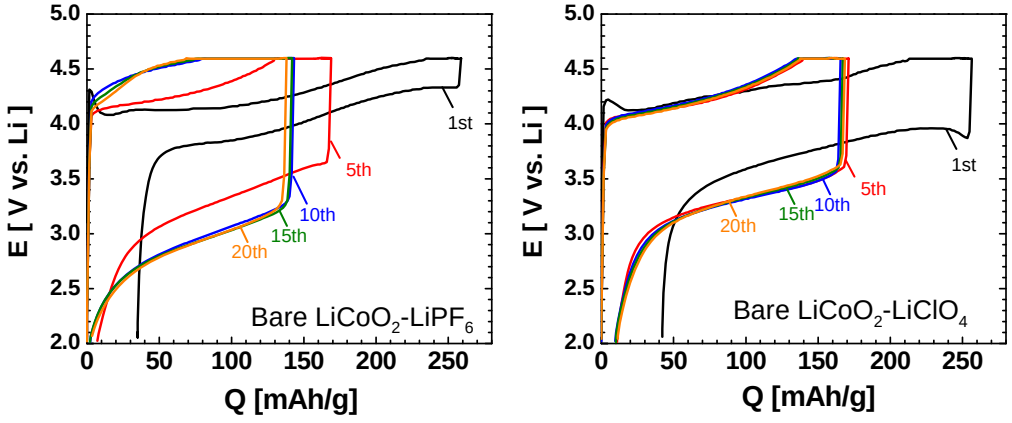

Figure V - 31: Voltage capacity profiles for bare LiCoO2 electrodes cycled in lithium cells with $LiPF_6$ and $LiClO_4$ in EC:DMC, C/5.

In an effort to increase the depth of information analyzed by XPS, we have taken advantage of synchrotron radiation on beamline X24A at NSLS and collected the spectra utilizing monochromatic X-rays with energy of 2555 eV compared to conventional Al K_α X-rays with energy of 1487 eV. In this way, the depth of the analyzed region increased from ~4 to ~11 nm for photoelectrons associated with the Co 2p region. Half of each electrode was analyzed by conventional X-rays while the other half was analyzed using synchrotron X-rays. The spectra collected with conventional X-rays are consistent with spectra reported earlier and will not be shown here. The

Co 2p synchrotron XPS data (Figure V - 32) for the bare $LiCoO_2$ electrode are consistent with conventional data showing mostly a contribution from $LiCoO_2$. However, the Co 2p synchrotron data for the coated $LiCoO_2$ electrode cycled in $LiPF_6$ display a contribution from Li_xCoO_2 (mostly absent in the conventional XPS data) in addition to the CoF_x contribution. Therefore, the depth of the region that contains only CoF_x for the coated electrode cycled in $LiPF_6$ is greater than 4 nm but less than 11 nm on average.

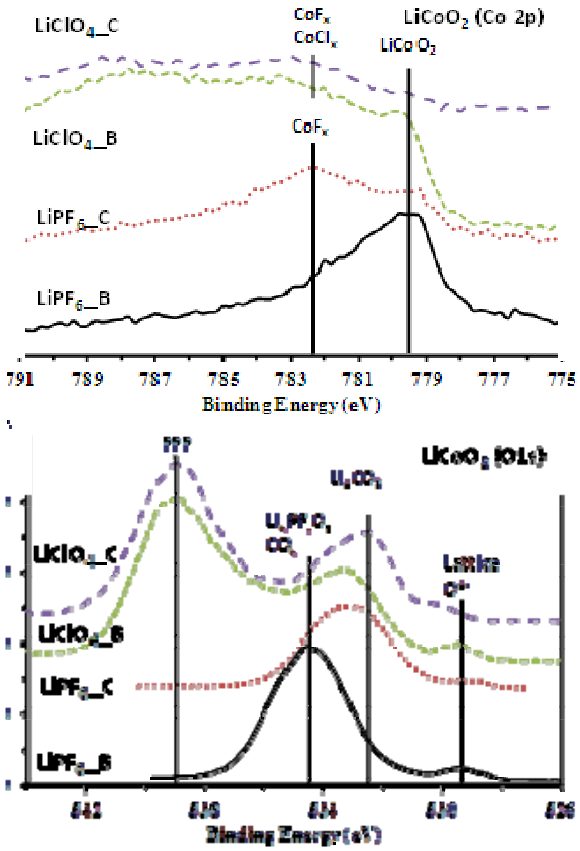

Figure V - 32: CO 2p and O1s spectra for coated and bare $LiCoO_2$ electrodes cycled in $LiPF_6$ or $LiClO_4$.

It is noted that the Co 2p spectra of electrodes cycled in $LiClO_4$ also shift to higher binding energy, which might be associated with $CoCl_x$ and CoF_x as the surface does not contain enough chlorine to account for all of the highly oxidized Co. The extent of the formation of $CoCl_x$ and CoF_x in $LiClO_4$ electrolyte is greater in the case of the coated electrode, which has the lowest degree of capacity retention among all electrodes, relative to the bare electrode. Such high binding energy Co peak was also observed in conventional XPS data and is unlikely due to differential charging. In this case, the formation of $CoCl_x$ and CoF_x for the electrodes cycled in $LiClO_4$ suggests an interaction with the PVDF binder since it is the only source of F. Such an interaction could lead to degradation of PVDF and the loss of electrical connectivity between particles and be responsible for the poor performance. The O 1s spectra shown in Figure V - 32 are qualitatively similar to conventional spectra with one very noticeable exception. The electrodes cycled in $LiClO_4$ but not those cycled in $LiPF_6$ have a large peak at high binding energy due to differential charging and, therefore, suggests that some of the species formed on the surface of the $LiClO_4$ cycled electrodes are more resistive in nature than those formed as a result of cycling in $LiPF_6$. High binding energy peaks due to sample charging were also observed in the F 1s as well as the Al 2p and Al 2s spectra and were all shifted by the same amount. Sample charging occurs more frequently when monochromatic X-rays rather than conventional X-rays are used.

The rate capability of Li-O_2 cells: combined XRD and (O, Li) K edge XANES studies. Rechargeable Li-O_2 batteries have the potential to provide 3-5 times the gravimetric energy density of conventional Li-ion batteries. Here, we demonstrate that the O_2 positive electrode in the Li-O_2 cells exhibit gravimetric energy densities (~2000 Wh/kg considering the total weight of positive electrode in the discharge state) 3-4 times that of $LiCoO_2$ (~600 Wh/kg) with comparable gravimetric power, as shown in a Ragone plot in Figure V - 33.

In order to understand the nature of the discharge products, pristine and discharged Vulcan carbon (VC) and 40 wt% Au on Vulcan carbon (Au/C) electrodes at 100 mA/g_{carbon} and 2000 mA/g_{carbon} were examined by XRD (Figure V - 34), where discharged electrodes were protected in Ar during XRD data collection. The results show that Li_2O_2 is the dominant crystalline ORR product. In addition, considerable broadening was noted in the peaks of lithium peroxide, which could be attributed to the broadening of small crystallite sizes of lithium peroxide, structural defects and/or nonstiochiometry in lithium peroxide such as lithium vacancies resembling $Li_{2-x}O_2$. Moreover, the peaks of lithium peroxide in the discharged electrodes of Au/C are broader than those in the discharged electrodes of VC. Different crystallite sizes and/or different amounts of structural defects and compositional nonstoichiometry may explain this difference.

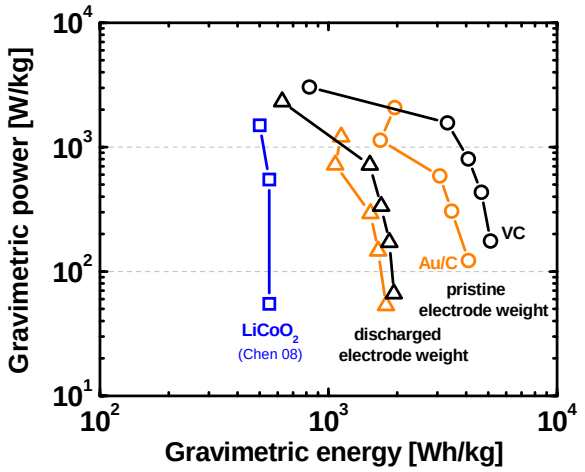

Figure V - 33: Ragone plot for Li-O2 cells with Vulcan carbon (VC) electrode by pristine electrode weight in black circles; by discharged electrode weight in black triangles), Au/C electrode by pristine electrode weight in orange circles; by discharged electrode weight in orange triangles) and conventional Li-LiCoO2 cell reported previously in blue squares (Tarascon et al., Chemsuschem, 2008).

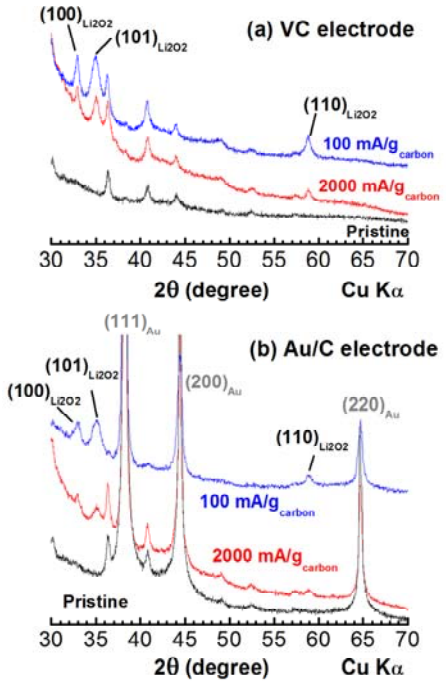

Figure V - 34: XRD patterns of pristine and discharged electrodes supported on a Celgard 480 separator (100 and 2000 mA/gcarbon) for VC (a) and Au/C (b). The reflections appeared in the pristine VC electrode came from Celgard C480 and those appeared in the pristine Au/C electrode came from Au nanoparticles and Celgard C480.

We further applied O and Li K edge XANES technique to probe the local enviornment of oxygen and lithium in the discharge products. O and Li K edge XANES of discharged VC and Au/C electrodes at 100 mA/g_{carbon} and the spectra of reference materials including Li_2O_2, Li_2O and $LiCoO_2$ are shown in Figure V - 35. Figure V - 35a shows that the bulk sensitive fluorescence yield (FY) O K edge XANES of discharged VC and Au/C electrodes are in reasonable agreement with both FY and surface sensitive total electron yield (TEY) spectra of Li_2O_2 reference powder, suggesting that the O local environment of the discharge product is Li_2O_2-like. The small difference in the FY O K edge XANES between discharge products and reference Li_2O_2 may suggest the presence of structural defects and/or nonstoichiometry such as lithium vacancies. Li K edge XANES of the discharge products shown in Figure V - 35b were found to have a major peak at 62.0 eV having a small pre-edge (at 58.0 eV) followed by a broad peak at ~ 70.0 eV. In contrast, the Li K edge XANES spectra of the discharge products do not match well with that of reference Li_2O_2 nor any other references (i.e., Li_2CO_3, LiOH, not shown). This result suggests that although XRD data show direct evidence of long-range ordering of lithium and oxygen in an Li_2O_2-like crystal structure, the Li^+ local environment in the lithium peroxide of discharged electrodes is different from that of Li_2O_2. Interestingly, Li K edge XANES spectra of discharge products resemble that of Li_xTiO_2 in both energy and shape while they resemble that of $LiCoO_2$ in shape and have a binding energy about 0.5 eV higher, where Li^+ ions are coordinated with 6 oxygen in Li_xTiO_2 and $LiCoO_2$. It is hypothesized that the spectrum difference between discharge products and reference Li_2O_2 can be attributed to the presence of structural defects in lithium peroxide such as oxygen and/or lithium vacancies, which has been suggested previously in a DFT study (Norskov et al., J. Chem. Phys. 2010). Further studies to understand the role of catalyst on affecting the growth mechanism and the nonstoichiometry and structural defects of the discharge product(s) are needed to verify the proposed hypothesis.

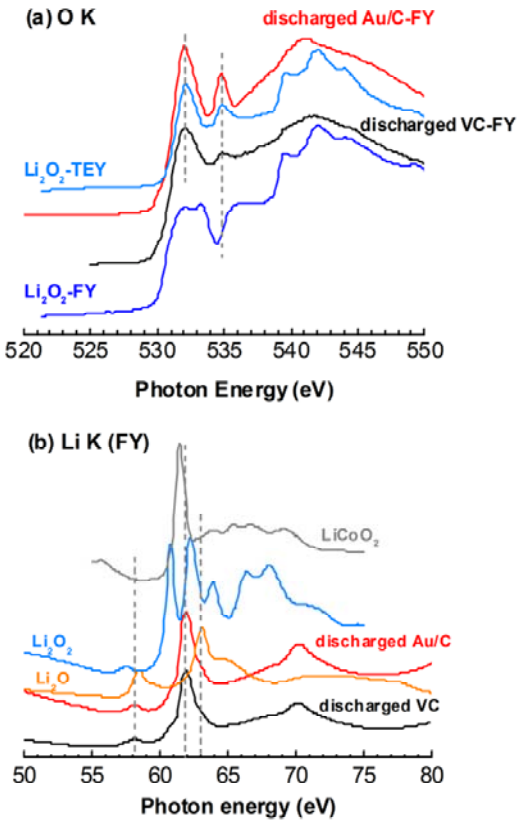

Figure V - 35: (a) O K edge and (b) Li K edge XANES FY spectra of reference compounds Li2O2, Li2O, LiCoO2 and discharged VC and Au/C electrodes at 100 mA/gcarbon.

XPS studies of discharge products in Li-O_2 cells. We have used conventional XPS to identify the role of the Pt and Au catalysts on the discharge products from O_2 reduction with lithium ions in Li-O_2 cells. The cell consisted of a Li foil, two pieces of Celgard separator (C480) and a Nafion-bonded cathode coated on a Celgard C480 using pure VC, Au/C (Au/C) and 40 wt% Pt/C (Pt/C) from Premetek. The cells were discharged at 100 mA/g_{carbon} to 2.0 V_{Li} in 0.1 M $LiClO_4$ in DME. The XPS measurements were conducted using conventional Al X-rays. Li_2O and Li_2O_2 powders were used as standards. All samples were transferred from an argon-filled glove box to the test chamber of the spectrometer without exposure to ambient conditions. The XPS multiplexes of the Li 1s, C 1s, O 1s and F 1s were recorded and those of O and Li are presented in Figure V - 36 and Figure V - 37, respectively. The C 1s regions (not shown) for the pristine electrodes display a high binding energy band (291-292 eV) due to fluorinated carbon from Nafion in addition to the hydrocarbon component at 284.6 eV. Those for the discharged electrodes display some carbon bonded to oxygen with binding energies at 286.2 and 289.4 eV in addition to the hydrocarbon component. The majority of the F 1s regions (not shown) have binding energy near 689 eV and can be attributed to fluorine chemistry in Nafion.

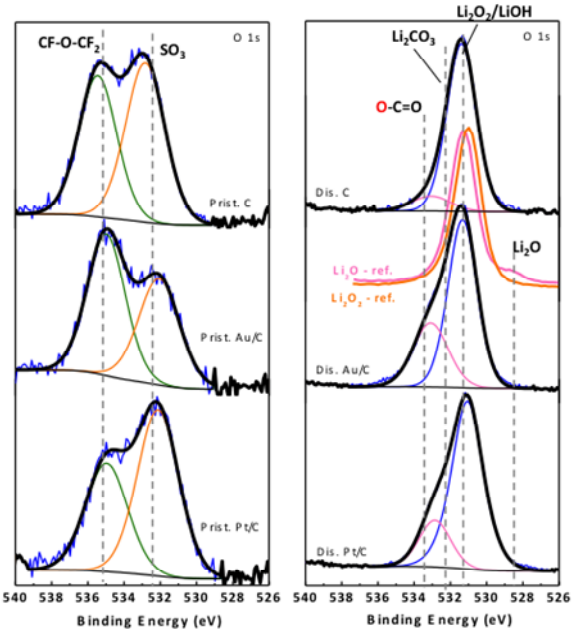

Figure V - 36: O 1s photoemission lines of pristine and discharged carbon, Pt/C and Au/C electrodes along with Li2O and Li2O2 standards.

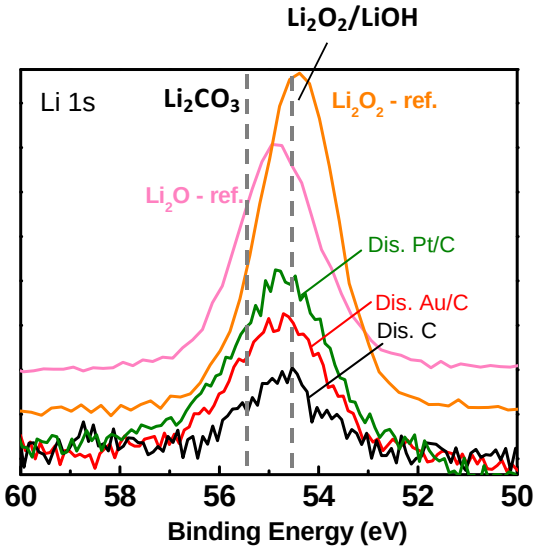

Figure V - 37: Li 1s photoemission lines of pristine and discharged carbon, Pt/C and Au/C electrodes along with Li2O and Li2O2 standards.

The O 1s binding energy of Li_2O_2 reference powder (Figure V - 36, right panel) was found to be 530.7 eV, which is comparable to that reported for LiOH (531.2 eV). This observation can be explained by 1) difficulties in differentiating Li_2O_2 and LiOH based on XPS data and 2) the surface of reference Li_2O_2 is covered by LiOH.

Considering XPS analysis of powder LiOH (not shown) indicated that the surface region of LiOH consisted mostly of lithium carbonate, the surface region of reference Li_2O_2 powder observed here more likely consists of Li_2O_2. The O 1s spectrum of Li_2O reference powder (Figure V - 36, right panel) consists of two components: 1) a major component at 530.9 eV, which is close to those reported for LiOH; 2) a minor component (~2%) at 528.4 eV, which is attributed to O^{2-} ion in Li_2O. Based on the major component at 530.9 eV, it is postulated that the surface of reference Li_2O is largely LiOH in nature as Li_2O is known to be extremely moisture-sensitive.

The O 1s regions for the pristine electrodes (Figure V - 36, left panel) display a double peak structure that can be associated with oxygen bond to CF_x groups (i.e., CF-O-CF_2) at 535 eV and SO_3 groups at 532 eV in Nafion. After discharge (Figure V - 36, right panel), the CF-O-CF_2 component at 535 eV from Nafion disappeared, which indicates the buildup of discharge products on the electrode surface. The majority of the oxygen signal for the discharged electrodes is attributed to the formation of Li_2O_2 at 531.0 eV for all discharge electrodes. However, the formation of LiOH cannot be ruled out. The formation of Li_2O can be ruled out by the lack of an oxygen component with binding energy in the range of 528-529 eV. In addition, a second component was identified at ~533.0 eV for the discharged electrodes, which can be associated with Li_2CO_3 and/or O-C=O (532.1 eV) and oxygen singly bonded with carbon atom in O-C=O (533.5 eV). The formation of Li_2O_2 (majority) and minority Li_2CO_3 for all discharge electrodes is also supported by the Li 1s spectra of Figure V - 37.

Electrochemical activity of high-energy Li-rich $(Li_2O)_x(MO_2)y$ systems. Positive electrodes of lithium peroxide and lithium oxide (Li_2O_x) were shown to exhibit higher energy densities compared to $LiCoO_2$ cells (Bruce et al., JACS 2006). However, the overpotential required to charge the Li-Li_2O_x cells is ~1.5 V owing to the slow reaction rate associated with decomposing Li_2O_x. In order to efficiently operate the high energy Li-Li_2O_x cells, we have applied nanoparticles of platinum (Pt) and gold (Au) to facilitate the charging reaction rates where Pt was shown to have the highest charging activity among Pt, Au and carbon (Shao-Horn et al. ESSL, 2010). However, the utilization of precious Pt metal is not ideal. Therefore, it is crucial to identify highly active catalyst with abundant elements such as Mn, Fe. Co, and Ni for high energy Li-Li_2O_2 and Li-Li_2O cells. Here we report the electrochemical activity for electro-oxidation of Li_2O_2 on pure carbon, Pt/C, and 40 wt% Co_3O_4/C (Co_3O_4/C) by anodic polarization of Li_2O_2-filled positive electrodes in 1 M LiTFSI DME at 5 mV/s. Co_3O_4 nanoparticles (NPs) were synthesized as follows: A solution of 10 mL dichlorobenzene and 10 mL of oleylamine was prepared at room temperature (20°C) in a four-neck flask. The mixture was heated to 160°C under Ar atmosphere with continuous stirring. 400mg of $Co_2(CO)_8$ in 4mL of dichlorobenzene was quickly injected into the above solution and left for 1 hr. The solution was cooled down to room temperature, and CoO NPs were precipitated by ethanol addition and collected by centrifugation. The product was re-dispersed in hexane and separated by ethanol addition and centrifugation. This procedure was repeated 2 times. The as-synthesized CoO NPs were transferred to a porcelain boat and was annealed in a tube furnace at 500°C for 3 hrs under O_2 which lead to Co_3O_4 NPs. The heat-treated Co_3O_4 NPs were loaded onto Vulcan Carbon (Co_3O_4: Carbon = 2:3 w/w) yielding 40 wt% Co_3O_4/C. The particle dispersion of Co_3O_4 NPs was uniform with average particle size ≈10 nm, as shown in Figure V - 38a.

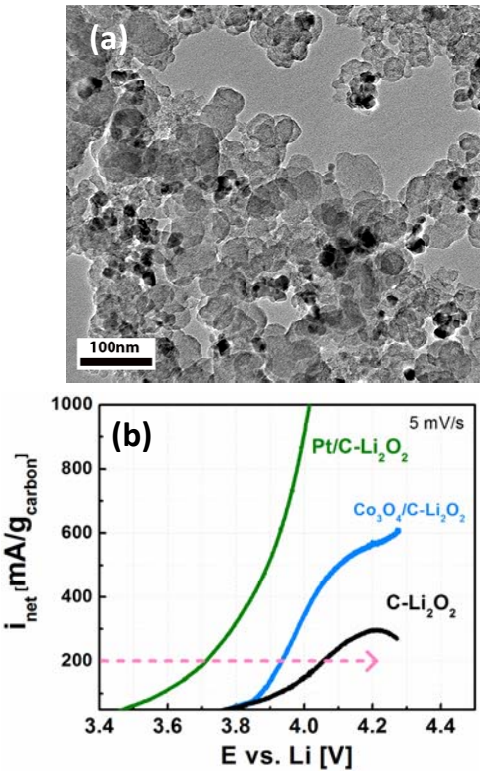

Figure V - 38: (a) TEM image of 40 wt% Co_3O_4/C (b) Li_2O_2 oxidation curves of pure Carbon, Pt/C, and Co_3O_4/C in 1 M LiTFSI DME at 5 mV/s

Figure V - 38b shows the net Li_2O_2 electro-oxidation currents (carbon-mass normalized), which were obtained by subtracting carbon-mass normalized currents of Li_2O_2-free electrodes from those filled with Li_2O_2. For C-Li_2O_2 cells, net currents of 200 mA/g_{carbon} were obtained at 4.05V_{Li}, which agrees well with the literature (Bruce et al., JACS 2006, JPS 2007, Shao-Horn et al. ESSL, 2010). In addition, net currents of 200 mA/g_{carbon} were obtained at 3.70 V_{Li} for Pt-Li_2O_2 cells, which is consistent with our previous study (Shao-Horn et al. ESSL, JACS, 2010). The application of Pt NPs decreases the charge overpotential by 350 mV compared to that of pure Carbon. Furthermore,

for Co_3O_4/C-Li_2O_2-cells, net currents of 200 mA/g_{carbon} was obtained at 3.93 V_{Li}. It is interesting to note that the application of non-precious Co_3O_4 NPs decreases the charging overpotential by 120 mV compared to that of pure Carbon. On-going work on developing the activity trend for electro-oxidation of Li_2O_2 and Li_2O on various metal oxides would provide further insights into the design principles of active catalyst for high energy Li-rich $(Li_2O)_x.(MO_2)_y$ (where M = Mn, Co, Ni, etc.) positive electrodes.

TEM studies of $0.5Li_2MnO_3 + 0.5LiNi_{0.44}Co_{0.25}Mn_{0.31}O_2$ (with M. Thackeray, ANL). Transmission electron microscopy (TEM) was used to study the atomic structure of the $0.5Li_2MnO_3$+$0.5LiNi_{0.44}Co_{0.25}Mn_{0.31}O_2$ layered-layered composite positive electrode materials. The results suggest that a nanoscale integration between $LiCoO_2$ structured material (space group R-3m) and Li_2MnO_3 (space group C2/m) was identified. Figure V - 39a shows the high resolution TEM (HRTEM) image of the $0.5Li_2MnO_3$+$0.5LiNi_{0.44}Co_{0.25}Mn_{0.31}O_2$ layered-layered materials. The electron diffraction patterns (Figure 10b) show that the material contained Li_2MnO_3-structured material. This was confirmed by fast Fourier transforms of the HRTEM taken from the same areas (Figure V - 39c). In order to study the spatial distribution and morphology of the Li_2MnO_3 structure material, an inverse Fourier transform that included only the g vectors unique to Li_2MnO_3 was performed, as shown in Figure V - 39d. It shows islands of Li_2MnO_3-ordered nanocrystals (Figure V - 39e and Figure V - 39f) separated by random phase noise. The random phase noise represents the $LiCoO_2$-structured portions of the crystal. This result is broadly similar to the results of J.G. Wen et al. (Solid State Ionics 2011), but we were able to achieve them for more general crystallographic orientations and with a non-aberration corrected TEM.

Conclusions and Future directions

We have used a number of analytical tools such as XPS, XRD, and TEM to examine the interfacial stability between electrode and electrolyte during cycling in lithium cells. The bare $LiCoO_2$ and "$AlPO_4$"-coated $LiCoO_2$ were used as a model compound to identify the role of surface coating of active material on interfacial stability during cycling. Our previous results have shown that the excellent cycling performance associated with $AlPO_4$ coating is related to the formation of CoF_x on the surface of "$AlPO_4$"-coated $LiCoO_2$ compared to that of bare $LiCoO_2$. Using synchrotron XPS, we are able to reveal that the thickness of this critical coating, CoF_x, is between 4-11 nm. This result will be used to guide the surface design to improve the efficiency and cycle life of positive electrode materials such as $LiNi_{0.5}Mn_{0.5}O_2$. We also applied XPS to study the surface chemistry of the discharged carbon, Au/C and Pt/C electrodes in Li-O_2 cells. The results indicate that discharge products of all electrodes can be assigned mostly to Li_2O_2 and Li_2CO_3 on the surface and to Li_2O_2 in bulk by XRD. No Li_2O were identified by XPS. The electrochemical activities of $(Li_2O)_x.(MO_2)_y$ (where M = Mn, Co, Ni, etc.) materials were evaluated by anodic polarization of Li_2O_2-filled positive electrodes in 1 M LiTFSI DME at 5 mV/s. The results show that the application of non-precious Co_3O_4 NPs decreases the charging overpotential by 120 mV compared to that of pure Carbon. TEM studies provided direct evidence for the integration of $LiCoO_2$-ordered material and Li_2MnO_3 -ordered material in the as-prepared $0.5Li_2MnO_3$+ $0.5LiNi_{0.44}Co_{0.25}Mn_{0.31}O_2$ layered-layered composite positive electrode material.

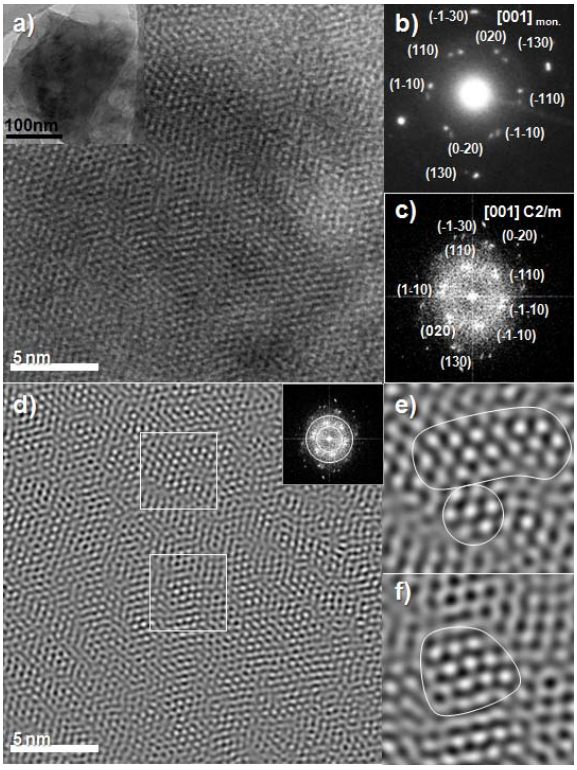

Figure V - 39: (a) HRTEM of $0.5Li_2MnO_3$+ $0.5LiNi_{0.44}Co_{0.25}Mn_{0.31}O_2$ layered-layered materials, (b) selected area diffraction pattern from Fig. (a), (c) FFT of Fig. (a), (d) inverse Fourier transformation of (c) that are unique to Li_2MnO_3, which are shown in the inset. (e) and (f) highlight parts of (d) showing well defined Li_2MnO_3 symmetry.

Future directions include 1) applying the insights gained in "$AlPO_4$"-coated $LiCoO_2$ model compounds to design stable surfaces coatings for $LiNi_{0.5}Mn_{0.5}O_2$ positive electrodes to improve the cycle life and efficiency of the system; 2) systematic evaluation of the electrochemical activities of $(Li_2O)_x.(MO_2)_y$ (where M = Mn, Co, Ni, etc.) materials for high energy storage applications. Conventional XPS, XRD, synchrotron XPS XRD and XAS will be used to investigate the surface chemistry of $(Li_2O)_x.(MO_2)_y$ positive electrodes upon cycling. In

addition, *in situ* differential electrochemical mass spectroscopy (DEMS) will be used to understand how the oxygen is realized during charge and the reversibility upon cycling. Electrochemical and gas evolution data will be correlated at different voltages as a function of cycling and of lithium overstoichiometric content.

Furthermore, we will continue to apply hard X-rays at the National Synchrotron Light Source of Brookhaven National Laboratory to increase the depth of the region analyzed by XPS and ARXS. This will provide a nondestructive way of increasing the depth of the analyzed region. Furthermore, we would like to explore collaborations with Robert Kostecki in the area of FT-IR and Raman studies.

FY2011 Publications/Presentations:

Publications:

1. Y.C. Lu, Z.C. Xu, H.A. Gasteiger, S. Chen, K. Hamad-Schifferli, Y. Shao-Horn, Platinum-Gold Nanoparticles: A Highly Active Bifunctional, Electrocatalyst for Rechargeable Lithium-Air Batteries. Journal of the American Chemical Society 132, (35), 12170-12171 (2010)
2. Y.C. Lu, H.A. Gasteiger, M.C. Parent, C. Vazrik, and Y. Shao-Horn, The Influence of Catalysts on Discharge and Charge Voltages of Rechargeable Li–Oxygen Batteries, Electrochem. Solid-State Lett., 13, A68-A72 (2010)
3. Y.C. Lu, H.A. Gasteiger, E. Crumlin, R. McGuire, and Y. Shao-Horn, Journal of The Electrochemical Society 157, (9), A1016-A1025 (2010).
4. N. Yabuuchi, Y.C. Lu, A. N. Mansour, T. Kawaguchi and Y. Shao-Horn, The Role of Surface Chemistry on the Electrochemical Reactivity of $LiNi_{0.5}Mn_{0.5}O_2$ in Lithium Cells, Electrochem. Solid-State let., 13(11), A158-A161 (2010).
5. N. Yabuuchi, Y.C. Lu, A.N. Mansour, S. Chen and Y. Shao-Horn, The Influence of Heat-Treatment Temperature on the Cation Distribution of $LiNi_{0.5}Mn_{0.5}O_2$ and its Rate Capability in Lithium Rechargeable Batteries, Journal of The Electrochemical Society, 158, (2) A192-A200 (2011).
6. Y.C. Lu, H.A. Gasteiger, and Y. Shao-Horn, Method Development to Evaluate the Oxygen Reduction Activity of High-Surface-Area Catalysts for Li-Air Batteries, Electrochem. Solid-State Lett., 14(5) A70–A74 (2011).
7. Y.C. Lu, D.G. Kwabi, K.P.C. Yao, J.R. Harding, J. Zhou, L. Zuin and Y. Shao-Horn, The Discharge Rate Capability of Rechargeable Li-O_2 Batteries, Energy Environ. Sci., 4(8) 2999-3007 (2011).
8. R.R. Mitchell, B. Gallant, C. Thompson and Y. Shao-Horn, All-Carbon-Nanofiber Electrodes for High-Energy Rechargeable Li-O_2 Batteries, Energy Environ. Sci., 4(8) 2952-2958 (2011).
9. Y.C. Lu, H.A. Gasteiger, and Y. Shao-Horn, Catalytic Activity Trends of Oxygen Reduction Reaction for Nonaqueous Li-Air Batteries, Journal of the American Chemical Society, ASAP (2011).

Presentations

1. Y.C. Lu, H.A. Gasteiger, and Y. Shao-Horn, "Catalysis studies and electrode design considerations for Lithium-air batteries" American Chemical Society, August 22, 2010, Boston, MA, USA.
2. Y.C. Lu, J.R. Harding, Y. Tsukada, H.A. Gasteiger, and Y. Shao-Horn, "Catalysis studies and electrode design considerations for Lithium-air batteries" American Chemical Society, August 24, 2010, Boston, MA, USA.
3. Y.C. Lu, H.A. Gasteiger, and Y. Shao-Horn, "Electrocatalytic Activity Studies of Select Metal Surfaces and Implications in Li-Air Batteries" 15th International Meeting on Lithium Batteries, July 2, 2010, Montréal, Canada.
4. Y.C. Lu, M. Parent, V. Chiloyan, and Y. Shao-Horn "The Influence of Catalysts on Discharge and Charge Voltages of Rechargeable Li-Oxygen Batteries" 15th International Meeting on Lithium Batteries, July 1, 2010, Montréal, Canada.
5. Y. Shao-Horn, Tajima Prize Award lecture "Oxygen Reduction Reaction Kinetics on Select Catalysts in Aqueous and Nonaqueous Solutions and Implications for Fuel Cells and Li-Air Batteries." 61st Annual Meeting of the International Society, September 29, 2010, Nice, France.
6. Y.C. Lu, H.A. Gasteiger, and Y. Shao-Horn, Oxygen Reduction on Supported Catalysts Using a Rotating Disk Electrode Configuration for Li-Air Batteries, 219th ECS meeting, Montréal, 2011.
7. B. Gallant, R.R. Mitchell, C. Thompson, and Y. Shao-Horn, High-Capacity Nanostructured-Carbon Electrodes for Lithium-Air Batteries, 219th ECS meeting, Montréal, 2011.
8. A. Mansour, Y. Lu, R. Quinlan, N. Yabuuchi, and Y. Shao-Horn, Interfacial Chemistry of LiNi0.5Mn0.5O2 Electrodes Cycled in LiPF6 Based Electrolytes, The 219th Meeting of The Electrochemical Society, Montreal, Canada, 2011.
9. R. Quinlan, Y. Lu, A. Mansour, and Y. Shao-Horn, XPS Study of the Discharge Products of a Li-O2 Cell, The 219th Meeting of The Electrochemical Society, Montreal, Canada, 3 May 2011.
10. Y.C. Lu, J.R. Harding, K.P.C. Yao, D.G. Kwabi, Y. Tsukada, Y. Lee, H.A. Gasteiger and Y. Shao-Horn Electrocatalysis of Oxygen Reduction and Oxygen Evolution Reactions for Li-air Batteries, E-MRS 2011 Spring Meeting, Nice, 2011.

V.B.8 Characterization of New Cathode Materials using Synchrotron-based X-ray Techniques and the Studies of Li-Air Batteries (BNL, U. Mass)

Kyung-Wan Nam and Xiao-Qing Yang (PIs)

Brookhaven National Laboratory
Upton, NY 11973-5000
Phone: (631) 344-3663; Fax: (631) 344-5815
E-mail: knam@bnl.gov
xyang@bnl.gov

Project Start Date: October, 2008
Project End Date: September, 2012

Objectives

- Determine the contributions of electrode materials changes, interfacial phenomena, and electrolyte decomposition to cell capacity and power decline.
- Develop and apply synchrotron based *in situ* X-ray techniques to study materials in an environment that is close to the real operating conditions
- Screen and study the potentially low cost and high energy density materials such as Li_2MnO_3-$LiMO_2$ and $LiFe_{1-y}Mn_yPO_4$.
- Synthesize and characterize high voltage cathode and high voltage electrolytes for high energy density lithium batteries for PHEVs.
- Carry out fundamental studies of high energy density Li-air batteries and gas diffusion electrode materials for Li-air batteries.
- Design, synthesize and characterize new electrolyte and electrolyte additives to increase O_2 solubility and/or with capability to dissolve Li_2O and Li_2O_2 oxides for Li-air batteries.
- Develop new diagnostic tools for battery studies.

Technical Barriers

- Li-ion and Li-metal batteries with long calendar and cycle life
- Li-ion and Li-metal batteries with superior abuse tolerance
- Reduced production cost of a PHEV batteries

Technical Targets

- PHEV: Specific energy 56-96 Wh/kg; Specific power 316-750 W/kg; 15-year life (40°C); 3,000-5,000 cycles
- EV: Specific energy 200 Wh/kg; 1,000 cycles

Accomplishments

- Developed new *in situ* XRD to study cathode materials for Li-ion batteries during chemical delithiation.
- Completed combined *in situ* hard XAS and *ex situ* soft XAS studies on high energy $Li_{1.2}Ni_{0.2}Mn_{0.6}O_2$ cathode materials during charge-discharge cycling. Important information about the roles of Mn cations was obtained.
- Completed *in situ* XAS and XRD studies on mesoporous $LiFe_{1-y}Mn_yPO_4$ ($0.0 \leq y \leq 0.8$) cathode materials during charge-discharge cycling. The effects of particle size and morphology on the phase transition behavior and performance of Li-ion cells have been studied.
- Modified the surface of carbon materials for gas diffusion electrode (GDE), which significantly improved the discharge capacity of the Li-air cell.
- Developed a novel new electrolyte which can increase the solubility of O_2 dramatically. The discharge rate of the Li-air cell using this new electrolyte is increased more than one order of magnitude compared to the conventional electrolytes.
- Developed a family of new boron based additives with good SEI formation capability and anion receptor functionality for lithium battery electrolyte.
- Designed and synthesized new solvents for lithium battery electrolytes.

✧ ✧ ✧ ✧ ✧

Introduction

Achieving the DOE goals for batteries for HEVs, PHEVs, and EVs require fundamental understanding of how current materials function – including how to improve rate, capacity and long-term cycling performance as well as the guidance on discovery of new materials and new mechanisms. This project attacks these issues by

developing new diagnostic tools to investigate battery materials both *in situ* and *ex situ*, and then applies these to explain the relationships between structure and function for new materials.

Approach

1. *In situ* XAS and XRD studies of new electrode materials such as $LiFe_{1-y}Mn_yPO_4$ and high capacity $Li_{1.2}Ni_{0.2}Mn_{0.6}O_2$ during electrochemical cycling to carry out the diagnostic studies to improve the energy density and cycle life of Li-ion batteries.
2. Soft XAS on the L-edges of Mn and Ni to distinguish the difference between the surface and the bulk structural changes caused by charge-discharge cycling for new cathode materials such as $Li_{1.2}Ni_{0.2}Mn_{0.6}O_2$.
3. *In situ* and *ex situ* transmission electron microscopy (TEM) coupled with selected area electron diffraction (SAED) to study the structural changes of electrode materials with high location specification and spatial resolution.
4. Electrochemical studies of GDE for Li-air batteries.
5. Improve the performance of the GDE by surface modification.
6. Design and synthesis of new electrolyte system with capability to dissolve Li_2O and Li_2O_2, and/or high solubility of O_2 for Li-air batteries.

Results

Continued the *in situ* x-ray absorption and time resolved XRD studies of G2 and G3 cathode materials during heating

A new synchrotron based *in situ* XRD technique shown in Figure V - 40 for studying the structural changes of cathode materials of Li-ion batteries during chemical lithium extraction in a NO_2BF_4/CH_3CN solution has been developed. This new technique was used to investigate the phase transitions of $LiFePO_4$

As shown from Figure V - 41, taking the advantage of the high resolution linear position sensitive silicon detector, the reflections from $LiFePO_4$ and $FePO_4$ can be clearly distinguished and identified. The changes of peak intensity as a function of oxidation reaction time (about 48 minutes total) or XRD scan number (total 50 scans) are plotted in Figure V - 41b. The intensity of pattern corresponds to the color scale (in the left). With increasing reaction time, the peak intensities for $FePO_4$ increase while those for $LiFePO_4$.decrease. The formation of second phase $FePO_4$ can be observed at scan 4, indicating a short time (about 4 minutes) was needed for the newly formed $FePO_4$ phase to grow enough crystal size to be detected by XRD. This is quite different than the *in situ* XRD results using electrochemical delithiation, where the appearance of $FePO_4$ takes a much longer time.

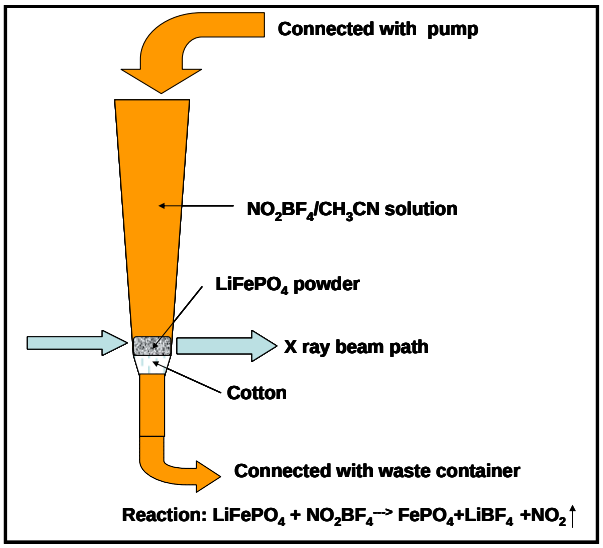

Figure V - 40: The schematic of experimental set-up for in situ XRD studies during chemical lithium extraction

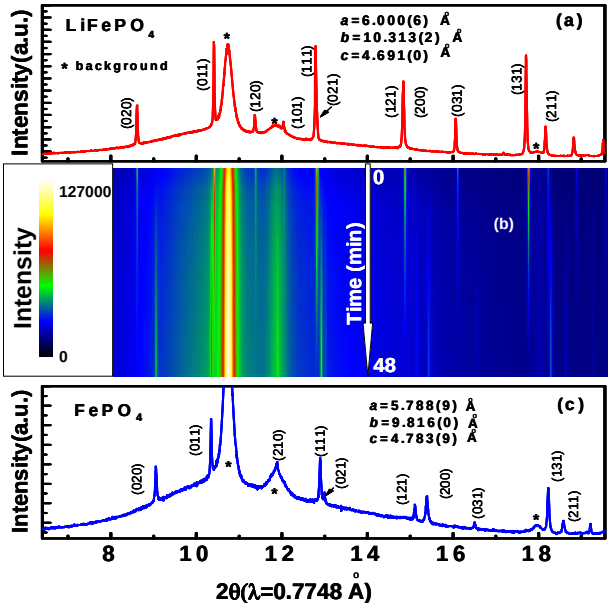

Figure V - 41: XRD patterns during in situ chemical lithium extraction of $LiFePO_4$: (a) XRD pattern for $LiFePO_4$ at the beginning of reaction; (b) contour plot of peak intensities as a function of reaction time. (c) XRD pattern for final $FePO_4$ at the end of reaction.

In collaboration with Prof. Hong Li and his research group at Institute of Physics, Chinese Academy of Sciences, a comparative study of the structural changes between $LiMn_{0.4}Fe_{0.6}PO_4$ cathode material samples with and without mesoporous structure during electrochemical cycling has been carried out using *in situ* and *ex situ* XRD (Figure V - 42). The phase transformation behaviours are quite different in these two samples. As shown in Figure V - 43, the structure of the mesoporou sample changed back to the original phase during first discharge with a high

degree of reversibility. As shown in Figure V - 44, in contrast to Figure V - 43, the phase transitions back to intermediate phase 2 and original phase 1 are not reversible at all. Large amounts of the sample remain in intermediate phase 2 at the end of discharge. These results provide valuable information about the poor reversible capacity and cycling performance of the sample without mesoporous structure from the structural change aspects.

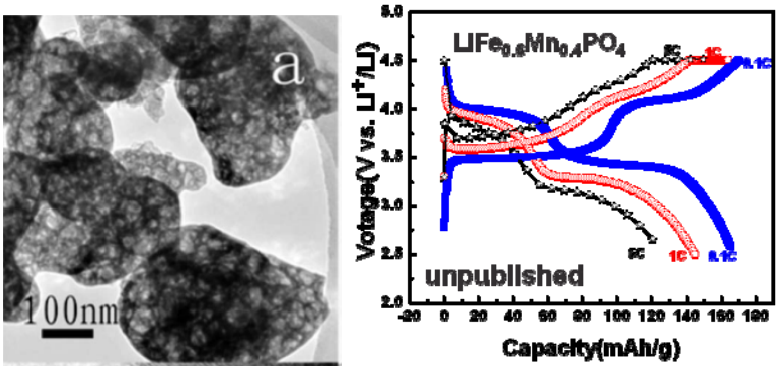

Figure V - 42: (a) The TEM image of morphology of mesoporous $LiMn_{0.4}Fe_{0.6}PO_4$ Meso-46 sample; (b) The charge-discharge capacity of the Meso-46 at different rates.

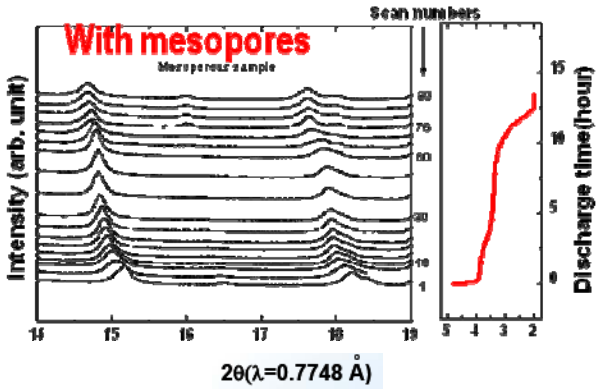

Figure V - 43: In situ XRD patterns of $LiMn_{0.4}Fe_{0.6}PO_4$ with mesoporous structure during first discharge

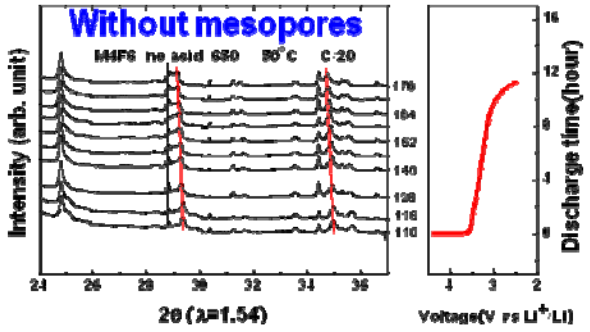

Figure V - 44: In situ XRD patterns of $LiMn_{0.4}Fe_{0.6}PO_4$ without mesoporous structure during first discharge

In collaboration with ANL, *in situ* and *ex situ* XAS studies were carried out to investigate the mechanism of the activation process in the $Li_{1.2}Ni_{0.2}Mn_{0.6}O_2$ cathode material at the National Synchrotron Light Source (NSLS) beamlines by the BNL team. The *ex situ* x-ray absorption near edge spectra (XANES) at the Ni K-edge for high energy $Li_{1.2}Ni_{0.2}Mn_{0.6}O_2$ cathode material before cycling and after 1st, 2nd, and 3rd charge and discharge are shown in Figure V - 45.

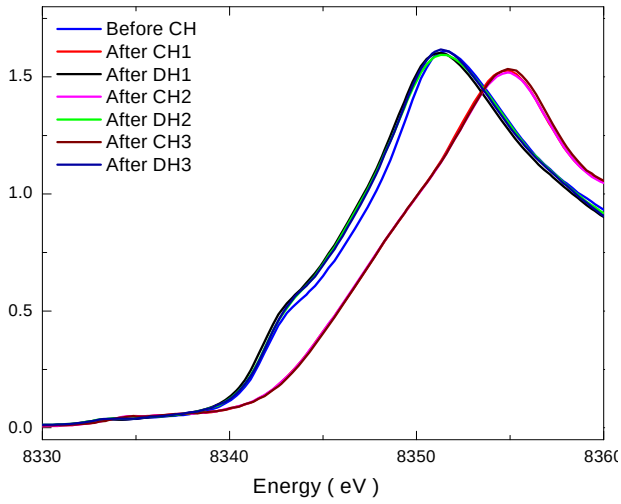

Figure V - 45: Ex situ XAS spectra at Ni K-edge of high energy Li1.2Ni0.2Mn0.6O2 cathode before cycling and after 1st, 2nd, and 3rd charge and discharge.

The Ni K-edge moves to higher energy position after the 1st charge indicating the Ni^{2+} to Ni^{4+} oxidation. It moves to a even lower energy position than that for the sample before cycling, indicating the reduction of Ni^{4+} to a state lower than the pristine sample before cycling. The *ex situ* XANES at the Mn K-edge for high energy $Li_{1.2}Ni_{0.2}Mn_{0.6}O_2$ cathode material before cycling and after 1st, 2nd, and 3rd charge and discharge are shown in Figure V - 46. In contrast to the results shown in Figure V - 45, no

rigid shift of Mn K-edge was observed, indication that the Mn ions remain at the oxidation state closer to the Mn^{4+} state.

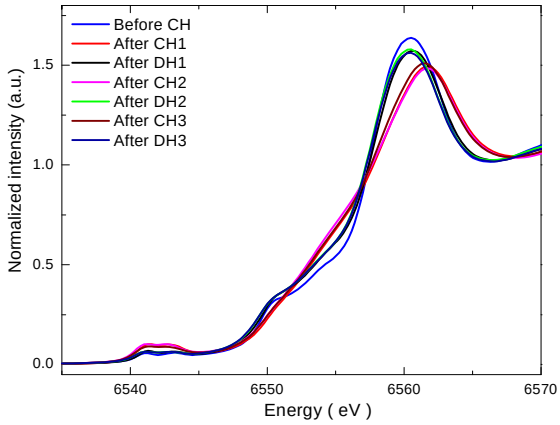

Figure V - 46: Ex situ XAS spectra at Mn K-edge of high energy $Li_{1.2}Ni_{0.2}Mn_{0.6}O_2$ cathode before cycling and after 1st, 2nd, and 3rd charge and discharge

In collaboration with Prof. Qu at the University of Massachusetts (UMASS) at Boston, a new electrolyte with higher ionic conductivity and oxygen solubility has been developed and studied. Up to now, the discharge rate of Li-air cell is too low (about 0.1 mA/cm^2). As shown in Figure V - 47, using our new electrolyte with increased O_2 solubility and mobility by the FTBA additives and new solvents, almost 100 times higher discharge rate has been achieved, making it closer to the Li-ion battery level.

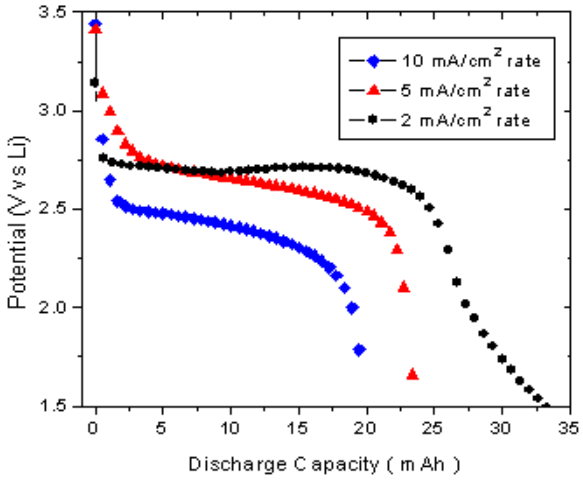

Figure V - 47: Constant-current (1 mAcm^{-2}) discharge of Li-O_2 cells using electrolyte with and without perfluorotributylamine (FTBA) additives

Conclusions and Future Directions

1. In collaboration with ANL, and GM R&D Center, Li_2MnO_3-$LiMO_2$ (M=Ni, Co, Mn) high energy density cathode materials have been studied using combined *in situ* hard XAS and *ex situ* soft XAS. The results of these studies provide useful information for improving the energy density and cycleability of high energy density Li-ion batteries.
2. In collaboration with Institute of Physics, CAS, the mesoporous $LiFe_{0.6}Mn_{0.4}PO_4$ cathode material are being studied by *in situ* XRD and XAS in comparison with the same composition without mesoporous structure. The results of these studies provide important information about the effects of meso-pores on the phase transition behavior and performance of these new cathode materials with low cost potential.
3. Developed new *in situ* XRD to study cathode materials for Li-ion batteries during chemical delithiation.
4. Developed a novel new electrolyte with dramatically increased O_2 solubility. The discharge rate of the Li-air cell using this electrolyte is almost 100 times greater than the conventional electrolytes.
5. Collaborations with US industrial partners such as Dow Chem. and GM, as well as with US and international research institutions (ANL and UMASS in US, IOP in China, KIST in Korea) have been established. The results of these collaborations have been published or presented at invited talks at international conferences.

Future Directions

1. Complete soft and *in situ* hard XAS study of high energy Li_2MnO_3-$LiMO_2$ (M=Ni, Co, Mn, Fe) cathode materials during activation charge and multiple cycling.
2. Complete comparative *in situ* XRD and XAS studies of $LiFe_{1-x}Mn_xPO_4$ (x=0 to 1) cathode materials with different particle size and morphology during chemical and electrochemical delithiations.
3. Develop and test the atomic layer deposition (ALD) surface coating on new cathode materials.
4. Use time resolved XRD to study the thermal stability of ALD surface coated Li_2MnO_3-$LiMO_2$ (M=Ni, Co, Mn, Fe) cathode materials during heating.
5. Further develop surface and interface sensitive techniques, such as soft x-ray absorption, TEM, SAED, and electron energy loss spectroscopy (EELS) for diagnostic studies on surface-bulk differences and phase transition kinetics of electrode materials.
6. In collaboration with UMASS Boston, continue the effort to develop GDEs with 2 catalysts for Li-air batteries. Start the preliminary studies of the rechargeable Li-air cells and *in situ* XRD and XAS on the GDE.
7. Develop new electrolyte systems to increase the solubility and mobility of O_2 in the electrolyte in order to increase the discharge rate of Li air cells.

FY 2011 Publications/Presentations

1. 2011 DOE Annual Peer Review Meeting Presentation, May 9th-13th 2011, Washington DC.
2. Chris Tran, Janak Kafle, Xiao-Qing Yang, Deyang Qu, "Increased discharge capacity of a Li-air activated carbon cathode produced by preventing carbon surface passivation", *Carbon*, Volume 49, Issue 4, (2011), Pages 1266-1271
3. Yufei Wang, Dong Zheng, Xiao-Qing Yang and Deyang Qu, "High rate oxygen reduction in non-aqueous electrolytes with the addition of perfluorinated additives", Energy & Environ. Science, V4 (2011), 3697-3702, DOI: 10.1039/C1EE01556G
4. Ho Chul Shin, Kyung Wan Nam, Won Young Chang, Byung Won Cho, Won-Sub Yoon, Xiao-Qing Yang, Kyung Yoon Chung, "Comparative studies on C-coated and uncoated $LiFeP_{O4}$ cycling at various rates and temperatures using synchrotron based *in situ* X-ray diffraction", *Electrochimica Acta*, Vol. 56, pp 1182-1189 (2011).
5. X. J. Wang, Y. N. Zhou, H. S. Lee, K. W. Nam, X. Q. Yang, O. Haas, "Electrochemical investigation of Al–Li/Li_xFePO_4 cells in oligo(ethylene glycol) dimethyl ether/$LiPF_6$", *J Appl Electrochem*, V41, (2011), 241-247, DOI 10.1007/s10800-010-0231-6.
6. Y. N. Zhou, X. J. Wang, H. S. Lee, K. W. Nam, X. Q. Yang, O. Haas, "Electrochemical investigation of Al–Li anode in oligo(ethylene glycol) dimethyl ether/$LiPF_6$", *J Appl Electrochem*, V41 (2011), 271-275, DOI 10.1007/s10800-010-0233-4.
7. Kyung-Yoon-Chung, Won-Sub Yoon, Kwang-Bum Kim, Byung-Won Cho, and Xiao-Qing Yang, "Formation of an SEI on a $LiMn_2O_4$ cathode during room temperature charge–discharge cycling studied by soft X-ray absorption spectroscopy at the Fluorine K-edge", *Journal of applied Electrochemistry*, V (2011) DOI 10.1007/s10800-011-0344-6.
8. Xiao-Jian Wang, Hai-Yan Chen, Xiqian Yu, Lijun Wu, Kyung-Wan Nam, Jianming Bai, Hong Li, Xuejie Huang, Xiao-Qing Yang, "New *in situ* synchrotron X-ray diffraction technique to study the chemical delithiation of $LiFePO_4$", *Chemical Communications*, V47 (2011), 7170-7172, DOI: 10.1039/C1CC10870K
9. Jie Xiao, Xiaojian Wang, Xiao-Qing Yang, Shidi Xun, Gao Liu, Phillip K. Koech, Jun Liu, and John P. Lemmon, "Electrochemically Induced High Capacity Displacement Reaction of PEO/MoS_2/Graphene Nanocomposites with Lithium", *Advanced Functional Materials*, V21 (2011), 2840-2846.
10. X.J. Wang, B. Zhang, K. W. Nam, Y. N. Zhou, J. Bai, H. Chen, H. Li, X. Huang, and X-Q. Yang "Phase transition behavior of mesoporous $LiFe_{1-x}Mn_xPO_4$", presented at the 218th Meeting of the Electrochemical Society, October 10-15, 2010, Las Vegas, Nevada, USA.
11. X.J. Wang, H. S. Lee, X. Q. Yang, K. W. Nam, Y. N. Zhou, X.Yu, L. F. Li, H. Li, and X. Huang, "The Studies of the Capability to Form Stable SEI on Graphite Anode of New Solvents and Additives for Lithium Battery Electrolytes", presented at the 218th Meeting of the Electrochemical Society, October 10-15, 2010, Las Vegas, Nevada, USA. **Invited**
12. X.J. Wang, X. Q. Yang, H. S. Lee, K. W. Nam, H. Li, and X. Huang, "The Synthesis and Characterization of New Additives and New Solvents for Lithium Battery Electrolytes", presented at the 2011 MRS Spring Meeting, April, 25-30, 2011, San Francisco, California, USA, **Invited**
13. X.J. Wang, C. Jaye, B. Zhang, Y.N. Zhou, K.W. Nam, H.Y. Chen, J.M. Bai, H. Li, X.J. Huang, D. Fischer, E.Y. Hu, and X.Q. Yang, "Investigation of Phase Transition Delay in $LiFePO_4$ /$FePO_4$ upon Charge Using Synchrotron Based X-ray Diffraction and Absoption Techniques", presented at the 2011 MRS Spring Meeting, April, 25-30, 2011, San Francisco, California, USA.
14. E.Y. Hu, Y. Lee, K-W. Nam, X.Q. Yu, X.J. Wang, and X.Q. Yang, "*In situ* X-ray absorption and diffraction studies of Ni and Fe substituted layer structured Li_2MnO_3 based cathode material during electrochemical cycling", presented at the 2011 MRS Spring Meeting, April, 25-30, 2011, San Francisco, California, USA.
15. Xiao-Qing Yang, "Lithium-ion Battery Diagnostic Studies for HEV,PHEV, and EV by Some US National Labs –ANL, BNL, LBNL, and ORNL", Presented at the "4th U.S. – China Electric Vehicle and Battery Technology Workshop", Argonne National Lab., Argonne, USA, August 4-5, 2011, **Invited.**
16. Xiao-Qing Yang, Xiao-Jian. Wang, Kyung-Wan Nam, Xiqian Yu, Hung-Sui Lee, Bin Zhang, Hong Li, Xuejie Huang, and Liquan Chen, "Studies of Surface and Bulk Structural Changes during Electrochemical Cycling for Olivine–structured $LiMn_xFe_{1-x}PO_4$ Cathode Materials Using Synchrotron Based XRD and XAS", presented at the "4th International Conference on Advanced Batteries for Automobile Application (ABAA4)", September 20-22, Beijing, China, , **Invited.**

V.B.9 Layered Cathode Materials (ANL)

Michael Thackeray

Argonne National Laboratory
9700 South Cass Avenue
Argonne, IL 60439
Phone : (630) 252-9184 ; Fax : (630) 252-4176
E-mail: thackeray@anl.gov

Collaborators:

ANL: S.-H. Kang, J. R. Croy, R. Benedek, V. G. Pol, S. V. Pol, C. S. Johnson, J. T. Vaughey, M. Balasubramanian (APS)
MIT: Y. Shao-Horn, C. Carlton
LBNL: V. Battaglia

Start Date: October 1, 2007
Projected End Date: September 30, 2011

Objectives

- Design high capacity, high-power and low cost cathodes for PHEVs and EVs.
- Improve the design, composition and performance of Mn-based cathodes.
- Explore new processing routes to prepare advanced electrodes with new architectural designs.
- Use atomic-scale modeling as a guide to identify, design and understand the structural features and electrochemical properties of cathode materials.

Technical Barriers

- Low energy density
- Poor low temperature operation
- Abuse tolerance limitations

Technical Targets (USABC - End of life)

- 142 Wh/kg, 317 W/kg (PHEV 40 mile requirement)
- Cycle life: 5000 cycles
- Calendar life: 15 years

Accomplishments

- Evaluated the electrochemical effects, such as voltage decay of 'layered-layered' electrode structures with a high Mn content.
- Identified a new, versatile processing technique for synthesizing composite electrode structures
- Evaluated sonochemical reactions for synthesizing electrode materials and coatings.
- Modeled interfacial structures and dissolution phenomena of $LiMn_2O_4$ electrodes.

✧ ✧ ✧ ✧ ✧

Introduction

Structurally integrated 'composite' electrode materials, such as 'layered-layered' $xLi_2M'O_3\bullet(1\text{-}x)LiMO_2$ and 'layered-spinel' $xLi_2M'O_3\bullet(1\text{-}x)LiM_2O_4$ systems in which M′ is predominantly Mn and M is predominantly Mn, Ni and Co, yield very high capacities approaching the theoretically-expected values (240-250 mAh/g) when discharged at relatively low rates. The rate and cycle life limitations of these materials have been attributed to structural degradation at the electrode surface when charged to high potentials.

Our research in FY2011 therefore continued to focus predominantly on developing methods to improve surface coatings and the electrochemical properties of high capacity $xLi_2M'O_3\bullet(1\text{-}x)LiMO_2$ electrodes. The following milestones were set for FY2011:

1. Improve and evaluate the electrochemical properties and surface stability of composite electrode structures with a high Mn content.
2. Evaluate aggressive synthesis reactions for coating metal oxide cathode particles with carbon and for fabricating stabilized surfaces with metal oxide and/or phosphate layers.
3. Model coatings and interfacial phenomena at the surface of $LiMn_2O_4$ electrodes.
4. Establish collaborative interactions with EFRC – Center for Electrical Energy Storage - Tailored Interfaces (Argonne-Northwestern University-University of Illinois (Urbana-Champaign). In particular, conduct X-ray absorption studies on BATT materials at Argonne's Advanced Photon Source (APS) to complement EFRC projects (see report V.F.1).

Approach

- Specifically, exploit the concept and optimize the performance of integrated ('composite') electrodes structures, particularly 'layered-layered' $xLi_2MnO_3\bullet(1\text{-}x)LiMO_2$ (M=Mn, Ni, Co) and novel 'layered-rocksalt' $xLi_2MnO_3\bullet(1\text{-}x)MO$ systems

- Design effective surface structures to protect the underlying metal oxide particles from the electrolyte and to improve their rate capability when charged (delithiated) at high potentials
- Explore alternative synthesis techniques to synthesize advanced electrode materials and surface structures and architectures: 1) autogenic reactions; 2) sonication methods
- Use first principles modeling to aid the design of bulk and surface cathode structures and to understand electrochemical phenomena.

Results

Stabilization of Composite Bulk Structures. Lithium- and manganese-rich mixed metal oxide electrodes with integrated structures, such as 'layered-layered' $xLi_2MnO_3•(1-x)LiMO_2$ (M=Mn, Ni, Co) can provide a very high rechargeable electrochemical capacity of 240-250 mAh/g if they are initially charged to 4.6 V. Over recent years, it has been established that if these composite electrode structures are continually cycled between 4.6 and 2.5 V, the cell voltage decays during discharge, compromising energy efficiency, cycling stability and cell performance. In FY2011, studies were initiated to address this issue.

The electrochemical charge/discharge profiles of $Li/Li_2MnO_3•LiNi_{0.44}Co_{0.25}Mn_{0.31}O_2$ cells cycled between 4.6 and 2.0 V at a ~C/15 rate at room temperature (RT) and at 55°C are shown in Figure V - 48a and Figure V - 48b, respectively; dQ/dV plots of the high temperature profiles (Figure V - 48b) are provided in Figure V - 48c. It is clear from these data that, at both room temperature and at 55°C, the discharge voltage is continuously suppressed on cycling, leading to a reduction in cell energy and energy efficiency; the voltage decay occurs more rapidly at 55°C. In particular, the dQ/dV data clearly indicate a gradual shift of the discharge potentials at approximately 3.7 and 3.3 V, characteristic of the original activated, layered electrode structure, to approximately 2.9 V after 50 cycles. Although the reasons for this behavior are not yet fully understood, the change in the electrochemical profiles strongly suggest that activation of the $Li_2MnO_3•LiNi_{0.44}Co_{0.25}Mn_{0.31}O_2$ electrode at 4.6 V and continued cycling to this high charging potential are likely accompanied by migration of manganese and nickel ions from the transition metal layers to the lithium layers, yielding a complex, composite structure in which spinel-like components become embedded within the layered component of the parent structure.

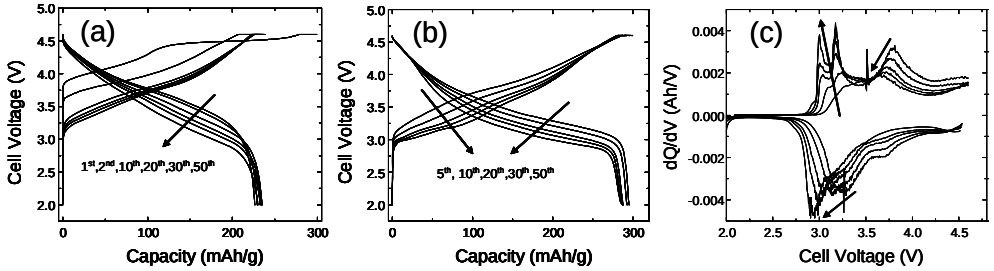

Figure V - 48: Plots of $Li/Li_2MnO_3•LiNi_{0.44}Co_{0.25}Mn_{0.31}O_2$ cells cycled between 4.6 and 2.0 V, ~C/15 rate, at (a) room temperature, and (b) 55°C; (c) dQ/dV plots of (b).

Recent work using Li_2MnO_3 as a template to prepare stabilized composite electrode structures has yielded very promising results; this aspect of the work will be continued as part of a new BATT cathode project in FY2012 (See BATT report in section V.B.14)

Surface Treatment Using Aggressive Reactions. Aggressive reactions, such as autogenic reactions, have been used to prepare electrode materials and surface-coated (specifically carbon-coated) electrodes, such as carbon-coated TiO_2, with considerable success. These studies were extended to explore other aggressive reactions, such as sonochemical reactions, as a route to fabricating surface layers to strengthen and protect composite $xLi_2MnO_3•(1-x)LiMO_2$ electrode structures and particles to electrochemical reactions.

For the initial studies, an Argonne standard electrode material with the composition $0.5Li_2MnO_3•0.5LiNi_{0.44}Co_{0.25}Mn_{0.31}O_2$ (referred to as NMC in Figure V - 48 and Figure V - 49) was used. The electrode particles were coated with a 10-30 nm layer of TiO_2 by pulsed sonication in an aqueous solution of $TiOSO_4$. The morphology of the parent electrode powder as determined by high-resolution scanning electron microscopy (HR-SEM) showed that 10-20 µm secondary particles consist of an assemblage of smaller primary nanoparticles. EDS spectra confirmed the expected composition (Mn, Ni, Co and O) of the compound, lithium being too low in atomic number to be detected by this method.

Figure V - 49 shows the results of a comparative rate study of $Li_2MnO_3•LiNi_{0.44}Co_{0.25}Mn_{0.31}O_2$ electrodes (both

uncoated and coated) carried out at (a) RT, and (b) 55°C. Cells were cycled between 4.6 and 2.0 V at various current densities of 15, 30, 75, 150, 300 and 750 mA/g. At RT, the average capacity of coated electrodes is higher than uncoated electrodes (Fig. 2a); furthermore, the first cycle coulombic efficiency at 15 mA/g improves from 71% for the uncoated electrode to 82% for the coated electrode. At 55°C, the performance of uncoated and coated electrodes were similar at the lower current rates (15-75 mA/g); at higher rates (150-750 mA/g), the coated electrodes clearly provide significantly higher capacities. Because of this promising result, this work will be extended in FY2012 to other sonicated metal oxide coatings, particularly those containing lithium that can act as protective solid electrolyte, specifically to obtain detailed information about surface structure and transport mechanisms that occur at the electrode/electrolyte interface.

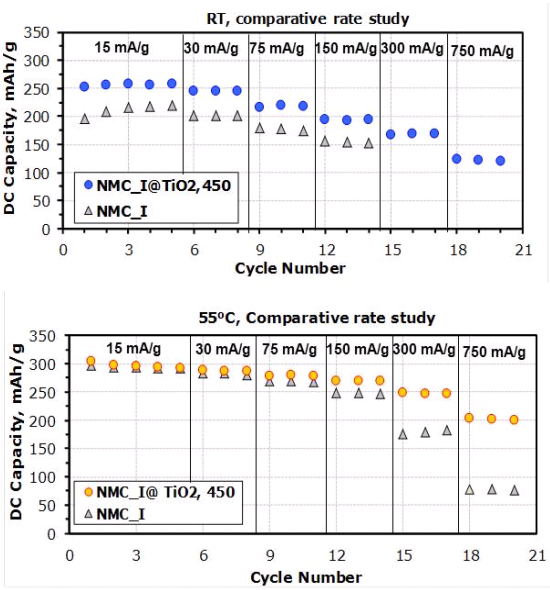

Figure V - 49: Top: Comparative rate study of uncoated and TiO_2-coated NMC electrodes vs. Li metal at 15, 30, 75, 150, 300 and 750 mA/g at RT; Bottom: Corresponding rate study at 55°C.

Theory: Surface Structure of $LiMn_2O_4$. Chemical and electrochemical reactions of lithium manganate spinel, $LiMn_2O_4$, are strongly influenced by surface and interface atomic structure. To help elucidate that structure, simulations were performed of (a) bare $LiMn_2O_4$ surfaces, both pristine and Ni-doped, (b) $LiMn_2O_4$ coated with AlF_3, and (c) $LiMn_2O_4$ slabs immersed in H_2O and acid (to simulate acid-promoted dissolution) at the GGA+U level of density functional theory. The most extensive results are for bare surfaces. In Figure V - 50a, coordination numbers of surface ions at surfaces of stoichiometric spinel slabs with different orientations and terminations are shown. (All of the surfaces contain vacancies introduced to cancel the long-range dipole moments that would be present in bulk-terminated surfaces, and thereby avoid electrostatic instabilities.) The relative stabilities of the different surface orientations agree, for the most part, with predictions for the prototype spinel $MgAl_2O_4$. Some of the surfaces show Mn with coordination numbers as small as 3 (compared to 6 in the bulk). The deficient surface ion coordination numbers result in lower Mn oxidation states, on average, than the bulk, as illustrated in Figure V - 50b. Most Mn ions near the surfaces exhibit trivalent oxidation states, whereas the mean oxidation state in the bulk is 3.5. Mn ions with coordination number of 3 are found to be divalent, a state that does not occur in the bulk, which would enhance vulnerability to dissolution. The preferred trivalent oxidation state of surface Mn influences the near surface chemistry of $LiMn_2O_4$. This was illustrated in simulations of Ni ion substitution for Mn near the surface of a spinel slab or wire. In the bulk, a Ni ion that substitutes for a trivalent Mn ion adopts a divalent oxidation state, and results in the oxidation of a neighboring Mn from a trivalent to a tetravalent state. Since near-surface Mn strongly prefers the trivalent state, however, suitable Mn-ion candidates for oxidation to 4+ are unavailable, which explains why energies of substitution near the surface are positive, and substitution is unfavorable. At a distance of about 1 nm from the surface, the structure is sufficiently bulk-like so that energies of substitution are close to the bulk limit. These results suggest that the near surface region of a Ni-doped spinel specimen would be depleted of Ni. As the Ni-depleted surface layer is eroded in a lithium-ion battery cathode (for example, by acid promoted dissolution), however, Ni-rich regions would be uncovered, which would be expected to give some protection against further dissolution, because the presence of Ni would diminish the number of Mn-ion candidates for oxidation to the tetravalent state, a necessary accompaniment to the dissolution of a surface trivalent Mn ion that would go into solution in a divalent state by disproportionation.

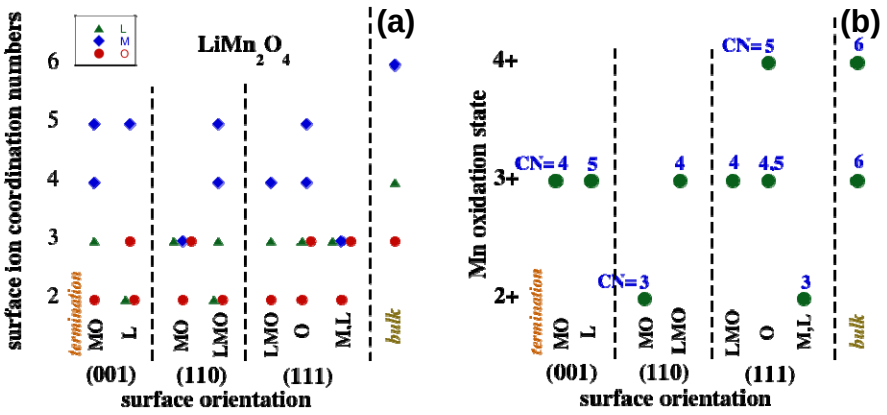

Figure V - 50: (a) Surface coordination numbers; (b) Mn oxidation states of $LiMn_2O_4$

Conclusions and Future Directions

Conclusions

- All milestones set for this project in FY2011 were met.
- The voltage-fade phenomenon in high-capacity $xLi_2MnO_3•(1-x)LiMO_2$ (M=Mn, Ni, Co) electrodes was evaluated.
- A new approach to synthesize composite electrode structures from a Li_2MnO_3 precursor was identified with promising results; this project will form the basis of a new cathode project in FY2012.
- Progress was made in stabilizing the surface, and improving the rate capability, of $xLi_2MnO_3•(1-x)LiMO_2$ electrodes using sonochemical reactions.
- Simulation of the surface structure of $LiMn_2O_4$ shows that near-surface manganese ions strongly prefer the trivalent state, which provided further insight into dissolution phenomena associated, for example, with Ni-substituted $LiMn_2O_4$ electrodes.

Future Work

(See New Cathode Project V.B.14.)

- Exploit novel processing methods using Li_2MnO_3 as a precursor to synthesize and optimize various composite electrode structures (composition and performance) with the goal of reaching/exceeding the energy and power goals required for 40-mile PHEVs and EVs. In particular, focus on 'layered-layered'-,'layered-layered-spinel'- and new 'layered-rocksalt' $xLi_2MnO_3•(1-x)MO$ systems.
- Focus on the stabilization of both surface and bulk structures. Use complementary experimental and theoretical approaches to improve the surface stability, rate capability and cycle life of high capacity Mn-rich oxide electrodes at high potentials.
- Further explore sonication to fabricate and evaluate stable surface architectures.
- Continue EFRC-related work and interact with DOE's energy storage centers.

FY 2011 Publications/Patents/Presentations

Publications

1. K. A. Walz, C. S. Johnson, J. Genthe, L. C. Stoiber, W. A. Zeltner, M. A. Anderson and M. M. Thackeray, Elevated Temperature Cycling Stability and Electrochemical Impedance of $LiMn_2O_4$ Cathodes with Nanoporous ZrO_2 and TiO_2 Coatings, J. Power Sources, **195**, 4943 (2010).
2. A. Rockett, Y. W. Chung, H. Blaichek, S. Butterfield, R. R. Chance, C. Ferekides, M. Robinson, S. W. Snyder and M. M. Thackeray, Transformative Research Issues and Opportunities in Alternative Energy Generation and Storage, Current Opinion in Solid State & Materials Science, **15**, 8-15 (2011).
3. R. Benedek and M. M. Thackeray. Simulation of the Surface Structure of Lithium Manganese Oxide Spinel, Phys. Rev. B, **83** (19): Art. No. 195439 (May 31 2011).
4. J. R. Croy, S.-H. Kang, M. Balasubramanian and M. M. Thackeray, A New Approach to Fabricating Li_2MnO_3-based Composite Cathode Structures for Lithium Batteries, Electrochem. Comm., **13**, 1063-1066 (2011).

Patents

1. M. M. Thackeray, S.-H. Kang, M. Balasubramaian and J. R. Croy, Electrode Structures and Surfaces for Li Batteries, US Patent Application, Serial No. 13/044038 (9 March 2011).

Presentations

1. K. G. Gallagher, D. Kim and S.-H. Kang, *Capacity and Power Fade of Graphite/xLi_2MnO_3•(1-x)$LiMO_2$ (M=Ni, Co, Mn) Li-ion Cells*, 218th Electrochem. Soc. Meeting, Las Vegas, 10-15 October, 2010.
2. L. A. Riley, S.-H. Kang, A. S. Cavanagh, M.M. Thackeray, S. M. George, S.-H. Lee, A. C. Dillon, *Li_2MnO_3-Stabilized $LiMO_2$ Cathode and ALD Coated MoO_3 Anode as a High Energy-Density Lithium-Ion Battery*, 218th Electrochemical Society (ECS) Meeting, Las-Vegas, 10-15 October (2010).
3. M. M. Thackeray, *Lithium Batteries: Challenges and Opportunities in an Evolving Lithium Economy,* Brown University, RI, 3 December (2010).
4. M. M. Thackeray, *Electrochemical Energy Storage for Transportation: Challenges and Opportunities in an Evolving Lithium Economy,* Fermilab Lecture Series, 4 February 2011.
5. M. M. Thackeray, *Electrochemical Energy Storage for Transportation: Materials Challenges and Opportunities in an Evolving Lithium Battery Economy,* The Future of Materials Science and Engineering in the 21st Century Workshop, Georgia Tech, Atlanta, GA, 24 February 2011.
6. M. M. Thackeray, *Electrochemical Energy Storage for Transportation: Materials Challenges and Opportunities*, Departmental Seminar, Northwestern University, 22 February (2011).
7. S.-H. Kang, K. G. Gallagher, D. Kim, W. Ryu, and M. M. Thackeray, *Enhanced Electrochemical Behavior of xLi_2MnO_3•(1-x)$LiMO_2$ (M=Mn, Ni, Co) Electrodes*, International Battery Association Meeting, Cape Town, South Africa, 12-15 April (2011).
8. M. M. Thackeray, *Design and Evaluation of Novel High Capacity Cathode Materials,* DOE Annual Merit Review, Washington DC, 9-13 May (2011).
9. J. R. Croy, S.-H. Kang, M. Balasubramanian and M. M. Thackeray, *Advances in Li_2MnO_3-based Electrodes for Lithium Batteries*, 5th International Conference on Polymer Batteries and Fuel Cells, (PBFC-5), Argonne National Laboratory, Illinois, 1-5 August (2011).
10. M. M. Thackeray, *Electrochemical Energy Storage for Transportation: Materials Challenges and Opportunities*, "Design - 2 - Devices: Advanced Materials for Energy Applications", Annual EFRC Energy Materials Symposium, Cornell University, Ithaca, NY, 12 August 2011.

V.B.10 Development of High Energy Cathode (PNNL)

Ji-Guang Zhang and Jun Liu
Pacific Northwest National Laboratory
902 Battelle Blvd., Mail Stop K3-59
Richland, WA 99352
Phone: (509) 372-6515; (509) 375-4443
E-mail: jiguang.zhang@pnl.gov; jun.liu@pnl.gov;

Start Date: October 1, 2010
Projected End Date: September 30, 2011

Objectives

- Develop high-energy cathode materials with improved safety.
- Develop low-cost synthesis routes for high-capacity and environmentally-benign cathode materials.

Technical Barriers

This project addresses the following technical barriers:

- High cost of cathode materials.
- Limited energy density and cyclability.
- Safety.

Technical Targets

- Investigate the electrochemical performances of $LiMnPO_4$ synthesized from non-stoichiometric Li/Mn ratio; evaluate thermal stability of electrochemically de-lithiated $LiMnPO_4$
- Develop a cost-effective method to prepare high-voltage spinel $LiNi_{0.5}Mn_{1.5}O_4$; identify appropriate electrolyte additives to improve Coulombic efficiency
- Explore the renewable organic cathode materials with $2e^-$ transfer per redox center.

Accomplishments

- Systematically studied the thermal stability of a de-lithiated $LiMnPO_4$ cathode
- Investigated the influence of lithium content in the starting material on the final structural and electrochemical performances of Li_xMnPO_4 ($0.5 \leq x \leq 1.2$)
- Developed a facile synthesis approach for high-voltage spinel. A Cr-substituted spinel, $LiNi_{0.45}Cr_{0.05}Mn_{1.5}O_4$, shows excellent cycle stability; the Coulombic efficiency and the first cycle loss were greatly improved after the addition of appropriate electrolyte additive.
- Synthesized poly(1,8-anthraquinonyl sulfide (P18AQS), a new organic cathode material, as a high-capacity cathode material.

✧ ✧ ✧ ✧ ✧

Introduction

- Li-ion batteries with high energy densities are required to reach DOE's goal regarding early commercialization of electrical vehicles, including hybrid electric vehicles and plug-in hybrid electric vehicles. To increase the energy of a cathode, the voltage and/or capacity of the material must be increased. During FY 2011, we further investigated the thermal stability of $LiMnPO_4$, and we were able to improve its synthesis approaches. By adding appropriate doping and electrolyte additives, we successfully developed a chromium doped high-voltage spinel, $LiNi_{0.45}Cr_{0.5}Mn_{1.5}O_4$. This material exhibited stable cycling and greatly improved efficiency. We also synthesized a novel renewable organic cathode, P18AQS, and we studied its electrochemical performance to advance our understanding on the renewable cathode materials.

✧ ✧ ✧ ✧ ✧

Approach

Investigate the final structural compositions and electrochemical performances of $LiMnPO_4$ synthesized with different lithium contents

- Characterize the phase transformation and oxygen evolution temperature of electrochemically delithiated $MnPO_4$ to evaluate thermal stability
- Synthesize high-performance $LiNi_{0.5}Mn_{1.5}O_4$ and its Cr-substituted phase, which will provide the basis for identifying electrolyte additives to improve the Coulombic efficiency for high-voltage cathodes.
- Synthesize and evaluate novel high-capacity organic cathodes based on the quinonyl group.

Results

Thermal stability of Electrochemically Delithiated $MnPO_4$. For thermal stability studies, the charged $LiMnPO_4$ paper electrodes and $MnPO_4 \cdot H_2O$ powder (as a control) were subjected to *in situ*, hot-stage XRD at every

30°C increment up to 534°C in a UHP-Ar atmosphere as shown in Fig. 1. We observed $MnPO_4$ reduction to $Mn_2P_2O_7$ with oxygen evolution at 490°C, which coincides with the phase changes in $MnPO_4 \cdot H_2O$. Between 180 and 490°C, the charged $MnPO_4$ undergoes amorphization (highlighted yellow area in Figure V - 51). TGA-MS results showed no oxygen released before reaching 490°C. However, initial CO_2 release between 200~400°C was observed for the charged $MnPO_4$ electrode consistent with the weight changes observed in the TGA plot indicating that the continuous weight loss up to 450°C resulted from decomposition of the SEI layer formed on the $LiMnPO_4$ electrode surface. CO_2 evolution is commonly observed during oxidation at the SEI layer and catalytic decomposition of carbonate-based organic electrolytes. The thermal stability and phase transformation of the de-lithiated $MnPO_4$ can be summarized by the following reaction:

$$\underset{Pnma}{MnPO_4} \xrightarrow{150\sim180^oC} \underset{Jahn\ Teller\ Distortion}{MnPO_4} \xrightarrow{490^oC} \frac{1}{2}\underset{C2/m}{Mn_2P_2O_7} + \frac{1}{2}O_2\uparrow$$

Our results demonstrate the intrinsic thermal stability of electrochemically lithiated or de-lithiated $LiMnPO_4$. However, the discharge rate of $LiMnPO_4$ needs to be improved for their practical application. Because heat evolution related to the $LiMnPO_4$ cathode is an extrinsic material property and not an intrinsic property, smart material design, such as carbon coating, can significantly reduce surface-electrolyte reactions better than $Li(NiCoX)O_2$ (X: Mn or Al) compounds in terms of both onset temperatures and specific heat evolution.

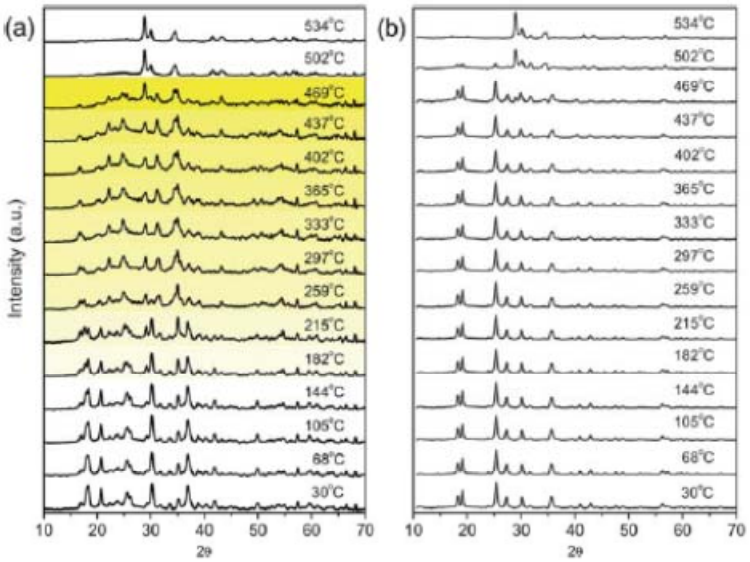

Figure V - 51: In situ, hot-stage XRD characterization of (a) the charged $MnPO_4$ electrode and (b) the $MnPO_4 \cdot H_2O$ powder under an UHP-Ar atmosphere (heating rate: 5°C /min).

$LiMnPO_4$ Synthesized from a Non-Stoichiometric Li:Mn Ratio. The influences of lithium contents in the starting materials on the final performance of Li_xMnPO_4 (x hereafter represents the starting Li content in the synthesis step, which does not necessarily mean that Li_xMnPO_4 is a single phase solid solution in this work) were investigated systematically. From the results of ICP mass spectroscopy, the Li:Mn ratio matched very well with the designed compositions, which confirms that the precipitation method is a feasible approach for tuning the lithium content in the final product. Rietveld refinement of the XRD data shown in Figure V - 52 revealed that $Mn_2P_2O_7$ is the main impurity when x <1.0 while Li_3PO_4 begins to form when x >1.0. Magnetic and XAS studies further confirmed that the main phase in Li_xMnPO_4 samples was $LiMnPO_4$, and the variation in Li content leads to the formation of additional Li-contained (Li_3PO_4) or Mn-contained ($Mn_2P_2O_7$) phases to accommodate the stoichiometry.

The as-prepared $Li_{0.8}MnPO_4$, which is a Li deficient phosphate, is quite different from chemically delithiated Li_xMnPO_4 because other byproducts, such as a Mn-deficient phase, may occur during the interactions between $LiMnPO_4$ and the oxidant (usually NO_2BF_4 dissolved in acetonitrile), thus influencing or hiding the physical and electrochemical properties of the material itself.

For $Li_{0.5}MnPO_4$ and $Li_{0.8}MnPO_4$, gradual increases in the reversible capacity with cycling were observed, Figure V - 53, which may be related to interactions between $Mn_2P_2O_7$ and $LiMnPO_4$. Among all the samples, $Li_{1.1}MnPO_4$ exhibits the most stable cycling probably because of the Li_3PO_4 coating on the surface of $LiMnPO_4$ nano-particles that functions as a solid electrolyte to facilitate ion transport. Therefore the electrochemical performance of

$LiMnPO_4$ can be tuned simply by adjusting the Li content in the synthesis step, which provides important clues on the activation and stabilization of phosphate-based cathode materials.

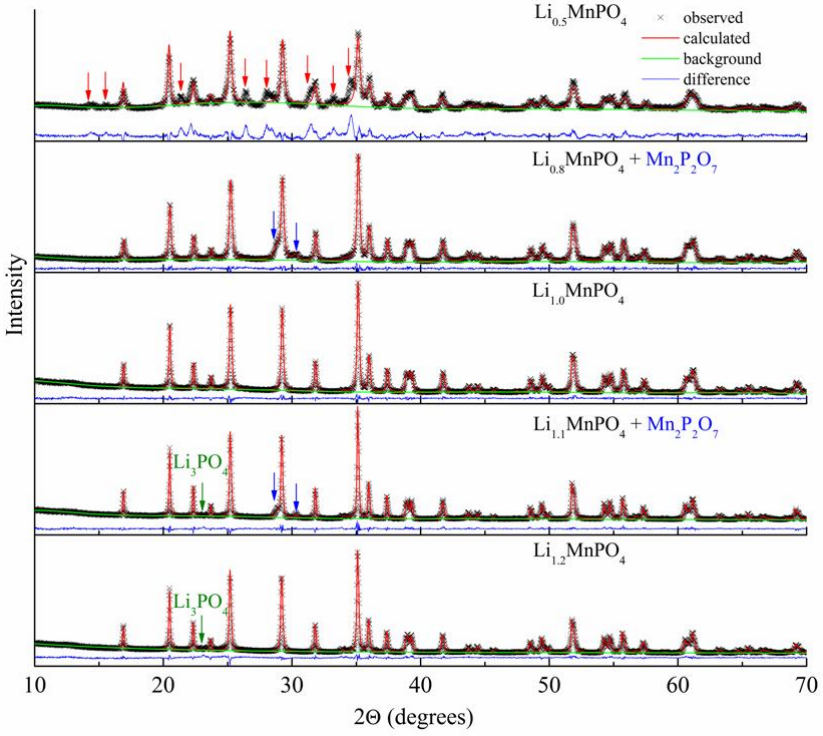

Figure V - 52: Rietveld refinement of XRD data of the Li_xMnPO_4 series. Refinements for x = 0.8 and 1.1 compositions are done using two phases, $LiMnPO_4$ and $Mn_2P_2O_7$. $Mn_2P_2O_7$ peaks are marked with blue arrows. Green arrows indicate small impurity peaks of Li_3PO_4. Red arrows indicate unidentified impurities in $Li_{0.5}MnPO_4$.

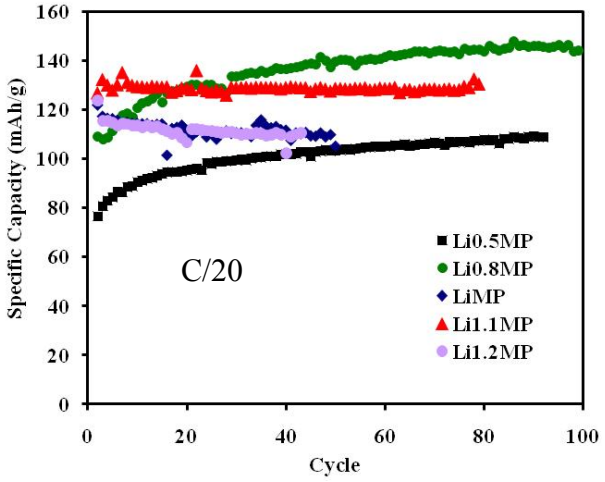

Figure V - 53: Cycling stability of Li_xMnPO_4 ($0.5 \leq x \leq 1.2$) between 2.0 and 4.5 V at C/20 rate. (1C=150 mA/g).

Synthesis of High-Voltage Spinel $LiNi_{0.5}Mn_{1.5}O_4$. We have developed a novel synthesis approach for preparing high-voltage spinel $LiNi_{0.5}Mn_{1.5}O_4$ and its Cr-substituted phase that involves only milling and heating. Both $LiNi_{0.5}Mn_{1.5}O_4$ and $LiNi_{0.45}Cr_{0.05}Mn_{1.5}O_4$ have cubic structures that can be indexed into the Fd-3m space group. For the undoped spinel, a trace amount of $Li_xNi_{1-y}O$ was identified. After 5% substitution of Ni by Cr in $LiNi_{0.5}Mn_{1.5}O_4$, no $Li_xNi_{1-y}O$ impurity was observed in the XRD pattern, which indicated a pure spinel phase. Rietveld refinements showed an increase of the lattice parameter from a = 8.17396(8) Å in $LiNi_{0.5}Mn_{1.5}O_4$ to 8.1860(1) Å after Cr-doping, which suggests an increased amount of the disordered phase.

Figure V - 54 compares the morphologies of the pure and Cr-substituted spinels. $LiNi_{0.5}Mn_{1.5}O_4$ exhibits a uniform particle size distribution as shown in Figure V - 54a. The octahedral particle diameters were around 2 μm and further aggregated into secondary particles. After Cr-doping, the morphology of the spinel did not change much. However, the octahedral shape of the spinel particles became more distinct as shown in Figure V - 54d. $LiNi_{0.5}Mn_{1.5}O_4$ consists of both ordered and disordered phases as revealed by Figure V - 54b and Figure V - 54c. The highlighted reflections are forbidden by the Fd-3m space group. The occurrence of the super lattice pattern was caused by the ordering between Ni^{2+} and Mn^{4+}, which indicates the coexistence of an ordered phase in the undoped spinel that cannot be directly observed from XRD pattern. However, after Cr-doping, the extra diffraction spots were no longer observable in Figure V - 54e and Figure V - 54f, both of which showed typical spinel patterns. In other words, Cr-doping

increased the amount of the disordered phase. This finding is consistent with the changes of lattice parameters calculated from XRD data.

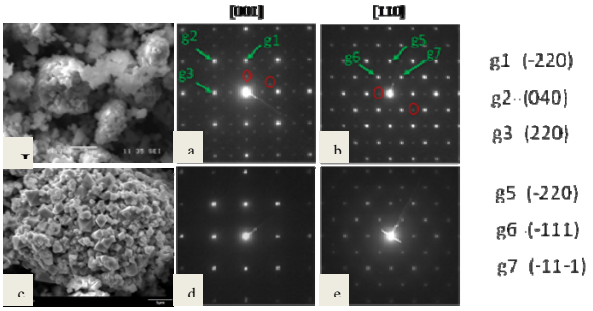

Figure V - 54: a) SEM image of $LiNi_{0.5}Mn_{1.5}O_4$; b) and c) electron diffraction patterns of $LiNi_{0.5}Mn_{1.5}O_4$ in the [001] and [110] zone, respectively; d)SEM image of $LiNi_{0.45}Cr_{0.05}Mn_{1.5}O_4$; e) and f) electron diffraction patterns of $LiNi_{0.45}Cr_{0.05}Mn_{1.5}O_4$ in the [001] and [110] zones, respectively.

Figure V - 55a reveals that, after Cr-doping, the cycling stability was significantly improved. This improvement may be assigned to the increased content of disordered phase and/or Mn^{3+} ions that facilitate Li^+ ion diffusion within the lattice. Meanwhile the surface modification caused by Cr-doping may alleviate Mn dissolution in the electrolyte. We note here that the intrinsic influencing parameter on performance is the content of Mn^{3+} instead of doping. In other words, if the Mn^{3+} concentration in pure $LiNi_{0.5}Mn_{1.5}O_4$ can be modified to the same amount as in $LiNi_{0.45}Cr_{0.05}Mn_{1.5}O_4$, the cycling stability also may be improved for the undoped spinel, which is now under investigation.

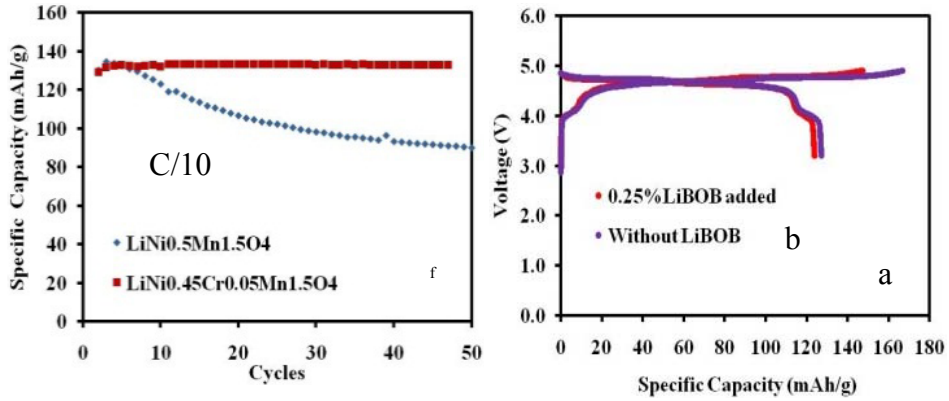

Figure V - 55: Comparison of a) cycling stability for $LiNi_{0.5}Mn_{1.5}O_4$ and $LiNi_{0.45}Cr_{0.05}Mn_{1.5}O_4$ and b) voltage profiles of $LiNi_{0.45}Cr_{0.05}Mn_{1.5}O_4$ tested with and without LiBOB.

We also found that the low concentration of Li bis(oxalato)borate (LiBOB) not only improves the first cycle efficiency of $LiNi_{0.45}Cr_{0.05}Mn_{1.5}O_4$ from 76% to 85%, but the rate capability also increases with 0.25% LiBOB (rate performances not shown here). LiBOB has an oxidation potential at around 4.5 V vs. Li/Li^+. When the voltage reaches 4.5V, LiBOB will be decomposed first via a ring-opening reaction to form a linear inorganic lithium metaborate film that covers the cathode surface. This protection film also is resistive to the trace amount of HF and POF_3 generated by the hydrolysis and thermal decomposition of $LiPF_6$ salt in the electrolyte. Therefore further decomposition of the solvents and the dissolution of Mn in the high-voltage spinel will be alleviated, thus improving the Coulombic efficiency and cycling stability. We also found that the coin-cells pans and separator membranes significantly influence on the Coulombic efficiency of the high-voltage cells, especially during the first cycle.

Renewable Organic Cathodes. In FY 2010, we investigated a novel organic cathode based on poly(anthraquinonyl sulfide) (PAQS). This renewable cathode was prepared using a simple poly-condensation that has been applied commercially to synthesize poly(p-phenylene sulfide). PAQS is different from traditional intercalation cathode materials because it allows 2e transfer that leads to a high theoretical capacity of 225 mAh/g. The electrochemically active site is O instead of S on the ring; therefore, the polysulfide dissolution issue encountered in Li/S batteries can be avoided.

We synthesized a new organic cathode material, poly(1,8-anthra-quinonyl sulfide) (P18AQS), and compared it with the previously reported poly(1,5-anthraquinonyl sulfide) (P15AQS) in terms of rate capability (see Figure V - 56). We found that the substitution position with less steric stress on the backbone is critical for the electrochemical performances, thus providing clues on the further design of new quinone-based cathodes.

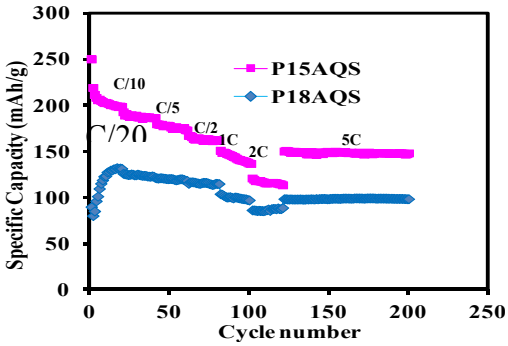

Figure V - 56: Comparison of the rate capabilities of novel organic cathodes with more than one redox center.

Conclusions and Future Directions

Different Li contents were used to synthesize Li_xMnPO_4 ($0.5 \leq x \leq 1.2$) materials, which then were systematically investigated in terms of structure, morphology, electrochemical behaviors, and magnetic properties along with an XAS study. We found that pure $LiMnPO_4$ forms within the whole range of $0.5 \leq x \leq 1.2$ while $Mn_2P_2O_7$ and/or Li_3PO_4 impurities coexist in the non-stoichiometric compositions. For $Li_{0.5}MnPO_4$ and $Li_{0.8}MnPO_4$, a gradual increase in the reversible capacity with cycling was observed, which may be related to interactions between $Mn_2P_2O_7$ and $LiMnPO_4$. Among all the samples, $Li_{1.1}MnPO_4$ exhibits the most stable cycling probably because of the Li_3PO_4 coating on the surface of $LiMnPO_4$ nano-particles that functions as a solid electrolyte to facilitate ion transport. This observation provides important clues on the activation and stabilization of phosphate-based cathode materials.

We investigated the phase transformations and thermal stabilities of the electrochemically charged $MnPO_4$ cathode. The $MnPO_4$ reduction to $Mn_2P_2O_7$ with oxygen evolution was observed at 490°C, which coincides with the phase changes in $MnPO_4 \cdot H_2O$. The charged $MnPO_4$ undergoes amorphization changes at temperatures ?180°C, and there is no oxygen released between 180 and 490°C. Although the kinetics of the $LiMnPO_4$ cathode needs to be improved, $LiMnPO_4$ can be a safe alternative to other high-voltage cathodes if its power can be further improved

A cost-effective approach has been developed for synthesizing the high-voltage spinel $LiNi_{0.5}Mn_{1.5}O_4$. After Cr substitution, the cycling performance was greatly improved because of the increased concentration of Mn^{3+} ions. The influence of Mn^{3+} concentration on performance will be investigated further next year. The addition of a low concentration of LiBOB (0.25%) improves the Coulombic efficiency especially for the first cycle. Cathode pans and separator membranes are now being evaluated with high-voltage cathode materials.

We also prepared a new renewable organic cathode based on quinonyl group, P18AQ. We found that the substitution position that results in less steric stress on the backbone is critical for designing a high-performance organic cathode. To improve the energy density and cycling stability of these high-capacity cathodes, novel organic cathode with other functional groups on the ring will be further investigated.

FY 2011 Publications/Presentations

1. D. Choi, J. Xiao, Y. J. Choi, J. S. Hardy, V. Murugesan, J. Liu, W. Wang, W. Xu, J.-G. Zhang, Z. Yang and G. L. Graff. "Thermal Stability of Electrochemically Charged/Discharged $LiMnPO_4$ Nanoplate Cathode for Li-ion Battery", *Energy Environ.Sci*. **4**, 4560(2011). **(Back cover article)**
2. J. Xiao, N. A. Chernova, S. Upreti, X. Chen, Z. Li, Z. Deng, D. Choi, W. Xu, Z. Nie, G. L. Graff, J. Liu, M. S. Whittingham and J.-G. Zhang, "Electrochemical Performances of $LiMnPO_4$ Synthesized from Non-Stoichiometric Li/Mn Ratio", *Phys. Chem. Chem. Phys*., **13,** 18099(2011).
3. A. Pan, D. Choi, J.-G. Zhang, S. Liang, G. Cao, Z. Nie, B. W. Arey, and J. Liu, "High-rate cathodes based on $Li_3V_2(PO_4)_3$ nanobelts prepared via surfactant-assisted fabrication", *J. Power Sources*, **196**, 3646 (2011).
4. A. Pan, J. Liu, J.-G. Zhang, G. Cao, W. Xu, Z. Nie, X. Jie, D. Choi, B. W. Arey, C. Wang, and S. Liang, "Template free synthesis of LiV_3O_8 nanorods as a cathode material for high-rate secondary lithium batteries", *J. Mater. Chem.*, **21**, 1153 (2011).
5. A. Pan, J.-G. Zhang, G. Cao, S. Liang, C. Wang, Z. Nie, B. W. Arey, W. Xu, D. Liu, J. Xiao, G. Li, and J. Liu, "Nanosheet-structured LiV_3O_8 with high capacity and excellent stability for high energy lithium batteries", *J. Mater. Chem.*, **21**, 10077 (2011).
6. D. Wang, J. Xiao, W. Xu, Z. Ni, C. Wang, G.L. Graff, J.-G. Zhang. "Preparation and Electrochemical Investigation of Li_2CoPO_4F Cathode Material for Lithium-Ion Batteries", Journal *of Power Sources* **196**, 2241–2245 (2011).
7. J. Yu, K. M. Rosso, J.-G. Zhang and J. Liu, Ab initio study of lithium transition metal fluorophosphate cathodes for rechargeable batteries, *J. Mater. Chem*., **21**, 12054(2011).
8. A. Pan, J. Liu, J.-G. Zhang, W. Xu, G. Cao, Z. Nie "Nano-Structured $Li_3V_2(PO_4)_3$/Carbon Composite for High-Rate Lithium-Ion Batteries", *Electrochem. Commun.*, **12**, 1674-1677 (2010).

V.B.11 Crystal Studies on High-energy Density Cathodes (LBNL)

Guoying Chen
Lawrence Berkeley National laboratory
Environmental Energy Technologies Division
Berkeley, CA 94720
Phone: (510) 486-5843; Fax: (510) 486-5467
E-mail: gchen@lbl.gov

Start Date: October 2009
Projected End Date: September 2012

Objectives

- Investigate phase transition mechanisms, explore kinetic barriers, and evaluate stability of high-energy cathode materials.
- Establish direct correlations between structure, composition, morphology, performance, and stability.
- Provide guidelines to design and develop electrode materials with improved energy density, rate capability, and safety, especially with regard to thermal stability.

Technical Barriers

- Low energy density
- Low power density
- Poor cycle life
- Safety

Technical Targets

- PHEV40: 142 Wh/kg, 320 W/kg, 5,000 cycles.
- EV: 200 Wh/kg, 1,000 cycles.

Accomplishments

- Demonstrated improved energy density, rate capability and phase stability in Li-excess layered $LiNi_{0.33}Mn_{0.33}Co_{0.33}O_2$. Effects of overlithiation illustrated.
- Developed synthesis approach and prepared phase-pure spinel $LiNi_xMn_{2-x}O_4$ single crystals with well-defined crystal structure, size, crystal facets and Mn^{3+} content.
- Identified superior transport properties and stability on spinel (111) crystal plane for the first time.
- Demonstrated the importance of particle surface facets on spinel performance.
- Developed a technique for qualitative measure of spinel Mn^{3+} content based on FTIR.

✧ ✧ ✧ ✧ ✧

Introduction

To meet the DOE targets for Li-ion batteries for vehicular applications, it is necessary to employ electrode materials that offer high-energy density and high stability. This project focuses on the development and optimization of two oxide cathodes that are presently most promising: layered $Li_{1+x}M_{1-x}O_2$ (M=Mn, Ni and Co) and spinel $LiNi_xMn_{2-x}O_4$.

Layered oxides are capable of delivering high capacity over 200 mAh/g. The cathodes, however, exhibit large irreversible capacity loss when charged through the activation plateau in the first cycle and suffer low rate capability and poor cycle life thereafter. Although much of the current effort focuses on mild-acid treatment and surface modification, it remains critical to obtain an in-depth understanding of the material's intrinsic properties and processes that enables rational design and optimization of the cathode.

Spinel $LiMn_{1.5}Ni_{0.5}O_4$ has a theoretical capacity of 147 mAh/g (700 Wh/kg) and fast three-dimensional Li-ion diffusion paths within the cubic lattice. Structural complexity of the material has led to synthesis-dependent properties and performance, particularly with regard to electronic and ionic conductivities, phase transformation behavior, chemical and thermal stabilities, and high-voltage reactivity with the electrolyte. It is known that physical properties, such as crystal structures (ordered vs. disordered), size, morphology and Mn^{3+} content, separately and collectively impact rate capability and stability of the material, but their individual contribution as well the synergy between them is unclear. In collaboration with the BATT Ni/Mn Spinel Focus Groups, we aim to prepare single crystals of $LiNi_xMn_{2-x}O_4$ with well-defined physical characteristics, investigate the kinetic and thermodynamic behavior, correlate the material's specific attributes to performance, and ultimately achieve electrode optimization with minimized side reactions and improved transport properties.

Approach

- Prepare well-formed crystals with various structure, composition, size and morphology using wet chemistry synthesis routes, such as solvothermal and molten salt reactions.
- Characterize their physical properties and investigate their solid state chemistry using advanced

spectroscopic, spectromicroscopic, scanning calorimetry and electron microscopic techniques.

- Optimize synthesis and processing conditions, improve performance and safety of the cathode materials based on the structural and mechanistic understandings.

Results

Layered Oxides. Through systematic studies on micron-sized, plate-shaped $Li_{1+x}(Ni_{0.33}Mn_{0.33}Co_{0.33})_{1-x}O_2$ (x=0 for stoichiometric and 0.14 for overlithiated) single crystals, the team has previously reported that excess Li increases the average oxidation state of the transition metal ions, facilitates the formation of an in-plane $\sqrt{3}a_{hex} \times \sqrt{3}a_{hex}$ superstructure that converts R-3m to $P3_112$ space group, improves the O3 phase stability and decreases the unit cell volume change upon chemical delithiation. The electrochemical performance of the oxides is further compared in Figure V - 57. At C/20 rate, an irreversible voltage plateau associated with O_2 release was observed at 4.4 V on the overlithiated oxide (Figure V - 57a). The cathode delivered a discharge capacity of 175 mAh/g, as compared to 140 mAh/g for the stoichiometric electrode.

On the dQ/dV plot (Figure V - 57b), a second discharge peak at 3.3 V was observed, and the charging peak at 3.9 V shifted to 3.6 V after charging through the activation plateau, indicating the participation of lower voltage components thereafter. When cycled between 2.5 to 4.8 V, the overlithiated oxide showed improved capacity retention and rate capability (Figure V - 57c), likely a result of the enhanced phase stability upon deep Li extraction at high voltages.

Spinel $LiNi_xMn_{2-x}O_4$. Well-formed spinel crystals were synthesized by a molten salt method. In the presence of a flux, phase-pure $LiNi_{0.5}Mn_{1.5}O_4$ single crystals formed at 550°C, well below the temperature typically used for solid state synthesis. A rock-salt type impurity phase appeared above 600°C when MnO_2 and $Ni(OH)_2$ were used as precursors (Figure V - 58), but the temperature increased to 700°C when $Mn(NO_3)_2$ and $Ni(NO_3)_2$ were used. In both cases, increasing synthesis temperature led to lattice expansion of the spinel phase but contraction of the rock-salt phase, suggesting changes in chemical compositions in both phases.

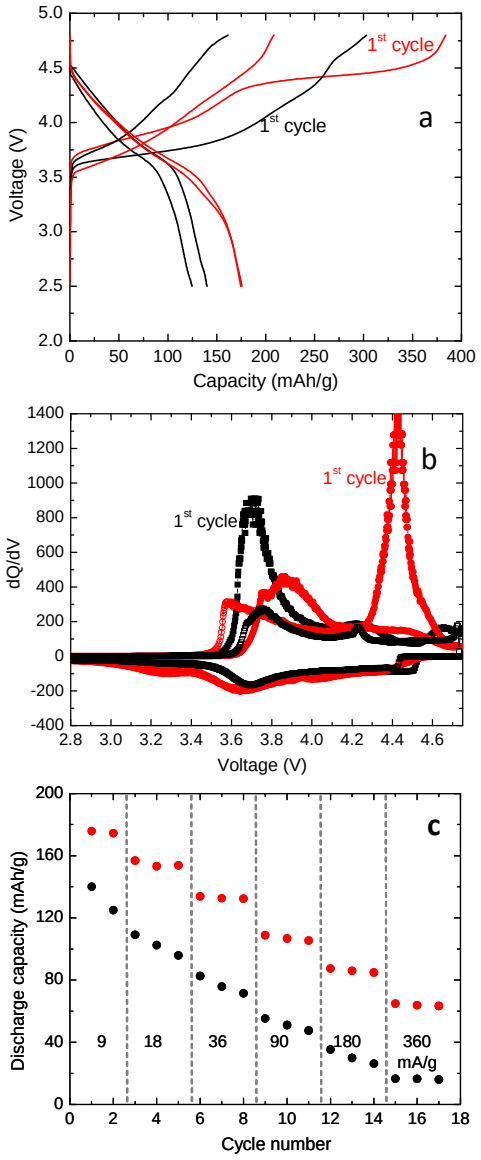

Figure V - 57: a) Charge-discharge profiles, b) dQ/dV plots for the first two cycles. Filled symbols: first cycle; open symbols: second cycle, and c) rate comparison of the oxides at the indicated current densities. Data for x=0 and 0.14 are shown in black and red, respectively.

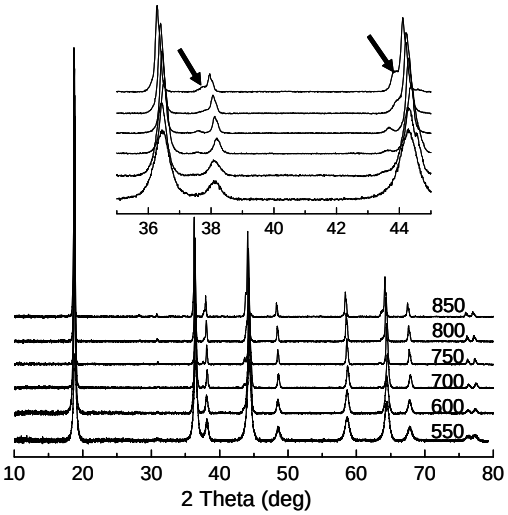

Figure V - 58: XRD patterns of the $LiNi_{0.5}Mn_{1.5}O_4$ crystals synthesized at indicated temperatures. Arrows indicate peaks from the rock-salt type impurity phase.

The choices of both reaction precursors and molten salt were found to have a large impact on crystal size and morphology. With the oxide precursors, octahedron-shaped crystals with an average size of 30 nm were obtained from a eutectic mixture of 0.58LiCl-0.42KCl, as shown in the SEM image in Figure V - 59a. When the nitrates were used, plate-shaped crystals, averaged at 1 μm in size and 100 nm in thickness, precipitated in LiCl flux at 750°C (Figure V - 59b), whereas octahedron-shaped crystals with an average size of 2 μm formed in the eutectic flux of LiCl-KCl at 700°C (Figure V - 59c). TEM and SAED analyses on the large crystals suggested that the octahedrons were predominantly enclosed by the (111) crystal planes, while the main surface facets on the plates were (112), as shown on the insets in Figure V - 59b and Figure V - 59c.

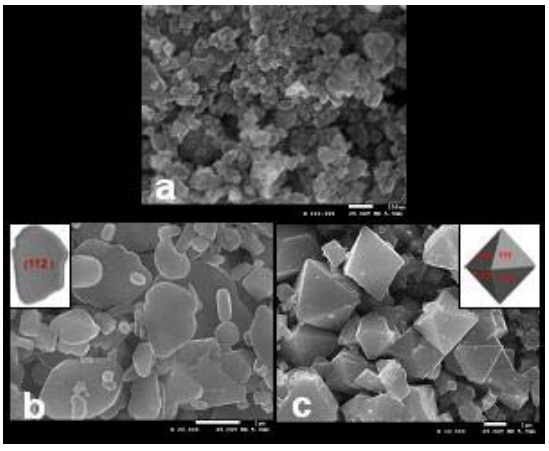

Figure V - 59: SEM images of $LiNi_{0.5}Mn_{1.5}O_4$ crystals prepared from a) oxide precursors in eutectic LiCl-KCl mixture, b) nitrate precursors in a LiCl flux, and c) nitrate precursors in eutectic LiCl-KCl mixture.

On the FTIR spectra, the bands at 430, 560 and 650 cm^{-1} that are characteristic of the cation ordered structure (space group of $P4_332$) appeared strongly in the large crystals made from the nitrates (Figure V - 60). The peak intensity ratio of 590/620, which has been used as a qualitative measure of transition-metal ordering in the structure, suggested that the octahedrons are most ordered among three samples. Superlattice peaks from the ordered structure, however, were not discernible in the XRD patterns.

The redox behavior and rate capabilities of the crystals are compared in Figure V - 61. The main peaks on the integrated capacity and voltage profiles are known to be associated with the Ni^{2+}/Ni^{3+} and Ni^{3+}/Ni^{4+} redox couples. For $LiNi_{0.5}Mn_{1.5}O_4$ plates with (112) surface facets, the charging peaks were separated by 55 mV, close to the reported value of 60 mV in the spinels with a disordered structure (space group of $Fd\bar{3}m$). The peaks also had a significant shift toward higher voltage, suggesting increased resistance for Li extraction from (112) crystal plane. Broad peaks at 4.1 V that is characteristic of the Mn^{3+}/Mn^{4+} transitions were observed, with the peak area integration estimating 18% Mn^{3+} in the sample. The amount decreased to 1.5% in the octahedron-shaped crystals with (111) surface facets, where the charging peaks were separated by a much smaller amount of 25 mV, close to the reported value of 20 mV for the ordered spinel. Despite the higher degree of ordering in the crystal structure and larger size, the octahedral crystals demonstrated superior rate capability, delivering a capacity of 138 mAh/g at C/5 rate. The smaller-sized crystals, on the other hand, had the worst performance among the three samples. The main surface facets on this sample remain to be analyzed, but the study clearly illustrates the importance of particle morphology on the performance of this cathode material.

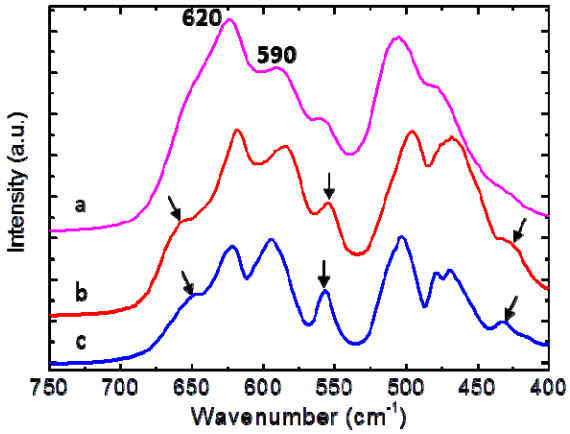

Figure V - 60: FTIR spectra of the $LiNi_{0.5}Mn_{1.5}O_4$ crystals. Arrows indicate peaks from the ordered structure.

Work was also initiated to investigate the effect of Mn^{3+} content on rate performance and stability of this high-voltage cathode. $LiNi_xMn_{2-x}O_4$ ($0.3 \le x \le 0.5$) single

crystals were prepared by the molten salt method, with the ratio between the Mn and Ni precursors carefully controlled to achieve the targeted stoichiometry. The crystals adapted the same octahedron shape and had a similar size of 2 μm. XRD patterns and lattice dimensions are compared in Figure V - 62a. The ionic radii of octahedral-coordinated Ni^{2+}, Mn^{3+} and Mn^{4+} are 0.83, 0.785 and 0.67, respectively. Decreasing Ni^{2+} content increases Mn^{3+}/Mn^{4+} ratio and therefore leads to a slight expansion in the cubic lattice, as shown in Figure V - 62b.

Figure V - 63a compares the FTIR spectra of the crystal samples. Bands at 620 and 560 cm^{-1} are attributed to Mn-O vibrations while the band at 590 to that of Ni-O. The replacement of Ni^{2+} by the smaller-sized Mn^{3+} leads to stronger Ni-O bonds and therefore a blue shift of the 590 peak at lower Ni content. The peak ratio of 590/620 increased nearly linearly with Ni content (Figure V - 63b), suggesting that it may be used as a measure for the Mn^{3+} content within this range. Peaks at 430, 560 and 650 are clearly present when Ni content is above 0.40, characteristic of an ordered crystal structure. Significant changes occurred on the spectrum when *x* decreased to 0.35, suggesting loss of the ordering in samples.

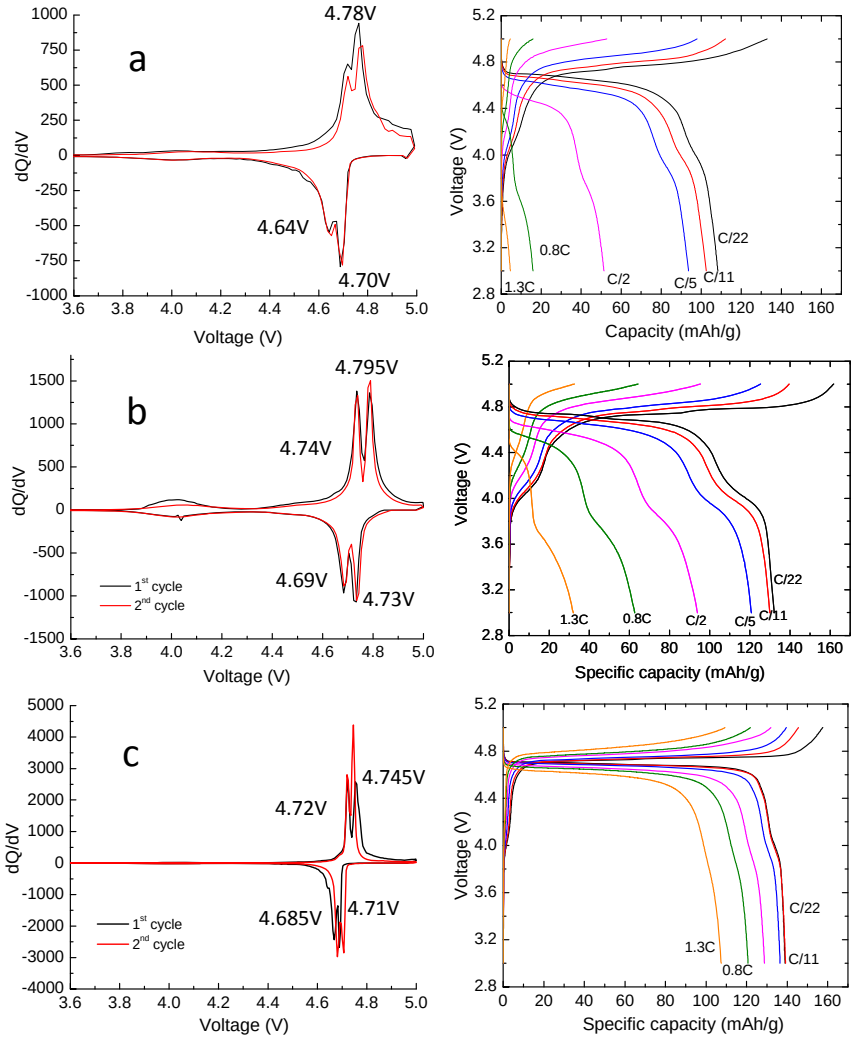

Figure V - 61: Rate capability comparison of $LiNi_{0.5}Mn_{1.5}O_4$ crystals. Results obtained from half-cell testing with Li foil as counter and reference electrodes, and 1M $LiPF_6$ in 1:1 ethylene carbonate: diethylene carbonate as electrolyte.

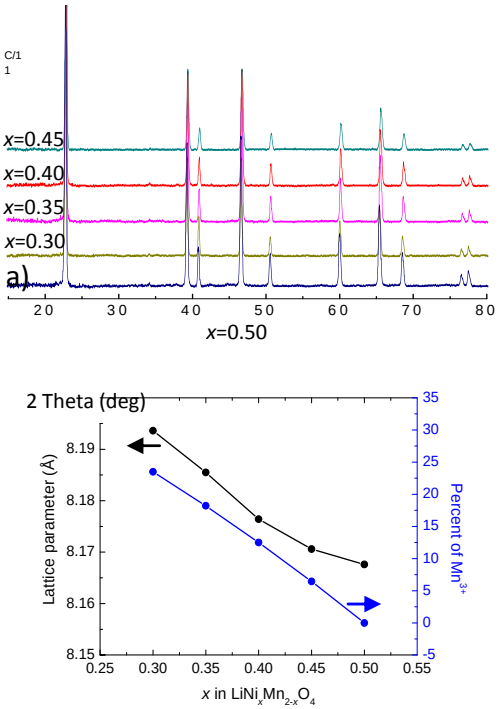

Figure V - 62: a) XRD patterns and b) lattice parameter and Mn^{3+} content in $LiNi_xMn_{2-x}O_4$ ($0.3 \le x \le 0.5$) crystals.

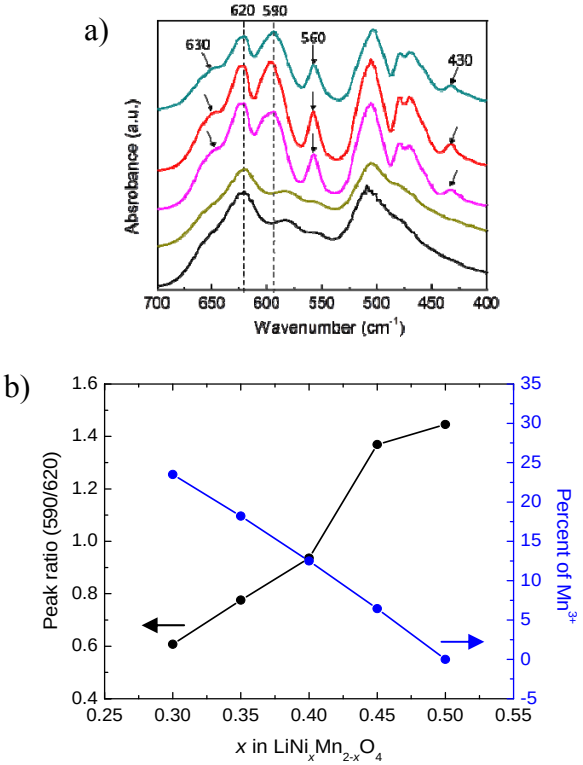

Figure V - 63: a) FTIR spectra and b) peak ratio of 590/620 and Mn^{3+} content in $LiNi_xMn_{2-x}O_4$ ($0.3 \le x \le 0.5$) crystals.

Conclusions and Future Directions

The value of using well-formed single crystals for property evaluation and mechanistic studies was further demonstrated. Detailed understanding on the effects of excess Li laid a foundation for the studies on Li and Mn-rich layered composite oxides. Future work will focus on structural, performance and stability effects of Li content and transition-metal ratios in the composite oxides, the mechanism of oxygen evolution at the high voltage, and synthesis conditions to produce composite cathodes with optimized characteristics for performance and safety.

Spinel crystals with controlled morphology and Mn^{3+} content were prepared by adjusting synthesis conditions. Superior transport properties and cycling stability were obtained from structurally ordered, large crystals with (111) surface facets, which suggests that morphology design is critical in achieving optimal rate capability and stability of the spinel. Future work will continue to optimize the cathode by further quantifying the impact of other physical properties on transport phenomena and stability.

FY 2011 Publications/Presentations

1. "Improved Kinetics and Stabilities in Mg-Substituted $LiMnPO_4$," G. Chen, A. Shukla, X. Song, and T. J. Richardson, *Journal of Materials Chemistry*, **21**, 10126 (2011).
2. "Thermal Instability of Olivine-type $LiMnPO_4$ Cathodes," G. Chen and T. J. Richardson, *Journal of Power Sources*, **195**, 1221 (2010).
3. "Continuity and Performance in Composite Electrodes," G. Chen and T. J. Richardson, *Journal of Power Sources*, **195**, 5387 (2010).
4. "MAS NMR Study of the Metastable Solid Solutions Found in the $LiFePO_4/FePO_4$ System," J. Cabana, J. Shirakawa, G. Chen, T. J. Richardson, and C. P. Grey, *Chemistry of Materials*, **22**, 1249 (2010).
5. "Structure and Performance of Layered $Li_{1+x}M_{1-x}O_2$ Crystals," ECS 218th meeting, Las Vegas, NV, October 11, 2010.
6. "Studies on Oxide Cathode Crystals," presented at the 2011 DOE Hydrogen Program and Vehicle Technologies Program Annual Merit Review and Peer Evaluation Meeting, Washington, DC, May 11, 2011

V.B.12 Developing Materials for Lithium-Sulfur Batteries (ORNL)

Chengdu Liang
Oak Ridge National Laboratory
Center for Nanophase Materials Sciences
Building 8610 MS 6493
Oak Ridge, TN 37831-6493
Phone: (865) 574-8408; Fax: (865) 574-1753
E-mail: liangcn@ornl.gov

Collaborators:
Nancy J. Dudney and Jane Howe (ORNL)

Start Date: June 2010
Projected End Date: September 2014

Objectives

- Expand the scientific understanding of lithium-sulfur chemistry and nanoporous cathode architecture to direct continued improvement in cycle life and capacity utilization to meet goals for PHEV and EV application.
- Optimize the nanostructure of the S/C composites to retain sulfur and suppress the migration of the polysulfide species.
- Improve the reversibility of Li_2S formation through optimization of the electrolyte composition.
- Establish a chemical mechanism to suppress the lithium dendrite formation or heal the damaged lithium anode.

Technical Barriers

Deployment of the Lithium-Sulfur (Li-S) chemistry in EV batteries has the potential to improve the energy density by a factor of 2 to 5 but suffers from poor cell performance and short cycle-life. The key challenge for Li-S batteries is the dissolution of sulfur and lithium polysulfides in liquid electrolytes. The soluble sulfur species create the polysulfide shuttle phenomenon inside the electrochemical cell, which carries sulfur from the cathode to the anode. The migrated sulfur species chemically react with the lithium anode and cause a "chemical short" of the battery. The "chemical short" leads to the loss of active materials, corrosion of the Li anode, and low coulombic efficiency. The mobile sulfur species cause the redistribution of sulfur in the battery and impose a poor cycle-life. New materials are crucial to enable Li-S battery chemistry in PHEV and EV applications.

Technical Targets

- Verify the previous ORNL discovery on the additives that prolong the cycle life of Li-S batteries
- Optimize the structure of carbon/sulfur composite electrode for the improvement of cycling performance.
- Invent new electrolyte compositions that are compatible with battery components
- Achieve long cyclability of lithium metal anode in Li-S batteries.

Accomplishments

- Demonstrated the additive effect of LiBr on Li-S batteries. A cycle-life of 1000 cycles was repeated using a Swagelok cell.
- Verified the battery chemistry of Li-S cell with LiBr as the additive by bench-top wet chemistry approach.
- Discovered new electrolyte additives that are less corrosive than LiBr.
- Explored approaches for lithium metal anode protection.
- Developed a sample transfer stage that can handle air-sensitive materials for the diagnosis of Li-S batteries.

Introduction

The DOE Vehicle Technologies Program is pursuing technologies to reduce U.S. petroleum consumption through vehicle electrification. Advances in lithium-ion battery development have enabled commercialization of both PHEVs and EVs. However, achieving significant market penetration and maximum petroleum reduction from advanced electric drivetrains will require lower costs and increased electric range. Li-S batteries provide a potential solution to both of these development challenges. Li-S batteries have significantly lower raw material costs and much higher energy density than lithium-ion batteries. However, Li-S batteries currently suffer from short cycle-life and poor efficiency. The goal of this project is to identify new materials and architectures that improve the cycle-life and performance of Li-S batteries.

Three key phenomena cause the short cycle-life of the Li-S batteries: (1) the irreversible deposition of Li_2S on the lithium anode through the intrinsic polysulfide shuttle, (2) the irreversible deposition of Li_2S and sulfur on the

cathode, and (3) the formation of lithium dendrites. In our previous development of Li-S batteries, we found that the aforementioned three phenomena can be overcome by the use of nanostructured S/C composite cathodes with electrolyte additives. As demonstrated in Figure V - 64, the cycle-life and capacity of the Li-S batteries have been significantly improved using a novel S/C nanocomposite material as the cathode and a simple electrolyte additive. For comparison purposes, the performance of a regular Li-S battery is also shown in Figure V - 64 [indicated by the red down triangle]. Shown in the inset of Figure V - 64, we were able to devise a cell that achieved a cycle-life of 1000 cycles without any indication of capacity decay. In spite of the dramatic improvement of cycle-life for Li-S batteries, the LiBr additive discovered at ORNL has significant drawbacks: the electrochemical intermediates of LiBr are highly corrosive. The LiBr additive causes severe problems with the current collectors and other metal parts in the battery. The incompatibility of LiBr with battery components drives the search for alternative additives that are free of the corrosion problem. In addition to the corrosion problem, the coulombic efficiency and the round trip energy efficiency are very low for Li-S batteries without suppression of the polysulfide shuttle.

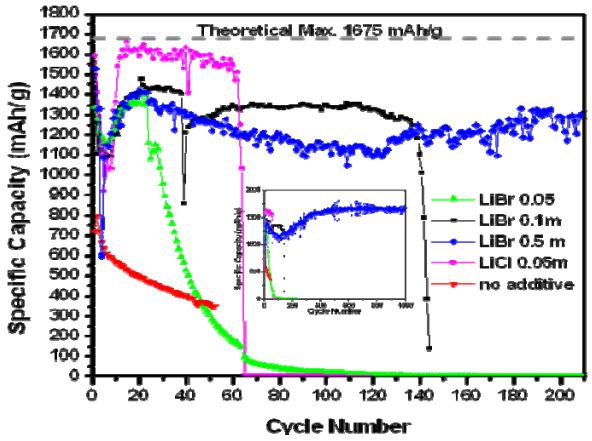

Figure V - 64: Cycle performance of Li-S batteries with/without electrolyte additives.

Approach

To achieve long-life Li-S batteries, the battery structure has to be able to suppress or eliminate the polysulfide shuttle and improve the electrochemical reversibility of Li_2S formation. The incorporation of sulfur into nanoporous carbon material serves to sequester the sulfur species at the cathode during electrochemical cycling. Although the physical adsorption of polysulfide cannot completely prevent the polysulfide shuttle, the S/C nanocomposites can significantly improve the cycling performance of Li-S batteries. The optimization of the S/C composite leads to better performance in terms of coulombic efficiency and energy efficiency. Besides the low energy efficiency, Li-S batteries suffer from severe capacity decay, which is mainly caused by the irreversible formation of Li_2S. Additives such as LiBr can accelerate the electrochemical cycling of the sluggish Li_2S by altering the battery chemistry. However, such additives have compatibility issues with battery components. We will explore new additives that are less corrosive than LiBr. To completely prevent the polysulfide shuttle, the protection of lithium metal anode will be an efficient approach for the improvement of both cyclability and the energy efficiency of Li-S batteries. We are seeking new materials that could improve both the energy efficiency and the cycle life of Li-S batteries by the following approaches: (1) optimizing the structure of sulfur/carbon composite to suppress the polysulfide shuttle thereby improving the coulombic efficiency; (2) exploring electrolyte additives that can reverse the formation of Li_2S; and (3) protecting the lithium metal anode by solid electrolyte coating.

In addition to discovering new materials for Li-S batteries, we develop a sample transfer stage for SEM characterization of air-sensitive materials to facilitate the material discoveries. This sample transfer stage is critical for the diagnosis of lithium metal anodes after battery cycling.

Results

Sulfur/Carbon Composites. Sulfur and its discharge products are neither electronic nor ionic conductors. To charge/discharge, a sulfur cathode needs both ionic and electronic conduction. Compositing sulfur with carbon imparts electronic conductivity to sulfur. The porosity of the sulfur/carbon composite accommodates liquid electrolytes and provides pathways for ionic conductivity. Hence, the porous structure of the hosting carbon materials determines the electrochemical performance of the composite. The contact area of sulfur with carbon is dictated by the surface area of carbon while the maximum sulfur loading is limited by the pore volume. Figure V - 65 shows the performance of two carbon materials with comparable surface area but differing pore volumes. Both materials have 50% sulfur loading. The carbon host with pore volume of 2.35 cm^3/g is significantly superior to the one with pore volume of 1.12cm^3/g for retaining the capacity of the sulfur cathode. The larger pore volume can accommodate more electrolyte and therefore enhance the retention of capacity. Tuning the pore sizes and porous structures is essential for the optimization of the electrochemical properties of the S/C composite. Both materials have similar coulombic efficiency of 95% at 0.5 C rate in a highly viscous tetraglyme electrolyte with 1.0 m LiTFSI as the lithium salt. The capacity decay that is observed is most likely due to the precipitation of Li_2S. An additive that accelerates the electrochemical process of Li_2S is highly desirable for improving the cycle-life of Li-S battery with optimized porous carbons.

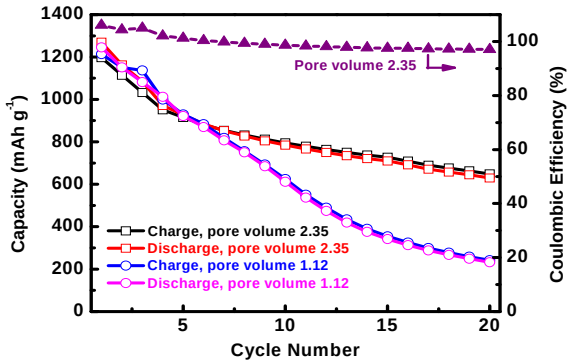

Figure V - 65: Cycling performance of S/C composites with 50% sulfur loading. Carbon hosts have pore volumes of 2.35 and 1.12 cm^3/g. Surface areas are ~ 800 m^2/g for both materials. Capacity is normalized by the sulfur alone.

Electrolyte Additives. To overcome the corrosion problem associated with the LiBr additive, a number of alternative compounds have been investigated. Organic alternatives include benzoquinone, Tetracyanoquinodimethane (TCNQ), and 2,3-Dichloro-5,6-dicyano-1,4-benzoquinone (DDQ). These compounds have electrochemical redox potentials between 2.5 and 3.9 V. However, the chemical compatibility of benzoquinone and TCNQ with bare lithium anode is a problem. DDQ has better chemical stability with lithium metal. It was found that using DDQ as the additive [5% in tetraglyme] reduces the capacity of S by half. The possible reason for this unexpected capacity loss could be the polymerization of DDQ at high concentration. The resulting polymer coats the carbon electrode surface and compromises the electrochemical performance of the cathode. When the concentration of DDQ was reduced to 1%, the electrochemical performance was improved comparing with the 5% DDQ in tetraglyme. Inorganic alternatives to LiBr were also investigated. Promising results were obtained when a phosphorous sulfide additive was used in the cell. As shown in Figure V - 66a, the charge/discharge curves have plateaus close to the ideal curves. The cell has a good retention of capacity at 0.1 C rate. The cut-off cell voltage has been set to 1.9 V because the additive can be reduced at the cathode when the discharge voltage is below 1.9 V. The stability of this phosphorous sulfide additive is still under investigation. The mechanism of how the additive works will be studied in future experiments.

Protection of Lithium Anode. To protect lithium from reacting with the sulfur species, a novel anode made of metal lithium with a pre-formed solid electrolyte interphase (SEI) on its surface was designed and implemented in the Li-S batteries. The tenet of the design is to have an ionic conductor covering the surface of lithium metal, thereby impeding surface reaction of lithium with polysulfide.

Lithium thiophosphate salts were chosen to form the SEI. Lithium thiophosphates are fast Li ion conductors. Their ionic conductivity ranges from 10^{-6} to 10^{-3} S/cm depending on the composition. It was found that Li_2S_x-P_2S_5 can react with lithium metal to form a solid electrolyte of lithium thiophosphate at the surface of lithium metal. This solid electrolyte conducts lithium ions while it blocks the access of polysulfide to the lithium. Because the polysulfide shuttle phenomenon is more severe at low cycling rates than at high rates, the cell was intentionally cycled at a low rate of 0.1 C to demonstrate the protection of lithium metal through this solid electrolyte coating. Shown in Figure V - 67a is the voltage profile of the first cycle. The discharge curve has two plateaus at 2.4 and 2.0 V, corresponding to the reduction of long chain polysulfides (sulfur atoms greater than 4) and short chain polysulfides (sulfur atoms less than 4), respectively. The ratio of the first plateau to the second plateau is exactly 1:3. The same ratio of the high to low plateaus was found in the charging curve. The constant ratio of 1:3 of these plateaus at both charging and discharge cycles proves that the polysulfide shuttle has been completely blocked by this solid electrolyte coating on the surface of lithium metal. The coulombic efficiency shown in Figure V - 67b is above 98% for all cycles. The energy efficiency is about 90% at 0.1 C. Capacity decay during cycling was still present. It is known that the capacity decay is caused by the precipitation of Li_2S in the liquid electrolyte.

Sample Transfer Stage. A new sample transfer stage has been developed for taking samples from a glove box to a scanning electron microscope (SEM) without exposure to air and moisture. The transfer stage operates by the difference of pressure inside and outside the SEM chamber: when a sample is loaded in a glove box and exposed to a slight vacuum, the atmospheric pressure pushes the lid against the o-ring seal. The sample is protected by the transfer stage as it is moved from the glove box to the SEM. After the sample stage is loaded inside the SEM chamber, the higher vacuum causes the lid to pop open, thus exposing the sample for imaging. This sample stage enables the analysis of lithium anodes after battery cycling.

Conclusions and Future Directions

Because of the poor electronic conductivity of sulfur, the high surface area carbon is the enabler of achieving the maximum utilization of sulfur under electrochemical cycling. The porosity is important for the retention of capacity. With the same sulfur loading, excess pore volume accommodates liquid electrolyte and facilitates the mass transport of lithium ions. Physical adsorption by porous carbon is insufficient to completely eliminate the polysulfide shuttle.

Electrolyte additives have the potential to accelerate the electrochemical cycling of the sluggish Li_2S. The compatibility of additives with cell components is the major issue of using additives. Organic additives could have problems with lithium anode that have not been previously recognized. Phosphorous sulfide is an excellent additive for Li-S batteries. The exact mechanism is unknown. Further investigation in this direction is needed.

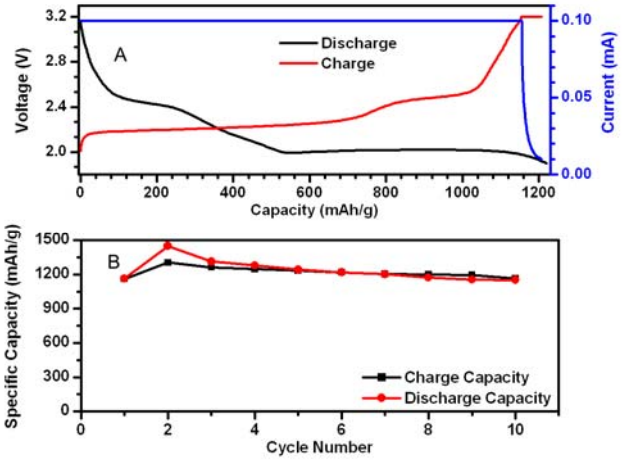

Figure V - 66: (a) Voltage profiles of Li-S cell with phosphorous sulfide additive. (b) cycling performance at 0.1 C in 1m LiTFSI.

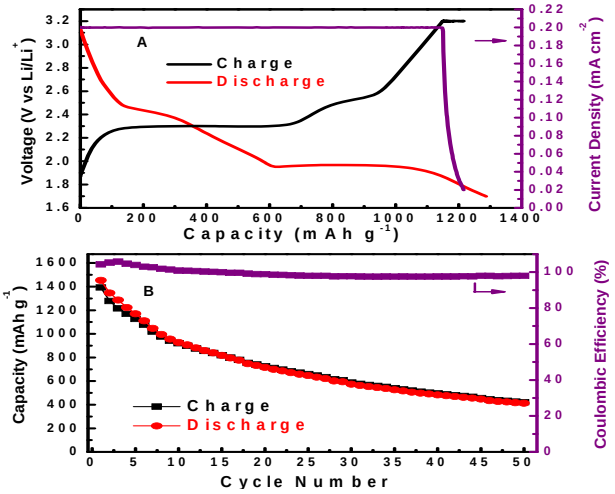

Figure V - 67: (a) Voltage profile of first charge/ discharge cycle of Li-S cell with a pre-formed SEI on Li anode. (b) coulombic efficiency and cycling performance of the cell after the blockage of polysulfide shuttle.

Protecting the lithium anode by sulfide-based solid electrolytes can efficiently block the polysulfide shuttle but the sluggish electrochemical cycling of Li_2S is still a problem for capacity retention. Diagnosis of lithium anode after cycling is necessary. A transfer stage for air-sensitive materials has been developed for the diagnosis of Li-S cells under SEM.

Future research will focus on the phosphorous sulfide-based electrolyte additives. The immediate next step will be the investigation of the long-term stability of the phosphorous sulfide additives. The mechanism of the additive effect will be studied in detail for the purpose of guiding the search of additives. The protection of the lithium anode will be studied intensively. Ultimately, the success of lithium anode protection will not only benefit the Li-S battery but also all other batteries which use lithium metal as the anode. Because of the dissolution of the sulfur species in the electrolyte, the cathode in Li-S batteries is considered a "liquid" electrode. Novel cell configurations will be explored to investigate the feasibility of Li-S in large format batteries for EV and PHEV applications.

FY 2011 Publications/Presentations

1. Zengcai Liu, Wujun Fu, Chengdu Liang (2011) "Lithium Sulfur Batteries". In "Handbook of Battery Materials" John Wiley & Sons, Ltd.

2. J.Y. Howe, L.A. Boatner, J.A. Kolopus, L.R. Walker, C. Liang, N.J. Dudney, and C.R. Schaich, "Vacuum-tight sample transfer stage for a scanning electron microscopic study of stabilized lithium metal particles", J. Mater. Sci., Mater. Res. online, Oct. 2011, DOI: 10.1007/s10853-011-6029-z
3. "Carbon/Sulfur Nanocomposites and Additives for High-Energy Lithium Sulfur Batteries," 2011 DOE Annual Peer Review Meeting Presentation, May 2011.
4. "Advanced Materials for Li-S Batteries," 4th Symposium on Energy Storage: Beyond Lithium Ion, Pacific Northwest National Laboratory, June 8, 2011
5. "Challenges and Solutions for Lithium-Sulfur Batteries," 4th US-China Electric Vehicle and Battery Technology Workshop, Argonne National Laboratory, Aug 4, 2011
6. "Sulfur-Carbon, Sulfide-Carbon Composites, and Electrolyte Additives for Lithium Sulfur Batteries," 220th ECS Meething, Boston, MA, Oct. 9-14, 2011.
7. "Solid electrolytes to enable lithium, lithium-sulfur, and lithium-air batteries," 220th ECS Meething, Boston, MA, Oct. 9-14, 2011.
8. "Mesoporous carbon/sulfur composite cathode for lithium batteries," 220th ECS Meething, Boston, MA, Oct. 9-14, 2011.
9. "Li_2S-P_2S_5 Solid Electrolytes for Lithium Ion and Lithium Sulfur Batteries," 220th ECS Meething, Boston, MA, Oct. 9-14, 2011.

Acknowledgment

This research at Oak Ridge National Laboratory, managed by UT Battelle, LLC, for the U.S. Department of Energy under contract DE-AC05-00OR22725, was sponsored by the Vehicle Technologies Program for the Office of Energy Efficiency and Renewable Energy. Parts of this research were performed at DOE user facilities including the Center for Nanophase Materials Sciences, the High Temperature Materials Laboratory, and the Shared Research Equipment (SHaRE) user facility.

V.B.13 Studies on the Local State of Charge (SOC) and Underlying Structures in Lithium Battery Electrodes (ORNL)

Jagjit Nanda (PI)
Materials Science and Technology Division
Oak Ridge National Laboratory
Oak Ridge, TN 37934
Phone: (865) 241-8361; Fax: (865) 574-4066
E-mail: nandaj@ornl.gov

Postdoctoral Worker: Dr. Surendra Martha
Industrial Collaborator: Dawn Bernardi and Andy Drews, Ford Motor Co.

Start Date: October 2010
Projected End Date: December 2013

Objectives

- Combined micro-Raman-AFM study of Li-ion electrodes subjected to various SOC's and stress cycles
- Understand cycle life and voltage depression issues in Li-rich NMC compositions and correlate the electrochemical performance with microstcructral phase changes

Technical Barriers

- Poor cycle life, structural stability, rate limitation and loss of energy due to voltage suppression during cycling. The Li-rich compostions also have very high 1st cycle irreversible capacity loss upon high voltage cycling.

Accomplishments

- Monitored SOC variation on the surface of commercial NCA electrodes as a function of SOC.
- Doubled the rate performance for Li-rich MNC from Toda.
- Conducted electrochemical benchmarking of Li-rich composition voltage suppression.

✧ ✧ ✧ ✧ ✧

Introduction

State of charge (SOC) of a battery is a macroscopic indicator of the amount of stored energy and is often used as a diagnostic tool for observing battery performance. The microscopic origin of the SOC in connection to Li-ion electrodes is related to the local lithium content in individual electrodes particles. However, electrodes for Li-ion are composite materials comprised of active electrode material, polymeric binders and carbon diluents. At an electrode level, the local SOC could be non-uniform. Such variations could then become more noticeable as the cell degrades resulting in power fade and/or capacity fade. Understanding the spatial variation of SOC on the electrode surafce therefore could provide a microscopic picture of the degradation occurring at a local scale. The other aspect of our study relates to understanding the electrochemical performance of the high voltage Li-rich MNC composition and correlating it to microstructural changes during cycling.

Approach

We have undertaken *ex situ* Raman mapping of electrodes which have been electrochemically cycled under different conditions. Utilizing a particle level SOC, we obtained a SOC Raman map showing their distribution at a micron length scale. The *ex situ* SOC map is expected to change as we cycle the electrodes at different rates and under extreme duty cycle conditions. This provides a statistical means for studying the micron scale SOC variation of commercially fabricated electrodes. The studies will provide key failure modes at the electrode (or materials) level that has impact on the cycle life of the Li-ion cell. Apart from these we also measure and benchmark electrochemcial performance of various capacity and high voltage cathode compostion and correlate those with microstrcutral analysis and degradation.

Results

SOC maps using confocal Micro-raman measurement of cycled electrodes. We first report the *ex situ* SOC analysis undertaken on production-ready commercial $LiCoNiAlO_2$ (NCA) electrodes obtained from SDI, Korea through our industrial collaborator Ford Motor Co. Part of the work was done at their Research and Innovation Laboraty and SOC analysis was carried out at ORNL. The NCA electrodes were left in a charaged state using a CCCV protocol and the difference of the surface SOC Raman maps were compared in Figure V - 68. The SOC distributions across the electrode were analyzed using a histogram analysis.

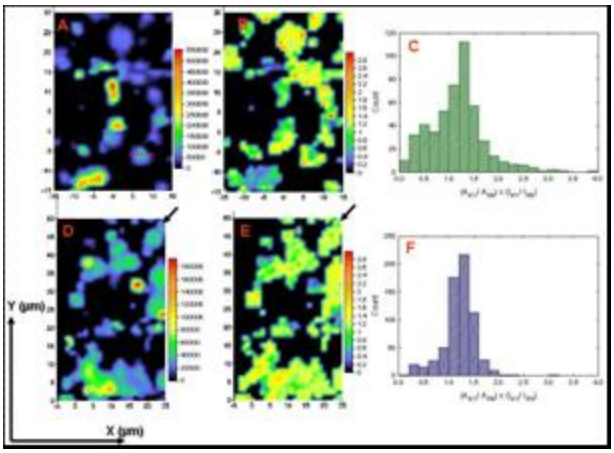

Figure V - 68: Raman maps showing local SOC varition across NCA electrodes cycled at 4.1 V under constant current condition at 3C with 1 hour PS. SOC plots show the local inhomogeneity across the electrode surface and could vary under electrochemical conditions.

Using a similar approach, we also undertook Raman mapping of high voltage Li-rich MNC composite cathodes under both cycled as well as pristine electrode conditions. Figure V - 69 shows the micro-Raman mapping/imaging of the pristine $Li_{1.2}Ni_{0.175}Co_{0.1}Mn_{0.525}O_2$ electrode showing the carbon and active material region at a micrometer resolution. We are currently comparing the SOC Raman maps with cycled Li-rich MNC electrodes.

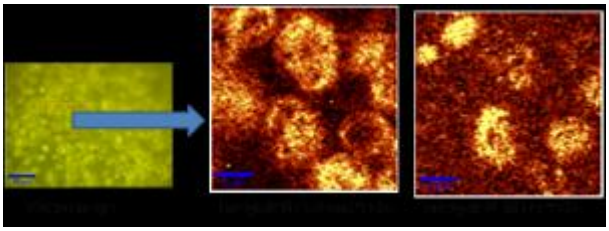

Figure V - 69: Micro-Raman mapping of the pristine $Li_{1.2}Ni_{0.175}Co_{0.1}Mn_{0.525}O_2$ electrode

Electrochemical benchmarking of Toda's high voltage Li-rich MNC composition. We have investigated the high voltage cycling performance of the excess Li MNC composition. Figure V - 70 and Figure V - 71 show the capacity versus the cycle number and the discharge voltage profiles at successive cycles. The typical compositions of these electrodes were 85 % active material, 6 % carbon black, 1.5 % carbon nanofibers (CNF) and 7.5% PVDF. They were cycled up to 4.9V using standard 1.2M $LiPF_6$/ EC-DMC (1:2 w/w). The bare $Li_{1.2}Ni_{0.175}Co_{0.1}Mn_{0.525}O_2$ composition showed a gradual capacity loss when cycled over 200 cycles (about 3.5 %) at 4.9 V. The CNF was used to improve the rate performance. (see next section).

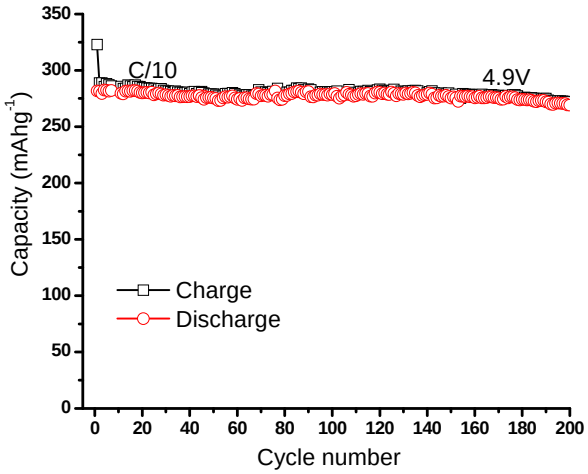

Figure V - 70: Capacity as a function of Cycle number for pristine $Li_{1.2}Ni_{0.175}Co_{0.1}Mn_{0.525}O_2$ with 1.5 wt% CNF

Figure V - 71 includes the first charging profile showing the high voltage plateaus at 4.5 V responsible for the higher capacity. The discharge profiles are shown at the end of 1, 5, 50 and 200 cycles. With successive cycling the discharge profile shifts to lower voltage indicating loss of energy, although the total capacity remains the same. This is an important technical barrier that needs to addressed or understood before moving forward for using this material for EV application. Literature results on similar compositions point to complex structural transitions during higher voltage charge-discharge as a possible loss of the voltage profile.

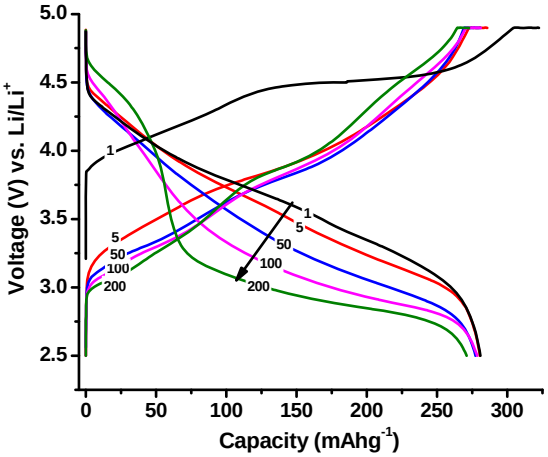

Figure V - 71: Voltage profile at 1st, 5th, 50th, 100th and 200th cycles.

Rate Performance. In order to address the issue of rate performance, we have for the first time reported an increase of about a factor of two rate capability of the excess Lithia composition by addition of a nominal amount of highly graphitic carbon nanofiber, CNF (1.5 wt%). In Figure V - 72 we show the comparison of the capacity and rate performance up to 100 cycles between the CNF electrode and the standard electrode composition

mentioned above. Figure V - 72a shows the improvement in the cycle life performance between the two. As shown in Figure V - 72b the rate performance improved a factor of two due to an overall increase of the electronic conductivity of the matrix due to addition of highly conducting CNF. Notably, after the 5C rate discharge going back to the C/5 rate; we continue to see good capacity retention for the CNF electrode whereas the standard composition showed decay with cycling. This shows that CNF additives serves as an electronic wiring around the Li-rich MNC particles improving the electronic conduction pathways to improve both rate performance and capacity retention.

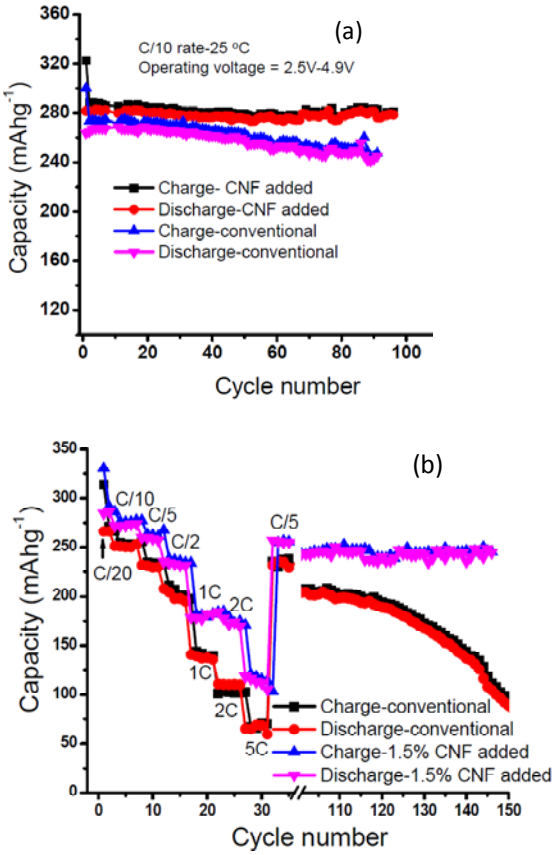

Figure V - 72: (a) Cycle life comparison between standard binder carbon black composition and with CNF addition and (b) the corresponding rate performance comparison.

Cyclic Voltammetry and Surface Studies. One of the key aspects here is to understand the origin of the first cycle irreversible capacity loss of the Li rich composition $Li_{1.2}Ni_{0.175}Co_{0.1}Mn_{0.525}O_2$ and to identify the electrochemical redox processes during the high voltage cycling. To this effect, we carried out detailed cyclic voltammetry (CV) studies at various scan rates. Figure V - 73 shows the first cycle anodic and cathodic peaks corresponding to Mn, Ni and Co red-ox transitions (shown as red dashed line). The second through fifth CV curves are shown as solid lines. The first cycle excess capacity obtained as a result of activation of Li_2MnO_3 (> 4.5 V) is illustrated by the large peak. This feature understandably disappears after the first cycle charging cycle, after the formation of MnO_2. The inset figure shows the CV cycles at a lower scan rate (25 mV S^{-1}) showing explicit contribution of Mn, Ni and Co to the overall capacity. We have also undertaken surface studies using X-ray photoelectron spectroscopy and Micro-Raman to identify various surface decomposition products during the high voltage cycling (results not shown here).

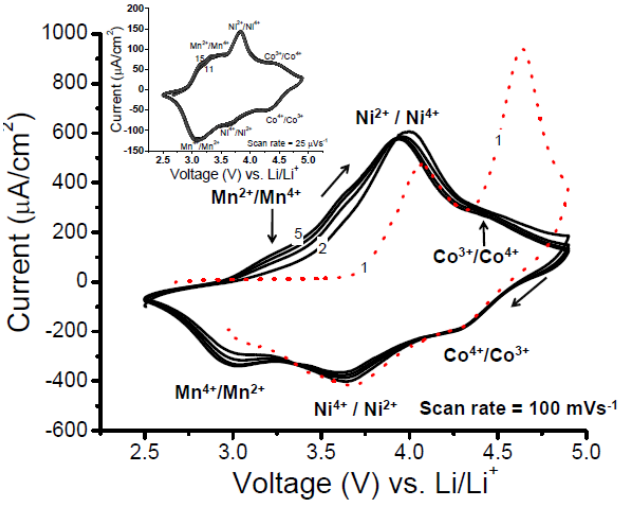

Figure V - 73: CV studies on $Li_{1.2}Ni_{0.175}Co_{0.1}Mn_{0.525}O_2$. first cycle anodic and cathodic peaks shown as red dashed line, the second through fifth CV curves are shown as solid lines.

Conclusions and Future Directions

We are undertaking detailed high resolution electron-microscopy at various SOCs of the Li-rich MNC composition to correlate the structural changes as the voltage profile changes from a layered-layered phase to a mixed layered-spinel type structure (low voltage). Experiments are also in progress to coat the Li-rich MNC with a nanometer thick solid electrolyte, LIPON, to reduce or minimize the side reaction at the surface due to high voltage cycling. We notice a dramatic enhancement of the electrchemcial performance. Full cell studies using Li-rich and carbon as positive and negative electrode material are in progress.

FY 2011 Publications/Presentations

Journal Publications

1. J. Nanda, J. T. Remillard, A. O'Neill, D. Bernardi, Tina Ro, Ken Nietering, Ted J. Miller, "Observation of Local State of Charge Distributions in Lithium-ion Battery Electrodes", Adv. Funct. Mater. 2011, 21, 3282–32900.

2. S. K. Martha, J. Nanda, Gabriel M. Veith, N. J. Dudney, Electrochemical and Interfacial Studies of High-Voltage Lithium-Rich Composition: $Li_{1.2}Mn_{0.525}Ni_{0.175}Co_{0.1}O_2$, J. Power Sources in press 2011.
3. V. Varadaraajan, Satishkumar B. C., J. Nanda and P. Mohanty, "Direct Synthesis of Nanostructured V_2O_5 Films using Solution Plasma Spray Approach for Lithium Battery Applications", J. Power Sources, 2011, 196, 10704

Conference Presentations

1. 2011 DOE Annual Peer Review Meeting Presentation, May 2011Washignton DC.
2. S. K. Martha, J. Nanda, W. D. Porter, N. J. Dudney, "Electrochemical and Interfacial Studies of High-Voltage Lithium-Rich Composition: $Li_{1.2}Mn_{0.525}Ni_{0.175}Co_{0.1}O_2$" MRS Spring Meeting 2011 San Francisco, 2011.
3. Jagjit Nanda, "High Energy Density Li-ion Electrodes: Current Status and Challenges" Battery Congress 2011, University of Michigan Ann Arbor

V.B.14 New Cathode Projects (LBNL)

Venkat Srinivasan
Lawrence Berkeley National Laboratory
1 Cyclotron Rd. MS62R0203
Berkeley, CA 94720-8168
Phone: (510) 495-2679
Fax: (510) 486-4260
E-mail: vsrinivasan@lbl.gov

Start Date: January 2012
Projected End Date: December 2016

Introduction

The FY 2011 Batteries for Advanced Transportation Technologies (BATT) Request for Proposals entitled "Novel Cathode Materials for High-energy Lithium Batteries" has resulted in four new projects that can help accelerate the application of such batteries in plug-in hybrid electric vehicles and electric vehicles. These projects focus on developing next-generation cathodes to increase the energy and decrease the cost of lithium-ion batteries while maintaining safety and cycle life.

Approach

The BATT program received 102 white papers and encouraged 28 applicants to submit full proposals. A selection committee composed of leading battery experts reviewed each proposal and recommended four for funding. In addition, some national lab researchers have been asked to submit another proposal directly to DOE for further consideration. DOE headquarters reaches funding decisions based on a peer review process, while maintaining and strengthening the national laboratory research capability.

Results

The awardees include three national laboratories and one university and are listed below, along with a brief description of their projects. The total requested funds are $5.81 million over four years.

High Capacity Composite Cathode Materials: New Synthesis Routes and Structures, Argonne National Laboratory. Li_2MnO_3-stabilized composite electrode structures, such as 'layered-layered' $xLi_2MnO_3\cdot(1-x)LiMO_2$ (M=Mn, Ni, Co) systems are receiving attention because they can provide capacities between 200 and 250 mAh/g between 4.6 and 2.0V vs. Li. These manganese-rich composite cathode structures have to be electrochemically activated above 4.4V in order to access the high capacity. Unfortunately, this process compromises the rate capability of these electrodes, which also suffer from voltage decay on cycling, thereby compromising the energy and power output of the cells and preventing their implementation in practical systems. This proposal addresses these limitations and challenges. A novel processing route using Li_2MnO_3 as a precursor to synthesize composite electrode structures is advocated, which is based on promising results obtained over the past few months. The technique is simple, versatile and seemingly low cost; it offers the possibility of opening the door to wide exploitation and, in particular, of synthesizing and tailoring composite electrode structures, including new systems, thereby enhancing the electrochemical properties of Li-ion cells to meet the performance targets of PHEVs.

***In situ* Solvothermal Synthesis of Novel High Capacity Cathodes, Brookhaven National Laboratory.** The development of high energy density, low cost Li ion electrodes will require improved understanding of the electrode preparation reactions in order to achieve control over material properties. In this effort we will develop and utilize *in situ* reactors designed to investigate solvothermal synthesis reactions in real-time using synchrotron techniques. This capability will allow us to identify intermediate or transient phases and better control phase nucleation, reaction rates and material properties. The following classes of high-energy materials will be investigated: (1) Li metal borates ($LiMBO_3$, M = Mn and Fe); (2) copper fluorides (CuF_2); (3) copper-vanadium oxides (CuV_3O_8); and (4) carbonophosphates and carbonofluorosulphates ($Li_3M(CO_3)PO_4$, $Li_3M(CO_3)SO_4F$ where M = Mn and Fe). Progress will be evaluated at the end of the second year with an up- or down-selection to continue research on those systems showing potential for achieving targets. The project deliverable is a reversible cathode with an energy density ≥700 Wh/kg, although these materials have the potential for much greater energy densities (e.g., 1400 Wh/kg).

Lithium-bearing mixed polyanion (LBMP) glasses as cathode materials, Oak Ridge National Laboratory. Li-bearing mixed polyanion (LBMP) glasses will be developed as cathode materials for Li ion batteries for use in EV applications. The composition of LBMP glasses can be tailored to provide higher electrical conductivities, higher redox potentials, and higher specific energies than similar crystalline polyanion materials. The disordered covalently bonded structures of LBMP glasses could provide excellent cycleability and safety. In addition, LBMP glass compositions may enable cycleable multi-valent changes in the transition metal cations, providing

the potential to provide specific energies of 1000Wh/kg. The experimental approach combines: (1) structure and property modeling, (2) glass processing, (3) glass characterization, (4) conventional cathode production, and (5) electrical and electrochemical testing. Computer modeling will be used to suggest the most promising LBMP glass compositions in terms of electrochemical performance and glass processing capability. Classical heat-quench glass forming and sol gel processing will be used to make the LBMP glasses. Electrical conductivity and glass uniformity are key properties that will be measured. Conventional cathodes will be made and electrochemical performance will be demonstrated in coin cells with LBMP glass cathodes.

High-capacity, High-voltage Cathode Materials for Lithium-ion Batteries, University of Texas at Austin. This project will design and develop materials based on polyanions that may cycle more than one Li ion per transition metal ion and/or operate above 4.3 V. Specifically, the high-capacity systems to be investigated are Li_2MSiO_4 (M = Mn, Fe, Co, Ni, and VO) with a theoretical capacity of ~ 330mAh/g and $Li_2MP_2O_7$ (M = Mn, Fe, Co, Ni, and VO) with a theoretical capacity of ~ 220mAh/g. The high-voltage systems to be studied are $LiMPO_4$ with M = Co and Ni, which operate at 4.8 and 5.1V, respectively, with capacities of ~ 170 mAh/g. Additionally, $Li_3V_2(PO_4)_3$ with a theoretical capacity of ~ 200mAh/g and an operating voltage between 3.6 and 4.6V and $Li_9V_3(P_2O_7)_3(PO_4)_2$ with a capacity of ~ 260mAh/g and an operating voltage between 3.6 and 4.8 V will be explored. However, synthesis and processing conditions play a critical role in realizing the full capacities of these polyanion cathodes. For example, we have shown that more than one Li ion could be reversibly extracted from carbon-coated nanostructured Li_2MSiO_4 (M = Fe and Mn) synthesized by a microwave-solvothermal (MWST) approach. We plan to extend this approach to other systems. The major issue with the high-voltage (> 4.5 V) cathodes is the chemical instability of the cathode electrolyte interface. We have shown that the 4.8 V spinel $LiMn_{1.5}Ni_{0.42}M_{0.08}O_4$ (M = Fe and Ga) exhibits good cyclability even with conventional electrolytes due to a self-segregation of Fe and Ga ions to the surface during synthesis, providing a robust cathode-electrolyte interface. We plan to adopt a similar surface-segregation strategy to improve the cyclability of the high-voltage polyanion cathodes.

V.C Anode Development

V.C.1 Nanoscale Composite Hetero-structures: Novel High Capacity Reversible Anodes for Lithium-ion Batteries (U Pitt)

Prashant N. Kumta

Swanson School of Engineering,
Departments of Bioengineering, Chemical and Petroleum Engineering, Mechanical Engineering and Materials Science,
University of Pittsburgh, Pittsburgh, PA 15261
Phone: (412)-648-0223; Fax : (412) 624-8069
E-mail: pkumta@pitt.edu

Start Date: January 1, 2011
Projected End Date: December 31, 2011

Objectives

- Identify new alternative nanostructured anodes to replace synthetic graphite providing higher gravimetric and volumetric energy densities.
- Similar or lower irreversible loss (≤15%) in comparison to synthetic graphite.
- Similar or better coulombic efficiency (>99.9%) in comparison to synthetic graphite.
- Similar or better cyclability and calendar life in comparison to synthetic graphite.
- Improve the coulombic efficiency, available energy density, rate capability and cycle life of high specific capacity Si based electrodes.
- Investigate nano-structured (*nc*-Si) and amorphous Si (*a*-Si) based composite or hybrid heterostructured anode.

Technical Barriers

The important technical barriers of alternative anodes for lithium ion batteries to be used in electrical vehicles or hybrid electrical vehicles are the following:

(A) Low energy density

(B) Large first cycle irreversible loss (ICL) (>25-30%)

(C) Inadequate coulombic efficiencies

(D) Poor cycle life

(D) Poor rate capability

(E) Low charge/discharge rates

Technical Targets

- Synthesize nano-structured (*nc*-Si) and amorphous Si (*a*-Si) based composite or hybrid structured anodes using cost effective processing techniques.
- Achieve reversible capacity of ~1000-1200 mAh/g.
- Reduce first cycle irreversible loss to less than ~15%.
- Improve coulombic efficiencies higher than 99.5%.
- Improve the rate capability.
- Characterize the nano-scale hetero-structures for structure and composition using electron microscopy techniques such as SEM, TEM and HREM.
- Investigate the origin and characterize the solid electrolyte interphase (SEI) layer.

Accomplishments

- Synthesized cost effective chemical and solid state approaches to nanostructured or amorphous Si based composites.
- Synthesized binder free electrodes using nanocrystalline Si and vertically aligned carbon nanotube (VACNT) hybrid nanostructures by simple, cost effective two step liquid injection CVD processes directly on INCONEL 600 alloy.
- Binder free Si/VACNT heterostructured anode exhibited a specific capacity in excess of ~1500 mAh/g and excellent rate capability.
- Identified conductive additives or conductive coatings (CA) on Si/C based anode materials to generate Si/C/CA nanocomposites with improved coulombic efficiency and rate capability.
- Synthesized nanocrystalline Si, graphite based nanocomposite (*nc*-Si/C/) containing additives by high energy mechanical milling exhibiting excellent cyclability (0.1-0.2% capacity loss/cycle), lower irreversible loss and high coulombic efficiency (~99.9%) with a specific capacity exceeding ~800 mAh/g.
- Synthesized amorphous Si films directly on Cu-foil by electrochemical reduction of silicon-salts which

exhibit reversible capacity ~1300 mAh/g with excellent stability.

- Explored novel thermoplastic (elastomeric) binders to improve the mechanical integrity of the electrode with improved cyclability of Si based composite structure.
- The novel Si/C composite and *nc*-Si/CNT hybrid nanostructures exhibit less than 20% first cycle irreversible loss.

✧ ✧ ✧ ✧ ✧

Introduction

Achieving the DOE-BATT technical targets will require improving the cycling stability, reduced irreversible loss, and improved coulombic efficiency and rate capability of Si based anodes. Hence it is essential to synthesize Si based composites using economical processes exhibiting excellent mechanical properties to endure the large cycling induced volumetric stresses of Li-Si alloys. In 2009, we conducted a systematic investigation of the electrochemical properties of HEMM derived Si/C based composite anodes. These HEMM derived composite anodes synthesized using polymer additives displayed a reversible capacity ~800 mAh/g or higher with a 0.01-0.03% capacity fade per cycle. Scale-up efforts to generate these novel composites are currently in progress; while efforts to further improve the capacities and other important electrochemical properties of these systems are also on-going. In addition, collaborative efforts to understand the SEI layers have been conducted with Dr. Kostecki and Dr. Battaglia at LBNL. Although Si/C based composites exhibiting capacity in excess of ~1000 mAh/g have been generated by HEMM, the system is commercially unsuitable due to high capacity fade of more than 0.2% per cycle. In order to improve the stability of Si/C based composite anodes, carbon nanotubes (CNTs) have been selected over graphite as a matrix. In 2010, a detailed investigation of Si/CNT hybrid structures was reported [1]. The CNTs possess some unparalleled attributes such as good electronic conductivity, high aspect ratio, structural flexibility, and tortuosity. Exploitation of these unique CNT attributes combined with its nano-scale dimensions will enable the generation of a nano-scale conductive network improving the electrical contact between the active Si particles. The Si/CNT hybrid structures exhibit high reversible capacity while also displaying excellent cyclability up to 50 cycles. However, the HEMM derived system exhibited larger than 25% ICL and/or low coulombic efficiency. The CVD derived Si/C nano-composite anode also shows a low coulombic efficiency (~98-99%) albeit a low irreversible loss (8-12%) in contrast. Thus for the Si/C nano-composite anode of capacity higher than ~1000 mAh/g to be commercially viable, the ICL should be lower than 15% and a coulombic efficiency in excess of 99.8%. In this regard, the present work was aimed at reducing the ICL below 20% and improving the coulombic efficiency above 99.8% for HEMM derived or CVD derived *nc*-Si/C composite by alloying with conductive additives, coating with conductive layers and generating novel microstructures such as hard "core-shell" morphologies. Synthesis of amorphous Si directly on copper foil by electrochemical reduction of silicon salts has also been performed. In addition, studies were also conducted to identify new binders for Si/C composites. PVDF, a commonly used binder in graphite electrodes is not ideal for Si based anodes because of its inability to endure the huge volumetric changes occurring during Li alloying and de-alloying. New high strength and elastomeric binders are needed to preserve the mechanical integrity of the electrode.

Approach

To meet the technical targets, our approach is to explore inexpensive Si and C based composite or hybrid nano-structured electrodes exhibiting 1) an electrochemical potential a few hundred mV above the potential of metallic Li, and 2) a capacity of at least ~1000 mAh/g or higher. To achieve these goals, we focused on exploring novel low cost approaches to generate nano-scale hetero-structures comprising nano-structured Si or amorphous Si and a variety of carbons derived from graphitic carbon as well as CNT. The Si/C composite has been coated or alloyed using various conductive metals as well as a variety of conductive layers to form Si/C/CA nanocomposites with improved rate capability, coulombic efficiency, and structural stability. In order to improve the structural integrity of the Si/C based electrode, which undergoes mechanical disintegration during long term cycling, a preliminary study has been conducted to identify high strength elastomeric binders for Si/C composites electrode. A detailed study of these Si/C based composite anodes has been recently presented at the 2011 DOE annual review.

A cost effective simple two-step CVD processes has been employed to synthesize binder free hybrid *nc*-Si/VACNT nano-structured electrodes on INCONEL 600 alloy. The vertically aligned carbon nanotubes (MWNT) were first synthesized on INCONEL 600 using xylene and ferrocene serving as the carbon and iron catalyst sources, respectively. Deposition of nanostructured Si on VACNTs has been achieved by cracking SiH_4 in the temperature range of 723K-1023K. Under the experimental conditions used, the CNTs grow perpendicular to INCONEL covered with Si nano-clusters deposited directly on VACNT at defined spacing. Si/C composite with conductive additives has been synthesized by HEMM of a mixture of graphite, silicon and additives with suitable polymers. The milled powder was thermally treated at 573K to generate C/Si composite containing the additives. In addition, conducting

layers have been coated on the Si/C composite anode derived from HEMM using electro less coating processes. Two new types of polymers of different molecular weight have been developed as a suitable binder for Si/C composite anode. Attempts were also made to synthesize amorphous Si films directly on copper foil by electrochemical reduction of silicon salt based electrolyte. Typical electrolyte comprises 0.5 M the Si-salt dissolved in propylene carbonate (PC) and tetrabutylammonium chloride (TBACL) used as supporting electrolyte to improve the ionic conductivity. A three electrode set up was used utilizing Cu foil of 11mm diameter as the working electrode. A Pt foil and wire served as counter and reference electrodes, respectively.

These promising systems were tested in half cells using metallic lithium as both counter and reference electrodes. Rate capability, long term cyclability, including origin and state of the SEI layers were investigated.

Results

Binder free Si/CNT hybrid nanostructures synthesized by CVD techniques on INCONEL 600. The long term cycling data (Figure V - 74) of binder free *nc*-Si/VACNT electrodes, comprising 54wt. % nanocrystalline Si deposited on VACNTs grown in INCONEL, shows a 1st discharge capacity of ~1870 mAh/g with a low irreversible loss (~16%). The rate capability study of *nc*-Si/VACNT performed at 100 mA/g (C/15), 200 mA/g (C/7) and 400 mA/g (C/3.5) shows a capacity retention of ~1350 mAh/g after 30 C/15 cycles ~1000 mAh/g after 60 C/7 cycles and ~700 mAh/g after 90 C/3.5 cycles. The capacity fade is a reflection of poor interface between Si and CNT which can be improved by engineering the interface. These studies are currently ongoing in order to improve the stability of the electrode.

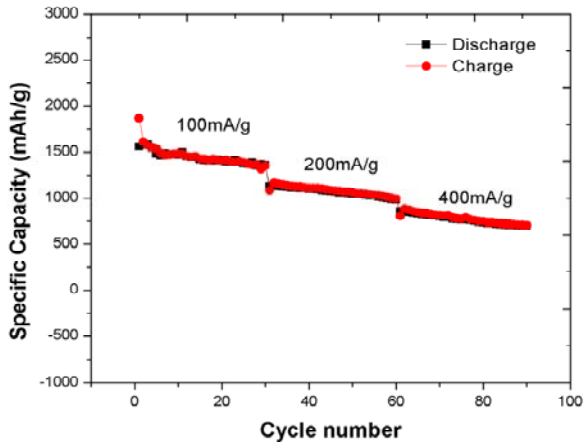

Figure V - 74: Variation of specific capacity vs. cycle numbers of nc-Si/CNT on INCONEL 600 cycled at a current rates of 100 mA/g, 200 mA/g and 400 mA/g.

Synthesis of Si/C/CA nanocomposites by HEMM. The cycling response of the C/Si/CA nano-composite, obtained by HEMM followed by thermal treatment at 773K, cycled for 30 cycles at ~C/5 rate, displayed in Figure V - 75, shows a 1st cycle discharge capacity of ~1020 mAh/g and a 1st cycle charge capacity of ~800 mAh/g with an irreversible loss ~20%. The composite shows excellent capacity retention with a 0.1% loss per cycle up to 30 cycles and an coulombic efficiency of ~99.84%. These results indicate the beneficial influence of the conducting additive (CA) to reduce the irreversible loss and improve the coulombic efficiency in contrast to microcrystalline Si/C which display higher ICL (≥ 30%) and lower coulombic efficiency (~99.4-99.5%). In order to understand the effect of the additive, preliminary electrochemical impedance spectroscopy (EIS) measurements have been conducted. It has been identified that the charge impedance decreases with addition of the additive which indicates a reduction in the charge transfer resistance of the composite electrode and a relatively stable SEI. The results will be fitted to an equivalent circuit model in the near future to understand the variation of SEI film resistance, charge transfer resistance and interphase electronic contact resistance with voltage and cycle number. The effect of additives to lower the irreversible loss and improve the coulombic efficiency will be studied in detail and reported in the near future.

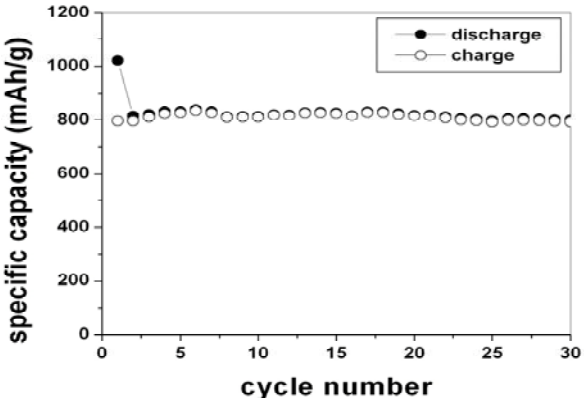

Figure V - 75: Variation of specific capacity vs. cycle number of C/Si/CA composite cycled at C/5 rate.

Novel Thermoplastic binders. New polymeric high strength binders denoted as Binder-1 and Binder-2 were developed which exhibit better electrode stability (Figure V - 76) than PVDF for the Si/C system. In the case of polymer 1, a citric acid and KOH based buffer (pH=3) was used as the solvent to enhance coupling of the hydroxyl ions present on Si to the polymer.

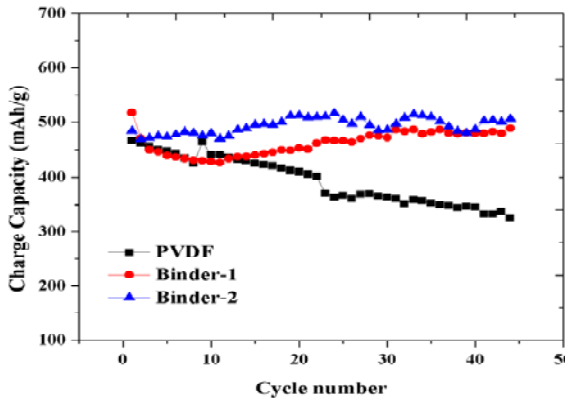

Figure V - 76: Charge capacities of Si/C based composite using PVDF, and the two novel polymer binders.

Synthesis of amorphous Si films directly on copper foil by electrochemical reduction of silicon salts. Formation of amorphous Si film on copper foil, obtained by electrochemical reduction of silicon salts, has been confirmed from Raman spectroscopy and scanning electron microscopy (SEM). A broad peak at ~ 485 cm^{-1} was observed in the raman spectrum which is characteristic of *a*-Si. No sharp peak at 520 cm^{-1} corresponding to crystalline silicon was observed indicating that the deposited films were mostly amorphous. The amorphous silicon (*a*-Si) films were electrochemically charged and discharged at ~400 mA/g current to evaluate their potential as suitable anodes for Li-ion batteries. As shown in Figure V - 77, a first discharge capacity of ~3400 mAh/g was obtained with an ICL of 60% probably due to impurities arising from the chemical reduction of the supporting electrolyte used and the expected surface oxidation of the amorphous Si. Efforts are in place to reduce it to the desired 15% level.. However, after the 1st cycle, a stable reversible capacity of ~1300 mAh/g was obtained. The columbic efficiency varied from 94% to 98% from 2nd to 5th cycle, after which it improved and remained close to the desired goal of 99.9% for the remaining cycles. A capacity fade of ~0.016% per cycle was observed resulting in a capacity of ~1260 mA/g at the end of the 100th cycle. This approach of developing thin *a*-Si films directly on Cu eliminates the use of binders and conducting agents, rendering the process simple, facile, and amenable to large scale manufacturing.

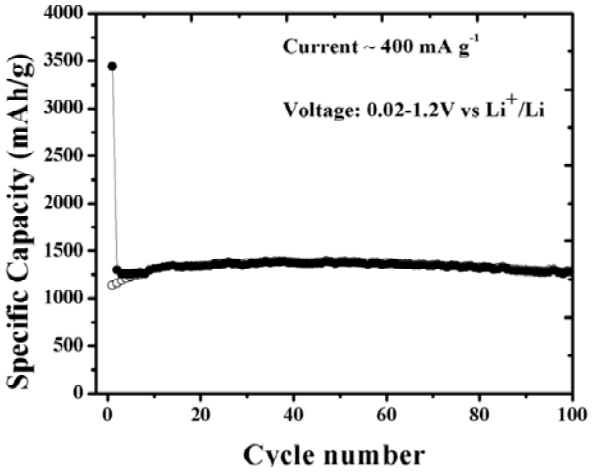

Figure V - 77: Cycling data for the deposited amorphous film cycled at ~400 mA/g.

Conclusions and Future Directions

The *nc*-Si/C composites synthesized by cost effective processing techniques such as HEMM, CVD, chemical reduction or electrochemical reduction processes exhibit a high reversible capacity of ~800-2000 mAh/g. However, the Si/C nanocomposite synthesized by these techniques show high ICL, low coulombic efficiency or limited structural stability depending on the synthesis procedure. In order to improve the coulombic efficiency, rate capability, or long term structural stability, various coatings, conducting additives and electronically conducting dopants have been pursued. A unique binder free hybrid Si/VACNTs based nanostructured electrode on INCONEL 600 alloy was synthesized using a simple cost effective CVD approach. The Si/VACNT exhibited a low irreversible loss (~16%), a reversible capacity ~1500 mAh/g and excellent rate capability. Addition of conducting dopants and additive layers with Si/C nanocomposites improved the coulombic efficiency and reduced the irreversible loss. Amorphous Si films obtained by electrochemical reduction of silicon salts shows a reversible capacity ~1300 mAh/g with excellent stability due to the improved adhesion of the deposited Si with the underlying copper foil. High strength thermoplastic and elastomeric binders were developed to improve the capacity retention by minimizing the colossal damage occurring due to the large volume changes upon lithium alloying and de-alloying.

Future work will be dedicated to improve the structural stability and couloumbic efficiency of *nc*-Si/C/CA or Si/CNT hybrid structures using core-shell morphology and developing new elastomeric binders. In addition, scale up activities using Si/C/CA composite and Si/CNT hybrid structures will be initiated and performed. Additionally, chemical reduction and mechano-chemical reduction approaches will be investigated to generate

amorphous Si (*a*-Si) and nano-crystalline Si (nc-Si) that exhibit capacities as high as 2000 mAh/g.

FY 2011 Publications/Presentations

1. W. Wang and P. N. Kumta, "Nanostructured hybrid silicon/carbon nanotube heterostructures: Reversible high-capacity lithium-ion anodes", ACS Nano, 4, 4, (2010), 222-2241.
2. W. Wang, R. Epur and P. N. Kumta, "*Vertically aligned silicon/carbon nanotube (VASCNT) arrays: Hierarchical anodes for lithium-ion battery*" Electrochem. Commu. 13 (2011) 429-432.
3. W. Wang, M. K. Datta, J. Maranchi, S. J. Chung, R. Epur, K. Kadakia, P. Jampani and P. N. Kumta, "*Amorphous silicon–carbon based nano-scale thin film anode materials for lithium ion batteries*" Electro. Acta. 56 (2011) 4717-4723.
4. Presentation at the 2011 DOE Annual Peer Review Meeting.
5. R. Epur, M. K. Datta, W. Wang, J. Maranchi, P. H. Jampani and P. N. Kumta, "Si/C based nanocomposite anodes for Li-ion batteries", 218th ECS meeting at Las Vegas, NV, USA.
6. R. Epur, M. K. Datta, A. Manivannan and P. N. Kumta, "Nanocrystalline Si/C/MWCNT based heterostructured electrodes – High capacity anodes for Li-ion batteries",219th ECS meeting at Montreal, Canada.
7. R. Epur, S. J. Chug, R. Kuruba, A. Manivannan and P. N. Kumta, "Nanocrystalline-amorphous Si composite anode by chemical reduction of Si salts", 220th ECS meeting at Boston, USA.

V.C.2 Interfacial Processes – Diagnostics (LBNL)

Robert Kostecki

Lawrence Berkely National Laboratory
Environmental Energy Technologies Division
1 Cyclotron Road, MS 90-3026D
Berkeley, CA 94720
Phone: (510) 486-6002; Fax: (510) 486-5454
E-mail: r_kostecki@lbl.gov

Start Date: October 1, 2010
Projected End Date: September 30, 2011

Objectives

- Establish direct correlations between BATT baseline electrodes' interfacial phenomena and surface chemistry, morphology, topology, and degradation mechanisms
- Evaluate and improve the capacity and cycle life of intermetallic anodes and high voltage cathodes
  - Determine physico-chemical properties of the SEI i.e., chemical composition, reactions kinetics, morphology, ionic/electronic conductivity etc.
  - Investigate electrocatalytic behavior of intermetallic anodes in organic electrolytes
  - Provide remedies to interface instability e.g., new alloys and/or structures, electrolyte additives, co-deposition of other metals etc.
  - Characterize degradation modes, improve SEI long-term stability in high-energy Li-ion systems
  - Evaluate the effect of surface composition and architecture on electrochemical behavior of the electrode

Technical Barriers

- This project addresses the following technical barriers related to the battery technology development effort of the DOE Office of Vehicle Technologies:
- Inadequate Li-ion battery energy (related to cost)
- Poor lithium battery calendar/cycle lifetime for PHEV and EV applications
- High electrode impedance that limits power density
- Need for new advanced battery materials and composite electrodes with acceptable specific energy, durability, costs, and safety characteristics

Technical Targets

- Cycle life: 5000 (deep) and 300,000 (shallow) cycles (40 mile).
- Available energy: 96 Wh/kg (40 mile).
- Calendar life: 15 years.

Accomplishments

- Characterization of the interfacial phenomena of a $LiMnPO_4$ composite cathode was completed
  - Charge/discharge of $LiMnPO_4$ composite cathode produces an unstable surface layer
  - Composition of the film changes continuously during cycling. Inorganic electrolyte oxidation products tend to gradually accumulate on the electrode surface
- Preliminary *in situ* and *ex situ* studies of $LiNi_{0.5}Mn_{1.5}O_4$ surface reactivity were carried out
  - $LiNi_{0.5}Mn_{1.5}O_4$ exhibits surface instability in EC/DEC/$LIPF_6$ electrolyte
- Fundamental study of interfacial properties at Sn electrode was completed
  - *In situ* study revealed that an effective SEI layer never forms on polycrystalline Sn in EC-DEC $LiPF_6$ electrolytes mainly due to high reactivity of (001) Sn surface orientation
  - The mechanism of interfacial reactions at Sn (001) and (100) electrode surface orientations was determined and characterized
- Effective strategies to suppress unwanted surface reactions on Sn electrodes were proposed

✧ ✧ ✧ ✧ ✧

Introduction

A primary aim of this project is to develop and use advanced diagnostic techniques and experimental methodologies to characterize basic physico-chemical properties and function of Li-ion electrode active and passive components that are being developed for use in PHEV and EV applications. The focus of this task is to understand and correlate fundamental interfacial processes that occur in Li-ion batteries with the cell electrochemical performance. The diagnostic evaluation of composite and model electrodes are used to determine cell failure

mechanisms, anticipate the system lifetime and develop new more-stable materials, composites and electrodes.

Approach

The main focus of this project involves the development and application of new instrumental techniques and novel enabling experimental methodologies to investigate and understand the basic mechanism of operation of Li-ion batteries. Advanced analytic methods are being developed and used *in situ* to characterize materials and cell active and passive components. *In situ* enhanced spectroscopic, microscopic and diffraction techniques as well as standard post-test analyses are applied to investigate the morphology, topology, structure, and composition changes of electrode materials and electrode/electrolyte interfaces during cell cycling.

This project employs the following approaches:

- Apply *in situ* and *ex situ* Raman microscopy, FTIR spectroscopy, and standard electrochemical techniques to probe and characterize chemical, structural and interfacial changes in $LiMnPO_4$ and $LiNi_{0.5}Mn_{1.5}O_4$ during charge/discharge
  - Perform *ex situ* FTIR-transmission and *in situ* FTIR-ATR measurements on composite cathodes
  - Design and construct a new spectro-electrochemical cell for *in situ* Raman microscopy measurements
- Apply *in situ* and *ex situ* Raman and FTIR spectroscopy, spectroscopic ellipsometry, AFM, SEM, HRTEM, and standard electrochemical techniques to detect and characterize interfacial processes at intermetallic anodes
- Use model single crystal electrodes to determine the mechanism and kinetics of detrimental processes associated with large irreversible capacity of polycrystalline Sn
- Determine implications of the basic interfacial phenomena for long–term electrochemical performance of intermetallic anodes in high-energy Li^+-systems

Results

Our first objective was to carry out diagnostic studies of surface phenomena on the high voltage cathode material $LiNi_{0.5}Mn_{1.5}O_4$ spinel. A model electrode with the LMNO spinel powder powder (material synthesized and provided by Jordi Cabana) pressed onto Al foil was prepared and assembled into the *in situ* spectro-electrochemical cell The cyclic voltammogram of the single particles electrode (Figure V - 78) shows the features characteristic for a typical LMNO electrode. The CV demonstrates good reversibility of the delithiation/lithiation process.

The Raman spectrum of the $Li_xNi_{0.5}Mn_{1.5}O_4$ (Figure V - 79) is characterized by a superposition of the Ni-Mn spinel Raman peaks at 400, 497, 600, and 636 cm^{-1}, and electrolyte peaks at 360, 524, 715, 730, and 740 cm^{-1}. Three intense new bands at 587, 540, and 482 cm^{-1} that vary in intensity with SOC are attributed to A_{1g} Mn^{4+}-O and Ni^{4+}-O vibrations. Also noticed upon charging was a large increase in the fluorescent baseline of the spectra, and the weakening intensity of peaks of EC (715 cm^{-1}) and $LiPF_6$ (730 and 740 cm^{-1}). These observations indicate that a layer of electrolyte decomposition products forms on the particle surface due to electrode/electrolyte interactions.

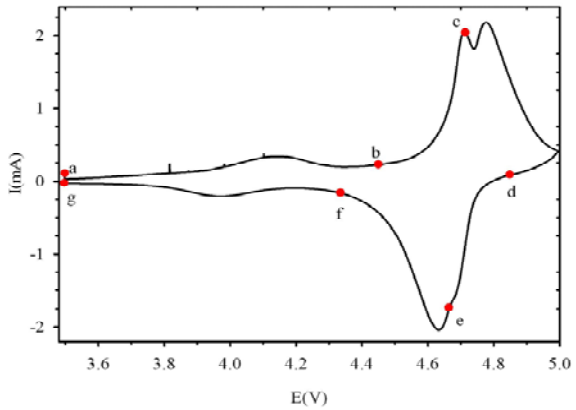

Figure V - 78: CV of LiNi0.5Mn1.5O4 powder pressed onto Al foil.

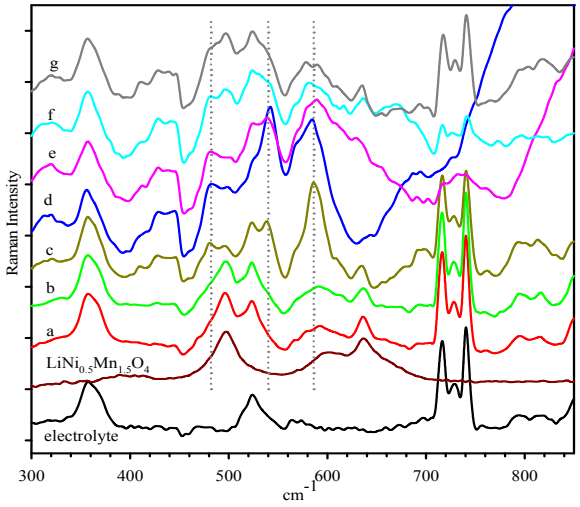

Figure V - 79: (a-g) Baseline subtracted Raman spectra of a $LixNi_{0.5}Mn_{1.5}O_4$ particle during CV scan (labels correspond to Figure V - 78).

Fluorescence, which originates from electrolyte decomposition products that form as a result of electrochemical and chemical side reactions, is an undesirable effect that interferes with observation of Raman features from the electrode. This time we decided to take advantage of this phenomenon by using *in situ* fluorescence spectroscopy of model LMNO electrodes to

provide a real-time probe of the formation of a surface electrolyte interphase (SEI) on the particle surface during cycling of the electrode.

During the first potential sweep to 5.0 V, a sharp rise in fluorescence intensity occurred (Figure V - 80) at the beginning of the Ni^{2+} oxidation reaction and continued until the reverse scan caused Ni^{4+} reduction. The fluorescence signal declined after this point until Ni^{2+} oxidation during the potential sweep on the second cycle occurred again. This pattern, repeated for all three cycles strongly suggests that electrolyte decomposition is catalyzed by the changes that occur upon Ni oxidation during the delithiation process. In addition, the loss of fluorescence intensity indicates that most of these fluorescent decomposition products either dissolve into the electrolyte, or decompose to other products right after formation. However, the rising fluorescence background intensity demonstrates that some fluorescent species remained at the particle surface. A similar increase in fluorescence has also been observed from 1 M $LiClO_4$ in EC:DEC electrolyte solutions. Therefore, the fluorescent species likely originate primarily from decomposition of the carbonate-based electrolytes, as opposed to $LiPF_6$.

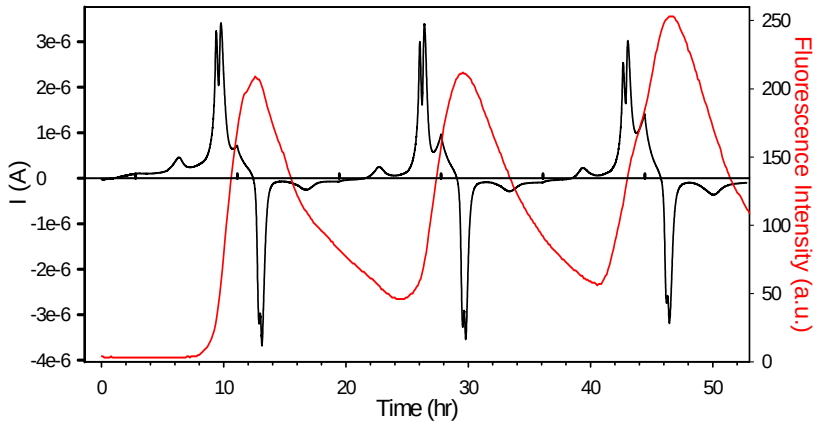

Figure V - 80: Current (left axis) and fluorescence intensity (right axis) vs. time during three CVs between 3.5 and 5.0 V at 0.05 mV/s.

Transmission FTIR and Raman spectroscopy were used to probe the structural changes of the LMNO spinel powder (synthesized and provided by Jordi Cabana) after aging in 1 M $LiPF_6$ in EC:DEC (1:2 w/w) electrolyte. Noticeable changes in FTIR spectra after 6 weeks at 55°C indicate changes in the local structure of the crystal. The Raman spectra of the aged LMNO powder suggest the surface Mn enrichment and possible Ni dissolution

The FTIR spectrum of delithiated MNO after one week at 60°C (Figure V - 79d) appears almost identical to the fully lithiated sample. Spontaneous relithiation of MNO (and corresponding reduction of the active metal) must be accompanied by electrolyte oxidation at the particle surface. The increased reactivity of LNMO in the charged state toward the electrolyte and its inability to retain charge during storage at elevated temperatures, are both critical issues that must be addressed for this material to be used in commercial Li-ion batteries.

Our second goal was to investigate the SEI layer composition on model Sn electrodes to gain insights into the different electrolyte degradation mechanisms at the highly reactive Sn (100) surface and the more stable Sn (001) surface. Preliminary soft X-ray XAS measurements were performed in the ALS (beam line 8.0.1) on Sn single crystals with the (100) and (001) orientations after cycling in EC/DEC 1M $LiPF_6$ electrolyte. Carbon, oxygen, and fluorine K-edges were probed with both florescent X-ray and Auger electron signals, which are proportional to the X-ray absorption. The surface sensitive Auger electron signal (escape depth of 50Å) indicates different compositions of the surface layers. Observation of C π^* and O π^* near-edge features at 290 eV and 534 eV respectively, on Sn (100), are identical to NEXAFS spectra of Li_2CO_3. The F K-edge pattern on Sn (001) suggests that F is in the form of LiF within the SEI layer.

Our third objective was to explore the feasibility and benefits of near-field microscopy and spectroscopy techniques to study interfaces and interphases in Li-ion systems at subwavelength resolution. Preliminary near-field measurements on HOPG model electrodes, Sn anodes and Li_xFePO_4 single particles were carried out using a near-field spectroscopy instrumentation at JASCO (Japan) and Neaspec (Germany). The initial results proved to be extremely encouraging revealing new surface features at subwavelength resolution, which is unavailable by any other existing techniques. A similar instrumental setup from Neaspec will be purchased in October 2011 with capital equipment funding recently received and will enable future in-house spectroscopic measurements at the nanoscale (nanoRaman, i.e. TERS and nano-FTIR) to characterize cathode and anode structure interfacial behavior.

Conclusions and Future Directions

- $LiMnPO_4$ composite cathode is unstable vs. $LiPF_6$, organic carbonate electrolytes
  - Electrolyte decomposition products do not form a stable layer on the surface of $LiMnPO_4$ composite cathode
  - Surface film forms at the exposed Li_xMnPO_4 active material. No surface film was detected on carbon black additive
- *In situ* Raman and fluorescence spectra of $LiNi_{0.5}Ni_{1.5}O_4$ single particle cathodes reveal a surface film rich in $Li_xPO_yF_z$ products
  - Composition and thickness of the film vary significantly during charge/discharge cycles
  - Large portion of electrolyte decomposition products diffuse away from the surface in the electrolyte – possible cross-talk with the anode SEI
- Prolonged exposure of $LiNi_{0.5}Mn_{1.5}O_4$ to EC/DEC/$LiPF_6$ leads to surface Ni^{3+} depletion, Mn^{3+} enrichment, and surface film formation of electrolyte decomposition products
- Surface and interfacial instability of $LiMnPO_4$ and $LiNi_{0.5}Ni_{1.5}O_4$ likely precludes these materials from achieving commercial viability without developing better routes for stabilizing the active material bulk and surface structure
- Fundamental study of interfacial processes on Sn electrode was completed
- *In situ* studies revealed that the nature and kinetics of interfacial processes are strongly dependent on the electrode surface structure and electrolyte composition
  - Stable surface film never forms on Sn (001) in EC/DEC/$LiPF_6$ electrolyte. The electrocatalytic behavior of Sn (001) surface possibly accounts for large irreversible charge losses observed for polycrystalline Sn anode
  - Effective SEI layer forms on Sn crystal domains (100)
  - Electrochemical reduction of DEC most likely occurs on Sn (001) surface whereas reduction of EC is promoted on Sn (100)
- Sn interface instability in organic carbonate electrolytes can be remedied by careful optimization of Sn electrode surface design, electrolyte composition, and use of additives that (re)produce a stable SEI layer
- It is critical for the long-term electrochemical performance of intermetallic anodes to suppress unwanted surface reactions. Coordinated electrode and electrolyte design must be carried out to achieve interfacial stability of Sn anodes in Li-ion battery applications.

Future Directions

- Design and apply *in situ* and *ex situ* experimental methodologies to detect and characterize surface processes in Li-ion intermetallic anodes
  - Comprehensive fundamental *in situ* spectroscopic ellipsometry in conjunction with AFM and FTIR/Raman surface analysis studies of the SEI layer formation on model monocrystal Sn and Si electrodes will be carried out
  - Cooperate with the BATT Task Group "SEI on Alloys“ and industrial partners (3M) to investigate the effect of material structure, morphology on formation of the SEI layer
  - Investigate correlations between physico-chemical properties of the SEI layer and long-term electrochemical performance of Li-ion electrodes
- Diagnostic evaluation of detrimental phenomena in high-voltage (>4.3 V) cathodes
  - Apply *in situ* and *ex situ* Raman and FTIR spectroscopy to detect and characterize surface and bulk processes in high voltage cathodes
  - Evaluate the effect of electrode passive additives and impurities on the electrochemical performance and long-term stability of the composite cathodes
  - Collaborate with BATT Task Group “Ni/Mn Spinel“ and industrial partners (HQ, Dow Chemical) to investigate detrimental processes that impede commercialization of new cathode materials
- Develop and introduce new *in situ* instrumental techniques and experimental methodologies to study mass and charge transfer processes in Li-ion systems
  - Improve sensitivity, selectivity and achieve sub-wavelength spatial resolution in optical microscopy/spectroscopy
  - Acquire, adapt and introduce near-field technques to our diagnostic effort

FY 2011 Publications/Presentations

1. Jeon, Ki-Joon; Lee, Zonghoon; Pollak, Elad; Moreschini, Luca; Bostwick, Aaron; Park, Cheol-Min; Mendelsberg, Rueben; Radmilovic, Velimir; Kostecki, Robert; Richardson, Thomas; Rotenberg, Eli, "Fluorographane: a wide bandgap semiconductor with ultraviolet luminescence", *ACS Nano*, 2011, 5 (2), pp 1042–1046

2. Elad Pollak, Bai-Song Geng, Ki-Joon Jeon, Ivan T. Lucas, Thomas J. Richardson, Feng Wang, and Robert Kostecki "The Interaction of Li^+ with Single-Layer and Few Layers Graphene", Nanoletters", 10 (2010) *10*, 3386–3388
3. Marie Kerlau, Jinglei Lei, Marek Marcinek, Frank McLarnon and Robert Kostecki, "Studies of Degradation Phenomena in Li-ion Batteries", The 28th International Battery Seminar & Exhibit, March 16, 2011, Fort Lauderdale, FL, USA (invited talk)
4. Nicolas S. Norberg, Robert Kostecki, "*In situ* Study of Interfacial Phenomena at $LiMnPO_4$ Cathode", 3rd International Conference on Advanced Lithium Batteries for Automobile Applications, September 7-11, 2010, Seoul, South Korea (invited talk)
5. M. Marcinek, J. Syzdek, G. Żukowska, W. Wosko, E. Dudek, P. Wieczorek and R. Kostecki, "Microwave Plasma CVD of Li-ion Composite Anodes", 218th ECS Meeting, Las Vegas, October 10-15, 2010
6. Elad Pollak, Bai-Song Geng, Ki-Joon Jeon, Ivan T. Lucas, Thomas J. Richardson, Feng Wang, and Robert Kostecki, "The Interaction of Li^+ with Single-Layer and Few Layers Graphene", 218th ECS Meeting, Las Vegas, October 10-15, 2010
7. N.S. Norberg, I.T. Lucas, E. Pollak, R. Kostecki, „Interfacial Phenomena at a Composite $LiMnPO_4$ Cathode", 218th ECS Meeting, Las Vegas, October 10-15, 2010
8. I. T. Lucas, M. Gervais, J.S. Syzdek, J.B. Kerr and R. Kostecki, "Electrocatalytic properties of Tin in Organic Carbonate Electrolytes", 218th ECS Meeting, Las Vegas, October 10-15, 2010
9. Jarosław Syzdek, Michel Armand, Robert Kostecki, Ivan Lucas, Marek Marcinek, Christian Masquelier, Jean-Marie Tarascon, Władysław Wieczorek, "Poly(oxyethylene)-based Composite Electrolytes – Structural Transformations and Electrochemical Performance", 218th ECS Meeting, Las Vegas, October 10-15, 2010
10. Elad Pollak, Ivan.T. Lucas and Robert Kostecki, "A Study of Lithium Transport in Aluminum Membranes", 218th ECS Meeting, Las Vegas, October 10-15, 2010
11. Robert Kostecki, Laurence J. Hardwick, Ivan T. Lucas, Elad Pollak, and Vijay A. Sethuraman, "Li^+ Transport Mechanism in Graphite and Li-Me Alloys", 61st Annual ISE Meeting, September 26th - October 1st, 2010, Nice, France (invited talk)
12. Robert Kostecki, "*In situ* SPM of Local Interfacial Phenomena in Li-ion Batteries", International Workshop on SPM for Energy Applications, Oak Ridge National Laboratory, September 16, 2010 (invited talk)
13. Robert Kostecki, "Batteries for Automotive Applications", 2nd Annual Workshop on Energy Research Energy Research Institute @ NTU, Singapore, June 16, 2010, (invited talk)
14. I. Lucas, E. Pollak, N. Norberg and R. Kostecki, "The Mechanism of Decomposition of EC-Based Electrolytes on a Tin Electrode", 15th International Meeting on Lithium Batteries Montreal, Canada — June 27–July 3, 2010
15. E. Pollak, I. Lucas and R. Kostecki, "A Study of Lithium Transport in Aluminum Membranes", 15th International Meeting on Lithium Batteries Montreal, Canada — June 27–July 3, 2010
16. M. Marcinek, L. Niedzicki, J. Syzdek, M. Kasprzyk, R. Borkowska, A. Zalewska, Z. Żukowska, W. Wośko, E. Dudek, M. Gumienniczuk, Ł. Łukaszczuk, M. Karłowicz, M. Armand, J.M. Tarascon, R. Kostecki, and W. Wieczorek, "New salts, ceramic sponges and MPACVD electrodes. Contribution to the lithium ion-batteries", 60th Anniversary Sadoway Symposium, MIT, June 2010.
17. Sherie Reineman, Ashok J. Gadgil, Susan E. Addy, Robert Kostecki, "Electrochemical Removal of Arsenic" US Patent Application No. 13/060

V.C.3 Search for New Anode Materials (UTA)

John B. Goodenough (PI)
University of Texas at Austin
Texas Materials Institute
ETC 9. 184,
Austin, TX 78712
Phone: (512) 471-1646; Fax: (512) 471-7681
E-mail: jgoodenough@mail.utexas.edu

Start Date: October 30, 2009
Projected End Date: December 31, 2011

Objectives

- Prior to 2010: To develop an anode material having a voltage $1.1 < V < 1.5$ V versus lithium for safe, fast charge without robbing capacity from cathode on initial charge (Completed).
- Post 2010: To develop a strategy that would allow use of lithium as the anode.

Technical Barriers

Identification and fabrication as a robust, thin membrane ceramic Li^+ electrolyte with a conductivity $\sigma_{Li} > 10^{-4}$ S cm^{-1} at room temperature that is stable in different liquid environments and on contact with lithium.

Technical Targets

- To demonstrate the feasibility of a Li battery having a solid Li^+-electrolyte separator and an aqueous, flow-through cathode.
- To identify an oxide Li^+ electrolyte having a $\sigma_{Li} > 10^{-4}$ S cm^{-1} that is stable on contact with a lithium anode.

Accomplishments

- Identified the $Fe(CN)_6^{3-}/Fe(CN)_6^{4-}$ redox couple and demonstrated its storage efficiency and cycle life for an aqueous flow-through cathode.
- Construction of a demonstration flow through cell with, as separator, a commercial Li^+ electrolyte having a $\sigma_{Li} > 10^{-4}$ S cm^{-1}, but not stable on contact with lithium. The demonstration showed feasibility of the concept of a flow-through liquid cathode.
- Investigation of the nominal oxide $Li_7La_3Zr_2O_{12}$ showed that adventitious Al^{3+} in the interstitial space of the host $Li_7La_3Zr_2O_{12}$ garnet framework is needed to stabilize the structure above 800°C and that the practical upper limit of Li in the interstitial space would be less that 7 Li/formula unit.
- Systematic investigation of the nominal $Li_{7-x}La_3Zr_{2-x}Ta_xO_{12}$ gave a maximum $\sigma_{Li} > 10^{-3}$ S cm^{-1} for 6.4±0.2 Li/formula unit, but with some uncertainty owing to the presence of Al^{3+} from the alumina boat in which the electrolyte was fired. The oxide did not react on contact with molten lithium.

Introduction

The LUMO of the organic liquid-carbonate electrolytes used today in Li-ion batteries is near 1.1 V versus a lithium anode. Therefore, any anode with a voltage $V < 1.1$ V versus lithium must form a passivating SEI layer permeable to Li^+, and the Li^+ in the SEI layer represents an irreversible loss from the cathode capacity on the initial charge. Moreover, to allow for a fast, safe charge, the anode voltage needs to be $V > 0.5$ V versus lithium. Therefore, there was motivation to find an insertion host for Li giving a voltage $1.1 < V < 1.5$ V versus lithium to better the $Li_4Ti_5O_{12}$ anode having a $V \approx 1.5$ V. In our prior work, we demonstrated that a layered oxide or sulfide could be tailored to have a voltage $1.1 < V < 1.5$ V versus lithium and that these anodes would give a fast, safe, long-lived charge/discharge. However, in order to realize a maximum voltage and specific capacity, a lithium anode should be the target.

Approach

A lithium anode is viable with a solid Li^+-electrolyte separator that blocks any dendrites from reaching the cathode. Moreover, the Li^+ of the passivating SEI layer on the lithium would come from the anode, not the cathode. However, this strategy requires identification of a solid Li^+ electrolyte having a $\sigma_{Li} > 10^{-4}$ S cm^{-1} at room temperature that is stable on contact with lithium and can be fabricated into a thin, dense membrane that is mechanically robust. Moveover, this strategy would allow use of a liquid cathode providing a higher capacity than can be achieved with a Li-insertion host. Our approach was, first, to test the feasibility of a liquid cathode and then to identify an oxide Li^+ electrolyte satisfying the criteria.

Results

In order to test the feasibility of a liquid cathode with a solid Li^+-electrolyte separator, we chose an aqueous alkaline cathode containing the redox couple $Fe(CN)_6^{3-}$

/$Fe(CN)_6^{4-}$ and a commercial Li^+ electrolyte with a $\sigma_{Li} \approx 10^{-4}$ S cm^{-1} containing Ti^{4+} and $(PO_4)^{3-}$ ions, neither of which is stable on contact with lithium.

It soon became apparent that a large capacity with this strategy would require a flow-through cathode, so we built the cell of Figure V - 81and showed it gave a V ≈ 3.5 V with no capacity fade on cycling. However, our use of an aqueous cathode requires an oxide separator. Weppener's group has reported a $\sigma_{Li} \approx 10^{-4}$ S cm^{-1} in a nominal $Li_7La_3Zr_2O_{12}$, which has Li^+ in the interstitial space of the garnet framework $La_3Zr_2O_{12}$. The interstitial space consists, per formula unit (f.u.), of three tetrahedral sites bridged at each face by an octahedral site sharing two opposite faces to give a total of 9 interstitial sites/f.u. It was also known that nominal $Li_7La_3Zr_2O_{12}$ contains adventitious Al^{3+} as a result of sintering above 1100°C in an alumina crucible. First, we obtained Al-free $Li_7La_3Zr_2O_{12}$ and found it decomposes above 800°C. Then we used neutron diffraction to locate the Al^{3+} in interstitial octahedral sites and, with our Al-free sample, to show that the maximum possible Li content in the garnet framework would be 7.5 Li/f.u., and then only if the Li vacancies were ordered on half the interstitial tetrahedral sites. The practical upper limit would be ≈ 7 Li/f.u., and since the Al^{3+} would be stabilizing the garnet framework perhaps by lowering the Li concentration to less than 7 Li/f.u., we undertook a study of the system $Li_{7-x}La_3Zr_{2-x}Ta_xO_{12}$ to determine the x at which σ_{Li} ia a maximum. With x = 0.6 and sintering in an alumina crucible, we obtain a $\sigma_{Li} \approx 10^{-3}$ S cm^{-1} in a narrow range at x as shown in Figure V - 82. However, the samples had a tan color, indicative of oxygen vacancies acting as color centers that appear to be associated with the adventitious Al^{3+}. Our white samples have proven difficult to densify at the low temperatures needed to retain the Li, indicating that the Al^{3+} is also acting as a sintering aid. We are concerned that Li_2O and/or Al_2O_3 in the grain boundaries will be attacked by an aqueous cathode, so we are in the process of examining how to make a dense ceramic membrane without a sintering aid.

Conclusions and Future Directions

The viability of a Li battery containing a Li^+-electrolyte separator and a liquid cathode has been demonstrated. An oxide Li^+ electrolyte stable on contact with lithium and having a $\sigma_{Li} \approx 10^{-3}$ Scm^{-1} has been identified, but the next challenge is fabrication of the electrolyte into a thin, dense membrane that is mechanically robust. We plan to construct cells that allow testing in electrolyte liquids, including oxidative salts, the Li^+ electrolyte is stable on cycling, whether thin membranes can be made that block dendrite growth, and to determine what charge/discharge rates are practical.

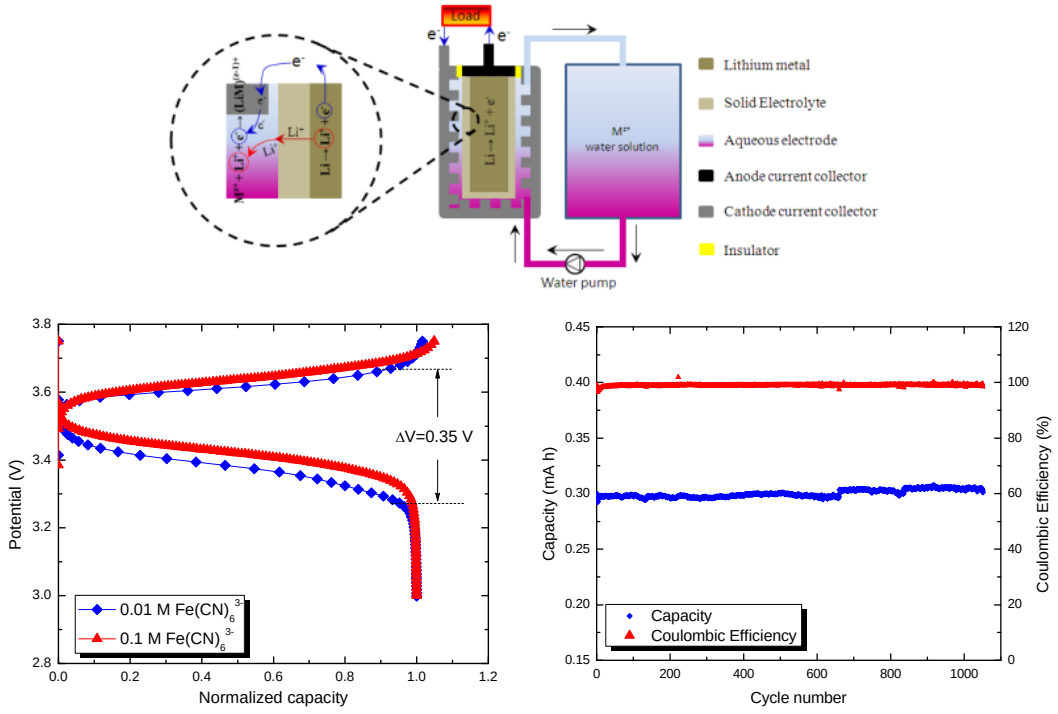

Figure V - 81: Structure of Lithium/aqueous cathode cell and its charge/discharge behavior.

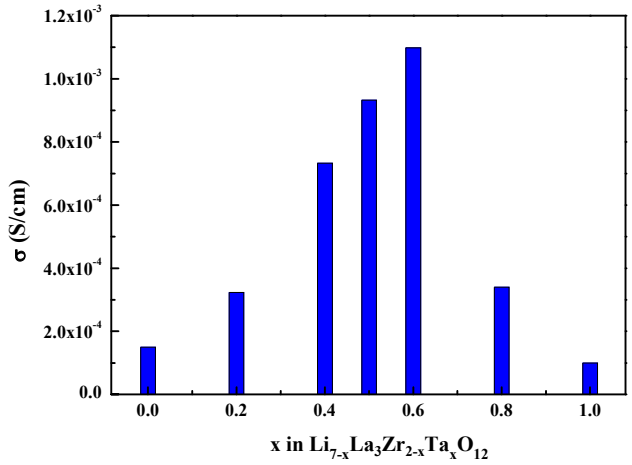

Figure V - 82: Relationship of conductivity and x in $Li_{7-x}La_3Zr_{2-x}Ta_xO_{12}$

FY 2011 Publications/Presentations

1. J.B. Goodenough and Y. Kim, "Challenges for Rechargeable Batteries", *J. Power Sources*, **196**, 6688-6694 (2011).
2. G. Yang, Y. Kim. J.B. Goodenough, "The Influence on Fermi Energy of Li-Site Change in $Li_zTi_{1-y}Ni_yS_2$ on crossing z=1", *J. Mater. Chem.*, **21**, 10160-10614 (2011).
3. J.T. Han, J.B. Goodenough, "3-V Full Cell Performance of Anode Framework $TiNb_2O_7$/Spinel $LiNi_{0.5}Mn_{1.5}O_4$", *Chem. Mater.*, **23**, 3404-3407 (2011).
4. Y. Lu, J.B. Goodenough, "Rechargeable Alkali-ion Cathode-Flow Battery", *J. Mater. Chem.*, **21**, 10113-10117 (2011)
5. Y. Lu, J.B. Goodenough, Y. Kim, "Aqueous Cathode for Next-Generation Alkali-Ion Batteries", *J. Am. Chem. Soc.*, **133**, 5756-5759, 2011.
6. H. Xie, Y. Li, J.B. Goodenough, "NASCICON-type $Li_{1+2x}Zr_{2-x}Ca_x(PO_4)_3$ with High Ionic Conductivity at Room Temperature", *RSC Advances* 2011, DOI:10.1039/C1RA00383F.
7. H. Xie, J. A. Alonso, Y. Li, M. T. Fernndez-Daz, J. B. Goodenough, "$Li_{1.2}Zr_{1.9}Ca_{0.1}(PO_4)_3$, a room-temperature Li-ion solid electrolyte", *J. Power Sources*, **196**, 7760-7762 (2011).
8. H. Xie, J. A. Alonso, Y. Li, M. T. Fernndez-Daz, J. B. Goodenough, "Lithium distribution in aluminum-free cubic $Li_7La_3Zr_2O_{12}$", *Chem. Mater.*, **23**, 3587-3589 (2011).
9. Y. Li, C.-A. Wang, H. Xie, J. Cheng, J. B. Goodenough, "High lithium ion conduction in garnet-type $Li_6La_3ZrTaO_{12}$", *Electrochem. Commun*.
10. doi:10.1016/j.elecom.2011.07.008

V.C.4 Nano-structured Materials as Anodes (SUNY)

M. Stanley Whittingham (Project Manager)
Binghamton University
Vestal Parkway East
Binghamton, NY 13902-6000
Phone: (607) 777-4623; Fax: (607) 777-4623
E-mail: stanwhit@binghamton.edu

Subcontractor: None

Start Date: June 1, 2007
Project End Date: December 31, 2010

Objectives

- Replace the presently used carbon anodes:
  - with safer materials that will be compatible with lower -cost layered oxide and phosphate cathodes and the associated electrolyte.
  - With materials having higher volumetric energy densities, twice that of carbon (1.6 Ah/cc and 0.5 Ah/g)

Technical Barriers

This project addresses the following technical barriers facing the use of Li-ion batteries in PHEVs and EVs:

(A) Materials and manufacturing cost of lithium-ion batteries

(B) Safety of lithium-ion batteries

(C) Volumetric capacity limitations of Li-ion batteries

Technical Targets

- Determine the limitations, besides cost, of the Sn-Co-C nanostructured anode.
- Identify the structural and surface changes of Sn anodes during cycling working collaboratively with LBNL (R. Kostecki)
- Explore nano-size Sn/Si alloys and metal oxides to identify their cycling characteristics.

Accomplishments

- Shown that bulk tin, in the form of foil, whether shallow or deep cycled, loses capacity at all depths of discharge.
  - SEI film is not protective, and increases continuously in resistance
- Shown that amorphous nano-size tin does not lose capacity whether shallow or deep cycled.
  - Shows high rates for lithium release
  - Shown that this material is charge-limited, that is lithium insertion is slow
- Technology transfer accomplished.
  - Working with several local battery companies, and many ex-students now in battery companies
- Students now have positions at BNL, NREL, and PNNL. Electrospinning technique transferred to NREL.

✧ ✧ ✧ ✧ ✧

Introduction

Achieving the DOE cost and energy/power density targets will require improved anode materials that have higher volumetric energy densities than carbon, and have lower cost production methods. At the same time the material must have higher lithium diffusion rates than carbon and preferably be at a slightly higher potential to improve the safety.

Approach

Explore, synthesize, characterize and develop inexpensive materials that:

- Have a potential around 500 mV above pure Li
- Have double the volumetric capacity of carbon
- Have a higher gravimetric capacity than carbon
- Emphasize nanostructures
  - Tin nanostructures
  - Compare with silicon based nanostructures
  - Keep aware of oxide-based anodes
    - We showed that Mn_3O_4 cycles well.

Results

Amorphous Nano-Sized Tin. We have completed our understanding of the capabilities of the amorphous tin anode developed by SONY. We showed that this material cycles well, holding its capacity at all depths of discharge in contrast to crystalline tin. These results are a clear indication that tin at the nano-size and in amorphous form can be cycled repetitively without capacity loss, and gave a clear direction for future work on tin-based systems. As a

result, we have found that the cobalt can be replaced by iron as described in our new project V.C.10.

We determined the rate-capability on both lithium insertion and removal. The results are shown in Figure V - 83.

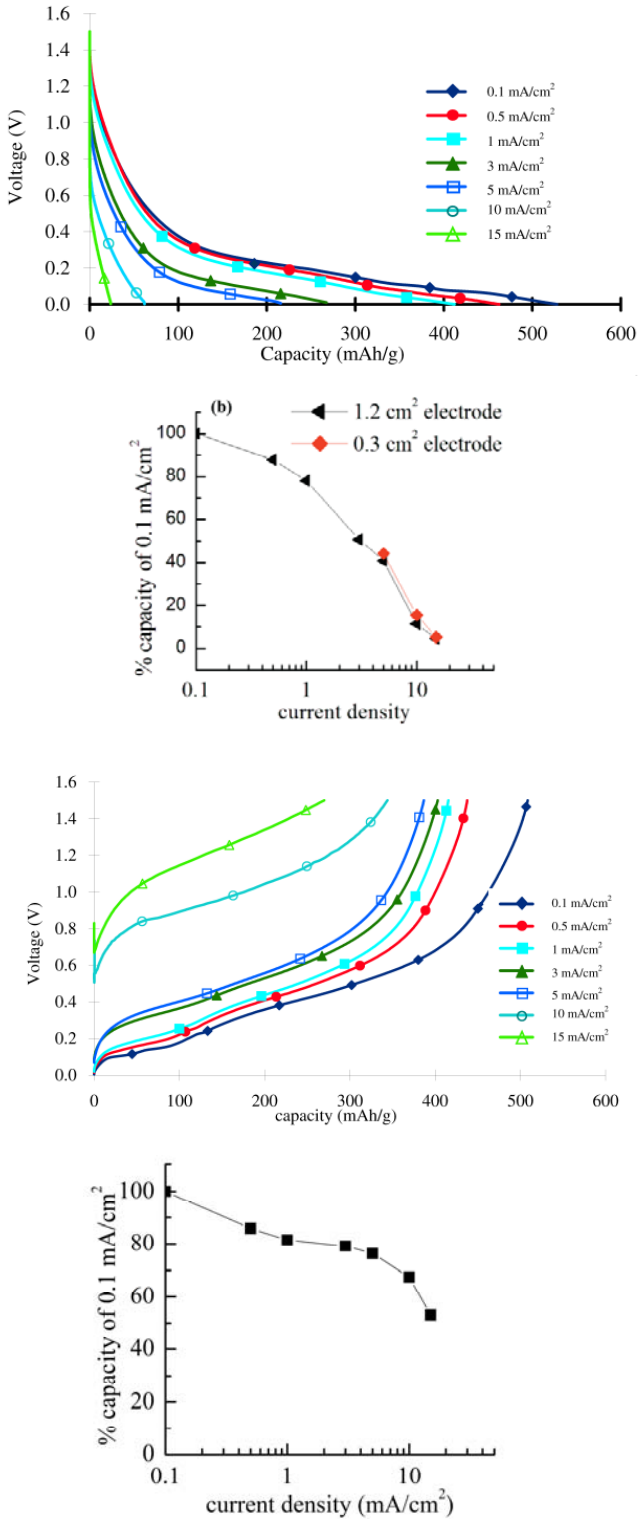

Figure V - 83: Lithium insertion and delivery rates from the Sn-Co amorphous material (top to bottom is a-d in discussion).

Figure V - 83a shows the lithium insertion curve, which is the charging of the battery using this material as an anode. Figure V - 83b shows the capacity as a percentage of the capacity at 0.1 mA/cm^2; for each data point, the lithium was first removed at the low rate of 0.1 mA/cm^2. It can be immediately seen that at the high rates used, the capacity falls off very rapidly. At a rate of 2 mA/cm^2 50% of the capacity is lost. In contrast, the capacity on lithium removal is maintained even at high rates; for example, around 70% of the capacity is retained at 10 mA/cm^2 (2.5C rate). Thus, this anode material can sustain high discharge rates (lithium delivery), and probably meets the technical needs of PHEV and EV. It is more limited on charging, Figure V - 83c and Figure V - 83d, and in this respect is comparable to carbon anodes, and might create problems with the fast charging needs of HEV batteries.

Bulk Tin Foil Anodes. In contrast to nano-amorphous tin, bulk tin foil loses capacity after about 10 to 12 deep cycles (or equivalent shallow cycles). This is due to a resistance build-up caused by the continuous formation of the SEI layer as the tin expands and contracts on reaction with the lithium. Robert Kostecki at LBNL has shown that the SEI layer formed on tin in the carbonate electrolytes is non-protective.

Other Anode Materials We are exploring other metal-based anode materials under our new project V.C.10.

Conclusions and Future Directions

A clear result from our study of understanding the cycling behavior of tin anode materials is that nano/amorphous materials work, and that bulk materials with their high expansion on lithium reaction do not and are therefore unsuitable for batteries. This project is now complete.

FY 2011 Publications/Presentations

1. Presentation to the 2011 DOE Annual Peer Review Meeting.
2. Ruigang Zhang and M. Stanley Whittingham "Electrochemical Behavior of the Amorphous Tin–Cobalt Anode", Electrochem. Solid State Letters, 2010, 13: A184-A187
3. Many invited presentations, incl.:
   - ECS, MRS, PPS
   - ORNL

V.C.5 Development of High Capacity Anodes (PNNL)

Ji-Guang Zhang and Jun Liu
Pacific Northwest National Laboratory
902 Battelle Blvd., Mail Stop K3-59
Richland, WA 99352
Phone: (509) 372-651; (509) 375-4443
E-mail: jiguang.zhang@pnl.gov; jun.liu@pnl.gov;

Start: Date: October 1, 2010
Projected End Date: September 30, 2011

Objectives

- Develop Si-based anodes with high capacities, cycle stabilities, and rate capabilities.
- Develop a low-cost synthesis route for Si-based anodes.

Technical Barriers

Low energy density, limited cycle life, and high cost.

Technical Targets

- Identify good composite structures and good conductive additives to improve the mechanical and electrical stability of Si-based anodes
- Develop a low-cost and scalable approach to synthesizing Si-based nanocomposite materials with improved capacity and stability.

Accomplishments

- Developed Si and Si-based anodes with a rigid skeleton support and nanostrucutered carbon coating. The anode demonstrates high capacity and improved cycle stability.
- Developed low-cost and scalable synthetic methods, such as mechanical ball milling, to anchor Si or SiO_2 on a skeleton support and create continuous conductive paths. Significant progress was made in developing high-capacity stable Si and SiO_x anodes. A stable capacity of ~600 mAh/g (based on the full electrode including the carbon additive and binder) over 90 cycles was obtained. A Si-anode with a similar structure provided a capacity of ~ 650 mAh/g (based on the full electrode including the carbon additive and binder) and 80% capacity retention over 90 cycles.
- In collaboration with Vesta Si, we developed and tested several batches of micron-sized porous Si for anodes. The pore sizes ranged from ~5 to 10 nm. The effect of pore size on battery performance was investigated. The cycle performance of a porous Si anode increases with increasing pore-size. A critical pore size:wall thickness ratio of ~3:1 was estimated to give stable cycle life.

Introduction

Si and Si-based materials are good high-capacity anode candidates for Li-ion batteries; however, because of large volume expansions and phase transformations upon lithiation and de-lithiation, they often show rapid capacity fading during cycling. The low conductivity and poor stability of these materials usually require the addition of conductive additives and/or coatings to enhance electron transport and electrical contact of the active materials. Good capacity retention could be obtained when a much larger amount of carbon was added to the material, but this will lead to a decrease in the capacity of the full electrode. To increase the cycle life of the anode without sacrificing the capacity, novel structured anode composites, with capacities more than double that of the state-of-the-art graphitic anodes need to be developed.

Approach

Using low-cost, scalable methods such as mechanical ball milling, we developed novel Si and Si-based composites with rigid skeleton supports and nanostructured carbon. Micron-sized Si/SiO_x were broken down into nanosized particles and attached to the surface of rigid mechanical supports. The Si/skeleton support then was coated with conductive carbon by ball milling to improve the electrical contact. The three-dimensional composites have high capacity and improved cycle life. Different rigid skeletons with high mechanical strengths can be used. The conductive coating can be graphene sheets, conductive carbon, metal, conductive polymer, etc. With an optimized ratio, the composite anode can have a stable and high capacity.

In another effort, we collaborated with Vesta Si and developed a simple chemical-etching method to synthesize micron-sized porous silicon with controllable pore size for anodes. After CVD coating, porous Si demonstrated high capacity and reasonable cycle stability. The effects of pore

size on battery performance were investigated systematically. Porous Si shows improved cycle stability with increasing pore size. This finding provides a guide for rational design of stable silicon anodes.

Results

SiO_x Anode with a Three-Dimensional Rigid Skeleton Support. We made significant progress in developing high-capacity stable SiO_x anodes. We obtained a stable capacity of ~600 mAh/g (based on the full electrode) over 90 cycles. This achievement was made by anchoring SiO_x on a rigid structural skeleton support and coating a conductive layer on outside of SiO_x to provide continuous electrical contact (Figure V - 84). We tested coin cells using this composite as the working electrode and Li metal as the anode between 0.02 and 1.5 V at a current density of ~100 mA/g.

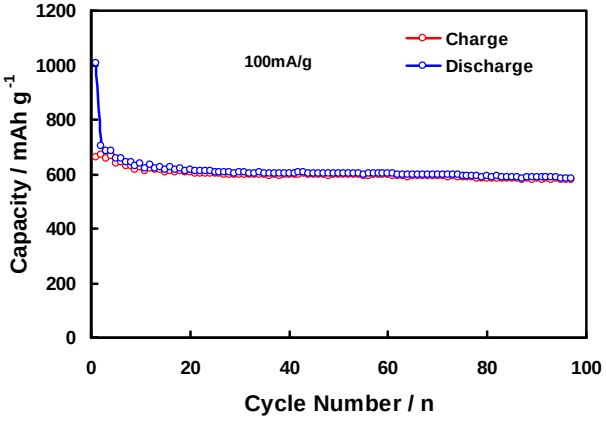

Figure V - 84: Stable cycling of SiO_x-based anodes with a rigid structural skeleton and continuous conductive carbon coating.

Si Anode with a Three-Dimensional Rigid Skeleton Support. Progress has been made in producing silicon anodes with rigid skeletons and continuous graphene coatings. A stable capacity of ~800 mAh/g (based on the active materials) over 90 cycles was obtained by anchoring Si on a rigid skeleton support and coating a conductive layer on the Si/skeleton support to provide continuous electrical contact (Figure V - 85a). We tested the coin cell between 0.02 and 1.5 V at a current density of ~1 A/g (three formation cycles are tested at a 100-mA/g current density). The Si anode also exhibited very good rate performance. Figure V - 85b showed the cycling performance under different current densities ranging from 0.5 to 8A/g. The capacity is ~500 mAh/g at 8 A/g.

We used the same Si anodes to investigate the effect of an electrolyte additive, fluoroethylene carbonate (FEC). With the FEC additive (the standard electrolyte is 1-M $LiPF_6$ in EC:DMC (1:2)), the cycling stability of the Si-based anode is improved significantly. As shown in Figure V - 85c, there is almost no capacity fading over 70 cycles with the addition of 10% FEC. As a comparison, the capacity is only ~50% of the initial capacity after 70 cycles when no FEC additive was used.

Porous Si Anodes and Pore-Size Effect. A porous Si sample with 10-nm pore size has ~25 wt% carbon after CVD coating. This carbon coating is thicker than those coated on porous silicon Si samples with smaller pore sizes of 7.5 nm (15 wt% CVD carbon) and 5 nm (5 wt% CVD carbon). TEM anlaysis showed that the porous Si (10-nm pore size) was coated with partially graphitized carbon both outside the particle and inside the pores. The primary silicon nanocrystallines have the size of tens of nanometers (see Figure V - 86a). We analyzed the pore-size change before and after CVD carbon coating using the Barrett-Joyner-Halenda pore-size distribution method. The pore size decreases from 10 to 7.5 nm after CVD C coating (Figure V - 86b). The pore volume decreases from 0.4 to 0.14 cm^3/g. The TEM and BJH results show that the carbon is coated both on the outside surface and also inside the pores. The continuous carbon coating greatly improves the conductivity of the silicon anode.

Battery test results showed that the porous Si with larger pore sizes have better cycle stability than those with smaller pore sizes (Figure V - 87a). Porous Si (10-nm pore size) has a capacity of ~2750 mAh/g calculated from the Si weight at a current density 100 mA/g. The cycle stability is much better than the porous Si samples with small pore sizes. At high current density, the porous Si samples with 10-nm pore size also show higher capacity and better cycle stability than the samples with small pore sizes. It has a capacity of ~800 mAh/g based on the whole electrode weight, including the carbon additives and binder (Figure V - 87b).

Conclusions and Future Directions

Si- and SiO_x-based anodes with rigid skeletons showed significantly improved capacity and stability. Investigation on the porous Si suggested that improved performance could be obtained by using large pore-size material and good carbon coatings. *In situ* characterization revealed that the accumulated damage on the Si layer is a major factor leading to the capacity fading. In future work, we will focus on the following three aspects:

1. Identifying the best structure-supporting and conductive-coating materials
2. Optimizing the ratios among the active material, the structure supporting material, and the conductive coating to balance the high capacity and cyclability
3. Developing new conductive additives and electrolyte additives to further improve cycling stability.

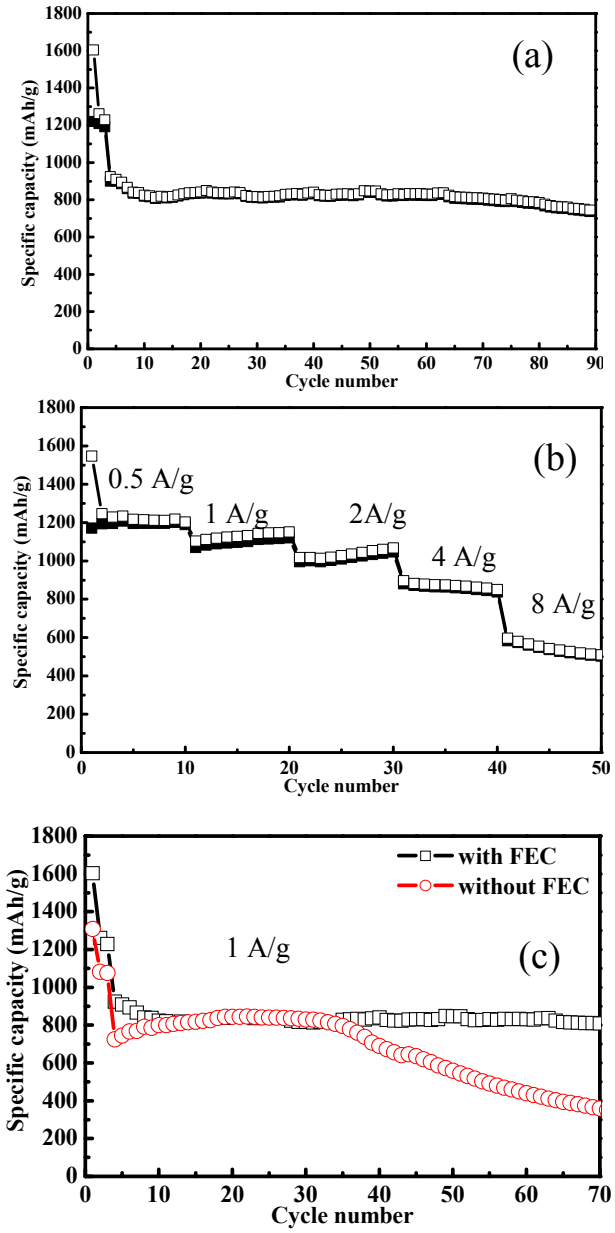

Figure V - 85: a) Stable cycling of Si anodes with rigid skeleton support and continuous conductive carbon coating. Good cycling stability and high capacity (~ 650 mAh/g anode in 90 cycles at 1 A/g) were obtained using commercial Si powder. b) Si anode cycling at different current densities from 0.5 A/g to 8 A/g. c) Si anode cycling stability with and without FEC as the electrolyte additive (as in (a). Capacities were calculated based on the full weight of the electrode, including carbon additive and binders.

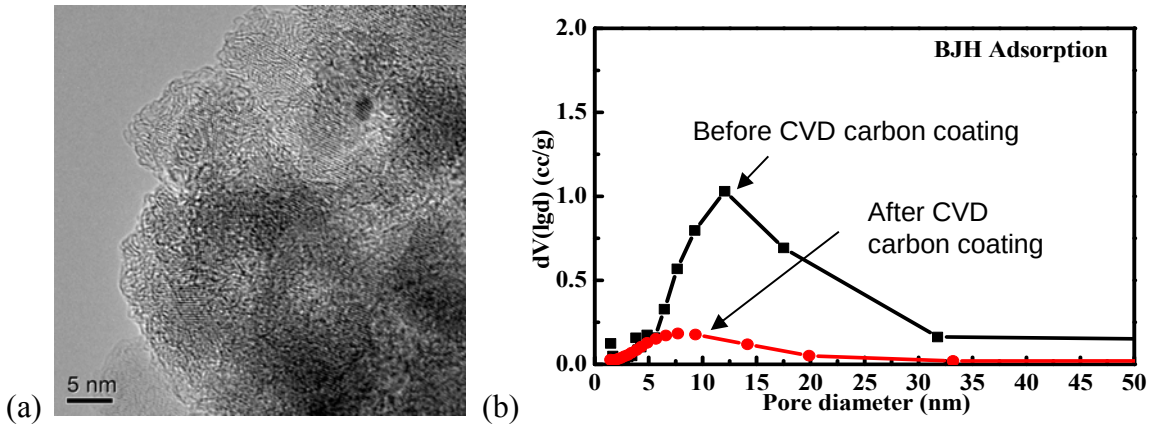

Figure V - 86: Structure characterization of porous Si with a 10-nm pore size. a) TEM image shows the carbon coated on porous Si. b) Pore size and pore volume change of the porous Si before and after carbon coating.

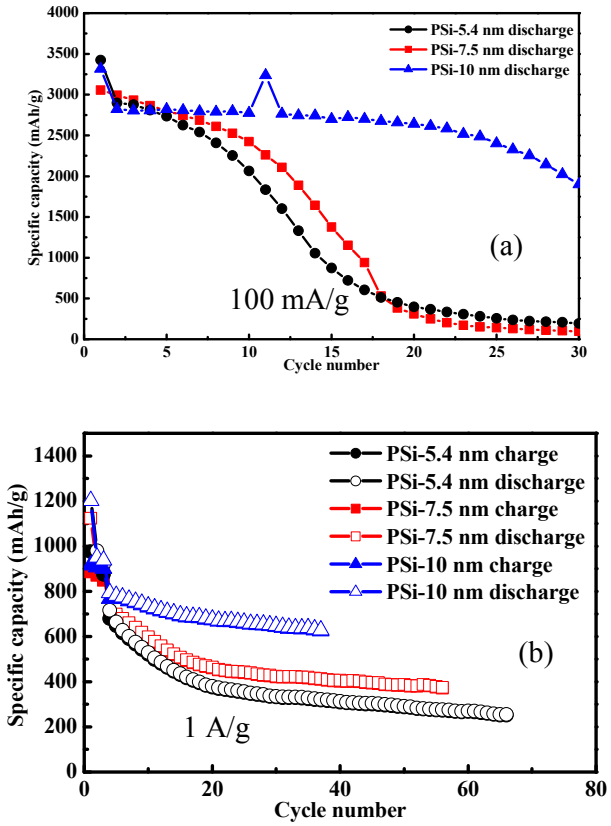

Figure V - 87: Cycle stability of anodes of porous Si with different pore sizes. a) Cycle stability at a low current density of 100 mA/g. b) Cycle stability at high current density of 1 A/g.

FY 2011 Publications/Presentations

1. Xiaolin Li, Praveen Meduri, Shanti Subramanian, Jie Xiao, Xilin Chen, Chongmin Wang, Ji-Guang Zhang, and Jun Liu. Pore size effect of porous silicon anodes for lithium rechargeable batteries. 220th ECS Meeting, Boston, MA. October 9-14, 2011.
2. Ji-Guang Zhang, Wei Wang, Jie Xiao, Wu Xu, Gordon L. Graff, Gary Yang, Daiwon Choi, Deyu Wang, Xiaolin Li, and Jun Liu. Silicon-Based Anode for Li-Ion batteries. To be published in Encyclopedia of Sustainability Science and Technology, a Springer Reference book edited by Robert A. Meyers et al.
3. Chong-Min Wang, W. Xu, J. Liu, D.W. Choi, B. Arey and L.V. Saraf, J.G. Zhang, Z.G. Yang, S. Thevuthasan, D.R. Baer, and N. Salmon. *In Situ* Transmission Electron Microscopy and Spectroscopy Studies of Interfaces in Li-Ion Batteries: Challenges and Opportunities. Journal of Material Research 25(8):1541 (2010).
4. Chong-Min Wang, Wu Xu, Jun Liu, Ji-Guang Zhang, Lax V. Saraf, Bruce W. Arey, Daiwon Choi, Zhen-Guo Yang, Jie Xiao, Suntharampillai Thevuthasan, and Donald R. Baer, *In Situ* Transmission Electron Microscopy Observation of Microstructure and Phase Evolution in a SnO_2 Nanowire during Lithium Intercalation, *Nano Lett.*, *11* (5): 1874 (2011).

V.C.6 Advanced Binder for Electrode Materials (LBNL)

Gao Liu
Enviornmental Energy Technologies Division
Lawrence Berkeley National Laboratory
Berkeley, CA 94720
Phone: (510) 486-7207; Fax: (510) 486-8619
E-mail: gliu@lbl.gov

Start Date: October 2010
Projected End Date: September 2012

Objectives

- Develop new conductive polymer binder materials to enable Si material in Li-ion negative electrode. Si has the highest Li-ion storage capacity at 4200 mAh/g. However, major issues presvent Si material from being used as negative electrode material in Li-ion cells, including limited life and low coulombic efficiency. The goal of this project is to develop negative electrode binder materials to improve the cycling performance of the Si-based electrode, and compatable with current Li-ion manufacturing process.
- Commercial Si particles come with different surface chemistries. The interface between the Si particle and conductive binders plays a critical role for the charge transport. The surfaces native to the Si particles are characterized and modified to improve charge transport at the interface.

Technical Barriers

This project addresses the following technical barriers from the Energy Storage section of the Vehicle Technologies Program Multi-year Research, Development and Demonstration Plan:

- Calendar and cycle life
- Energy density
- Cost

Technical Targets

Relevant USABC goals

EV

- $150/kWh
- 230 Wh/dm^3
- 1000, 80% capacity, discharge cycles
- 10-year system life

PHEV 40-mile

- $220/kWh
- 193 Wh/dm^3
- 2750, 75%-capacity, discharge cycles +80,000 HEV cycles
- 15-year system life

Accomplishments

- Synthesized a class of conductive polymer binders for Si materials with good electronic conductivity and good adhesion.
- The conductive polymer binder enables high capacity cycling of Si particles without conductive additives in the electrode.
- Correlated Si nanoparticle surface chemistry to their electrochemical performance.
- Developed processes to modify Si nanoparticle surface to improve their electrochemical performance.

✧ ✧ ✧ ✧ ✧

Introduction

Achieving the DOE energy, cycle life and cost targets will require materials of higher capacity and/or voltage and improved coulombic efficiency. High capacity Si based anode material has the potential to fulfill the energy density requirements for EV/PHEV applications. However, full capacity cycling of Si results in significant capacity fade due to a large volume change during Li insertion and removal. Decreasing the particle size to nanometer scale can be an effective means of accommodating the volume change; however, nanoparticle has large specific surface area, which makes the material prone to oxidation to form insulating SiO_2 layer. It is also challenging to make electric connections to all the Si nanoparticles in the electode by using similar size acetylene black nanoparticles. The repeated volume change of Si nanoparticles during cycling can lead to repositioning of the particles in the electrode matrix and result in particle dislocation from the conductive matrix. This dislocation of particles causes the rapid fade of the electrode capacity during cycling. In order to address this issue, Si/conductive polymer composite electrodes were developed. This new electrode can be fabricated with the current Li-ion manufacturing processes. We developed a new class of electric conductive binder materials, which provide improved binding force to the Si surface to help maintain

good electronic connectivity throughout the electrode. The electrodes made with these binders have significantly improved the cycling capability of Si.

Approach

Use functional polymer design and synthesis to develop new conductive polymers with proper electronic properties, strong adhesion and improved flexibility to provide electric pathways in the electrode, and to accommodate large volume change of the Si alloy active material during lithium insertion and removal. The rational design of binder is assisted with advanced diagnostic techniques such as XAS at Advance Light Sources and with advanced molecular computation at National Energy Reseearch Secientific Computing Center – both are DOE national user facilities.

Results

Conductive Polymer Binder with Tailored Electronic Properties. We developed new conductive polymers through a combination of material synthesis, X-ray spectroscopy, density functional theory, and battery cell testing (Figure V - 88). Contrasting other polymer binders, the tailored electronic structure of the new polymer enables lithium doping under the battery environment. The polymer thus maintains both electric conductivity and mechanical integrity during the battery operation.

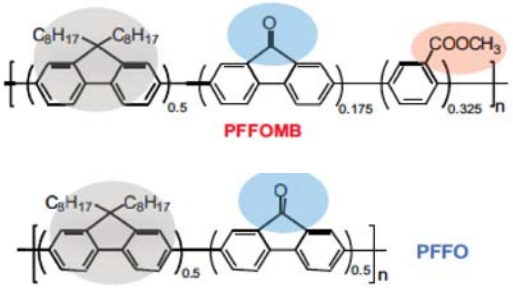

Figure V - 88: Molecular structure of conductive polymer binder.

The technical challenge stems from the reducing enviroment when the Si anode is lithiated. For example, the typically used p-type polyaniline (PAN) conductive polymer will not stay p-doped below 1 V (Li/Li^+), therefore losing electronic conductivity when used in the Si anode, which is operated between 0.01 V–1 V (Li/Li^+).

In order to solve the crucial problem on electric connectivity of the binder, we focus on developing polymer binders that could be cathodically (n-type) doped for high electronic conductivity under the reducing environment for anodes. Our strategy for accomplishing the goal is to tailor the energy levels of the polymer conduction state, i.e., the lowest unoccupied molecular orbital (LUMO), so that the electrons could cathodically dope the polymer to achieve adequent electronic conductivity. Mechanically, it is also crucial that the polymer is intimately adhered to Si particle surface. Both electrical and mechanical integrity of the electrodes will then be maintained throughout the battery operation

The molecular structures of the developed polymers, PFFO and PFFOMB are based on polyfluorene (PF)-type polymers (Figure V - 88) Two key functional groups, carbonyl C=O and methylbenzoic ester -$PhCOOCH_3$ (MB), were introduced for tailoring the LUMO electronic states and for improving the polymer adhesion respectively, as elaborated below.

In order to achieve a properly tailored electronic structure, we have extensively applied synchrotron based soft x-ray absorption spectroscopy (XAS) on a series of polymers to monitor the unoccupied conduction states. XAS provides a simple but direct probe of the excitations of core level electrons to the unoccupied states, i.e., the lowest-energy XAS peaks directly correspond to the LUMO states. Figure V - 89 shows the XAS data collected on three selected PF type polymers and the traditionally used p-type PAN. It is evident that the carbonyl groups in PFFO and PFFOMB generate a new LUMO state at 284.7eV in XAS (blue arrow), much lower than that of the PF (black arrow) and PAN (purple arrow). The additional MB units in PFFOMB do not change the low energy position of this LUMO. Therefore, the carbonyl is the key function group that lowers the LUMO energy level.

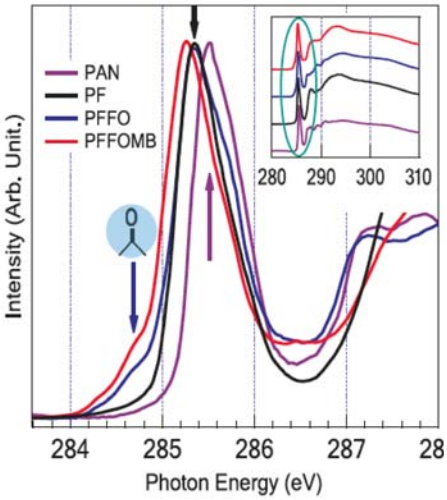

Figure V - 89: Carbon- 1s XAS spectra collected on a series of polymers.

Performance of Si/Conductive Polymer Composite Electrode. A commercial Si material was used to fabricate electrodes with the PFFOMB conductive binders. The Si material is NOT carbon coated. A standard slurry making process was used to fabricate all the composite Si/conductive binder electrodes. Figure V - 90 presents the performance of the PFFOMB/Si based anode that is cast with a Si to polymer weight ratio of 2:1. The electrodes based on PAN and polyvinylidine difluoride (PVDF)

showed poor performance due to the insulating nature of the polymer matrix. The Si/AB/PVDF and Si/PFFO electrodes are characterized by high starting capacity but fast fading, due to the loss of electrical and mechanical integrity respectively. With the designed electrical and mechanical properties, PFFOMB achieved both intimate electric contact for electron conduction and mechanical integrity, resulting in high specific capacity and stable cycling performance.

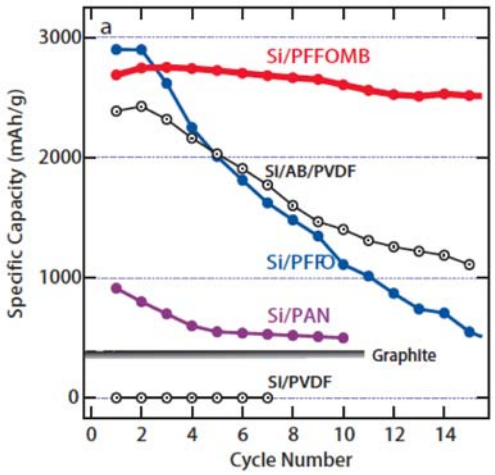

Figure V - 90: The initial cycling behaviors of Si particles in different conductive matrixes against lithium metal counter electrodes at C/10 rate.

Commercial Si Nanoparticle Surface and Modification. An important aspect that has not been well studied is the surface of the Si nanoparticles and its impacts on the initial cell performance. Nanomaterials, including spherical particles, wires or sponge structures, tend to have enhanced surface area compared to micron-sized particles. Surface impurities play a significant role in the performance of the nano-material; the initial performance of Si nanoparticles with similar size distribution can vary significantly from batch to batch even if they are from the same supplier. We demonstrate that the performance variation is due to variations in the native oxide surface layer on Si nanoparticles, and that the removal of this layer can significantly improve the Si nanoparticles' initial performance.

TEM images of Si nanoparticles before and after etching for 30 min. to remove surface layers are shown in Figure V - 91. Besides the large size distribution of the as-received sample, a core-shell structure was observed for most particles in Figure V - 91a,b. Shell thickness is around 4 -10 nm, with thicker shells on bigger particles. This amorphous shell layer is the native oxide layer from the manufacturing process. We have investigated different samples from various sources, and the thickness of this glassy amorphous layer varies significantly. After HF etching, this amorphous oxide layer was reduced to 1-2 nm (Figure V - 91c,d).

The SiO_2 content as a function of different etching times was investigated using TGA. As shown in Figure V - 92 SiO_2 content decreases from 26.5 % before etching to 18.9 % after 5 min. and 12.9% after 10 min. of etching. A simple calculation based on elemental analysis assuming 50-nm Si nanoparticles yields an initial surface SiO_2 layer of 4 nm, which is at the lower limit of the TEM observations for the as-received sample. The HF etching provides a facile process for generating Si nanoparticles with different SiO_2 content by controlling the etching time.

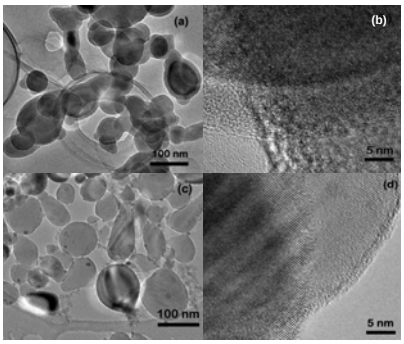

Figure V - 91: TEM images of Si nanoparticles [(a) and (b)] as-received from commercial supplier showing SiO_2 layer on the surface and [(c) and (d)] after 30 min of HF etching to remove the SiO_2 surface layer.

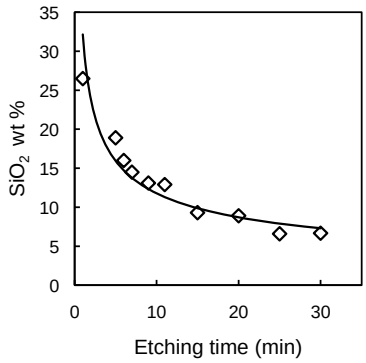

Figure V - 92: SiO_2 content in the samples, determined using TGA, as a function of etching time.

The as-received Si nanoparticles and those after 10 min. and 30 min. of etching were used as negative electrodes in coin cells with Li metal as the counter electrodes, and their initial electrochemical performance was evaluated for 10 cycles (Figure V - 93). The specific capacities in Fig. 3a,b,c are based on the overall weight of the Si nanoparticles, whereas those in Fig. 6a-1,b-1,c-1 are after discounting the weight of the SiO_2. Comparing the specific capacities based on Si powder weight in Fig. 3a,b,c, there is a clear correlation between the SiO_2 surface layer thickness and measured reversible capacity. The reversible capacity of the as-received Si nanoparticles is less than 970 mAh/g (Figure V - 93a), and even after discounting SiO_2, it is 1320 mAh/g (Figure V - 93a-1),

which is still far short of the 3750 mAh/g expected from Si materials. The kinetics of reducing SiO_2 is very slow. The specific capacities improve steadily after 10 min. (Figure V - 93b, Figure V - 93b-1) and 30 min. (Figure V - 93c, Figure V - 93c-1) of etching to reach the theoretical capacity limit for Si. Therefore, the thick SiO_2 layer has an insulating effect on the Si cores, preventing some of the Si from reacting with Li, and removal of this layer via an HF etch significantly improves the reversible capacity.

Conclusions and Future Directions

We have successfully developed a class of conductive polymer binder that is suitable for Si anode. Extended cycling tests have demonstrated the effectiveness to accomondate Si volume change, provide electric conduction within the electrode, and stability during cycling. We have characterized the Si nanoparticle surface and understood the surface properties to the Si electrochemical performances. In the future we will develop an electrode that has high Si material loading and high capacity per unit area to meet the EV/PHEV energy density goals. We will combine the conductive polymer binder with other functionalities and additives to further stabilized Si surface, minimize side reactions and increase coulombic efficiency.

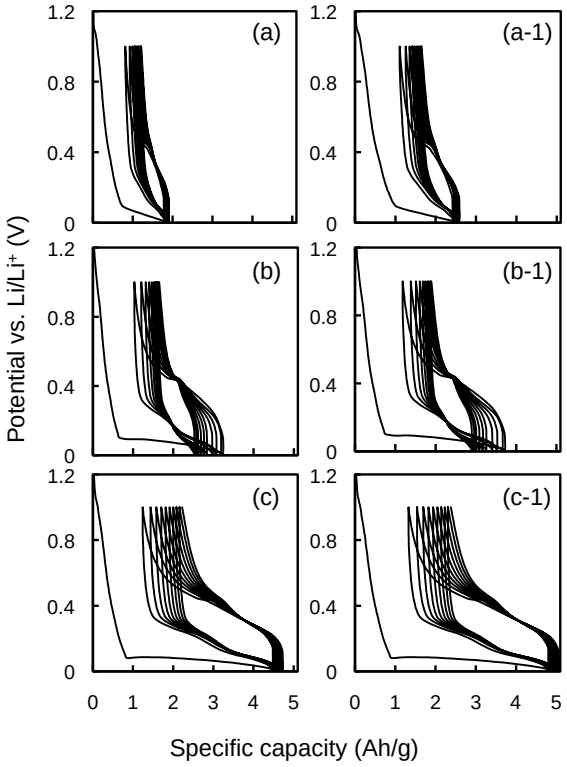

Figure V - 93: Specific capacity vs. potential of the first 10 cycles of Si electrode. (a) and (a-1) As-received Si, (b) and (b-1) Si after 10 min of etching, (c) and (c-1) Si after 30 min of etching. (Specific capacities in (a), (b) and (c) are based on gross Si particle weight; specific capacities in (a-1), (b-1) and (c-1) are based on pure Si weight after discounting SiO_2.)

FY 2011 Publications/Presentations

Patents and Patent Applications

1. U.S. patent application No. PCT/US2008/063101, "Improved High Discharge Rate Lithium-Ion Rechargeable Batteries" Gao Liu, Vince Battaglia, and Honghe Zheng, filed in May 2008.
2. U.S. patent application No. PCT/US2010/035120 "Electrically Conductive Polymer Binder for Lithium-ion Battery Electrode" Gao Liu, Shidi Xun, Vince Battaglia and Honghe Zheng, filed in May 2010.
3. U.S. patent application PCT/US2011/038420 "Si Composite Electrode with Li Metal Doping for Advanced Lithium-ion Battery" Gao Liu, Shidi Xun and Vince Battaglia, filed in May 2011.
4. U.S. patent application no. PCT/US2011/047546, "Nanostructure-Surface Modified Cu Thin Film for Lithium-ion Negative Electrode Application" Gao Liu, Ziyan Zheng, Xiangyun Song and Vince Battaglia, filed in Aug. 2011.

Publications

1. Liu, G.; Xun, S.; Vukmirovic, N.; Song, X.; Olalde-Velasco, P.; Zheng, H.; Battaglia, V. S.; Wang, L.; Yang, W, Polymers with Tailored Electronic Structure for High Capacity Lithium Battery Electrodes, *Adv. Mater.* **2011** to appear.
2. Xun, S.; Song, X.; Wang, L.; Grass, M. E.; Liu, Z.; Battaglia, V. S.; Liu, G., The Effects of Native Oxide Surface Layer on the Electrochemcial Performance of Si Nanoparticles-Based Electrodes. *J. Electrochem. Soc.* **2011** to appear.
3. Xiao, J.; Wang, X; Yang, X. Q.; Xun, S.; Liu, G., Koech, P. K.; Liu, J., Lemmon, J. P., Electrochemically Induced High Capacity Displacement Reaction of PEO/MoS_2/Graphene Nanocomposites with Lithium. *Adv. Funct. Mater.* **2011** to appear.
4. Xun, S.; Song, X.; Grass, M. E.; Roseguo, D. K.; Liu, Z.; Battaglia, V. S.; Liu, G., Improved Initial Performance of Si Nanoparticles by Surface Oxide Reduction for Lithium-Ion Battery Application. *Electrochem. Solid State Lett.* **2011,** *14* (5), A61-A63.
5. Kim, S.; Park, M. J.; Balsara, N. P.; Liu, G.; Minor, A. M., Minimization of focused ion beam damage in nanostructured polymer thin films. *Ultramicroscopy* **2011,** *111*, 191-199.
6. Zheng, H. H.; Liu, G.; Song, X. Y.; Ridgway, P.; Xun, S. D.; Battaglia, V. S., Cathode Performance as a Function of Inactive Material and Void Fractions. *J. Electrochem. Soc.* **2010,** *157* (10), A1060-A1066.

Inivted presentations

1. *Particles and Polymer Binder Interaction - A Controlling Factor in Lithium-ion Electrode Performance,* General Motors Global R&D Symposium-Automotive Lightweight Materials and Battery Technology in Shanghai China, Nov. 2011.
2. *New Materials and Electrode Designs for Lithium-ion Rechargeable* General Motors, Warren Michigan, Nov. 2011.
3. *Probe Material and Interface Changes of an OLED Device,* U.S. DOE EERE-BES SSL Roundtable meeting in Bethesda Maryland, Oct. 2011
4. *Developing and understanding battery materials with combined techniques Part I. Introduction and materials*, Soft X-Ray Spectroscopy of Energy Storage Materials Section of Advanced Light Sources user meeting at Lawrence Berkeley National Laboratory in Berkeley CA, Oct. 2011.

V.C.7 Three-Dimensional Anode Architectures and Materials (ANL)

Jack Vaughey
Argonne National Laboratory
9700 South Cass Avenue
Argonne, IL 60439
Phone : (630) 252-9184 ; Fax : (630) 252-4176
E-mail: vaughey@anl.gov

Collaborators: ANL: L. Trahey, Fulya Dogan, Fikile Brushett, Aude Hubaud

Start Date: October 1, 2010
Projected End Date: September 30, 2014

Objectives

- Design electrode architectures containing main group metal, metalloid or intermetallic components that can tolerate the volumetric expansion of the materials and provide an acceptable cycle life
- Exploit electrochemical deposition reactions to improve the design and performance of tin-based intermetallic electrodes
- Develop methods to assess the internal changes within the electrode on cycling as a tool to improve performance.

Technical Barriers

- Low energy
- Poor low temperature operation
- Abuse tolerance limitations

Technical Targets (USABC - End of life)

- 142 Wh/kg, 317 W/kg
  (PHEV 40 mile requirement)
- Cycle life: 5000 cycles
- Calendar life: 15 years

Accomplishments

- Designed and implemented a process to use metallic copper as both the binder and conductive additive for a silicon-based lithium-ion battery anode
- Devised and carried out detailed NMR studies to determine relationship between annealing and cycling stability.
- Devised and constructed a cell for micro CT tomography techniques to 'look inside' electrodeposited three dimensional electrode architectures as they cycle.
- Interactions with the EFRC – Center for Electrical Energy Storage - *Tailored Interfaces* (Argonne-Northwestern University-University of Illinois (Urbana-Champaign) were initiated around the micro CT tomography effort.

Introduction

The search for an alternative anode to replace graphite in lithium-ion batteries has been underway for many years. Several types of materials have been investigated, notably: i) metals, ii) metalloids, iii) intermetallic compounds, and iv) metal oxides. Metals (e.g., Sn), metalloids (e.g., Si) and intermetallic compounds (e.g., Cu_6Sn_5) are of particular interest because they offer significantly higher theoretical volumetric and gravimetric capacities compared to graphite (372 mAh/g and 818 mAh/ml, respectively), and because they react with lithium several hundred millivolts above the potential of metallic lithium. However, these materials have densely packed structures and therefore expand considerably on reaction with lithium. Within the overall BATT-Anode effort, a particular focus on silicon has been initiated for all participants.

A major objective of our research is to design three-dimensional, microporous copper architectures that can 1) simplify the lithium-ion battery electrode by combining requirements for a binder, and conductive additive and extending the current collector into the active phase, and 2) provide a sufficiently large void volume to accommodate the volumetric expansion during reaction with lithium of main group metals. This project was a new start in the BATT-Anode program starting October 2010.

The previous BATT-Anode effort (FY2007-10, PI Mike Thackeray) focused on developing intermetallic anodes with a reversible capacity of > 600 mAh/g with a cycle life exceeding 250 cycles using either half or full lab-scale cells. Materials development focused on bulk intermetallic systems, thin films, and microporous electrodes where a thin film of a main group metal (e.g. tin) was electrodeposited onto a copper foam substrate and annealed to form a three-dimension intermetallic anode structure. The new program builds on these electrode architecture concepts but modified to use high gravimetric energy density silicon and tin active materials rather than high volumetric capacity intermetallics.

Approach

- Design new electrode architectures by electrodeposition techniques in which a Cu foam provides an electronically connected substrate onto which electrochemically active metals can be deposited.
- Develop methods to build electrodes where copper metal acts as a binder and conductive additive for high capacity main group metals, e.g. silicon.
- Develop characterization methods that allow for a better understanding of the electrochemically active interfaces with in the electrode architecture.

Results

The initial focus was to develop a method to encase micron-size Si particles with a Cu net or mesh formed *in situ*. The use of micron-size Si particles (10 to 20 µm) allows for lower surface area contact with the electrolyte, thus eliminating losses due to SEI formation and allowing for easier handling of the raw materials. Initial attention centered on generating a thin and dispersed Cu coating on the Si particles. After evaluating various methods, an electro-less deposition method was chosen for its simplicity and coating characteristics (see Figure V - 94).

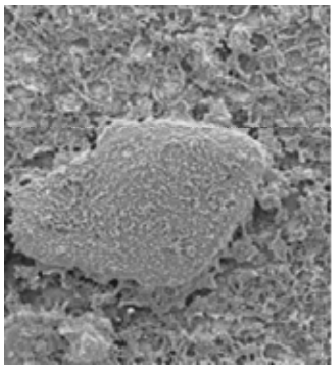

Figure V - 94: A SEM image of the copper-coated silicon particle (20-25 µm) after annealing.

After a detailed annealing study, a set of conditions were identified where the deposited Cu coating annealed to form a three-dimensional network over the Si, binding it to the underlying Cu foil (Figure V - 95). Preliminary XRD studies showed that below 700°C there was only a minimal amount of reaction between Cu and the Si particles to form the intermetallic phase, CuxSi, in agreement with the reported phase diagram. Using this method, a mesh was created over the Si *in situ*, binding it to the current collector without the need for additional binders or conductive additives. In an effort to better understand the interface between the annealed copper mesh and the electrochemically active silicon, solid state ^{29}Si NMR has been used a probe of the system on annealed laminates processed at various temperatures, Figure V - 96.

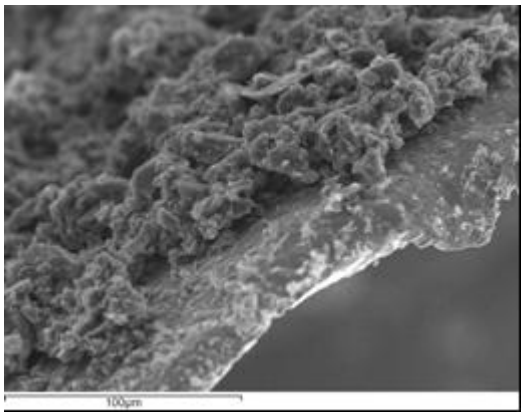

Figure V - 95: Demonstration of how silicon is bound to the copper foil (edge-on view) after annealing.

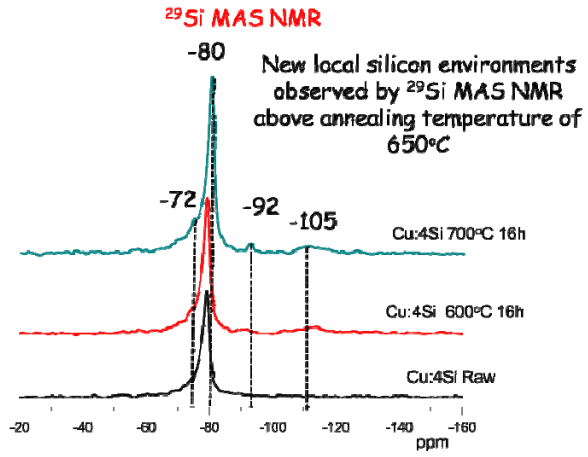

Figure V - 96: MAS-NMR study of species formed on annealing of electrode materials.

Early work, in conjunction with X-ray diffraction studies, indicated that the predominant alloy phases formed on long term heating are Cu_3Si and maybe Cu_4Si. MAS-NMR studies have indicated that the best cycling electrodes have very little alloy formation and little silicon surface oxidation (from annealing process). Electrodes with larger numbers of Si species did not cycle as well as other electrodes. Since many silicon oxides are electrochemically inactive, their presence on the particle surface from the processing may be blocking lithium insertion. In addition electrodes annealed at higher temperatures were found to have peaks that can be associated with Cu_3Si. Due to the small amounts of intermetallic materials present in the laminates, the identification of the interfacial phases was not achievable using powder XRD methods.

Because there are no insulating organic binders and other additives in the electrode, a comparison to a standard electrode was done. Electrochemical studies of these copper-silicon electrodes showed a four-fold enhancement in power capability compared to more standard PVDF-based electrodes and a similar volume-expansion dependence on cycle life. Analysis of the MAS-NMR data also showed under certain annealing conditions the process used oxidized the surface of the silicon particles hindering their activity. This coating would probably also hinder power capability and its formation process is being investigated.

The electrodes have been evaluated for cycle life as a function of the capacity. By varying the capacity of the underlying Si materials, the impact of a variety of electrode volume expansions (LiSi has ~ 120%, based on crystallographic data) can be evaluated. In Figure V - 97, the cycling of materials of the electrode composition $CuSi_4$ is plotted against various lithium contents. For samples cycled to the approximate composition "$LiSi_2$", the electrode can maintain this capacity for nearly 50 cycles, for higher volume expansion (Li_3Si_4, LiSi) the cycle life is lower. Figure V - 98 highlights the first 10 cycles for the $CuSi_4$ laminate cycled to the composition $LiSi_2$.

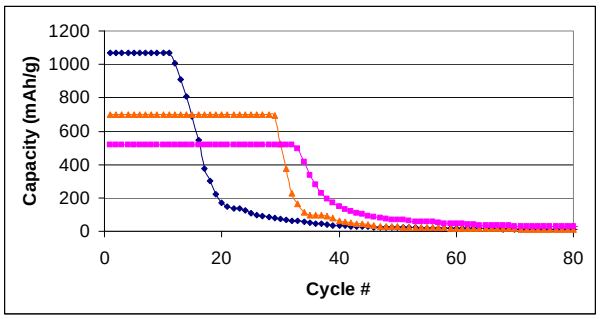

Figure V - 97: The cycling capacity of a series of $CuSi_4$ electrodes cycles to LiSi, Li_3Si_4, and $LiSi_2$.

Based on cycling data to date, the more copper in the sample relative to silicon the better the laminate holds together and the more controlled the silicon's volume expansion the better the cycling. Plots of the cycling profile over time and an individual profile are shown in Figure V - 98.

Tomography

Improving the performance and lifetime of volume-changing anode materials requires a detailed knowledge of 3d structure as a function of synthesis parameters and cell operating conditions. To that end, high resolution, high speed synchrotron-based microtomography experiments at the 2-BM-A beamline at Argonne's Advanced Photon Source have been used to 'look inside' a cycling electrode. Microtomography enables non-destructive visualization of complex electrode architectures, including buried pore networks and sub-surface interfaces.

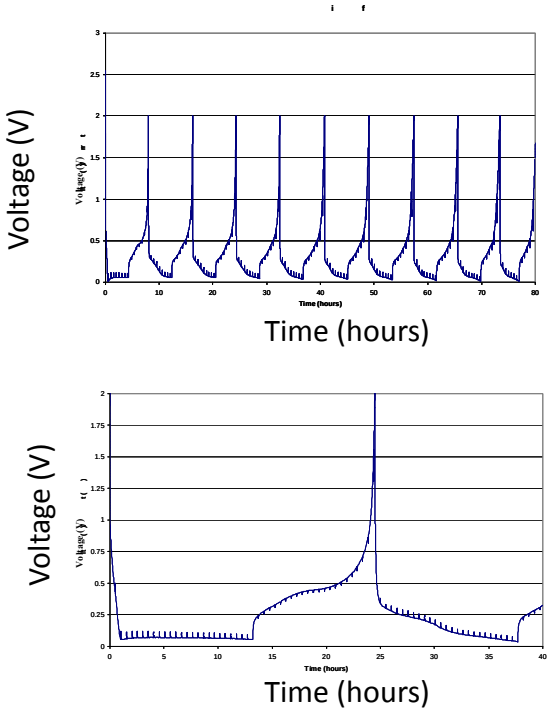

Figure V - 98: The cycling profile for $CuSi_4$ electrodes cycled to the composition $LiSi_2$.

Copper substrate current collectors were electrodeposited with a wide range of parameters in order to develop two robust, yet distinctly different morphologies (in terms of porosity and tortuosity). Applied current, deposition time, additive concentration, annealing temperature, and annealing time were systematically altered and the resulting substrates were analyzed by scanning electron microscopy. It was determined that 1 A depositions for 30 seconds with 2 different Cl^- concentrations (one 4x the other), and annealing at 500°C for 48+ hours reproducibly produced strong substrates with surface features well-suited for microtomography.

Both electroless and electrodeposition were used to coat the copper substrates with tin. It was expected that the electroless bath would be ideal due to its tailored throwing power (ability to coat subsurface features with the same ease as high-altitude features), yet the electroless trials applied very thick tin coating despite short immersion times. Four electrodeposition procedures (3 galvanic square waves and 1 galvanostatic) were tested, all designed to deposit the same number of moles of tin onto the copper surfaces. The galvanic square waves, as expected, produced the least dendritic tin coatings. The final deposition procedure was determined to be (-10 mA, 1 s / -1 mA, 5 s) x 240, from a solution of tin sulfate,

sodium sulfate, and tartaric acid. SEM images of these depositions on the two different copper substrates are shown in Figure V - 99.

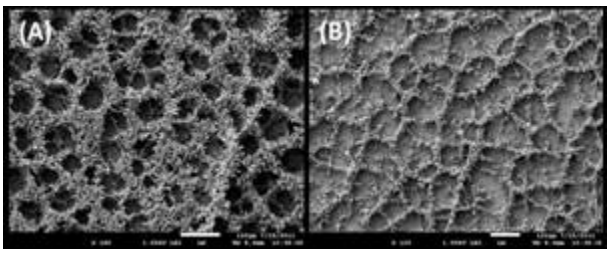

Figure V - 99: SEM images of the two types of Cu substrates generated for the micro-tomography study.

Microtomography of the copper substrates, substrates coated with tin, and electrodes cycled (vs. lithium) is currently underway including *in situ* electrochemical cycling at the microtomography beamline, continued efforts on electroless tin deposition on the substrates, and annealing the Sn-coated substrates to produce an intermetallic interlayer between the active tin and the current collector.

Conclusions and Future Directions

- Designing and building three dimensional electrode architectures that eliminates non-conductive and insulating electrode components has been found to increase the power capability of a silicon electrode.
- MAS-NMR studies of the Cu-Si electrodes have found that the electrodes with the smallest amount of intermetallic formed (Cu_3Si) cycle the best.
- Tomography experiments of electrodeposited 3-D composite Sn on Cu electrodes have identified a non-isotropic volume expansion in the active species that has implications for researchers concerned about binder design.
- Work will continue on these related electrode designs to gain further insights on how electrode construction for these high volume expansion systems can be optimized for better performance and cycle life.

FY2011 Publications/Patents/Presentations

1. Lynn Trahey, John T. Vaughey, Harold H. Kung, Michael M. Thackeray "Porous Copper Current Collectors for Advanced Anode Architectures" NEDO-Argonne Meeting on Lithium-Ion Batteries, Argonne, IL, October, 2010.
2. L. Trahey, J. Vaughey, A. Jansen, M. M. Thackeray "Binder Free Intermetallic Sn Electrodes" Argonne-PNNL Joint Workshop on Energy Storage, Argonne National Laboratory, November, 2010.
3. Lynn Trahey, John T. Vaughey, Michael M. Thackeray "Porous Sn-based Electrode / Electrolyte Systems for Li-Ion Batteries" 216th Meeting of the Materials Research Society, San Francisco, CA, April, 2011.
4. J. Vaughey, L. Trahey "Metallic Copper Binders for Li-Ion Batteries: Synthesis and Characterization" BATT-Anode Workshop, Washington DC, May, 2011.
5. L. Trahey, F. Dogan, B. Johnson, J. Vaughey "Applications of X-Ray Tomography to Three Dimensional Anode Architectures" Joint BATT-Anode Workshop, Berkeley, CA, August, 2011.
6. Fikile Brushett, Andrew Jansen, Jack Vaughey, Zhengcheng Zhang, Fulya Dogan "Exploratory Research of Non-Aqueous Flow Batteries for Renewable Energy Storage" 219th Meeting of the Electrochemical Society, Boston, MA, October, 2011.
7. Fulya Dogan, Lynn Trahey, Michael M. Thackeray, John T. Vaughey "Three-Dimensional Anode Architectures and Materials" 219th Meeting of the Electrochemical Society, Boston, MA, October, 2011.
8. A. N. Jansen, J. Clevenger, A. Baebler, J. T. Vaughey "Variable Temperature Performance of Intermetallic Lithium-Ion Battery Anodes" *J. Alloys and Compounds*, **509**, 4457 (2011).
9. L. Trahey, H. Kung, M. M. Thackeray, J. T. Vaughey "Effect of Electrode Dimensionality and Morphology on the Performance of Cu_2Sb Thin Film Electrodes for Lithium-Ion Batteries", *Eur Journal of Inorganic Chemistry*, 3984 (2011).
10. C. Joyce, L. Trahey, S. Bauer, F. Dogan, J. T. Vaughey "Copper Metal Binders: the Copper-Silicon System" *J. Electrochem Soc.,* submitted 2011.

V.C.8 Metal-Based High-Capacity Li-Ion Anodes (SUNY)

M. Stanley Whittingham (Project Manager)
Binghamton University
Vestal Parkway East
Binghamton, NY 13902-6000
Phone: (607) 777-4623; Fax: (607) 777-4623
E-mail: stanwhit@binghamton.edu

Subcontractor: None

Start Date: January 1, 2011
Project End Date: December 31, 2014

Objectives

Replace the presently used carbon anodes:

- With safer materials that will be compatible with lower cost layered oxide and phosphate cathodes and the associated electrolyte.
- With materials having higher volumetric energy densities, twice that of carbon (1.6 Ah/cc and 0.5 Ah/g)

Technical Barriers

This project addresses the following technical barriers facing the use of lithium-ion batteries in PHEV and all-electric vehicles:

(A) Materials and manufacturing cost of lithium-ion batteries

(B) Safety of lithium-ion batteries

(C) Volumetric capacity limitations of lithium-ion batteries

Technical Targets

- Synthesize nano-size tin materials by at least two different methods.
- Characterize these materials and determine their electrochemical behavior
- Initiate studies on nano-silicon materials. Synthesize by at least one method.

Accomplishments

- Synthesized nano-size tin compounds using a mechanochemical reductive reaction.
  - Electrochemical behavior is comparable to that of the SnCo anode.
  - Volumetric capacity is double that of carbon.
- Synthesized a nano-silicon material using a mechanochemical reductive reaction.
  - Shows stable cycling
  - Volumetric capacity is double that of carbon.
- Technology transfer accomplished.
  - Working with several local battery companies, and many ex-students now in battery companies
  - Students now have positions at BNL, NREL, and PNNL. Also at Toyota (Ann Arbor, MI) and Primet Precision (Ithaca, NY)

✧ ✧ ✧ ✧ ✧

Introduction

Achieving the DOE cost and energy/power density targets will require improved anode materials that have higher volumetric energy densities than carbon, and have lower cost production methods. At the same time the material must have higher lithium diffusion rates than carbon and preferably be at a slightly higher potential to improve the safety.

Approach

Explore, synthesize, characterize and develop inexpensive materials that:

- Ideally have a potential around 500 mV above pure Li
- Have double the volumetric capacity of carbon
- Have a higher gravimetric capacity than carbon
- Emphasize simple metal alloys/composites from bulk to nano-size
  - Build on our understanding of the SnCo anode nanostructures
  - Emphasize tin compounds and compare with silicon based nanostructures

Results

Tin Anode Materials. Sn based alloy materials were prepared by mechanical milling using Ti, Al and Mg as the reducing agent and different grinding media. It was found that both the reductive metal and grinding media significantly affect the material formed and the resulting electrochemical behavior. Titanium reduction provided materials with excellent capacity, 600 mAh/g which is close to the theoretical capacity, and excellent capacity

retention on cycling. The electrochemical behavior was further enhanced by the use of iron grinding media, which resulted in the alloying of some or all of the tin with iron giving Sn_2Fe. The capacity and rate capability of these iron containing materials is comparable to those of the Sn-Co-C compounds, and much better than bulk Sn_2Fe. Their electrochemical behavior is shown in Figure V - 100, Figure V - 101, and Figure V - 102; all are cycled vs lithium metal.

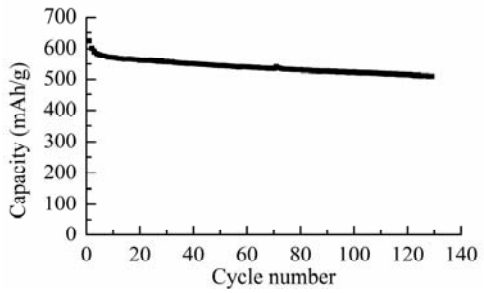

Figure V - 100: Capacity retention on cycling of Sn-Fe formed by titanium reduction using hard iron grinding media and cycled between 0.01 and 1.2 volts at 0.2 mA/cm^2.

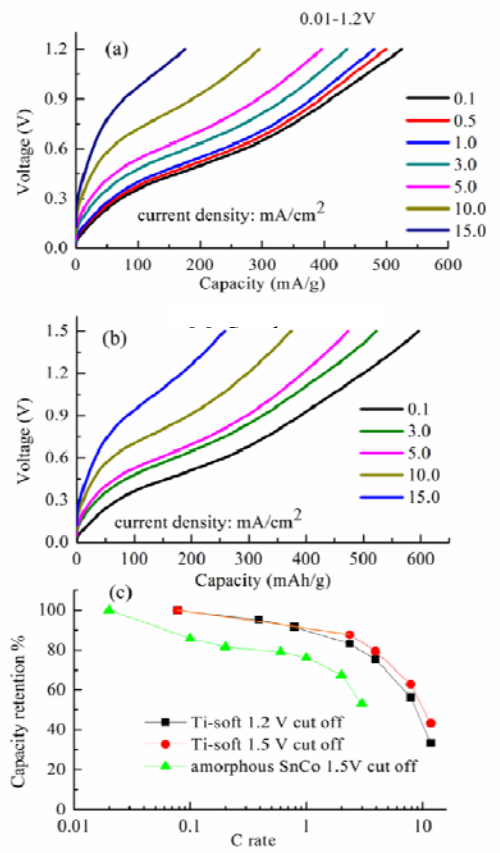

Figure V - 101: Lithium removal from the Sn-Fe electrode synthesized by titanium reduction in soft-iron media. (a) cycled between 0.01 and 1.2 volts, (b) between 0.01 and 1.5 volts, and (c) Ragone plots comparing this material with the SONY SnCo anode.

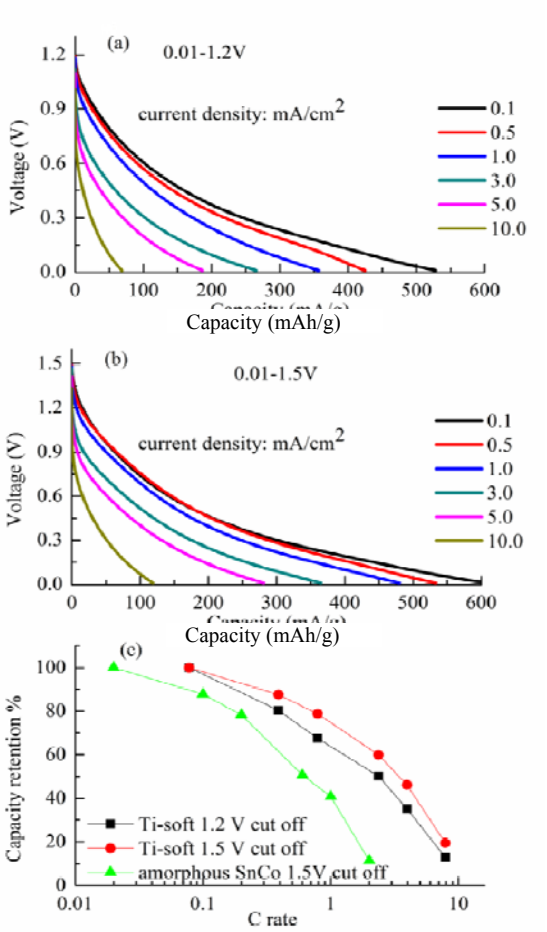

Figure V - 102: Lithium insertion into the Sn-Fe electrode synthesized by titanium reduction in soft-iron media. (a) cycled between 0.01 and 1.2 volts, (b) between 0.01 and 1.5 volts, and (c) Ragone plots comparing this material with the SONY SnCo anode.

These materials were prepared by titanium reduction using soft-iron grinding media, where the tin was present as nano-sized Sn_2Fe, and the iron came from the grinding media. The volumetric energy density is 2.2 Ah/cc, more than double that of carbon.

Silicon Anode Materials. A Si/MgO/graphite (SMOG) composite was synthesized by a two-step high energy ball-milling process. Equal molar amounts of SiO and Mg (99%, Aldrich) powder were ball-milled for 4 hours. Then an equal weight of graphite was added and it was further ball-milled for 0.5 hour. The average crystallite sizes of the Si and MgO are 26 nm and 22 nm, and these form agglomerates from 100 nm to 3 µm. The Si, Mg and O are evenly distributed throughout the composite. The electrochemical behavior of this composite material is shown in Figure V - 103. As shown in Figure V - 103 (a) the capacity remains over 600 mAh/g for over 40 cycles, this compares to the 372 mAh/g of carbon. An initial theoretical calculation of the volumetric capacity indicates 1.7 mAh/cc double that, 0.8 Ah/cc, of carbon.

Little loss of capacity was observed up to 3 mA/cm^2, with a slight loss at 8 mA/cm^2, equivalent to a 3C rate. The cycling efficiency exceeded 99% for currents of 3 mA/cm^2 or less. At 8 mA/cm^2 the efficiency dropped to 98%. Figure V - 103 (b) shows that the hysteresis in the cycling curve increases markedly at 8 mA/cm^2. The Ragone plot in the inset shows the excellent rate capability.

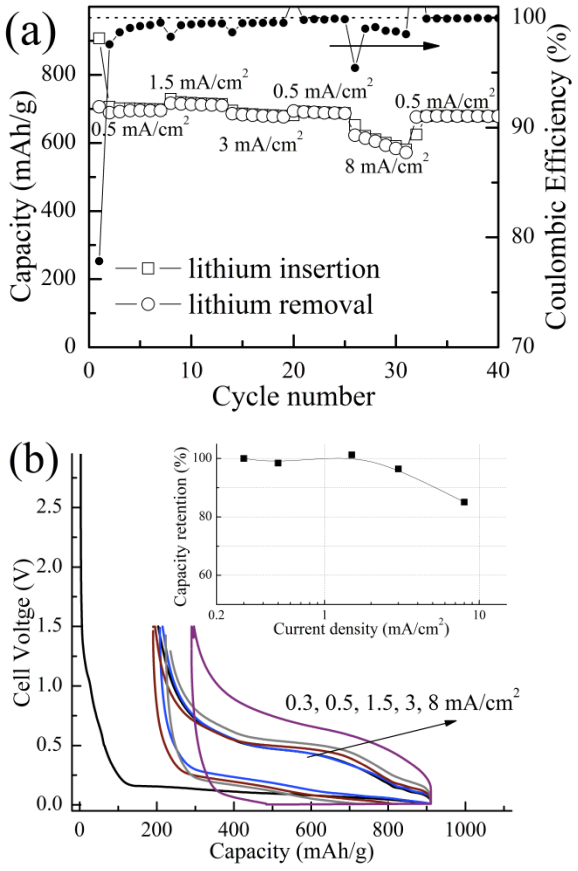

Figure V - 103: Rate capability of Si/MgO/graphite electrode between 0.01 V and 1.5 V. (a) capacity cycling at different current density; (b) lithium insertion/removal curve at different rates, and Ragone plot for Li insertion. 1 C rate = 2.8 mA/cm^2. The first cycle current density was 0.3 mA/cm^2. For current = 1.5, 3, 8 mA/cm^2, the Li/SMOG half cell was discharged to 0.01V and held at 0.01 V for 2 hours before charged.

Conclusions and Future Directions

A clear result from our earlier understanding of the cycling behavior of amorphous nano SnCo anode materials is that nano/amorphous materials work, and that bulk materials with their high expansion on lithium reaction do not and are therefore unsuitable for batteries. Thus, our project targeted mimicking the SnCo material, and this was successfully accomplished using the Sn_2Fe compound. However, it has an unacceptably high first cycle capacity loss which must be overcome. Silicon formed in a reductive mechanochemical reaction showed good cycling and capacity retention. Our future work will include preparing these tin and silicon compounds by at least one more method and evaluating the effect of synthesis approach on the electrochemical properties.

FY 2011 Publications/Presentations

1. Presentation to the 2011 DOE Annual Peer Review Meeting.
2. Wenchao Zhou, Shailesh Upreti and M. Stanley Whittingham "Electrochemical performance of Al-Si-Graphite composite as anode for lithium-ion batteries", Electrochemistry Communications, 2011, 13: 158-161.
3. Wenchao Zhou, Shailesh Upreti, and M. Stanley Whittingham, "High performance Si/MgO/graphite composite as the anode for lithium-ion batteries", Electrochemistry Communications, 2011, 13: 1102-1104.
4. Ruigang Zhang, Shailesh Upreti and M. Stanley Whittingham, "Tin-Iron Based Nano-Materials as Anodes for Li-Ion Batteries", J. Electrochem. Soc., 2011, (12): in press.
5. Many invited presentations, including:
   - Electrochemical Society, Materials Research Society, Pacific Power Sources Conf., IBA
   - U. C. San Diego, Stony Brook U., Wake Forest U., Michigan State U.
   - ORNL, Haldor Topsoe-Copenhagen
   - Local outreach

V.C.9 New Layered Nanolaminates for Use in Lithium Battery Anodes (Drexel U)

Yury Gogotsi and Michel Barsoum
Drexel University
Materials Science and Engineering Department
3141 Chestnut St, MSE Dept. Lebow 344.
Phone: (215) 895-6446; Fax: (215) 895-1934
Email: gogotsi@drexel.edu, barsoumw@drexel.edu
Subcontractor: None

Start Date: Jan 1, 2011
Projected End Date: December 30, 2015

Objectives

- To replace graphite in Li-ion battery (LIB) anode with new materials: layered ternary carbides and nitrides (MAX phases). The strategy may offer anodes with higher charge density than graphite, lesser expansion, longer cycle life and, potentially, a lower cost than Si nanoparticles.

Technical Barriers

This project aims to address the following technical barriers facing the modern LIB technology:

(A) short life-span of modern batteries,

(B) low charge density, and

(C) compromised safety.

Technical Targets

- Perform the a*b initio* simulation of Li incorporation into MAX phase carbides.
- Perform electrochemical experiments on a variety of MAX phases to select the most promising ones for more detailed study.
- Study the effect of particle size on the capacity of the three best MAX phase materials.
- Improve capacity by selective extraction of M or A atoms, to add space for the Li.
- Investigate SEI formation on selected MAX phase carbides.
- Optimization of the material. Testing the rate capability of the anode.
- *In situ* study of charge/discharge processes and better understanding of the mechanism of Li insertion.
- Comparison of powder *vs.* MAX phase solids with 10-20% porosity.

Accomplishments

- Successful synthesis of porous anodes composed of MAX phase requiring neither binder nor carbon black additives.
- DFT simulations of Li intercalation into different MAX phases were carried out, allowing us to gain an insight into the dynamics controlling the process.
- Complete electrochemical study and characterization of different MAX phases.
- Selective etching of an "A" layer was achieved resulting in the exfoliation of MAX phases forming new graphene-like 2-D structures composed of transition metal carbides and/or nitrides ("MXene").

✧ ✧ ✧ ✧ ✧

Introduction

Lithium metal, although providing the highest energy density anode material, cannot be used due to its high reactivity, electrolyte depletion, and dendrite formation issues. As a substitute for Li, graphitic carbon is currently used. We are exploring the feasibility of using layered ternary carbides and nitrides (MAX phases) as new generation anodes for LIB. These materials promise increased capacity (above the 372 mAh $g^{-1}$of graphite, and to address concerns such as safety, cycle-life, and storage-life.

We believe the MAX phases can deliver to the strictest LIB demands due to the following: (i) their vastly superior mechanical properties relative to graphite, (ii) their (at least one order of magnitude) better electronic conductivity than graphite; (iii) the possibility to make anodes without binders by first forming thin wafers followed by a sintering step, (iv) given the higher density of MAX phases they can potentially outperform the volumetric capacity of graphite, even if their gravimetric capacity would be found wanting, (v) large choice of chemistries available, allowing one to fine tune the performance of the system, (vi) the latter can be further expoited by the preparation of the sub-stoichiometric MAX phases in A and/or M elements. We estimate, for example, that if 50% of the Si and Ti atoms are removed from Ti_3SiC_2 and 4 Li atoms surround each Si, the theoretical capacity increases to 738 mAh g^{-1}. Such a value would exceed the capacity of graphite by a factor of ≈ 2. Even higher values can potentially be reached by using

other MAX phases and varying the amounts of A and M atoms extracted from the carbides or nitrides. In addition we believe given the outstanding mechanical properties of the MAX phases such issues as electrode degradation due to solvent induced volume change shall be minimized.

Overall based on the known properties of MAX phases one can expect the following improvements to be obtained: (i) higher energy density; (ii) higher power density; (iii) small irreversible capacity, and, (iv) longer cycle life due to moderate expansion and much better mechanical properties.

Approach

Since at this time the relationship between capacity and MAX phase chemistry is unknown, a rapid screening of as many MAX phases as possible shall be carried out to find out the most promising chemistry, by testing their performance in LIB. This process will be guided by *ab initio* calculations. Reducing particle size, selective etching of an A element from the MAX structure, and exfoliation of these layered structure also will be investigated to increase the Li uptake of these structures and increase the charge density.

Results

Ab intio calculations- using density functional theory (DFT) using the plane-wave pseudo-potential approach, with ultrasoft pseudopotentials and Perdew Burke Ernzerhof (PBE) exchange - Wu-Cohen (WC) correlation functional, as implemented in the CASTEP code in Material Studio software - showed possibility of Li–intercalation inside MAX phases with volume expansion around 30 %. The elechtrochemical measurments for Li uptake, however, into different MAX phases (~20 µm particle size) was however found to be low. Reduction of particle size to around 1 µm resulted in doubling the capacity, but it was still low (see Figure V - 106). In order to increase the Li uptake, selective etching of the "A" layer was carried out to introduce more space for Li in the structure. Selective etching of the Al out of Ti_3AlC_2 (a typical MAX phase) structure using diluted hydrofluoric acid at room temperature, followed by ultrasonication resulted in the formation of the exfoliated Ti_3C_2 layers (that are calling "MXene" to emphasize its graphene-like morphology). The exposed Ti surfaces appear to be terminated by OH and/or F. Not only individual layers are formed (Figure V - 104, a-d), but also conical scrolls and nanotubes (Figure V - 105, a-d). The elastic modulus (predicted by *ab initio* simulation) of a single, exfoliated $Ti_3C_2(OH)_2$ layer, along the basal plane, is calculated to be around 300 GPa, which is within the typical range of transition metal carbides and significantly higher than most oxides and clays. *Ab initio* calculations also predict that MXene band gap can be tuned by varying the surface terminations. When terminated with OH and F groups, the band structure has a semiconducting character with a clear separation between valence and conduction bands by 0.05 eV and 0.1 eV, respectively. The good conductivity and ductility of the exfoliated powders suggest uses in Li-ion batteries, pseudocapacitors and other electronic applications. Assuming 2 Li atoms layers can be accommodated inside the structure (viz. $Ti_3C_2Li_2$) a theoretical capacity of 320 mAh g^{-1} - which is comparable to the 372 mAh g^{-1} of graphite for (LiC_6) – is predicted.

There are over 60 currently known MAX phases and our discovery opens the door for the synthesis of a large number of 2-D $M_{n+1}X_n$ structures, including the carbides and nitrides of Ti, V, Cr, Nb, Ta, Hf and Zr. The latter could include 2-D structures of combination of M-atoms, (*e.g.* $(V_{0.5}Cr_{0.5})_3C_2$) and/or different carbo-nitrides (*e.g.* $Ti_3(C_{0.5}N_{0.5})_2$).

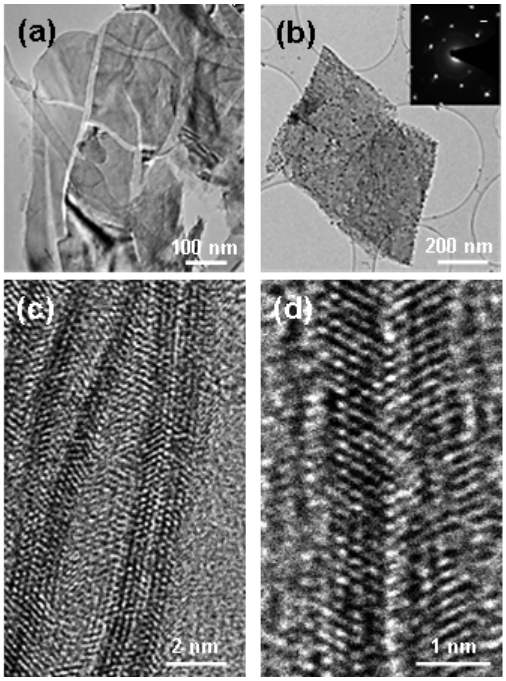

Figure V - 104: TEM images of exfoliated MXene nanosheets. (a) TEM micrographs of exfoliated 2-D nanosheets of Ti-C-O-F. (b) Exfoliated 2-D nanosheets; inset SAD shows hexagonal basal plane. (c) HRTEM image showing the separation of individual sheets after ultra-sonic treatment. (d) HRTEM image of bilayer $Ti_3C_2(OH)_xF_y$.

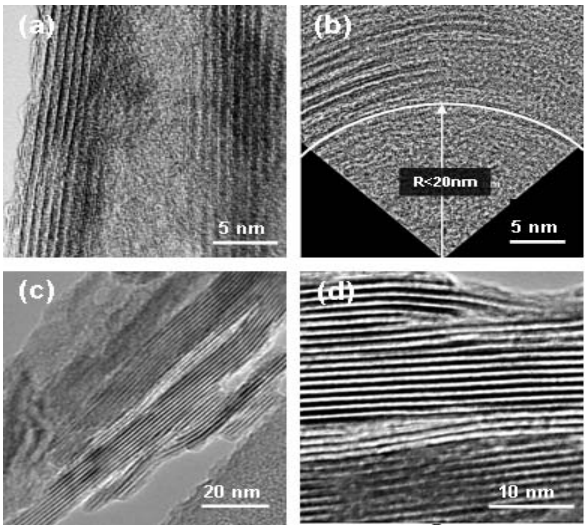

Figure V - 105: TEM images of exfoliated MXene nanosheets. HRTEM image of a bilayer $Ti_3C_2(OH)_xF_y$. (a) Conical scroll of about 20 nm in outer diameter. (b) Cross sectional TEM image of a scroll with inner radius less than 20 nm. (c) TEM micrographs for stacked layers of Ti-C-O-F. Those are similar to multilayer graphene or exfoliated graphite that finds use in electrochemical storage. (d) The same as c but at a higher magnification.

Exfoliated Ti_3AlC_2 powders showed a capacity of 250 mAh g^{-1} for the first cycle and a reversible capacity 5 times higher than pristine T_3AlC_2 (Figure V - 106). These results justify the change in research direction to focus on exfoliated MAX phases (MXenes), with significantly better Li uptake.

The irreversibility of the first cycle can be explained by the presence of hydroxyl, OH, groups on the MXene surface sheets, which presumably react with Li. At this point, work is in progress on reducing those OH groups to enhance the overall Li capacity. At this time, it is reasonable to assume that exfoliated Ti_2AlC would have a Li capacity that is 1.5 times higher than Ti_3AlC_2, due to the lower number of atomic layers per each MXene sheet (3 atomic layers in case of Ti_2C *vs*. 5 for Ti_3C_2).

Conclusions and Future Directions. Using *ab initio* calculation methods we were able to perform the assessment of the MAX phases in view of their potential applications in LIB anodes. The experimental capacity of the anodes made of MAX phases, however, was significantly lower than theoretical.

Selectively etching the A-element from several MAX phases using wet-chemistry was achived. In particular the hydrofluoric acid treatment of the Ti_3AlC_2 MAX phase resulted in a formation of layered Ti_3C_2 – a new 2-D crystalline material.

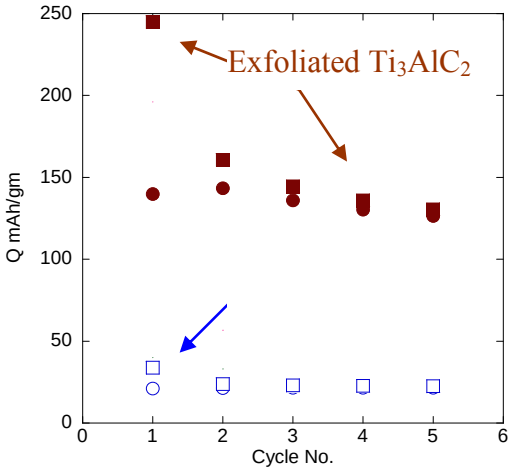

Figure V - 106: Lithiation and de-lithiation charge density as a function of the cycle number for pristine Ti_3AlC_2 and exfoliated Ti_3AlC_2 (Ti_3C_2 MXene).

Overall the strategy of the selective removal of the A-element from the MAX phases allows for the formation of a new class of 2-D early transition metal carbides/nitrides soldis that we propose to call "MXene".

We have demonstrated that the utilization of the MXene based anodes allowed us to quintuple the capacity of LIB anodes as compared with untreated MAX. Work is currently in progress in order to optimize the exfoliation process, as well as broaden the scope of MAX phases which can potentially be used as a source of MXenes.

Understanding the lithiation and delithiation mechanisms is needed to increase the capacity and decrease the irreversibility.

FY 2011 Publications/Presentations

Refereed Publications

1. Naguib, M.; Kurtoglu, M.; Presser, V.; Lu, J.; Niu, J.; Heon, M.; Hultman, L.; Gogotsi, Y.; Barsoum, M. W., Two Dimensional Nanocrystals Produced by Exfoliation of Ti_3AlC_2, Advanced Materials 2011, 23 (37), 4248-4253.
2. Naguib, M.; Kurtoglu, M.; Presser, V.; Lu, J.; Niu, J.; Heon, M.; Hultman, L.; Gogotsi, Y.; Barsoum, M. W., Two-Dimensional Nanocrystals: Two-Dimensional Nanocrystals Produced by Exfoliation of Ti_3AlC_2 (Adv. Mater. Cover 37/2011). Advanced Materials 2011, 23 (37), 4207-4207. (see Figure V - 107).
3. Naguib, M.; Presser, V.; Lane, N.; Tallman, D.; Gogotsi, Y.; Lu, J.; Hultman, L.; Barsoum, M.W., Synthesis of a New Nanocrystalline Titanium Aluminum Fluoride Phase by Reaction of Ti_2AlC with Hydrofluoric Acid, RSC Advances 2011, DOI:10.1039/C1RA00390A
4. Presser, V.; Naguib, M.; Chaput, L.; Togo, A.; Hugd, G.; Barsoum, M.W., First-order Raman scattering of

the MAX phases: Ti_2AlN, $Ti_2AlC_{0.5}N_{0.5}$, Ti_2AlC, $(Ti_{0.5}V_{0.5})_2AlC$, V_2AlC, Ti_3AlC_2, and Ti_3GeC_2, J. of Raman Spectroscopy 2011, DOI: 10.1002/jrs.303

5. Naguib, M.; Presser, V.; Tallman, D.; Lu, J.; Hultman, L.; Gogotsi, Y.; Barsoum, M.W., On the Topotactic Transformation of Ti_2AlC into a Ti-C-O-F Cubic Phase by Heating in Molten Lithium Fluoride in Air, J. American Ceramic Society 2011, DOI: 10.1111/j.1551-2916.2011.04896.x
6. Lane, N.; Naguib, M.; Presser, V; Hugd, G.; Hultman, L.; Barsoum, M.W., First-Order Raman Scattering of the MAX phases Ta_4AlC_3, Nb_4AlC_3, Ti_4AlN_3 and Ta_2AlC, J. Raman Spectroscopy 2011. In press.
7. Naguib, M.; Mashtalir, O.; Carle, J.; Presser, V.; Gogotsi, Y.; Barsoum, M. W., Two-Dimensional Transition Metal Carbides and Carbonitrides. ACS Nano 2011, (submitted).

Presentations

1. Naguib, M.; Kurtoglu, M.; Presser, V.; Lu, J.; Niu, J.; Heon, M.; Hultman, L.; Gogotsi, Y.; Barsoum, M. W. Two-Dimensional Nanocrystals of Ternary Transition Metal Carbides and Nitrides Produced by Exfoliation of MAX Phases, 2011 MRS Fall meeting.
2. Gogotsi, Y.; Barsoum, M.W.; Naguib, M.; Mashtalir, O.; Ruvinskiy, P., New Layered Nanolaminates for Use in Lithium Battery Anodes, 2011 BATT Anode Focus Group Meeting, Washington.

It is worth noting that our paper published in Advanced Materials was the feature article of that issue. Our micrograph, shown below was used for the cover.

This work has garnered much publicity in several languages. The press release and the links to press articles can be found at:

http://max.materials.drexel.edu/mxene-–-a-new-family-of-2-d-transition-metal-carbides-and-nitrides/

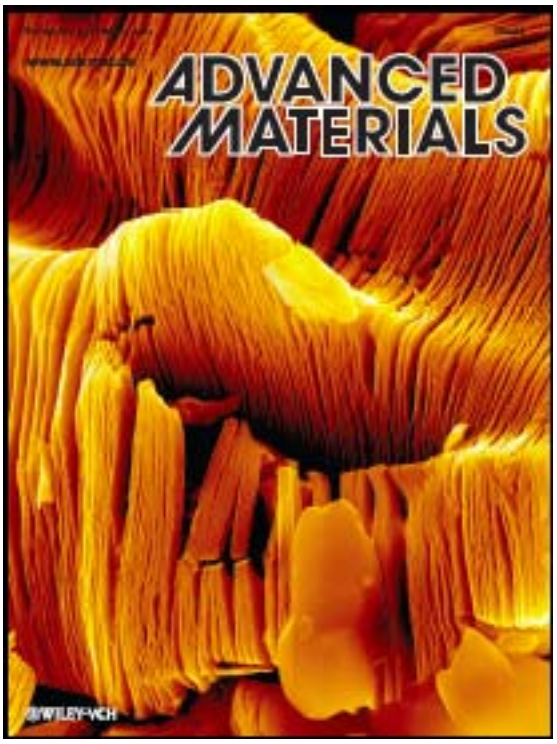

Figure V - 107: Cover of Advanced Materials in which our paper appeared. This colorized SEM micrograph of a typical exfoliated Ti_3C_2 grain was taken at Drexel University by B. Anasori.

V.C.10 Atomic Layer Deposition for Stabilization of Amorphous Silicon Anodes (NREL, U Col)

Anne C. Dillon (Project Manager)

National Renewable Energy Laboratory
1617 Cole Blvd. Golden, CO
Phone: (303) 384-6607; Fax: (303) 384-6432
E-mail: anne.dillon@nrel.gov

Subcontractor: University of Colorado: co-P.I.'s Prof. Steven M. George and Prof. Se-Hee Lee

Start Date: October 2010
Projected End Date: September 2014

Objectives

- Use inexpensive and scalable deposition techniques for the production of either amorphous silicon (a-Si) or nano-Si powders and/or doped a-Si or nano-Si.
- Develop novel atomic layer deposition (ALD) coatings that will enable durable cycling to be achieved for the high volume expansion (~ 400 %)Si materials.
- Explore the importance and mechanism of various coatings via the new *BATT Coating Group*.
- Collaborate within the BATT program with the aim of developing high-rate plug-in hybrid electric (PHEV) compatible electrodes (both anodes and cathodes).

Technical Barriers

Major barriers addressed include:

(A) Cost: Inexpensive processing techniques are employed to fabricate conventional thick electrodes.

(B) High Capacity: Silicon is predominantly being explored as a high capacity anode material. There is also a collaborative emphasis to enable high capacity cathode materials.

(C) High Rate: Both ALD coatings and nanostructured materials are being developed such that high-rate capability is demonstrated for emerging materials.

(D) Safety: The ALD coatings are targeted to improve safety for a variety of electrode materials.

Technical Targets

- Demonstrate that ALD coatings can enable durable cycling for high-volume expansion Si anodes with a capacity ≥ 1000 mAh/g.
- Demonstrate ALD coatings and nanostructured or amorphous materials for prolonged high rate cycling.
- Demostrate that ALD coatings may serve as an artificial solid electrolyte interphase (SEI) and will importantly help minimize degradation upon volume expansion.
- Explore ALD coatings to minimize the first cycle capacity loss in Si anode materials.

Accomplishments

- This is a new award and NREL/CU have met all of the year one milestones as outlined briefly below:
  - Demonstrate scale-up of hot wire chemical vapor deposition (HWCVD) a-Si or nano-Si powder.
  - Optimize HWCVD produced a-Si or nano-Si in conventional coin cell.
  - Demonstrate an ALD coating for improved performance of Si anodes.
  - Optimize coated electrode and demonstrate durable cycling.
- A new *Coatings Group* to better understand the importance of coatings in next-generation material has been formed.
  - Explored internally a variety of systems including full cells to achieve better coating understanding.
  - Established collaborations with external BATT partners including, Stan Whittingham, Clare Grey, Arugumum Mantharam and Gao Lui to better understand coatings via the *Coatings Group.*
- Assisted in employing NREL techniqes to enable high capacity cathodes via collaboration within BATT.
  - NREL established collaboration with Marca Deoff for spray deposition of spinel structures.

- In collaboration with Stan Whittingham, NREL has helped to show that $LiNi_yMn_yCo_{1-2y}O_2$ have inherent high rate capabilities.

✧ ✧ ✧ ✧ ✧

Introduction

Significant advances in both energy density and rate capability for Li-ion batteries will be necessary for implementation in next generation EVs. In our previous BATT award, NREL/CU demonstrated that thick MoO_3 (~15 µm) could be stabilized with a thin ALD coating of Al_2O_3 despite the relatively extreme volume expansion > 100%. In the proposed efforts, both inexpensive routes for the synthesis of Si as well as the Al_2O_3 ALD coating and other new coatings to enable Si anodes will be employed.

Both high rate and durable cycling of Si will be achieved by employing the Al_2O_3 ALD coating and/or by developing new molecular layer deposition (MLD) techniques to develop elastic (polymer-like) coatings and also coatings with low elastic moduli that are similar to polysiloxanes. Extensive collaboration is emphasized to employ both the ALD coatings and demonstrated nano-sturctured materials expertise to enable development of both high capacity anodes and cathodes within the BATT program that exhibit durable high rate capability.

Approach

The utilization of silicon as a Li-ion anode material is very desirable because of its high theoretical capacity of 4200 mAh/g. Unfortunately, crystalline Si (c-Si) exhibits a rapid capacity degradation resulting from large volume expansion that produces fracturing, loss of electrical conductivity and mechanical degradation. Amorphous silicon (a-Si) and nano –silicon (n-Si) have been demonstrated to exhibit improved cycling performance but have not achieved durability and rate capability for application in PHEVs and EVs. In addition, Si has only been demonstrated for thin films (< 1µm) and in nanostructured electrodes that are not suitable for large-scale vehicular applications. Here inexpensive and commercial techniques for the formation of thick Si electrodes are employed.

In the first year the demonstration of inexpensive Si production techniques has been performed. ALD coatings have also been employed to demonstrate reversible high capacity Si for thick electrodes. Finally, mechanistic understanding of the new coatings is being obtained via both internal and collaborative work (*Coatings Focus Group*). Through collaborative efforts, various technologies are being employed to assist in the development of high capacity cathode materials.

Results

Material: Scale-up of the inexpensive HWCVD process to achieve phase pure a-Si has been achieved. For the HWCVD depositions of a-Si powders, the substrate temperature (T_s) was at room temperature. In theory this should completely remove the possibility of growing any crystalline silicon species (c-Si). However, instead local hot spots depending on proximity of the filament to the substrate and duration of the run/film thickness resulted in the nucleation of c-Si particles. Figure V - 108(a) displays an *in situ* microscope image taken of an unutilized a-Si powder. The magnification is 100 times, and the green spots represent the µ–Raman spot size. In Figure V - 108(a) the large particles are ~ 30 µm in diameter and in general had a Raman line consistent with c-Si, the blue curve in Figure V - 108(b). Other portions of the initial samples appeared completely amorphous, red curve Figure V - 108(b), and a mixed phase was also observed, depicted by the orange curve in Figure V - 108(b).

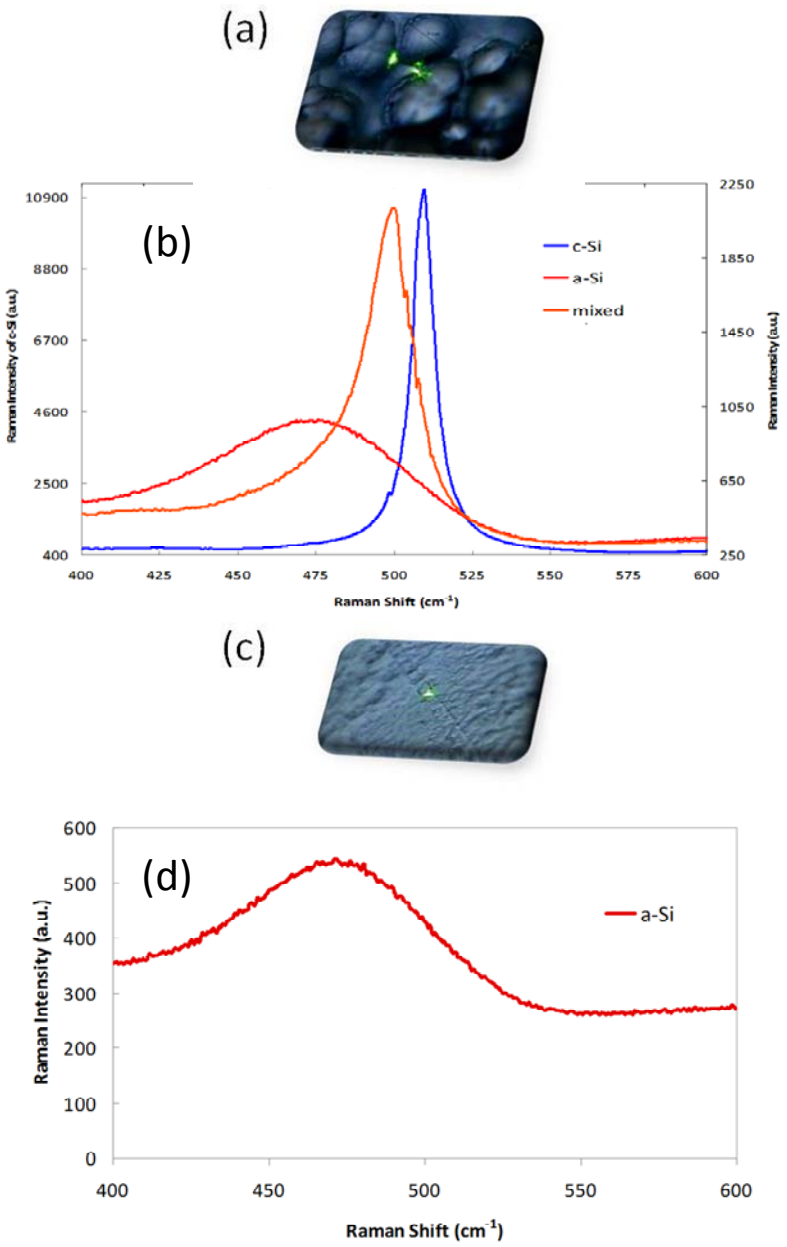

Figure V - 108: a) Image of mixed phase HWCVD Si and b) corresponding Raman spectra compared with c) image of optimized a-Si and d) corresponding Raman spectrum.

By optimizing the synthesis conditions, it was possible to produce pure amorphous powder as shown in the micrograph of Figure V - 108(c) and the Raman spectrum of Figure V - 108(d). X-ray diffraction of the a-Si powders also did not exhibit any crystalline peaks.

Coin Cell Testing of HWCVD Materials: Initially the a-Si was tested in a conventional coin cell electrode that was ~15 µm thick. Unfortunately, in this conventional electrode containing 60:20:20 Si:AB:PVDF, the first cycle irreversible capacity loss was ~ 30%, and stable cycling was not observed. Thus a unique technique employing copper as both the binder and conductive additive was employed. Figure V - 109 displays the cycling performance of both the initial attempt (60:20:20 Si:AB:PVDF) as well as that of the new electrode fabrication technique. The new technique enables the creation of an electrode that is ~ 30-40 µm thick. The electrode has an initial first cycle irreversible capacity loss of only ~ 13% and a total reversible capacity of ~2500 mAh/g. After the first cycle capacity loss, the electrode has a Coulombic efficiency of ~ 95 %. This represents a very significant improvement over the conventional electrode with AB and PVDF (Figure V - 109).

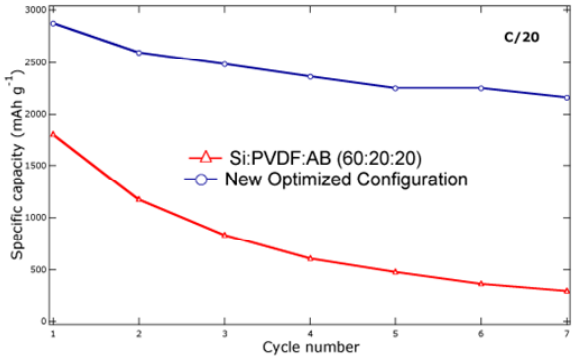

Figure V - 109: Cycling performance of a 15 µm thick electrode containing 60:20:20 Si:AB:PVDF compared to our new 30-40 µm thick electrodes fabricated with a novel technique.

ALD Coatings for Improved Si Durability: Thick coin cells with only copper as a conductive additive were employed for both amorphous Si and various sizes of crystalline nanoparticles (including commercial particles). In general, initial capacities of approximately 2500 mAh/g and a Coulombic efficiency of ~ 95% are observed for all of the various different materials.

As part of the coating focus group presentation in August, it was shown that by applying an ALD Al_2O_3 coating to these materials the initial capacity is reduced to ~ 1200 mAh/g, but the Coulombic efficiency is increased to > 99%. Coating thicknesses from 0.5 -2.5 nm were explored, and it was found that 1 nm is the optimal ALD Al_2O_3 coating thickness. Figure V - 110(a) shows that a 1 nm Al_2O_3 ALD coated electrode, containing commercial crystalline nano-Si particles, has a capacity of over 1000 mAh/g for 160 cycles. Furthermore, there is no fade in the Coulombic efficiency. The ALD coating may limit the lithium insertion and simultaneously improve durability.

Figure V - 110(b) shows the voltage discharge and charge curves for a bare electrode and the coated electrode at the 50th cycle, using the novel configuration. Note, that the capacity of the bare electrode has faded to ~1200 mAh/g (from ~ 2500 mAh/g) and is now roughly the same as the coated electrode. Importantly, after only 2 cycles (not shown) the discharge curves look significantly more similar than those shown in Figure V - 110b). Specifically, the Li^+ insertion voltage drops over time for the bare electrode but not for the coated electrode. This indicates that the structure of the ALD coated Si is not altered as much with cycling as that of the bare electrode. Thus, it is possible that limiting the number of Li^+ ions that are inserted allows more structural integrity to be maintained and extends the durable cycling.

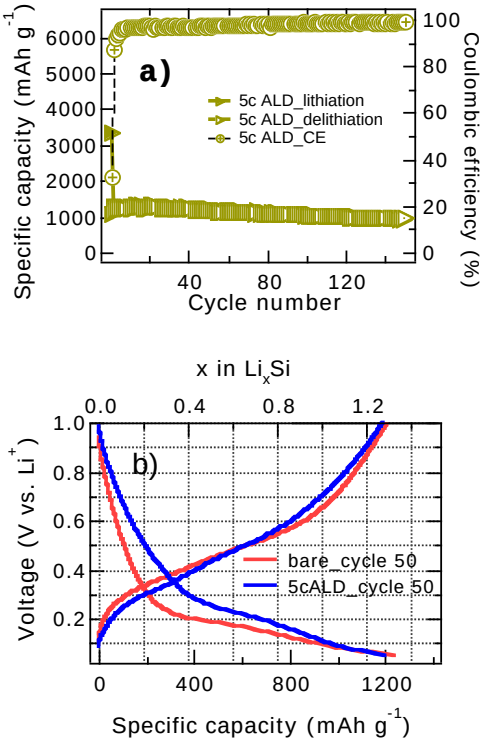

Figure V - 110: a) Durable cycling performance and Coulombic efficiency of an ALD coated nano-Si electrode employing the novel matrix with copper employed as both the conductive additive and binder. b) Voltage discharge and charge profiles of both bare and coated electrodes at cycle 50.

Mechanistic Studies of ALD Coatings: Coating a variety of materials such as nano-$LiCoO_2$, that will be sent to Clare Grey will enable mechanistic studies of Al_2O_3. NREL/CU has also fabricated full cells of natural graphite (NG) and $LiCoO_2$ where both electrodes, one or the other electrode, as well as neither electrode were coated. In creating these full cells, some surprising results that led to greater understanding of the ALD coatings were observed. Figure V - 111 shows the cycling behavior of the various electrodes that were cycled to 4.45 V vs. Li/Li^+, representing a very high voltage for $LiCoO_2$. The uncoated electrodes are represented by (c) and the bare by (b). Note that as expected when both electrodes were coated, as well as when the cathode was coated, improved cycling was observed. Surprisingly, when only the anode was coated improved cycling was also observed. Extensive characterization studies including impedance analysis, x-ray photoelectron spectroscopy, and time of flight secondary ion mass spectrometry were employed to analyze this effect. It was found that the surface species of the anode and cathode interact. Thus, coating only the anode dramatically affects the cathode.

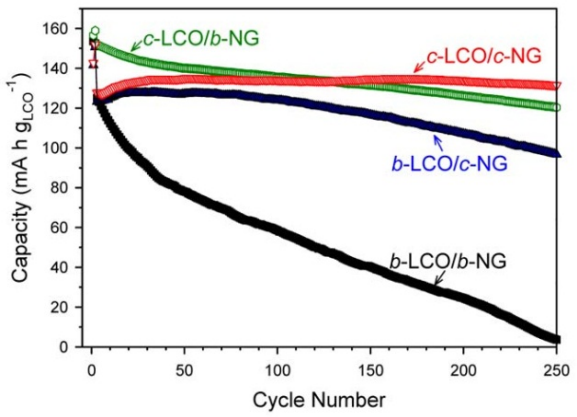

Figure V - 111: Cycling performance of NG and $LiCoO_2$ full cells where various electrodes are coated with Al_2O_3.

Noteworthy First-Year Collaborations: NREL worked with Stan Whittingham's group at SUNY Binghamton to show that $LiNi_yMn_yCo_{1-2y}O_2$ can cycle stably for 500 cycles at both 5C and 10C with capacities of approximately 130 and 110 mAh/g, respectively. (See report V.B.5.). The cathode was enabled by using carbon single-walled nanotubes as both the conductive additive and binder with an active material loading of 95 wt.%. Anodes containing Si and a conductive binder developed by Gao Lui at LBNL were also coated with Al_2O_3, and preliminary results indicate that the performance of thicker electrodes is improved.

Conclusions and Future Directions

It has been demonstrated that ALD coatings of Al_2O_3 improve the durable cycling of thick Si-electrodes containing various forms of Si. A *Coatings Group* to better understand the mechanism of various coatings on new electrodes has been formed. In future work, the mechanism of the Al_2O_3 and other coatings will also be explored. In FY12 exploration of the mechanism as well as enabling durable high rate capability for thick Si electrodes will be emphasized.

FY 2011 Publications/Presentations

1. Jung, Y.S., et al., "Unraveling the Unexpected Improved Performance of ALD Coated $LiCoO_2$/Graphite Li-ion Batteries" *JACS* (Submitted).
2. E. Kang, et al., "Magnetite Nanoparticles Confined in Mesocellular Carbon Foam for High Performance Anode Materials of Lithium-Ion Batteries," *Adv. Funct. Mater.*, **21**, 2430 (2011).
3. Dillon, A.C., et al., "HWCVD MoO_3 Nanoparticles and a-Si for Next Generation Li-Ion Anodes" *Thin Solid Films* **519**, 4495 (2011).
4. Ban, C. et al. "Extremely Durable High-Rate Capability of an $LiNi_{0.4}Mn_{0.4}Co_{0.2}O_2$ Cathode Enabled with Single-Wall Carbon Nanotubes" *Advanced Energy Materials* **1**, 58 (2011).
5. Riley, L.A. et. al. "Improved mechanical integrity of ALD-coated composite electrodes for Li-ion Batteries", Electrochemical and Solid State Letters **14**, A29 (2011).
6. Riley, L.A. et. al. "Electrochemical Effects of ALD Surface Modification on Combustion Synthesized $LiNi_{1/3}Mn_{1/3}Co_{1/3}O_2$ as a Layered-Cathode Material," **196**, 3317 (2011).
7. Scott, I.D. et al. "Ultrathin Coatings on Nano-$LiCoO_2$ for Li-Ion Vehicular Applications" *Nano Lett.* **11**, 414 (2011).
8. Dillon, A.C. "Carbon Nanotubes for Photoconversion and Electrical Energy Storage." *Chem. Rev.* **110**, 6856 (2010).

Invited Presentations (contributed not listed)

1. Dillon, A.C. ALD of Al_2O_3 for Highly Improved Performance in Li-ion Battery Electrodes *invited*, ALD2011, Boston, MA, July 2011.
2. Ban, C., *invited* "Binder-free High Rate Capability Li-ion Electrodes" Materials Research Society Spring Meeting, San Francisco, CA, April 2011.
3. Dillon, A.C. *invited* International Battery Association Meeting, Cape Town, South Africa, April, 2011. (Presented by M.S. Whittingham.)
4. Dillon, A.C. "Methods to Achieve Durable High Rate with High Capacity for Li-ion Batteries" *key note* Special ACS Symposium in Honor of Debra R. Rolison, Anaheim, CA March 2011.
5. Dillon, A.C., "High Rate and High Capacity Metal Oxide Anodes" *invited* American Vacuum Society Fall Meeting, Albuquerque, NM, Oct. 2010.

V.C.11 Synthesis and Characterization of Si/SiO_x-Graphene Nanocomposite Anodes and Polymer Binders (PSU)

Donghai Wang and Michael A. Hickner (PI)
The Pennsylvania State University
Department of Mechanical and Nuclear Engineering
Department of Materials Science and Engineering
328 Reber Building
University Park, PA 16802

Phone: (814)-863-1287; (814) 867-1847
E-mail: dwang@psu.edu; mah49@psu.edu

Start Date: January 1, 2011
Projected End Date: October 1, 2014

Objectives

- Design, synthesize and test novel polymer binders with varying mechanical properties and surface linker groups for Si anodes
- Synthesize and characterization of Si/SiO_x-graphene nanocomposites,
- Identify and evaluate the electrochemical performance of the Si/SiO_x-graphene nanocomposites and the polymer binder.
- Improve management of volume change characeristics of Si-based anodes, impede the capacity fading with enhanced capacity reliability, decrease initial irreversible capacity loss, and improve the specific capacity and coulombic efficiency of Si/SiO_x-based anodes.

Technical Barriers

There are several technical barriers to developing Si/SiO_x-based anodes for lithium-ion batteries including:

- Poor capacity cycling
- Large initial irreversible capacity and corresponding low coulombic efficiency
- Need to add a high percentage of conductive carbon to obtain good rate (C/3) performance

Technical Targets

- Prepare Si nanoparticles with controlled particle size, and demonstrate Si-graphene nanocomposite anodes.
- Synthesize and evaluate novel polymer binders with controlled SiO_x binding groups and Li-conducting blocks.
- Determine electrochemical properties of Si/SiO_x nanoparticle, Si/SiO_x-graphene nanocomposites and the polymer binders in lithium half cell.
- Achieve stable reversible capacity in excess of ~1,000 mAh/g.
- Obtain above 40% first cycle coulombic efficiency as well as 90% coulombic efficiency cycle to cycle.

Accomplishments

- Demonstrated Si nanoparticles with controlled diameter ranging from 5 nm to 20 nm and Si-graphene nanocomposite synthesis through solution synthesis approach.
- Successful synthesis of Si nanoparticles with diameter ranging from 50-100 nm, and Si-graphene nanocomposites by using magnesiothermic reduction method.
- Random and block copolymers with surface binding silanes have been synthesized.
- Successful synthesis of a novel mechanically robust polymer binder (i.e., sulfonated Radel binder), which have been tested in battery cells for cycle performance and nearly equivalent performance to CMC/SBR.
- As-prepared Si-graphene nanocomposites exhibit specific capacity in excess of ~1,000mAh/g with good cycling stability and rate capability.
- The novel Si-graphene composites exhibit less than 20% first cycle irreversible loss as well as 90% coulombic efficiency cycle to cycle thereafter.

✧ ✧ ✧ ✧ ✧

Introduction

An increase in energy and power densities of Li-ion cells depends in a decisive way on improvements in electrode materials performance. As the commercial anode, graphite has the theoretical capacity of 372 mAh/g, which is low relative to the requirement of high-energy application fields. Thus, the search for an alternative anode to replace graphite in Li-ion batteries has been underway for many years. So far, silicon has the highest theoretical

capacity ($Li_{4.4}Si \approx 4200\ mAhg^{-1}$) of all known materials, and is abundant, inexpensive, and safer than graphite (it shows a slightly higher voltage plateau than that of graphite, and lithiated silicon is more stable in typical electrolytes than lithiated graphite). Unfortunately, the practical use of Si powders as anodes in Li-ion batteries is still hindered several problems. One of the problems is severe volume changes during Li insertion/extraction, leading to loss of electric contact and poor cycling performance.

One approach to obtain a high-performance Si anode is to use silicon/carbon composites. Graphene is an excellent conductive carbon substrate to host active Si nanomaterials due to its high conductivity, large surface area, flexibility, and chemical stability. In this project, we will aim to develop novel Si/SiO_x-graphene nanocomposite to improve cycling performance of Si anodes. On the other hand, many important battery characteristics, including stability and irreversible capacity losses, are critically dependent on the polymer binder's properties. High capacity electrochemically active Si particles that exhibit significant volume changes during insertion and extraction of Li require improved binder characteristics to ensure electrode integrity during use.

Inspired by these features, in this project we sought to mitigate the electrochemical limitations of Si-based anodes during charge/discharge by designing novel Si/SiO_x-graphene nanocomposite and polymer binders to tolerate volume change, improve electrode kinetics, and decrease initial irreversible capacity loss. The new electrodes made with these polymer-coated SiO_x-graphene nanocomposites have significantly improved the cycling capability of Si-based anodes.

Approach

Our approach is 1) to synthesize SiO_x-graphene nanocomposites and identify noval commercially available binders to tolerate volume change upon lithiation/delithiation so as to improve cycling performance of Si-based anodes; and 2) to develop novel polymer binder with controlled elastic properties, ion-conductive moieties, and SiO_x surface binding functionality, in order to stabilize and bridge SiO_x particles to improve cycling performance of Si-based anodes.

Results

Si-Graphene Naoncomposite Anodes. We first prepared Si nanoparticles with controlled particle size through a solvothermal synthesis approach using reduction of silicon precursor at the presence of capping ligands. The as-prepared Si nanoparticles were uniform with the size of 4~6 nm (Figure V - 112a). Similarly, Si-graphene nanocomposite were also synthesized following one-step solvothermal synthesis of Si nanoparticles with addition of dispersed functional graphene sheets. As shown in Figure V - 112b, Si nanoparticles were evenly distributed onto the functionalized graphene sheets, and the particle size of Si nanoparticles was about 4~6 nm.

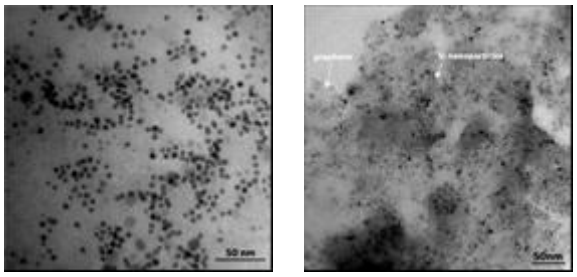

(a) (b)

Figure V - 112: TEM images of (a) as-prepared Si nanoparticles and (b) Si-graphene nanocomposites

In addition, Si nanoparticles with average particle diameter of 50-100 nm were synthesized by magnesiothermic reduction approach. To obtain Si-graphene nanocomposites, the resulting Si nanoparticles were mixed thoroughly with functionalized graphene sheets followed by thermal treatment. The TEM image of Si/graphene nanocomposites (Figure V - 113a) revealed that Si nanoparticles were well distributed onto the graphene conductive support, and XRD patterns (Figure V - 113b) demonstrated the pure-phase crystalline structure of Si nanoparticles and Si-graphene nanocomposites.

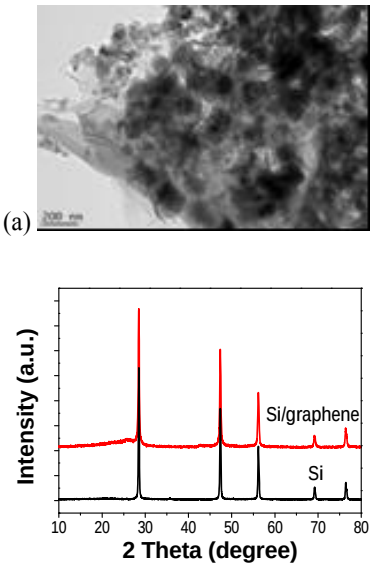

Figure V - 113: (a) TEM image of as-prepared Si-graphene nanocomposites; and (b) XRD patterns of as-prepared Si nanoparticles and Si-graphene nanocomposites.

Electrochemical tests were performed on as-prepared Si-graphene nanocomposite anode materials between a lower cut-off voltage at 0.01 V and an upper cut-off voltage of 1.5 V. The anode electrodes were prepared by mixing Si/graphene nanocomposites, Super-P carbon and a

commercial binder of PVDF at a weight ratio of 8:1:1 and pasted on Cu foils. Figure V - 114a shows the discharge and charge curves during the first five cycles in a coin-type half-cell at a rate of 200 mA/g. The Si-graphene nanocomposite anode shows first discharge and charge capacities of 1461 and 1238 mAh/g, that is, a coulombic efficiency of 85%. The electrode maintains a capacity over 1300 mAh/g in the following cycles with the coulombic efficiency of ca. 96%. In addition, we also investigated the cycling performance of Si-graphene nanocomposites at a high current density of 2000 mAh/g (Figure V - 114b). At the first cycle, Si-graphene nanocomposites show a specific discharge capacity of approximately 863 mAh/g and charge capacity of 751 mAh/g (i.e., the coulombic efficiency of 87%). With increase in cycling number, the capacity of Si-graphene nanocomposites remains relatively constant (900~1000 mAh/g) with the coulombic efficiency of over 97%, indicating that these Si-graphene anodes have good cycling stability. Further investigation on the anode performance of Si-graphene nanocomposites is still underway.

A series of PEO and trimethoxy silane-based binders have been synthesized. An example chemical structure of these polymers is shown in Figure V - 115. These types of polymers have been made in random and block architectures. Also, other functional groups such as quaternary ammonium groups and sulfonate groups have been explored as the Si-binding moiety. In addition, mechanically robust binders composed of RADEL® poly(sulfone) variants have also been synthesized.

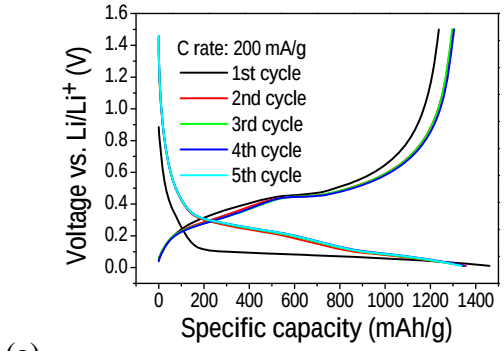

(a)

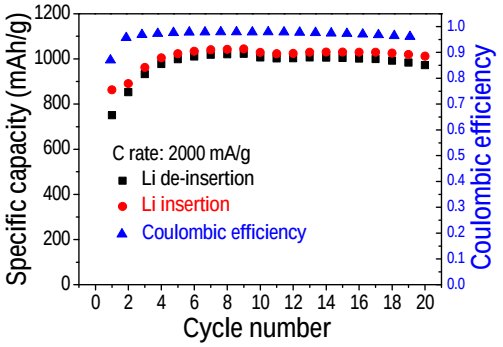

(b)

Figure V - 114: (a) Charge-discharge curves of Si-graphene nanocomposites at a rate of 200 mA/g between 0.01 and 1.5 V; (b) Cycling performance of Si-graphene nanocomposites at a high current density of 2000 mA/g.

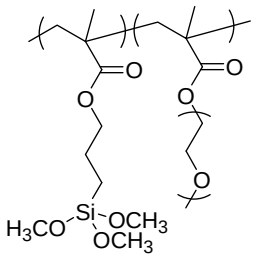

Figure V - 115: Silane-PEO containing copolymers.

Synthesis and Evaluation of Polymer Binders. To evaluate the electrochemical performance of as-prepared polymer binders, commercial silicon nanoparticles were mixed with Super-P carbon and the as-prepared polymer binder in a weight ratio of 7:2:1. The cells were cycled at a current density of 200 mA g^{-1} in a voltage range from 0.01 to 1.5 V. The performance of several PEO and trimethoxy silane-based polymer binders is shown in Table V - 1. The first cycle efficiencies and cycle life of the silane-PEO and sulfonate PEO binders is not reasonable compared to the CMC-SBR baseline. The poor performance is probably due to high swelling in the EC/DMC battery electrolyte. Thus, our work on new synthesis of block copolymer Si nanoparticle binders is ongoing with stiffer, less swellable blocks to maintain the structural integrity of the binder.

Table V - 1: Charge-Discharge Performance for 1st and 10th cycle for Silane-PEO (Si PEO) and sulfonate-PEO (S PEO) copolymer binders.

Binder	1st Discharge	1st Charge	Efficiency	10th Disharge	10th Charge	Efficiency
Si-r-EO 50:50	2388	1110	0.465	12.8	8.2	0.641
	2557	1486	0.577	25.7	15.5	0.603
S-r-EO 50:50	1182	553	0.468	27.8	17	0.612
	1592	670	0.421	26.1	12.9	0.494
S-r-EO 50:50	1250	405	0.324	11.2	5.4	0.482
	1166	423	0.363	10.3	3.7	0.359
PVDF	2697	1470	0.545	17.7	10.7	0.605
	2001	1052	0.526	23.2	13.4	0.578
CMC/ SBR	2693	2247	0.834	1060	963	0.908
	1921	1675	0.872	1075	993	0.924

In addition, the electrochemical performance of mechanically robust binders composed of RADEL® poly(sulfone) variants have also been tested. Figure V - 116 shows their 1st and 10th cycle performance compared to conventional PVDF and CMC/SBR binders. The Radel and sulfonated Radel (S-Radel) materials show comparable performance to CMC/SBR. Longer-term cycling and optimization of these electrodes is underway. Interestingly, these Radel binders do not contain carboxylate groups found on CMC. We are currently testing their swelling properties in EC/DMC and evaluating new Radel structures for high performance binders.

Conclusions and Future Directions

Si-graphene nanocomposites have been prepared through one-step solvothermal synthesis of Si nanoparticles with addition of dispersed functional graphene sheets, or one-step magnesiothermic reduction of SiO_2-graphene nanocomposites. The electrochemical performance of Si-graphene nanocomposites has been evaluated in coin-type cells. Results demonstrate that the as-prepared Si-graphene composites exhibit specific capacity in excess of ~1,000 mAh/g (gram of composite) with excellent stability and rate capability at a rate of 2000 mA/g, and exhibit less than 20% first cycle irreversible loss as well as 90% coulombic efficiency cycle to cycle thereafter. With regard to novel polymer binders, we have successfully developed a class of polymer binders for Si anode. Initial tests have demonstrated that the Radel and sulfonated Radel (S-Radel) binders show comparable electrochemical performance to CMC/SBR, indicating that Radel-based binders are suitable for Si anode.

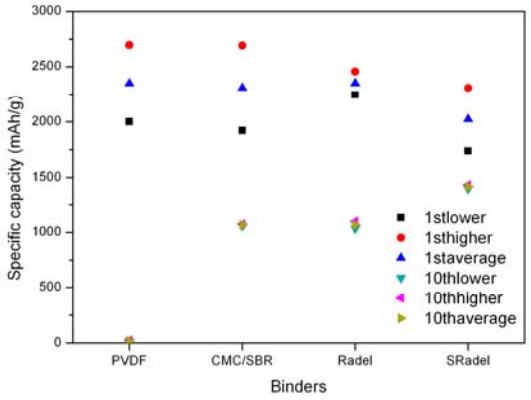

Figure V - 116: Comparison of PVDF and CMC/SBR binders with Radel and S-Radel.

During the remainder of the project period, future work will focus on: 1) optimizing the composition of Si-graphene to balance the high capacity and cyclability; 2) optimizing the size and morphology of Si and graphene in the Si-graphene composite to increase the utilization rate of Si; 3) optimizing the composition and structure of as-prepared polymer binders for Si anodes; and 4) exploring the application of the optimized polymer binders in the anode system to further improve the cycling capability of Si-graphene nanocomposites.

FY 2011 Publications/Presentations

1. Contributed to Prashant Kumta " Novel Lithium Ion Anode Structures Overview of New DOE BATT Anode Projects" 2011 DOE Annual Peer Review Meeting presentation.

V.C.12 Synthesis and Characterization of Silicon Clathrates for Anode Applications in Lithium-Ion Batteries (SwRI)

Kwai S. Chan and Michael A. Miller
Southwest Research Institute
Department of Materials Engineering
Mechanical Engineering Division
6220 Culebra Road
San Antonio, TX 78238
Phone: (210) 522-2053; Fax: (210) 522-6965
E-mail: kchan@swri.org; mmiller@swri.org

Start Date: January 1, 2011
Projected End Date: December 31, 2014

Objectives

- Develop scalable synthesis methods for producing empty and substituted silicon clathrates
- Design, synthesize, and characterize silicon clathrate compounds for anode applications in Li-ion batteries
- Fabricate and characterize prototype silicon clathrate anodes designed to exhibit small volume expansion during lithiation, high specific energy density, while avoiding capacity fading and improving battery life and abuse tolerance

Technical Barriers

This project addresses the following technical barriers of the lithium-ion battery technology, especially focusing on the silicon clathrate anode materials:

- Low-energy density
- Low-power density
- Short calendar and cycle lives

Technical Targets

- Develop silicon clathrate anodes to meet PHEV and EV goals by exceeding current benchmarks (Conoco Phillips CPG-8 Graphite/1 M $LiPF_6$+EC:DEC (1:2)/ Toda High-energy layered (NMC) in the following metrics:
- Energy density
- Power density
- Calendar and cycle lives

Accomplishments

- Prepared 12 gram quantities of Type I barium aluminum-substituted silicon clathrates ($Ba_8Al_8Si_{38}$) by an arc-melting technique
- Synthesized 100 milligram quantities of Ba_8Si_{46} by a high-pressure, high-temperature multi-anvil technique
- Synthesized 10 milligram quantities of empty Si_{46} by a plasma magnetron sputtering technique
- Performed first-principles computations to identify possible reaction pathways for the formation of empty clathrates Si_{46}, Li_xSi_{46}, $Ba_xLi_yAl_zSi_{46-z}$ and $Li_{15}Si_4$
- Constructed and evaluated electrochemical half-cells using silicon clathrate materials synthesized in this program

✧ ✧ ✧ ✧ ✧

Introduction

To achieve the DOE's performance targets for PHEV and EV applications, low-cost advanced anode materials with high-energy density, high-power density, and longer calendar and cycle lives are needed. To address this need, this project focuses on the development of synthesis methods, characterization of electrochemical performance, and the design and fabrication of prototype silicon clathrate anodes for potential applications in Li-ion batteries for PHEV and EV.

Silicon clathrate, a polymorph of silicon, is an emerging anode material that is composed of sp^3 bonded silicon atoms arranged in cage-structures. The silicon clathrate, Si_{46}, consists of crystalline Si with a regular arrangement of 20-atom and 24-atom cages fused together through 5 atom pentagonal rings (Type I clathrate). It has a simple cubic structure with a lattice parameter of 10.335 Å and 46 Si atoms per unit cell. The crystal structure (Space Group $Pm\bar{3}n$) of the Si_{46} clathrate is different from the common form of crystalline Si (c-Si), which is diamond cubic (Space Group $Fd\bar{3}m$) with a lattice parameter of about 5.456 Å.

First-principles computations performed at SwRI have revealed that significant amounts of Li ions can be

inserted into and extracted from the cage structure of silicon clathrates without substantial volume changes or pulverization of the cage structure. Theoretical computations of the total volume, occupiable volume, and accessible volume within the Type I silicon clathrate structures indicate that the empty spaces within the cage structure are accessible to Li and amenable to Li intercalation through electrochemical means, thus making silicon clathrate a potential anode material for Li-ion battery applications.

Approach

SwRI is working with LBNL to develop silicon clathrate anodes for PHEV and EV applications. The approach is to synthesize guest-free Type I silicon clathrate (Si_{46}) using a number of high-temperature processing methods, while concurrently exploring an investigational route for direct synthesis of guest-free clathrate and performing *ab initio* and classical molecular dynamics (MD) computations to identify lithiation pathways. Silicon clathrates will be utilized to fabricate prototype anodes. Electrochemical characterization will be performed to evaluate and improve, if necessary, anode performance including cyclic stability. The final year of the program will be directed at the design, assembly, and characterization of a complete (anode/cathode) small-scale, prototype battery suitable for concept demonstration.

Results

Arc-Melt Synthesis. An arc-melting technique was utilized to synthesize metal-substituted clathrate (Type I) structures of the form $Ba_8M_8Si_{38}$ (M = Al, Cu), starting from pellets of pure Si, Al or Cu, and Ba and melting the admixture of pellets under an argon atmosphere. The product – either containing Al or Cu – was brittle and grey-silver in color. After forming powders of each product, powder X-ray diffractometry (PXRD) confirmed that Al- or Cu-substituted silicon clathrate (Type I) was indeed formed. The formation of the clathrate I structure requires the addition of Al or Cu in the starting admixture; namely, Ba_8Si_{46} is not formed without metal addition. Twelve grams of $Ba_8M_8Si_{38}$ Type I clathrates were produced. Figure V - 117 shows the PXRD pattern for $Ba_8Al_8Si_{38}$ produced by the arc-melting technique. These materials were utilized to fabricate half-cells for characterization of electrochemical performance.

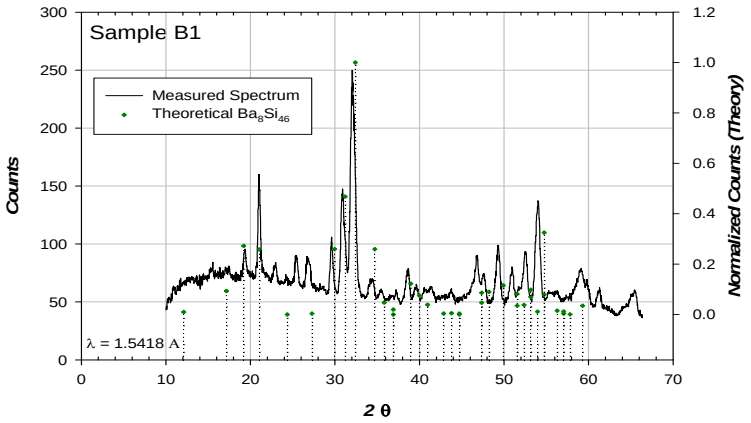

Figure V - 117: PXRD pattern of $Ba_8Al_8Si_{36}$.

Multi-Anvil Synthesis. High-pressure, high-temperature Walker-type multi-anvil techniques were used to synthesize small quantities (~100 mg) of barium-intercalated silicon clathrate (Type I, Ba_8Si_{46}) by structurally converting barium silicide ($BaSi_2$) to the clathrate I structure at 800°C with 3, 4, and 5 GPa of mechanical pressure. An image of the products is shown in Figure V - 118 for each of the three pressure points. Initial PXRD results (Figure V - 119) suggested that conversion of $BaSi_2$ to the clathrate (Type I) structure (Ba_8Si_{46}) was incomplete. However, upon close inspection, it was subsequently discovered that the spectrum was partially obscured by the presence of h-BN, indicating that the technique's conversion yield was, in fact, very good.

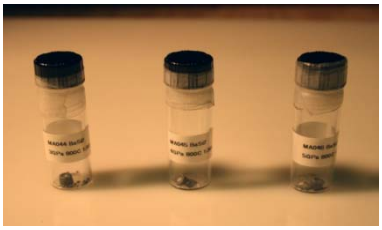

Figure V - 118: Image of barium-intercalated silicon clathrate (Type I, Ba_8Si_{46}) pellets formed from the high-pressure, high-temperature multi-anvil structural conversion of barium silicide ($BaSi_2$) at three different pressure regimes.

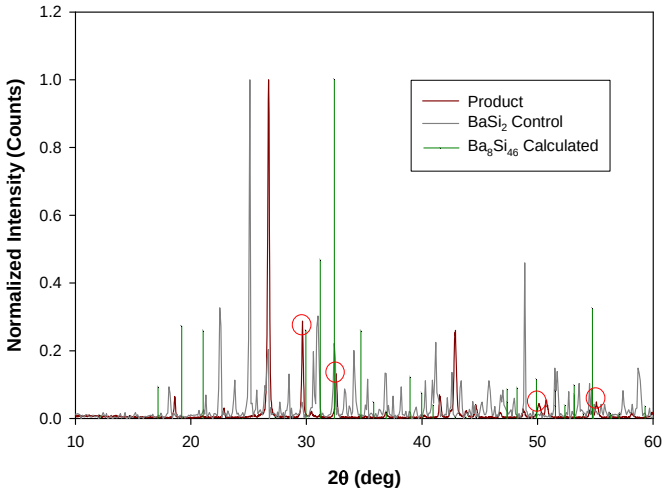

Figure V - 119: Powder X-ray diffraction pattern of the 5 GPa product is compared with that of $BaSi_2$ and the positions of major reflections theoretically predicted for pure Ba_8Si_{46}.

Direct Synthesis of Guest-Free Clathrate. A plasma-enhanced magnetron sputtering (PEMS) vacuum deposition chamber was set up to explore the synthesis of guest-free silicon clathrate particles by directing a silicon-argon plasma into a pool of ionic liquid (IL), as illustrated in Figure V - 120.

Two different ionic liquids were utilized and both produced small quantities of guest-free Si_{46}, which was confirmed by Raman Spectroscopy. Figure V - 121 presents an image of empty Si_{46} synthesized by PEMS, while Figure V - 122 shows the results of Raman spectroscopy.

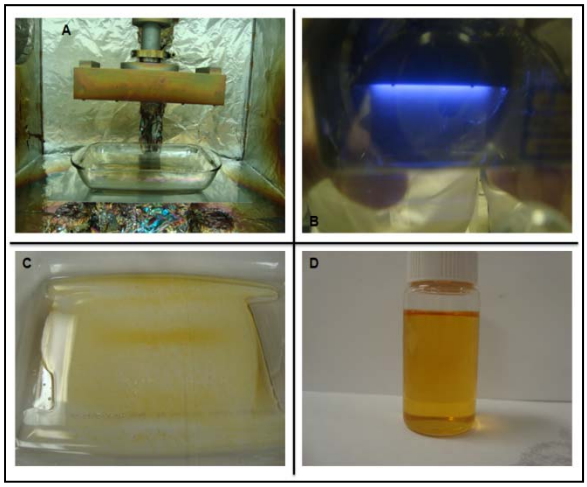

Figure V - 120: (A) PEMS deposition chamber and setup for depositing nano-particles of silicon clathrate (guest free) into a pool of IL. (B) Image of deposition plasma directed over pool of IL. (C) Image of IL pool following PEMS deposition and recovered IL containing nano-particles of silicon clathrate (D).

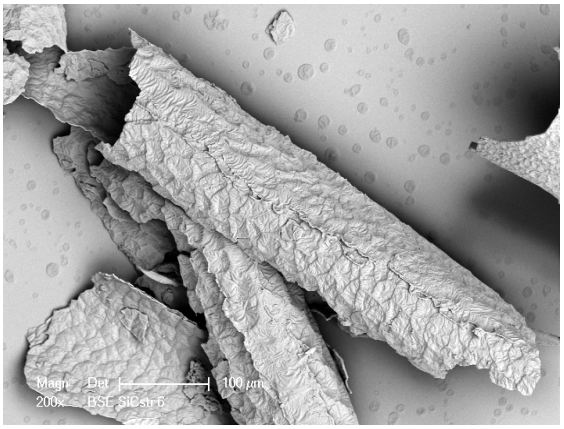

Figure V - 121: Image of empty Si_{46} produced by PEMS.

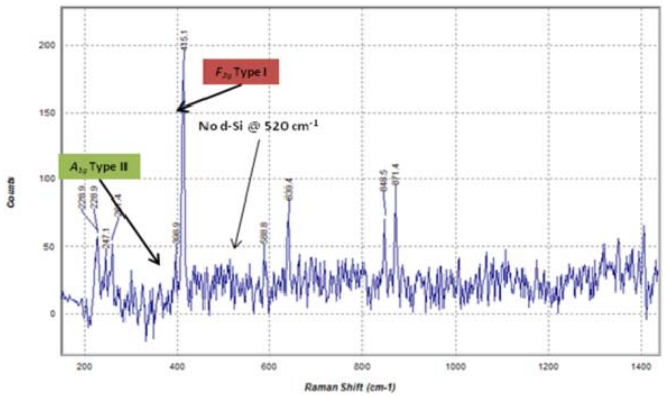

Figure V - 122: Raman spectropic analysis of the Si_{46} produced by PEMS deposition into an ionic liquid

Batch Synthesis via Soft Oxidation of $BaSi_2$. A synthetic pathway was designed and the necessary hardware (manifolds and glass reactor) was set up to conduct direct, batch synthesis of guest-free Type I silicon clathrates at elevated temperature. First, the thermochemical stability of candidate ionic liquid (IL) solvents needed to carry out the synthesis at temperatures at or slightly above 300°C for periods in excess of 48 hours was evaluated. Differential scanning calorimetry coupled with thermal gravimetric analysis (DSC-TGA) showed that the PF_6^- salt of 1-butyl-3-methylimidazolium was not sufficiently stable for the reaction due to its degradation onset near 300°C. Subsequently, an alternate, proprietary IL, consisting of the *bis*(trifluoromethylsulfonyl)imide anion was discovered to show excellent thermochemical stability up to 400°C over 48 hours with negligible mass loss. This IL was incorporated into the reactor setup and guest-free silicon clathrates were synthesized via soft oxidation of $BaSi_2$. Several reaction schemes are currently being attempted.

Molecular Modeling of Silicon Clathrates. The possible routes for extracting Ba atoms from Ba_8Si_{46} and $Ba_8Al_6Si_{40}$ were investigated by performing first-principle energetic computations using the Car-Parrinello molecular dynamics code. The energy change due to the presence of a guest Ba atom residing in a Si_{46} cage or an alloyed Al_6Si_{40} cage was computed as a function of the number of Ba atoms. The results, shown in Figure V - 123, indicate that the energy required to extract a Ba atom from the Si_{46} or Al_6Si_{40} cage ranges from 2.43 eV to 3.66 eV at 0K. The energy change was also computed as a function of temperature and Li content to identify potential pathways and processing windows for extracting guest Ba atoms from the clathrates.

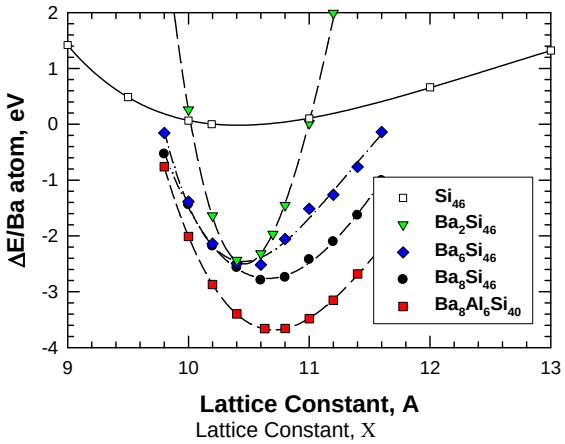

Figure V - 123: Energy change of Si_{46} due to Ba guest atoms or Al substitution of the Si framework.

Half-Cell Electrochemical Characterization. A method was devised to fabricate anodes consisting of previously synthesized $Ba_8M_8Si_{38}$ conformed to ~1 cm diameter thin disks. The anode material was pulverized to a very small particle size using a simple mini-ball and capsule anvil system. The fine powders were then pressed into a thin disk in a mini-press apparatus. Mechanically stable anode-disks were successfully prepared without the use of any binder material. A method was also devised to bond the pressed disk to a current collector (metal foil) for use in an electrochemical half-cell apparatus. A three-electrode bulk-electrolysis cell was first used to deintercalate Ba^{2+} from the electrode material. Subsequently, a three-electrode split-cell was used to intercalate Li^+ into the clathrate anode and measure the capacity. These tests are still on-going. Preliminary results, shown in Figure V - 124, indicated that Ba^{2+} ions were extracted during oxidation and Li^+ ions were inserted into the anode during reduction.

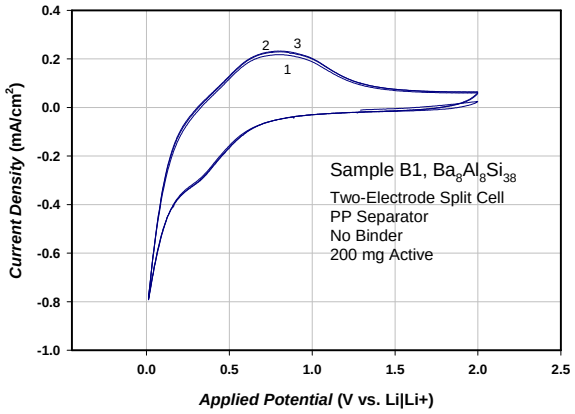

Figure V - 124: Cyclic voltammetry of $Ba_8Al_8Si_{38}$ for the reductive intercalation and oxidative deintercalation of Li^+ after the formation of a stable SEI.

Conclusions and Future Directions

1. Barium aluminum-silicon clathrate can be fabricated by arc melting in small (12 gram) quantities. First-principles computations indicated that some of the barium guest atoms in the aluminum-substituted Si framework can be replaced by Li atoms. Encouraged by these findings, part of the future efforts will be directed toward making barium deficient aluminum-substituted silicon clathrates and lithium aluminum-silicon clathrates.
2. Empty silicon clathrates can be synthesized by plasma-enhanced magnetron sputtering of silicon into an ionic liquid. Future work will be directed toward refining the technique to improve the yield of this process.
3. High-pressure, high-temperature synthesis has produced about 100 mg of Ba_8Si_{46}. This batch of material will be made into half-cells for electrochemical evaluation.
4. Ionic liquids with suitable thermal stability for soft oxidation of $BaSi_2$ at 300ºC to 400ºC have been identified and incorporated into a reactor set-up. Synthesis of guest-free silicon clathrates via soft oxidation has been initiated. This effort will be continued to evaluate several reaction schemes based on the Hoffman elimination reaction.
5. First-principles computational results showed that the stabilization energy of the Si framework (cage structure) by Li is smaller than that of Ba, meaning that Li can be inserted and extracted more easily from the Si framework than Ba. Future work will directed toward predicting the kinetic barriers for various lithiation pathways.
6. Cyclic voltammetry performed on $Ba_8Al_8Si_{38}$ indicated extraction of Ba^{2+} ions during oxidation and Li ions were inserted into the anode during reduction. Electrochemical characterization of silicon clathrate anodes will be continued and expanded to include materials synthesized by other synthetic routes.

FY 2011 Publications/Presentations

1. 2011 DOE Annual Peer Review Meeting Presentation.

V.C.13 Wiring Up Silicon Nanoparticles for High-Performance Lithium-Ion Battery Anodes (Stanford U)

Yi Cui (PI)
Stanford University
476 Lomita Mall, McCullough 343
Stanford, CA 94305
Phone: (650) 723-4613
E-mail: yicui@stanford.edu

Start Date: January 2011
Projected End Date: December 2015

Objectives

- Go beyond the charge capacity limitation of conventional carbon anodes by designing nano-architectured silicon electrodes.
- Design, synthesize and characterize Si nanostructure-based anodes to overcome the volume change-induced materials challenges and to realize high performance.
- Understand the fundamendal structure-property relationship on electrode materials with large structure and volume change.
- Develop low-cost materials processing methods.

Technical Barriers

The large structure and volume changes of Si during battery cycling cause multiple materials challenges: 1) Mechanical breaking 2) Unstable solid electrolyte interface. 3) Challenge to maintain good electrical connection. These fundamental challenges result in technical barriers in battery performance:

- Large first cycle irreversible loss
- Poor cycle life
- Inadequate coulombic efficiencies

Technical Targets

- Develop fundamental materials guideline through structure and property correlation and design nanostructured Si anodes with the features to address the three material challenges outlined above.
- Develop synthesis techniques to produce the designed nanostructured Si anodes.
- Develop techniques for structure-property correlation at the single nanostructure level.
- Demonstrate high performance Si anodes with cycle life above 3000 at 1000mA/g and 5C rate, and first cycle irreversible loss less than ~15%.

Accomplishments

- Developd synthesis strategy to connect Si particles electrically.
- Developed *ex situ* TEM to study Si volume changes and discovered the dependence of volume change on surface oxide layer and on size.
- Developed synthesis methods to produce Si electrodes with engineered pore sizes.
- Obtain detailed information on the volume expansion and contraction of Si.
- Determining size effects on fracture upon electrochemical lithiation/delithiation of silicon nanopillars.
- Developed conductive, mechanically robust, electrochemically inactive nanoscale scaffolding for supporting Si active material.
- Develop a prelithiation method to load lithium into Si anodes.

✧ ✧ ✧ ✧ ✧

Introduction

Next generation high capacity electrode materials are needed in order to generate high energy battery technology to meet the demands of transportation. Silicon is an exciting and promising anode material to replace carbon in Li-ion batteries due to: 1) a high gravimetric capacity of ~4200 mAh/g, ten times higher than graphite (~370 mAh/g); 2) a high volume capacity of 9786 mAh/cm^3; 3) its relatively low working potential suitable as an anode (~ 0.5 V Vs Li/Li$^+$); 4) abundance of Si element, safe and environmentally benign; 5) The fundamental and manufacturing knowledge established in Si semiconductor industry and solar industry can be leveraged. However, there exist several scientific and technical challenges for silicon anodes: 1) Mechanical breaking caused by large volume change. The electrochemical alloying reaction of Li with Si involves volume expansion of up to 400% and significant contraction during lithium extraction. The stress induced by the large volume changes causes cracking and pulverization of silicon, which leads to loss of electrical

contact and eventual capacity fading. 2) Unstable solid electrolyte interface (SEI). The repetitive volume expansion and contraction cause the continuous movement of the interface between Si and organic electrolyte and it is challenging to form a layer of stable SEI, resulting in low Coulombic efficiency and capacity loss during cycling. 3) Challenge to maintain good electrical contact between Si materials and current collector. Even though mechanical breaking does not take place in Si nanostructures below critical sizes, large volume change can still cause the movement of Si nanostructures and the detachment from the conducting environment during long-term battery cycling. 4) Challenge to generate Si materials to address the above three challenges with low-cost and scalable processing.

This goal of this project is to study the fundamental principles related to alloy anodes, to design nanostructured Si anodes to over the three fundamental challenges and to develop low-cost and scalable procesing.

Approach

This project develops the *ex situ* and *in situ* electron microscopy to understand the structure and property correlation of nanostructured Si anodes, which helps developing the materials design principles. Based on the principles, this project also designs and synthesizes nanostructured Si which can overcome the three fundamentals materials challenges. The project also develops low-cost and scalable nanomaterials which have the designed functionality.

Results

Connecting Si particles electrically with "inorganic glue". A method was developed to fabricate Si-based powder electrodes without using polymer binders or conductive carbon additives. The expansion/contraction of Si particles in slurry anodes usually results in loss of electrical contact and capacity decay, even with sub-micron particles. To combat this issue, we have developed "inorganic glue" that serves to bind Si particles together in an electrode architecture and provides better electrical contact than conductive additives. In this process, slurry electrodes containing Si particles or nanowires were fabricated, and then chemical vapor deposition was used to deposit ~50 nm of doped amorphous Si onto the electrodes. This a-Si layer fuses the particles together and also binds them to the underlying current collector substrate. In this way, a porous, electrically connected structure of crystalline Si particles in an a-Si framework is created. 200 nm Si particles in this framework showed high capacity (~2500 mAh/g) and good cycling performance, but micron-sized particles showed fast capacity decay, as shown in Figure V - 125.

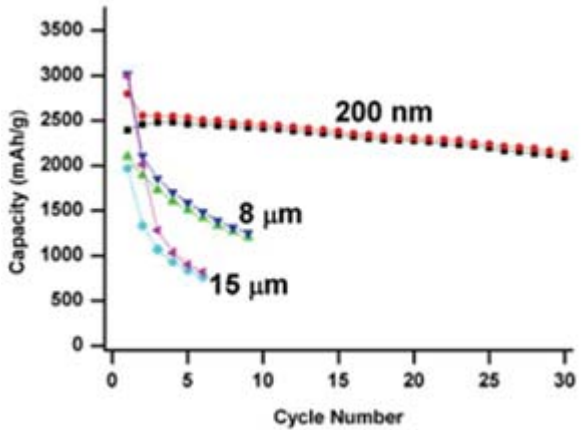

Figure V - 125: Specific capacity with cycling for anodes with different Si particle sizes bound together with inorganic glue

***Ex situ* TEM to study Si volume changes.** Other work utilized transmission electron microscopy (TEM) to study in detail the volume changes in individual Si nanostructures. In this technique, Si nanostructures are dispersed directly on a metal-coated TEM grid, and single nanostructures can be imaged before and after electrochemical charge/discharge. TEM is useful because the volume and structural changes in single NWs during lithiation can be studied simultaneously. Figure V - 126 shows TEM images and selected-area diffraction patterns of the same two nanowires before and after lithiation. The crystalline nanowires become amorphous and expand in diameter after lithiation.

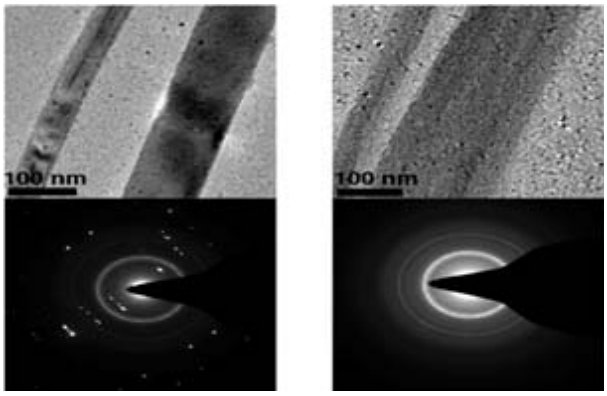

Figure V - 126: TEM images and diffraction patterns of the same two nanowires before (left) and after (right) lithiation

Using this technique, we have studied differences in volume changes between nanowires with and without a surface oxide layer. We observed that smaller NWs with oxide shells tend to expand to a lesser extent than those without oxide. We expect that this could be useful in engineered hollow nanostructures, where a constraining layer could be used to control volume expansion away from the surface in contact with the electrolyte.

Determining size effects on fracture upon electrochemical lithiation/delithiation of silicon nanopillars. The circumstances causing fracture of Si nanostructures during lithiation/delithiation are not completely understood. To determine the effect of nanostructure size and structure on fracture characteristics, nanopillars with controlled size and crystallographic orientation were fabricated and observed with SEM after lithiation/delithiation. Surprisingly, we found that many nanopillars fractured upon initial lithiation, which has not been predicted by many computational simulations. Pillars with <100>, <110>, and <111> axial orientations all show cracks that run along their length after lithiation. Interestingly, the cracks are usually located between directions of preferred radial anisotropic expansion. Because of this, we propose that the cracks develop due to regions of concentrated tensile hoop stress between the preferred radial expansion directions. In addition, we found that pillars with diameters > 360nm consistently fractured upon lithiation, while pillars with diameters < 240nm usually did not fracture. The fraction of fractured pillars was dependent on lithiation rate only for pillars of intermediate diameter (240nm). Overall, these data indicate a critical size for fracture upon lithiation between ~240 and 360nm.

Interconnected hollow Si nanoparticles as anodes. We developed a novel interconnected Si hollow nanosphere electrode that is capable of accommodating large volume changes without pulverization during cycling (Figure V - 127). We developed a finite element model to simulate the diffusion-induced stress evolution and investigated the volume expansion of the same single hollow spheres before and after lithiation using TEM. More interestingly, we achieved high initial discharge capacity of 2725 mAh/g and 700 cycles in electrochemical tests (Figure V - 128). Less than 8% capacity degrades for every 100 cycles. Even after 700 cycles, this Si hollow sphere electrode shows 1420 mAh/g capacity. Superior rate capability is demonstrated as well and attributed to fast lithium diffusion in the interconnected Si hollow structure.

Conductive, mechanically robust, electrochemically inactive nanoscale scaffolding for supporting Si active material. We fabricated titanium carbide/carbon core-shell nanofibers directly on a steel substrate, and then used CVD to coat amorphous Si onto this scaffolding. The nanoscale electronically conductive scaffolding allows for relatively high mass loading and good electronic connectivity, and the large mechanical stiffness and strength of the TiC/C nanofibers permit the silicon to mechanically deform during alloying/dealloying without damaging the underlying conductive backbone. This is in contrast to other one-dimensional nanostructures, such as Si nanowires, in which the entire structure reacts with Li during charge/discharge and is altered in the process. The specific capacity data with cycling shown in Fig. 5 shows that a capacity close to 2800 mAh/g can be maintained after 100 cycles for the TiC/C/Si composite (red dots), which exceeds that of Si nanowires (black dots). The Coulombic efficiency is also improved compared to silicon nanowires. This study shows the importance of interfacing large volume-expansion alloying anode materials with mechanically robust inactive materials for good battery performance.

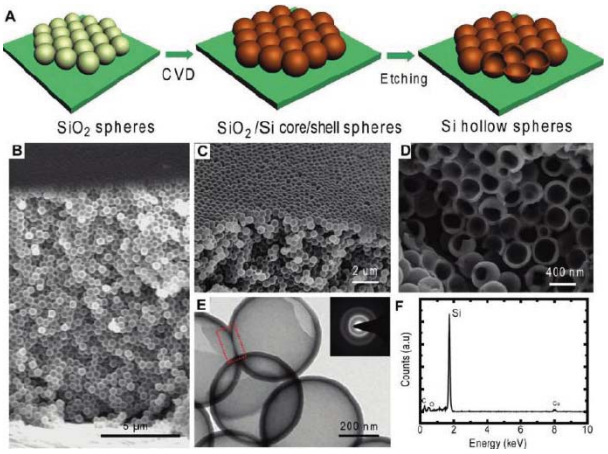

Figure V - 127: Hollow Si nanoparticle synthesis and images.

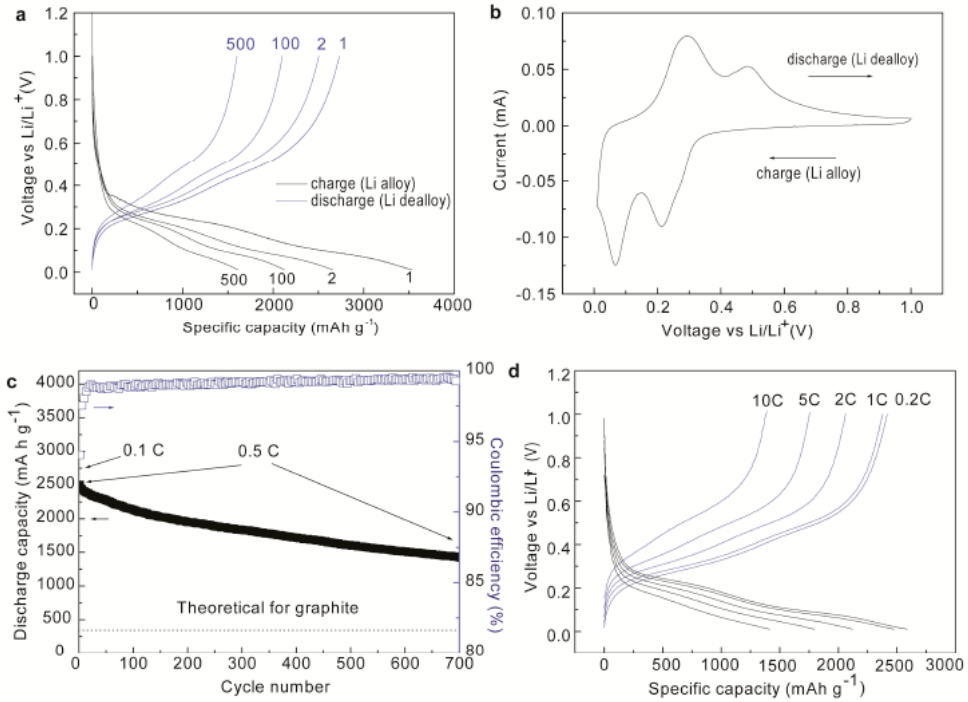

Figure V - 128: Electrochemical performance of hollow Si nanoparticles.

Conclusions and Future Directions

- We have developd synthesis strategies to connect Si particles electrically, *ex situ* TEM to study Si volume changes and discovered the dependence of volume change on surface oxide layer and on size. We have also developed synthesis methods to produce Si electrodes with engineered pore sizes. We have obtain detailed information on the volume expansion and contraction of Si. We have determining size effects on fracture upon electrochemical lithiation/delithiation of silicon nanopillars. We have developed hollow Si nanocrystalls and conductive, mechanically robust, electrochemically inactive nanoscale scaffolding to demonsrate high perframnce Si anodes.
- Future direction include 1) Further understand the structure-property correlation 2) Optimizing hollow space engineering inside Si anodes. 3) Design strategy in forming stable SEI. 4) Design low-cost and scalable methods for high performance anodes.

FY 2011 Publications/Presentations

1. M. T. McDowell, Y. Cui," Single Nanostructure Electrochemical Devices for Studying Electronic Properties and Structural Changes in Lithiated Si Nanowires ", *Advanced Energy Materials* , 1, 894 (2011).
2. Y. Yao, M. T. McDowell, I. Ryu, H. Wu, N. Liu, L. Hu, W. D. Nix, and Y. Cui, "Interconnected Silicon Hollow Nanospheres for Lithium-Ion Battery Anodes with Long Cycle Life ", *Nano Letters* , 11, 2949 (2011).
3. N. Liu, L. Hu, M. T. McDowell, A. Jackson, and Y. Cui, "Prelithiated Silicon Nanowires as an Anode for Lithium Ion Batteries ", *ACS Nano* , 5, 6487 (2011).
4. M. T. McDowell, S. W. Lee, I. Ryu, H. Wu, W.D. Nix, J.W. Choi, and Y. Cui, " Novel Size and Surface Oxide Effects in Silicon Nanowires as Lithium Battery Anodes ", *Nano Letters*, 11, 4018 (2011).
5. Y. Yao, K. Huo, L. Hu, N. Liu, J. J. Cha, M. T. McDowell, P. K. Chu, and Y. Cui, "Highly Conductive, Mechanically Robust, and Electrochemically Inactive TiC/C Nanofiber Scaffold for High-Performance Silicon Anode Batteries" *ACS Nano*, 5, 8346 (2011).
6. (Invited talk) “Ultrahigh Capacity of Silicon Nanowires for Lithium Ion Batteries”, 10X Battery R&D Conference, Santa Clara, California, Jan 10-12, 2011.
7. (Invited talk) “Designing Nanostructures and Interfaces for High Performance Batteries and Supercapacitors**”,** The38th annual Physics and Chemistry of Semiconductor Interfaces Conference, San Diego, CA, Jan 16-20, 2011.
8. (Invited talk) “One Dimensional Nanostructures: from Energy to Environment Materials” Materials Research Society Spring Meeting, San Francisco, Apr 25-29, 2011.
9. (Invited talk) “High Energy and Low-cost Energy Storage with Nanostructures” Materials Research

Society Spring Meeting, San Francisco, Apr 25-29, 2011.

10. (Invited talk) The Wilson Prize Lecture, "Rational Nanomaterials Design for Energy Transformation and Storage", Harvard University, Cambridge, MA, Apr 28, 2011.
11. (Invited talk) "Energy and Environment Nanomaterials," The Harvard Distinguished Energy Lecture, Harvard University, Cambridge, MA, Apr 29, 2011.
12. (Invited talk) "Batteries, Solar Cells and Water Filters with Nanomaterials", Stanford Energy and Environment Affiliate Program, Stanford University, Stanford, CA, May 4, 2011.
13. (Invited talk) "Rational Nanomaterials Design for Energy Storage" Symposium M, ICMAT 2011, Singapore, Jun 27-Jul 1, 2011.
14. (Invited talk) "Energy Nanomaterials by Rational Design", Pacific Northwest National Laboratory, Richland, WA, July 8, 2011.

V.C.14 Hard Carbon Materials for High-Capacity Li-ion Battery Anodes (ORNL)

Sheng Dai
Oak Ridge National Laboratory (ORNL)
1 Bethel Valley Rd.
P.O. Box 2008, MS-6201
Oak Ridge, TN 37831-6053
Phone: (865) 576-7307; Fax: (865)-576-5235
E-mail: dais@ornl.gov

Collaborators: Xiao-Guang Sun, Miaofang Chi, ORNL

Start Date: June 2010
End Date: September 2012

Objectives

The objective of this project is to develop low-cost hard carbon materials with a high capacity (>372 mAh g^{-1}) and reliable performance for applications in lithium ion batteries.

Technical Barriers

Challenges for application of lithium ion batteries in electric vehicles include low energy density, poor cycle life, large irreversible capacity loss, poor rate capability, and calendar life.

Accomplishments

- Evaluated the carbonization temperature effect on the carbon half cell performance.
- Ealuated the effect of binder amount and pore size on the carbon half cell performance.
- Evaluated the surface coating and bulk doping effect on the electron conductivity of the carbon and the accompanying carbon half cell performance, especially the rate capability and long cycle stability.
- Evaluated the surface coating of single ion conductor on improving the initial coulombic efficiency and cell cycling stability.
- Finished the comparison of cell performance of mesoporous carbon with commercial carbons

✧ ✧ ✧ ✧ ✧

Introduction

Thousands of carbonaceous materials are commercially available, and lithium can be inserted reversibly within most of these. The structure of carbons depends strongly on the type of organic precursors used to make them. Carbonaceous materials have traditionally been divided into two groups: soft and hard. The soft carbons can be graphitized completely upon heating to above 3000°C, whereas the hard carbons are very difficult to graphitize. The capacity of graphite (soft carbon) is limited to 372 mAh g^{-1}, which is associated with its maximum LiC_6 stage. On the other hand, disordered hard carbons with different degrees of graphitization have been reported to exhibit stable capacities exceeding 500mAh/g. The reversible capacities of many hard carbons for lithium depend on both pyrolysis temperature and precursor type. In addition, the mechanism of lithium insertion in carbonaceous materials also depends on the carbon type.

Approach

Hard carbon materials with tailored surface areas and nanoscopic architectures have been synthesized in our group via a self-assembly method [1,2]. The unique ORNL methodology for synthesis of these hard carbon materials has several advantages: (1) tunable pore sizes (2–18 nm), (2) adjustable surface areas, (3) controlled variation of carbon/hydrogen ratios and chemical compositions through carbonization temperature and precursors, (4) tunable interfacial structures, and (5) controllable morphologies. The unique characteristics of our hard carbon materials permit us to systematically correlate the synthesis conditions with their reversible lithium intercalation capacity and provide a rare opportunity to investigate the structure-function relationship associated with hard carbons for energy storage. The lithium intercalation mechanism will also be studied in detail to guide the future synthesis of carbon materials with high, stable capacities against cycling for applications in lithium ion batteries.

Results

The mesoporous carbons obtained at different temperatures under nitrogen atmosphere all had a similar BET surface area of around 500m^2/g with pore sizes in the range of 6-9 nm. However, the intercalation capacity of the mesoporous carbon obtained at 550°C (MC550) showed much higher capacities than those obtained at 650, 750 and 850°C under the same testing conditions. So we have focused on improving the cell performance of MC550. To test the rate capability of MC550, we used the theoretical capacity of graphite, 372 mAh g^{-1}, to calculate the needed current. During the optimization of the electrode, we found

that 10wt% carbon black (CB) delivered the best cell performance. A cell with 15wt% CB showed initial higher capacities, but it became lower under higher rate conditions (Figure V - 129A). Therefore, 10wt% CB was used to fabricate mesoporous cabon electrodes. Figure V - 129B illustrates the benefit of meso-pores within MC550, which delivered much higher capacity than that of micro carbon (C550) under the same cycling condition.

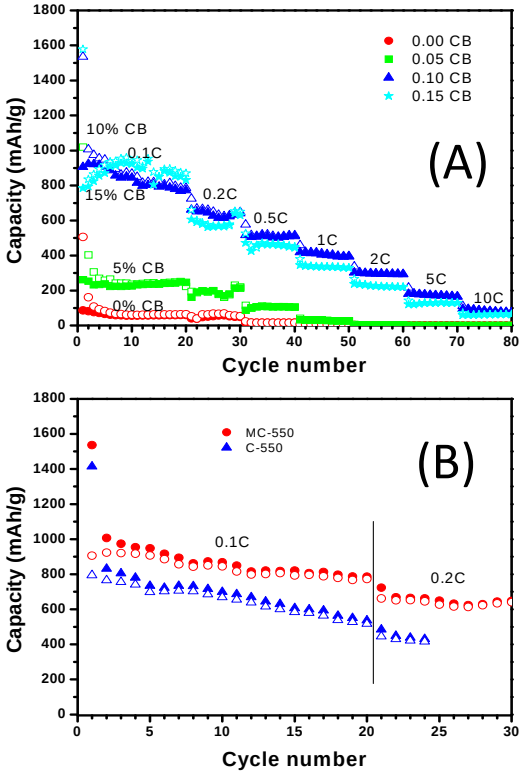

Figure V - 129: (A) Cycle performance of MC550 under different rate conditions and (B) comparison of cell performance between mesoporous carbon MC550 and non-porous carbon C550 under same rate conditions (the electrode area is 1.327cm^2).

Considering that the electronic conductivity of MC550 is lower than that of natural graphite and other carbons obtained at higher temperatures, we tried to improve its electronic conductivity by coating the surface with a good electron conductor, polypyrrole (PPy), which is doped with toluene sulfonic acid. As shown in Figure V - 130A under all rate conditions the capacities of the cells with 10wt% and 20wt% PPy were lower than that of the cell without surface coating. However, the cycling stability of the cells with surface coating was much improved over that of the cell without surface coating, which is mainly attributed to a reduction in surface defects.

The decrease in capacity after surface coating prompted us to improve the bulk electron conductivity rather than the surface electron conductivity. Multiwall carbon nanotube (CNT, 10wt% and 20wt%) was chosen as the doping agent to improve the electronic conductivity. Figure V - 130B shows that, under all rate conditions, the cells based on CNT doped MC550 had a 100 mAh g^{-1} higher capacity than the cell based on un-doped MC550. The increased capacity is primarily due to the optimized transport properties of the doped carbon samples. The meso pores within the carbon matrix provide fast Li+ transport channels, wheras the CNTs within the carbon matrix provide fast electron transport channels, and thus provide higher rate capabilities.

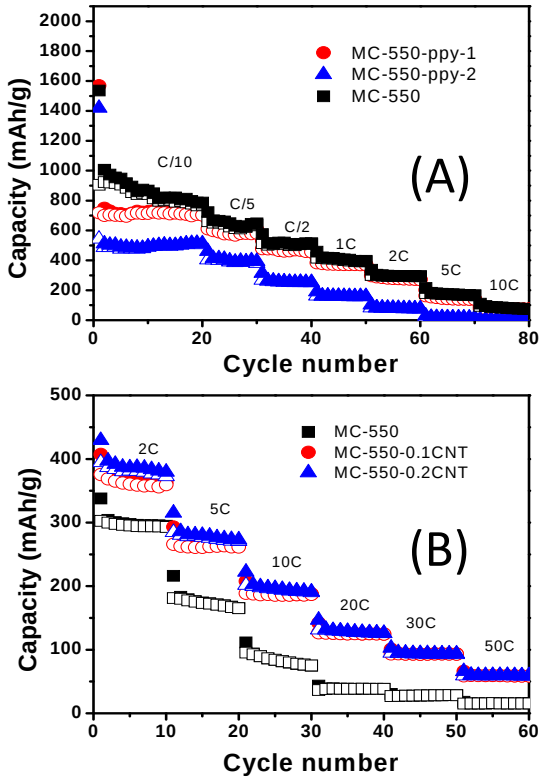

Figure V - 130: (A) Cycle performance of MC550 with Polypyrrole (PPy) surface coating (10wt% and 20wt%) under different rate conditions; (B) Cycle performance of MC550 with carbon nanotube (CNT) doping (10wt% and 20wt%) under different rate conditions.

The initial coulombic efficiency of the cells based on MC550 is only in the range of 50-55%. Therefore, we have tried different ways to improve the initial coulombic efficiency. First, single ion conductors were used to mimic the composition of the solid electrolyte interphase (SEI) to prevent the continual electrolyte decomposition. We used polyacrylic acid lithium salt (PALi) and poly(styrenesulfonic acid-co-methacrylic acid) lithium salt (PSSA-co-MALi) as surface coating agents to coat the carbon surface, followed by casting electrodes. As shown in Figure V - 131A, the improvement in coulombic efficiencies after surface coating was very limited. In addition, it is accompanied by decrease in both charge and discharge capacities, which suggests that the surface coating reduces the surface defect sites and therefore initial lithium storage capacity. However, the cycling stability of

the carbons after surface coating is improved, especially under high rate conditions (Figure V - 131B).

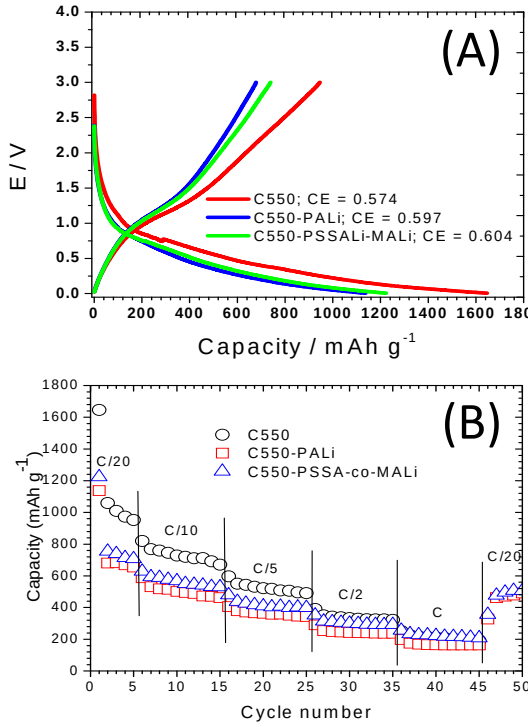

Figure V - 131: (A) First cycle of MC550 with 10wt% surface coating of single ion conductors under the rate of C/20 (B) Cycle performance of MC550 with 10wt% surface coating of single ion conductors under different rate conditions.

While we were trying different techniquse to improve the performance of our mesoporus carbon as a potential anode for electric vehicle applications, we were asked to focus on evaluating commercial carbons. We systematically investigated the performance of commercial carbons from Pred Materials and MTI Corporation versus our mesoporous carbon under the same rate conditions. As seen in Figure V - 132, all the commercial carbons have poor rate capability compared to the mesoporus carbon under the same rate conditions. For example, at low 1C rate the capacities of natural graphite, Potato Graphite, Mesophase Graphite and MesoCarbon MicroBeads (MCMB) are all lower than 250 mAh g^{-1} while that of mesoporous carbon delivers a capacity that is more than 400 mAh g^{-1}, which is higher than the theoretical capacity of graphite (372 mAh g^{-1}). With increasing cycling rate, the difference between our mesoporous carbon and the commercial carbons becomes bigger. At 10C rate, the capacities of commercial carbons drop to nearly zero while that of mesoporous carbon remains around 100mAh g^{-1}.

The above comparisons show that the mesoporous carbon is superior to those commercial carbons under high rate conditions, which is an important factor to consider for electric vehicle applications where high power and high energy is needed.

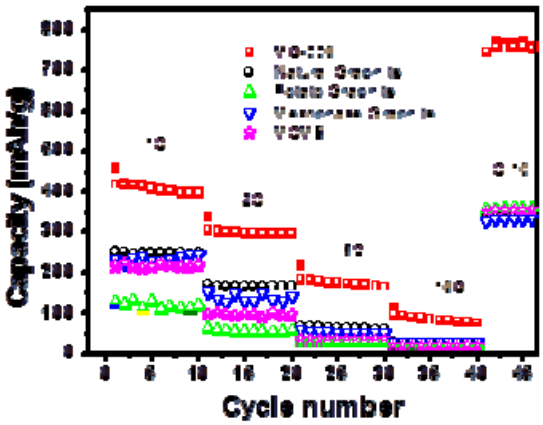

Figure V - 132: Comparison of the rate capability of different commercial carbons with the house synthesized mesoporous carbon. Natural graphite, potaot graphite and mesophase graphite all come from Pred. Materials. MCMB (MesoCarbon MicroBeads) comes from MTI Corporation.

Conclusions and Future Directions

Mesoporous carbon has clear advantages over commercial carbons in terms of capacity and rate capability. However, the cycling stability and the initial coulombic efficiency clearly need to be improved. Coating the carbon surface with single ion conductor can prevent the initial contact of the electrolytes with electrodes, however, the electrolyte can swell the surface coating and eventually contact the electrode and decompose, which results in capacity loss with cycling. Inelastic coatings such as crosslinked materials or inorganic lithium compounds could eliminate the swelling effect and thus improve the initial coulombic efficiency and cycling stability.

FY 2011 Publications/Presentations

1. 2011 DOE Annual Peer Review Meeting Presentation.
2. B. K. Guo, X. Q. Wang, M. F Chi, S. M. Mahurin, X. G. Sun, S. Dai, “One-step Synthesis of Mesoporous Carbon for Lithium-ion Batteries with High Capacity and Rate Capability”, abstract #1399, the 220th Electrochemical Society Meeting, Boston, Oct. 9-14, 2011.
3. B. K. Guo, X. Q. Wang, M. F Chi, S. M. Mahurin, X. G. Sun, S. Dai, Soft-Templated Mesoporous Carbon-Carbon Nanotube Composites for High Performance Lithium-ion Batteries, Advanced Materials, 2011, 23, 4661.

References

1. Dai et al., U.S. Patent 7,449,165
2. Dai et al., Angew. Chem. Inter. Ed. 2008, 47, 3696.

V.D Electrolyte Development

V.D.1 Polymer Electrolytes for Advanced Lithium Batteries (UC, Berkeley)

Nitash P. Balsara
University of California
201 C Gilman Hall
Department of Chemical and Biomolecular Engineering
Berkeley, CA 94720
Phone: (510) 642-8973; Fax: (510) 643-4778
E-mail: nbalsara@berkeley.edu

Start Date: October 2008
Projected End Date: December 2013

Objectives

- Fundamental characterization of self-assembled block copolymer electrolytes for stabilizing lithium metal anodes.
- Development of self-assembled polymer separators.
- Development of electronically and ionically conducting polymer binders.

Technical Barriers

Current lithium-ion cells use polymers for two applications: they serve as a binder to hold the active materials in place and as a porous separator to hold the liquid electrolyte and keep the electrodes physically separated. The cost of the porous separators is large due to the delicate processing steps that are used in manufacturing. Defects in the separator can cause catastrophic failures. The binder is essentially an inactive component, while electron and ion transport are mediated by separate components - carbon and liquid electrolyte that floods the pores of a porous electrode, respectively. Cell energy and power performance deteriorate if the active materials loses contact with charge transporting components. Lithium metal electrodes are not used in rechargeable batteries due to dendrite growth.

Technical Targets

- Enable the use of a lithium metal electrode stabilized by a block copolymer electrolyte.
- Synthesize and characterize self-assembled porous battery separators.
- Synthesize and characterize electronically and ionically conductive polymer binders.

Accomplishments

- Measured conductivity, and salt diffusion coefficient as a function of morphology in block copolymer electrolytes.
- Quantified the relationship between conductivity and morphology of self-assembled, porous block copolymer separators.
- Successful synthesis of electronically- and ionically-conducting binder and its use in lithium battery electrodes.

✧ ✧ ✧ ✧ ✧

Introduction

The objective of this work is to comprehensively examine the role that polymers can play in the development of advanced lithium batteries – specifically addressing issues of safety, cycle life, and cost. Replacing conventional liquid electrolytes with a solid block copolymer enables the use of a lithium metal anode, which improves the energy density of the battery. The block copolymer comprises a hard non-conducting block that suppresses the formation of lithium dendrites while a soft block enables rapid transport of lithium-ions. In more recent work, we have replaced the hard non-conducting block with an electronically conducting block to serve as a polymer binder. Preliminary characterization data reveal the presence of both electron and ion transport capabilities in these materials. Finally, nanoporous separators have been synthesized by block copolymer self-assembly. These materials provide insight into the morphologyconductivity relationship in porous separators. The processing routes to create these separators may be more cost-effective and environmentally friendly than those under current industrial use.

Approach

Sequential polymerization is used to synthesize the block copolymers for all of the projects. Physical characterization includes determination of morphology by X-ray scattering and electron microscopy, and electrochemical characterizations are performed using either blocking or non-blocking electrodes. Equipment for

cycling cells as a function of temperature and for making pouch cells with a solid electrolyte is now available.

Results

Material. We have synthesized three different kinds of block copolymers: poly(styrene)-*b*-poly(ethylene oxide) (SEO) copolymers for stabilizing the lithium metal electrode, polystyrene-*b*-polyethylene-*b*-polystyrene (PS-PE-PS) copolymers for self-assembled porous separators and poly(3-hexylthiophene)-*b*-polyethylene oxide (P3HT-PEO) copolymers for electronically and ionically conducting binders.

Block Copolymer Electrolyte Characterization. The salt diffusion was studied in a series of nanostructured block copolymer electrolytes using the restricted diffusion technique. The decay of the open-circuit potential of a symmetric Li-polymer-Li cell was analyzed by a Laplace inversion algorithm to give the distribution of relaxation processes characteristic of the electrolytes. The distribution function was characterized by two parameters, an average diffusion coefficient, D_{avg}, and a polydispersity index, $PDI_{diffusion}$, which is a measure of the width of the distribution of diffusion coefficiens. We compare the parameters obtained from a series of nearly symmetric SEO block copolymer electrolytes containing lithium bis(trifluoromethanesulfone)imide salt (LiTFSI) with those obtained from a homogeneous poly(ethylene oxide) (PEO)/LiTFSI mixture. D_{avg} of the SEO/LiTFSI mixtures increases with increasing molecular weight of the PEO block, M_{PEO}, and reaches a plateau of 2/3 D_{PEO} when M_{PEO} exceeds 50 kg/mol (D_{PEO} is the average salt diffusion coefficient in PEO homopolymer). The $PDI_{diffusion}$ values obtained for SEO copolymers are significantly higher than those obtained in PEO homopolymer (see Table V - 2).

Table V - 2: Average diffusion coefficient, D_{avg}, and $PDI_{diffusion}$ of the relaxation distribution functions for the polymers used in this study [see ref. 4 for details].

Polymer	D_{avg} (cm^2/s)	Average $PDI_{diffusion}$
PEO(27)	$(1.23 \pm 0.12) \times 10^{-7}$	1.16 ± 0.13
SEO(6 – 7)	$(2.36 \pm 0.49) \times 10^{-8}$	1.67 ± 0.32
SEO(16 – 16)	$(4.62 \pm 0.18) \times 10^{-8}$	1.59 ± 0.26
SEO(36 – 24)	$(5.79 \pm 1.2) \times 10^{-8}$	1.41 ± 0.18
SEO(37 – 25)	$(6.80 \pm 1.5) \times 10^{-8}$	1.64 ± 0.35
SEO(40 – 54)	$(7.44 \pm 0.6) \times 10^{-8}$	1.31 ± 0.15
SEO(53 – 68)	$(6.54 \pm 1.1) \times 10^{-8}$	1.36 ± 0.27
SEO(74 – 98)	$(8.45 \pm 0.8) \times 10^{-8}$	1.38 ± 0.21
SEO(240 – 269)	$(7.83 \pm 1.5) \times 10^{-8}$	1.35 ± 0.26

Self-assembled Separators. Nanoporous battery separators were made by blending a poly(styrene-block-ethylene-block-polystyrene) copolymer (SES) and polystyrene (PS) homopolymers, casting films of the blend, and selectively dissolving the homopolymer. The volume previously occupied by the homopolymer chains in the cast films are thus converted into pores. This approach enabled systematic variation of the pore structure at fixed void fraction by changing the normalized chain length of the sacrificial PS homopolymer. The efficacy of the resulting separators was determined by measurement of the ionic conductivity of separators soaked in a standard lithium battery electrolyte, 1M lithium hexafluorophosphate in ethylene carbonate/diethyl carbonate (1:1 v/v, Novolyte Technologies, Inc.). The effect of the chain length of the sacrificial homopolymer on separator morphology and ion transport was then determined using impedance measurements.

In highly porous separators with a nominal pore volume fraction of 0.43, conductivity peaked at $\alpha = 0.22$, where values as high as 0.39 mS/cm were achieved (α is the molecular weight of the PS homopolymer normalized by that of the PS block in the SES copolymer). Nitrogen adsorption experiments and scanning electron microscopy were used to determine the underpinnings of this observation. At $\alpha = 0.12$, extremely small pores with low surface area are formed. Increasing α to 0.22 results in a film with well-connected nanoscale pores. A further increase in α to 2.02 results in films with micron-sized pores that are not effective for ion transport. Figure V - 133 shows SEM images of these porous separators.

The main advantage of our approach relative to conventional separator manufacturing is that the pore structure is determiend by equilibrium thermodynamics and thus strict control over processing conditions is not necessary.

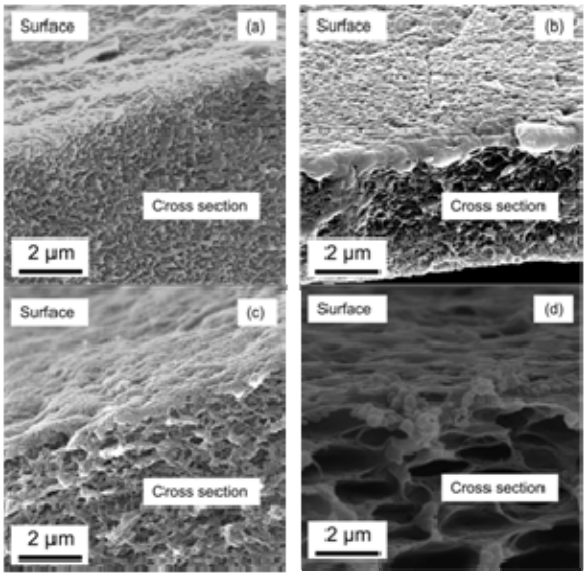

Figure V - 133: Scanning electron micrographs of separators with void fraction, $\mathbb{V} = 0.43$ at a) $\alpha = 0.12$ b) $\alpha = 0.22$ c) $\alpha = 0.43$ and d) $\alpha = 2.02$ obtained by cryofracturing washed out films. (Images taken from Wong et al., paper under review.)

Multi-purpose Binder. A block copolymer that exhibits simultaneous electronic and ionic conduction was

synthesized as shown in Figure V - 134. Separate values for the electronic and ionic conductivity of the P3HT-*b*-PEO copolymer mixed with LiTFSI, were determined using a combination of ac and dc impedance measurements. The P3HT-*b*-PEO/LiTFSI mixture was then used to make a lithium battery cathode with $LiFePO_4$ as the only other component. All-solid lithium batteries composed of the cathode described above, SEO solid electrolyte and a lithium foil as the anode showed capacities within experimental error of the theoretical capacity of the battery (Figure V - 135). The ability of P3HT-*b*-PEO to serve all of the transport and support functions required in a lithium battery electrode is thus demonstrated. The fact that P3HT is a semiconductor enables design of responsive electrodes.

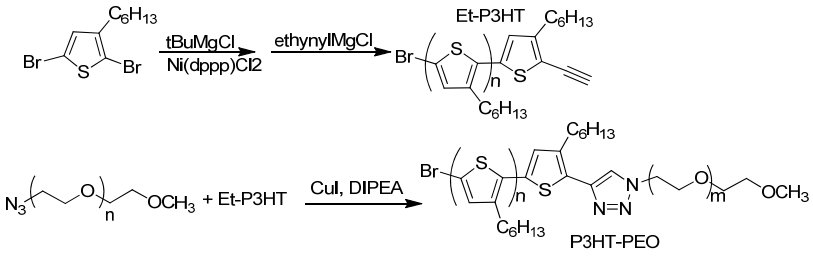

Figure V - 134: Synthesis of P3HT-b-PEO.

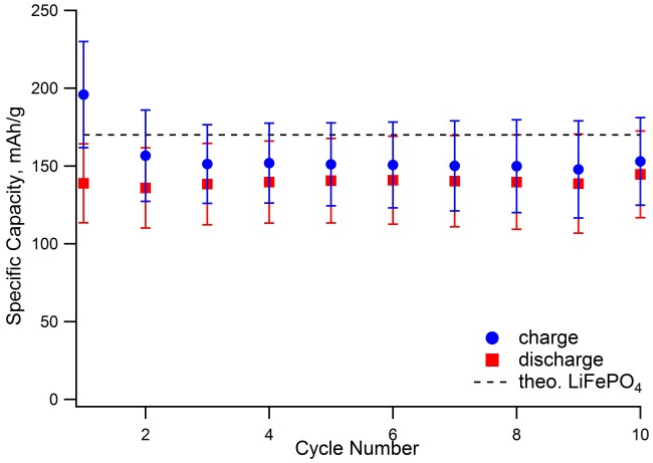

Figure V - 135: Average specific capacities for the first 10 cycles of 10 cells.

Conclusions and Future Directions

We have measured salt diffusion coefficients as a function of block copolymer morphology. We have successfully synthesized polymer separators with self-assembled pores, and are in the process of characterizing a wider array of morphologies to understand the underpinnings of ion transport in these systems. Our in-house assembly and analysis for pouch cells is now fully opereational with our first full cell data published in ref. 3. These data demonstrated that our binder conducted both ions and electrons to the reaction sites within the cathode.

FY 2011 Publications/Presentations

1. "Effect of Lithium Polysulfides on the Morphology of Block Copolymer Electrolytes", A.A. Teran, N.P. Balsara, Macromolecules, accepted 2011.
2. "Effect of Molecular Weight on Conductivity of Polymer Electrolytes", A.A. Teran, M.H. Tang, S.A. Mullin, N.P. Balsara, Solid State Ionics, doi:10.1016/j.ssi.2011.09.021, 2011.
3. "Simultaneous Electron and Ion Conduction in a Block Copolymer: Application in Lithium Battery Electrodes", A.E. Javier, S.N. Patel, D.T. Hallinan, V. Srinivasan, N.P. Balsara, Angewandte Chemie (Communication), vol. 50, pp 9848–9851, 2011.
4. "Salt Diffusion Coefficients in Block Copolymer Electrolytes", S.A. Mullin, G.M. Stone, A. Panday,

N.P. Balsara, Journal of the Electrochemical Society, vol. 158, pp. A619-627, 2011.
5. "Chemical Mapping of a Block Copolymer Electrolyte by Low-Loss EFTEM Spectral Imaging and Principle Component Analysis", F.I. Allen, M. Watanabe, Z.H. Lee, N.P. Balsara, A.M. Minor, Ultramicroscopy, vol. 111, pp. 239-244, 2011.
6. Invited Lecture. "Role of Block Copolymers in All-Solid Rechargeable Batteries", Joint Meeting of the International Battery Association and Pacific Power Source Symposium, Big Island, Hawaii, January 9, 2012.
7. Invited Lecture, "Next Generation Battery Technology: EHS Impact", California Industrial Hygiene Council Conference, San Francisco, California, December 6, 2011.
8. Invited Lecture, "Simultaneous Electron and Ion Conduction in a Block Copolymer", Session in Honor of Professor Matthew Tirrell's 60th Birthday, Annual Meeting of the American Institute of Chemical Engineers, Minneapolis, Minnesota, October 17, 2011.
9. Plenary Lecture, "Microstructured Block Copolymer Membranes for Lithium Batteries and Alcohol Separation", Session on Emerging Areas in Polymer Science and Engineering, Annual Meeting of the American Institute of Chemical Engineers, Minneapolis, Minnesota, October 17, 2011.
10. Invited Lecture, "Block Copolymers for Lithium Batteries", Sustainable Energy Education and Research Center, University of Tennessee, Knoxville, Tennessee, September 27, 2011.
11. Invited Lecture, "Solid-State Batteries", American Vacuum Society, Northern California Chapter, San Jose, California, September 21, 2011.
12. Invited Lecture, "Characterization of Microstructured Block Copolymer Electrolytes for Lithium Batteries", Annual Meeting of the American Chemical Society, Denver, Colorado, August 28, 2011.
13. Invited Lecture, "Block Copolymer Membranes for Rechargeable Lithium Batteries", First International Symposium on Colloids and Materials, Amsterdam, Holland, May 8, 2011.
14. Invited Lecture, "Characterization of Microstructured Block Copolymer Electrolytes for Lithium Batteries", Fundamental Topics in the Physics and Theory of Novel Polymeric Systems, Annual Meeting of the American Chemical Society, Anaheim, California, March 27, 2011.
15. Department Seminar, "Block Copolymers for Lithium Batteries", Department of Chemistry and Biochemistry, Santa Clara University, Santa Clara, California, February 11, 2011.
16. Invited Lecture, "Block Copolymer Electrolytes for Lithium Batteries", Materials Research Outreach Program, University of California, Santa Barbara, February 3, 2011.

V.D.2 Interfacial Behavior of Electrolytes (LBNL)

John B. Kerr (Principal Investigator Name)
Lawrence Berkeley National Laboratory,
MS 62R0203, 1 Cvclotron Road,
Berkeley, CA 94720
Phone: (510) 486-6279; Fax: (510) 486-4995
E-mail: jbkerr@lbl.gov

PI has participated in BATT program since 1998.
1994-1999 USABC/3M/HQ project on Li/Polymer batteries.
FY10-12 Project started October 1, 2009
70% completed

Objectives

FY10

- Demonstrate whether single-ion conductor polyelectrolytes (gel and dry polymer) prevent concentration polarization in composite cathodes and facilitate thicker electrodes.
- Determine whether single-ion conductor polyelectrolytes (gels and dry polymers) are beneficial for large volume-expansion anodes.

FY11

- Determine whether available single-ion conductor polyelectrolytes function with the high voltage NiMn spinel cathodes.
- Determine the stability of base-line and single-ion electrolyte to NiMn spinel cathodes including chemical analysis of electrolyte degradation products.

Technical Barriers

This project addresses the following technical barriers

- Poor cycle and calendar life.
- Low power and energy densities.
- High manufacturing cost.
- Safety

Technical Targets

- Determine the contribution to the interfacial impedance of the salt structure in terms of reactivity versus intrinsic electrode kinetics.
- Determine the contribution to the interfacial impedance of the solvent or polymer structure in terms of reactivity versus intrinsic electrode kinetics.
- Determine the contribution to the interfacial impedance of the physical properties of the electrolyte – liquid vs. gel. vs. solid polymer electrolyte.
- Develop analytical methods for determination of side reaction products and chemical characterization of the SEI layer.

Accomplishments

- Prepared and tested new single ion conductor materials based on fluoroalkylsulfonylimide anions which appear stable to 5 Volts or higher.
- The new salts appear to have interesting and potentially beneficial effects in conventional lithium ion cells when used as additives.

✧ ✧ ✧ ✧ ✧

Introduction

The choice of electrolyte used in lithium ion batteries presents significant challenges. The impedances presented by the electrolyte are the bulk ohmic resistance (conductivity), concentration polarization (transport properties) and interfacial impedance (intrinsic electrochemical kinetics of charge transfer at the electrodes). Most of the attention of electrolyte researchers over the years has focused upon the ohmic resistance (conductivity) of the bulk electrolyte yet this impedance is usually smaller than that due to concentration polarization (especially in composite electrodes) and much smaller than that of the interface. Interfacial impedance is a critical barrier to the deployment of lithium ion batteries in traction vehicles.

Single-ion polyelectrolyte lithium conductors possess the solution for many of the problems with present electrolytes. They can be used with no liquid electrolyte thereby reducing the safety problem. They can be prepared and deployed in ways that avoid many of the reactivity issues both in the bulk of the electrolytes and at the interfaces and hence offer a solution to the lifetime problem. Because they possess a unity transference number, there is no concentration polarization through the composite electrodes. Thus, provided the conductivity is in excess of 10^{-4} S/cm, the single ion conductors (SIC) can facilitate the use of thicker composite electrodes thereby leading to higher energy and power densities. They further appear to have application to the operation of large volume expansion electrodes where concentration gradients have a considerable negative effect.

In past years, this group has demonstrated that SIC materials, both dry and as gels, possess the bulk transport properties required. However, the interfacial behavior of these materials has exhibited disastrously high impedances rendering the SIC materials unusable. It is imperative that the source of this impedance be elucidated and reduced to manageable values and hence the whole goal of the work is to elucidate the mechanisms that lead to interfacial impedance so that this critical factor may be minimized.

There is considerable continuing discussion in the literature about the effect of the solid electrolyte interphase (SEI) upon the interfacial impedance of Li ion battery electrodes. Growth of the impedance is one mode of failure that limits the calendar and cycle life of Li ion batteries. From studies of a variety of electrolytes ranging from single ion polyelectrolyte Li ion conductors through binary salt polymer electrolytes, polymer gels, ionic liquids and liquid electrolytes it has been noted that the properties of the electrolyte have a significant impact on the apparent intrinsic rates of electrode reactions quite apart from their reactions to form side products that may form the SEI layer. To separate out these effects we have attempted to study a variety of electrolytes that can allow the separation of the effect of side reactions from that of intrinsic kinetics. Needless to say, the effects of trace impurities and intrinsic instabilities in both the electrolytes and the electrodes can have a major impact upon the interfacial behavior and considerable effort is still required to properly characterize the materials for reproducible results.

Approach

A physical organic chemistry approach is taken to electrolyte design, where the molecular structure is varied to provide insight into the processes that may affect the performance of the battery. Figure V - 136 illustrates the approach taken for incorporation of immobilized anions into the separator and binder materials as well as into the composite electrode structure in order to facilitate control of the concentration of the lithium ions at the electrode surface. It turns out that the salt concentrations that are preferred for bulk ion transport are much less than that preferred for the surface concentration. Interfacial impedance is decreased as the exchange current density increases and the exchange current density is proportional to the concentration at the electrode surface

As is illustrated in Figure V - 136, different anions and different polymer backbones have been prepared and tested to investigate the effects of molecular structure on the behavior of the electrolytes when they are tested with different electrode materials.

To accomplish this work requires collaboration with other groups in BATT.

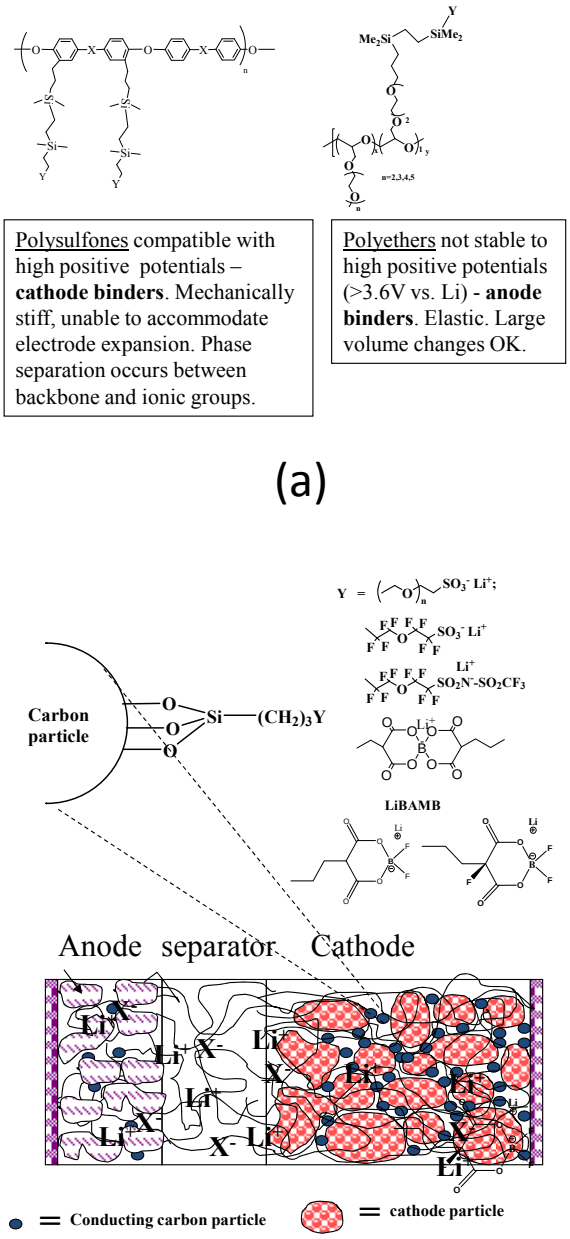

Figure V - 136: Methods of immobilizing electrolyte anions in lithium ion batteries. (a) Polyelectrolyte ionomers for use as separators and binders; (b) surface modified carbons for incorporation into composite electrodes to control lithium ion concentration.

- Surface analysis groups to identify side reaction products and reactive intermediates by combination of spectroscopy and product distribution analysis.
- Sharing data and materials with other electrolyte developers.

- MD and electrochemical systems modeling groups to provide experimental data.
- Deliver promising materials to cell testing group.

Results

Previous work has reported upon the tethering of borate ester anions derived from malonic acid which allows the anion to be fixed to the polymer to form a network polymer that is cross-linked through the anion. During the past year we have prepared new borate ester anions which provide insight into the effect of anion structure on the bulk and interfacial behavior. Figure V - 137 shows the structures of new salts that have been synthesized and tested. The hydrosilated salt is used to attach the anion to the polymer as illustrated in Figure V - 136 and this anion provides a material that is not cross-linked.

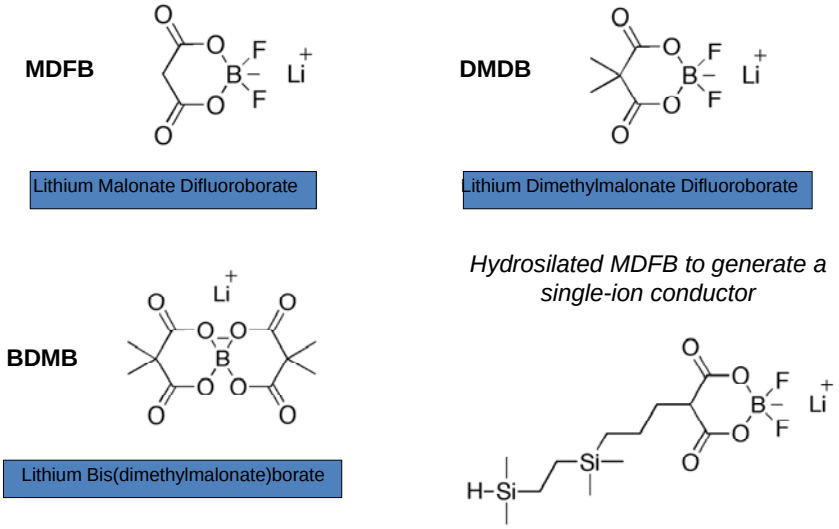

Figure V - 137: New salts synthesized and tested in FY10.

In FY10 these and the fluoroalkylsulfonyl imide salt were tethered to polymers based on polyether structures. In FY 2011 the polymer structures that these anions have been attached to have been extended to polyether-polysulfone backbones as shown in Figure V - 138. Which shows a polymer cross-linked using a bis(malonato) ester anion(BDMB) and with trifluoroalkylsulfonylimide anions (TFSI). The conductivities of these polymers formed into gels with EC:EMC solvents are plotted against 1/T inFigure V - 139, together with the conductivities of the corresponding PEO-based polymers. The large double-headed arrows are to highlight the difference in conductivity that is observed on replacement of the polyether with the polyether-polysulfone backbone.

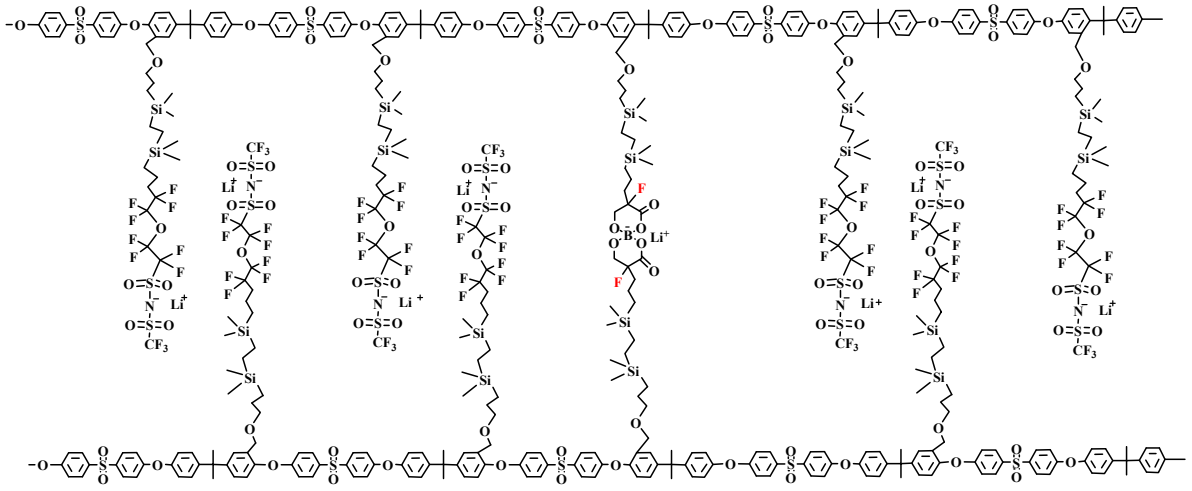

Figure V - 138: Structure of Polyether-polysufone Single ion conductor (PS-TFSI)

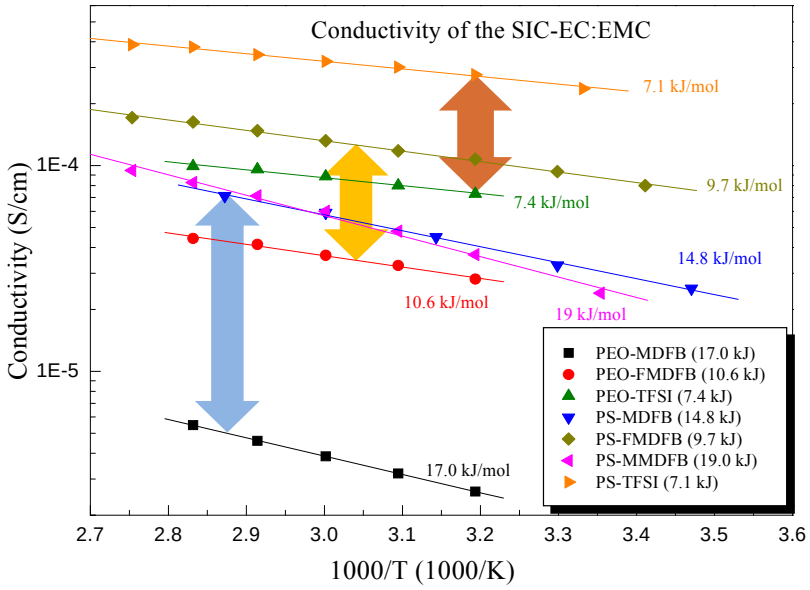

Figure V - 139: Conductivities of polyelectrolyte gels as a function of temperature. Gels are prepared with EC:EMC solvent.

The activation energies for Li ion conduction are also listed on the plot. It can be seen that switching from the polyether backbone to the polyether-polysulfone backbone resulted in a significant increase in conductivity without much change in the activation energy. However, the activation energy almost doubled on changing the solvent to tetraethyleneglycoldimethyl (TEGDME) ether from the carbonate solvents and the absolute value of the conductivity decreased by an order of magnitude that probably reflects the effect of the lower dielectric constant of the medium on the ion-pairing of the salts. Similar trends were also observed with the interfacial impedance of the gels at lithium metal where the impedance with the polyether-polysulfone is much smaller. Figure V - 140 shows the impedance of the PS-TFSI gel at lithium metal at 80°C which is an order of magnitude less than the polyether material. Even at 25°C the impedance is only 200 ohm.cm^2 which indicates that these single-ion conductor materials are now very close to being practical.

More important is the performance of these materials when used as binders in composite electrodes. Figure V - 141 shows the impedance of half cells of $LiFePO_4$ one with the single-ion conductor separator and binder and one with a conventional binary salt electrolyte. Figure V - 142 shows the discharge capacities of these two cells as a function of rate.

Figure V - 142 shows the much better capacity at high rates of the single-ion conductor binder which is expected due to the lack of concentration polarization. The stability of the PS-TFSI SIC gel at high voltages is illustrated in Figure V - 143, where it can be seen that the electrolyte system is stable to at least 4.5V. This indicates the material will be stable with the spinel –type cathodes and tests on this stability are under way.

The interfacial impedance of these SIC materials is still high but maybe reduced by functionalization of the surfaces in composite electrodes as illustrated in Figure V - 136 (b). Very encouraging results have already been obtained that will merit a patent application in due course. The results will be reported on in future.

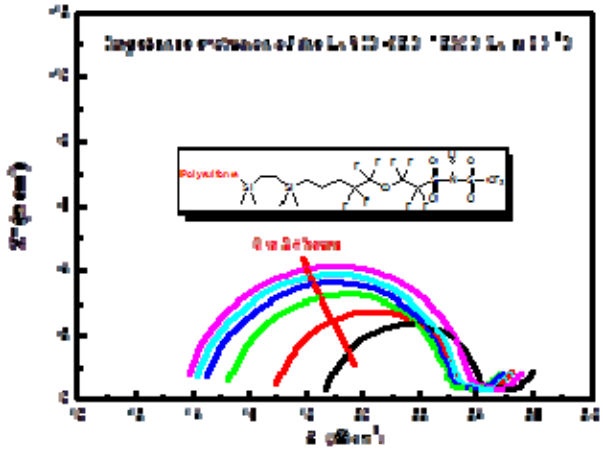

Figure V - 140: Nyquist plot of impedance of PS-TFSI Single-ion conductor gel against Li metal.

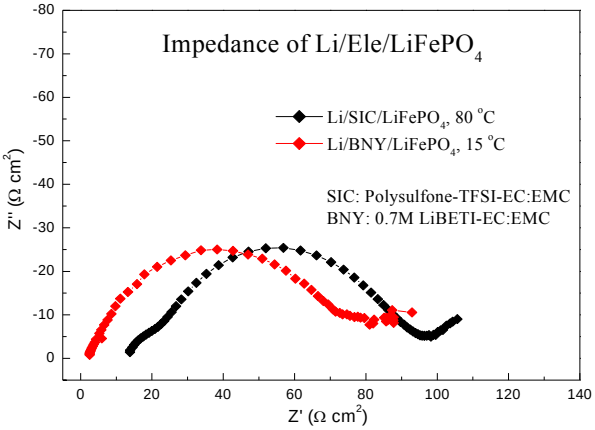

Figure V - 141: Nyquist plots of Half cells of $LiFePO_4$ one with a single-ion conductor separator and binder and one with a binary salt electrolyte

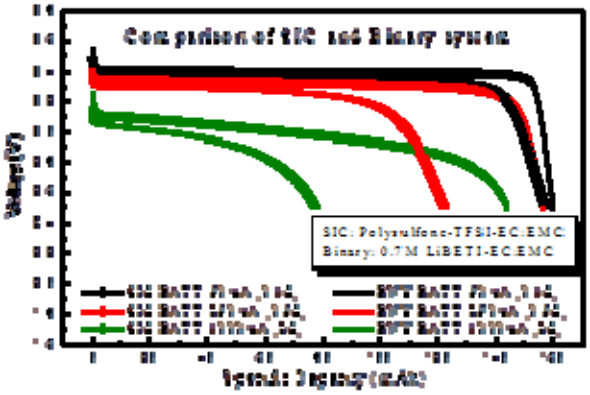

Figure V - 142: Discharge capacity as a function of rate comparison for single ion conductors versus binary salt electrolytes

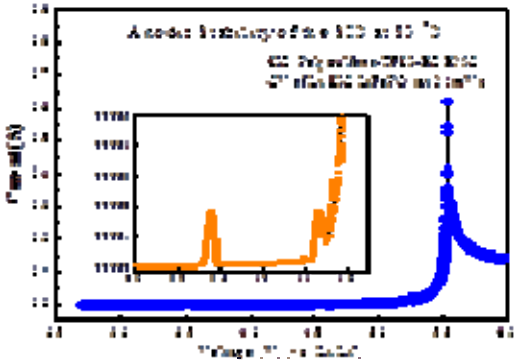

Figure V - 143: Voltammetry of Polysulfone SIC gel in Li/SIC/$LiFePO_4$ cell.

FY 2011 Publications/Presentations

1. "Synthesis of Lithium Malonate Difluoro Borate (LiMDFB) and Lithium Bis (Trifluoro-methanesulfonyl) Imide (LITFSI) based single ion conductor and its Electrochemical Performance", Li Yang, Peter F. Driscoll, Matthieu Gervais, Ravindra Potrekar, Jianli Cheng, John B. Kerr, ECS Fall Meeting, Oct 2011, Boston, MA. Abstr. #183
2. "Polymer modified MWCNT as conductive additive in LiFePO4 cathode with high rate capability" Jianli Cheng, Li Yang, John B. Kerr, ECS Fall Meeting, Oct 2011, Boston, MA. Abstr. #1371.
3. "Electrolytes - R&D for Advanced Lithium Batteries. Interfacial Behavior of Electrolytes" Presentation to the DOE Annual Merit Review, Arlington, VA, May 2011. #ES089.
4. "Single Ion Conductor Polyelectrolytes for Increased Capacity, Dendrite Inhibition and Safety", John B. Kerr, Li Yang, Xioaguang Sun, Adam Miller, Peter Driscoll and Ravindra Potrekar, DowKokam, Advanced Battery Technology Exchange, Lee's Summit, MO, October 2011.

V.D.3 Molecular Dynamics Simulation Studies of Electrolytes and Electrolyte/Electrode Interfaces (Univ Utah)

Grant D. Smith and Oleg Borodin
University of Utah
Department of Materials Science and Engineering
122 S. Central Campus Dr. Rm. 304
Salt Lake City, UT
Phone: (801) 585-3381
E-mail: gsd8@utah.edu

Subcontractor: Penn State University

Start Date: March 2008
Projected End Date: December 2012

Objectives

- Use molecular simulations to gain understanding into the chemical composition of the electrode/electrolyte interface as a function of electrode potential
- Understand double layer structure, capacitance and transport at the anode and cathode interface as a function of potential and temperature
- Use *ab initio* calculations to gain insight into high voltage electrode surfaces and electrolyte oxidation (cathode) and reduction (anode) mechanisms
- Use molecular simulations to predict the chemical composition and structure of SEI layers at the anode and cathode
- Use molecular simulations to understand the role of additives in the formation of SEI layers
- Gain molecular level understanding of Li^+ cation transport mechanisms in SEI layers
- Gain molecular level understanding of Li^+ cation transport mechanisms in electrolytes comprised of new salts and solvents in collaboration with experimental BATT projects
- Provide guidance for design of electrolytes with improved lithium transport, reduced interfacial resistance and/or improved electrochemical stability

Technical Barriers

- Poor low-temperature operations
- Poor transport through SEI layers
- High interfacial transport resistance
- Oxidative stability of the electrolyte in contact with high voltage cathode materials

Technical Targets

- Develop a cell to meet the 10-mile PHEV goal.
- Develop an electrolyte or electrolyte additives that allow use of cathodes in the high-potential range (4V – 5V *vs.* Li/Li^+).
- Develop and utilize a high-potential, stable electrolyte system that can operate in the temperature range of -30°C to 55°C.

Accomplishments

- Improved understanding of the outer SEI formation via single electron reduction of ethylene carbonate, including identification of major components
- Improved understanding of the structure, dynamics and desolvation energetics of the graphite/electrolyte interface as a function of electrode potential
- Identification of the low energy surfaces of $LiNi_{0.5}Mn_{1.5}O_4$
- Calculation of the oxidation potential and decomposition pathways for important electrolyte components and the determination that the presence of the lithium salt anion significantly influences both the oxidative stability and the preferred decomposition pathways

✧ ✧ ✧ ✧ ✧

Introduction

The interfaces between electrodes and the bulk electrolyte in secondary lithium batteries are complex. Often in direct contact with the anode is the solid electrolyte interphase (SEI) comprised of species formed primarily by the electrochemical decomposition of the electrolyte, salt, and additives. The SEI layer in turn is in contact with the electrolyte (solvent + salt) whose structure and dynamics are likely strongly perturbed by the presence of the interfaces. Electrode/electrolyte interfaces influence cell performance in numerous ways. For example, the SEI layer, particularly at the anode but perhaps also at the cathode, stabilizes the electrode against solvent intercalation/dissolution and stabilizes the electrolyte against electrochemical decomposition but can result in high interfacial transport resistance, particularly at lower temperatures. Formation of SEI layers with good transport

properties, good mechanical properties and electrochemical stability is of paramount importance. Particularly challenging is development of electrolytes and/or additives that allow use of high voltage cathode materials.

Approach

Our approach to simulation of bulk electrolytes, SEI layers, and electrode/electrolyte interfaces is multi-fold. First, we carry out high-level quantum-chemistry (DFT and correlated methods) to study the structure of electrode materials, their surfaces, interactions between electrodes and electrolytes (including reactions), and the interaction between electrolyte components. Second, where possible and appropriate, we utilize quantum-chemistry based force fields and non-reactive simulation methods. These studies include bulk electrolytes, model SEI layers and electrode/electrolyte interfaces. Third, we utilize an electroactive interface model to study electrolyte structure and charge transfer processes at electrode/electrolyte interfaces where control of electrode potential is paramount. Finally, we utilized atomistic MD simulations with ReaxFF, a reactive force field developed by Adri van Duin at Penn State and William Goddard at Caltech. This simulation method combines accuracy in modeling reaction energies and barriers with the capability to simulate systems large enough and over sufficiently long time to capture the diffusive properties of molecules necessary to adequately capture important chemical and structural reorganization during SEI formation. The ReaxFF is an empirical potential that is parameterized to reproduce results from quantum chemistry calculations.

Results

Quantum chemistry studies of the influence of anion (PF_6^-) on the solvent oxidative stability and oxidative decomposition pathways were performed in collaboration with the Army Research Laboratory. Oxidative stability of PC/PF_6^- complex was found to be reduced compared to the intrinsic oxidative stability of PC solvent due to the formation of HF upon oxidation of PC/PF_6^-. Importantly, the presence of the PF_6^- anion also altered the PC oxidative decomposition pathways.

In collaboration with van Duin (Penn State), the reactive molecular dynamics simulation methods utilizing ReaxFF has been extended to accurately treat both oxidation and reduction at electrode interfaces. This effort required modification of the ReaxFF code to allow for control of electrode charge. The new ReaxFF code (q-ReaxFF) will handle inert (carbon, metal) electrodes and active (graphite, $LiNi_{0.5}Mn_{1.5}O_4$) electrode materials.

For the purpose of parameterizing both reactive (ReaxFF) and non-reactive (Lucretius) molecular dynamics simulation models for metal and $LiNi_{0.5}Mn_{1.5}O_4$ electrodes we have carried out DFT studies of bulk crystal and surfaces utilizing the Vienna *ab-initio* simulation package (VASP). These calculations have allowed us to determine interactions between metal substrates and electrode materials and will allow us to parameterize partial charges, polarizabilities, dispersion/repulsion interactions and reactivity with $LiNi_{0.5}Mn_{1.5}O_4$. We have calculated basic properties (including energies, internal stresses, and unit cell geometries) for components of the $LiNi_{0.5}Mn_{1.5}O_4$ high voltage spinel as well as for the spinel directly in order to aid parameterization of the forcefield (ReaxFF) for reactive molecular dynamics simulations of the high voltage spinel. We have also investigated β-MnO_2 (pyrolusite) under a number of compression conditions ranging between 50 and 120 percent of the original volume. For investigations of the $LiNi_{0.5}Mn_{1.5}O_4$ spinel, we have begun by reproducing published results for the bulk spinel, including the predicted average voltage of the cell of approximately 4.7 V. The relaxed geometries and energies which will serve, in conjunction with the MnO_2 data, for parameterization of ReaxFF for the spinel. We have also utilized DFT to identify the lowest energy surfaces of $LiNi_{0.5}Mn_{1.5}O_4$.

Our reactive MD simulations have demonstrated that various alkyl carbonates are formed in the outer SEI layer at the anode due to single electron reduction. To improve our understanding of Li^+ transport through the electrolyte/SEI interface and through the SEI itself extensive simulations of model SEIs comprised of dilithium alkylcarbonates (ethylene and butylene) have been initiated using a new polarizable force field. The force field has been re-parameterized against higher-level quantum chemistry calculations and fit to accurately reproduce conformational properties of alkylcarbonates, electrostatic field around these molecules in vacuum, and molecular dipole moments.

Conclusions and Future Directions

We hope to continue investigating low energy surfaces of $LiNi_{0.5}Mn_{1.5}O_4$ by including oxygen in a non-stoichiometric ratio as necessary to cap unterminated transition metal bonds, or direct calculation of the reaction of elemental oxygen with the ideal surfaces to determine whether or not oxygen termination of the exposed surface plays an important role. These studies will be extended to include reactions with electrolyte components, including candidates for high-voltage electrolytes and additives for formation of stable cathode SEI layers. Oxidative decomposition pathways for these materials will also be determined. ReaxFF simulations of oxidation/reduction of electrolytes as a function of electrode potential will also be carried out, allowing us to see initial reactions and ultimately formation of SEI layers.

FY 2011 Publications/Presentations

1. 2011 DOE Annual Peer Review Meeting Presentation.
2. O. Borodin, J. Vatamanu, G. Smith "Molecular Insight into Ionic Liquid Behavior in Double Layer Capacitors and in Electrolytes for Lithium Batteries" 4th Congress on Ionic Liquids (COIL-4), June 15-18, 2011, Crystal City Hilton, Arlington, Virginia (http://coil-4.org/invited-speakers/)
3. O. Borodin, "Modeling of Liquid and Ionic Liquid Electrolytes for Energy Storage Applications" 10X Advanced Battery R&D, Future Storage Platforms, January 10-12, 2010 at Techmart in Santa Clara, CA
4. Lidan Xing, Jenel Vatamanu, Oleg Borodin, Grant D Smith "Understanding Electrolyte Stability from DFT Calculations and Double Layer Structure from MD Simulations" 4th Symposium on Energy Storage: Beyond Lithium Ion, Pacific Northwest National Laboratory, June 7-9, 2011 (poster)
5. Dmitry Bedrov, Grant D. Smith and Adri van Duin, "Molecular dynamics simulations using ReaxFF: Mechanisms of outer SEI formation via single electron reduction of ethylene carbonate (EC)", American Chemical Society, Denver, CO, August 27-September 1, 2011.
6. Grant D. Smith and Oleg Borodin, "Ionic Liquid Electrolytes for Lithium Ion Batteries: Insights from Molecular Dynamics Simulations", American Chemical Society, Denver, CO, August 27-September 1, 2011.
7. Grant D. Smith and Oleg Borodin, "Ionic Liquid Electrolytes for Lithium Ion Batteries: Insights from Molecular Dynamics Simulations", General Motors Central Research, Warren, MI, August 10, 2011.
8. Grant D. Smith and Oleg Borodin, "Polymer Electrolytes for Lithium Ion Batteries: Insights from Molecuar Dynamics Simulations", American Chemical Society, Anaheim, CA, March 27 – 31, 2011.
9. Dangxin Wu, Grant D. Smith and Dmitry Bedrov, "Simulations of Lithium Ion Batteries: Electrolytes, Electrodes and Interfaces", NAATBatt, Louisville, KY, September 7-8, 2011.
10. Grant D. Smith and Oleg Borodin, "Polymer Electrolytes for Lithium Ion Batteries: Insights from Molecuar Dynamics Simulations", IBM Almaden Research Center, San Jose, CA, October 10, 2011.
11. Grant D. Smith, Dmitry Bedrov and Adri van Duin, "Molecular dynamics simulations using ReaxFF: Mechanisms of outer SEI formation via single electron reduction of ethylene carbonate (EC)", Electrochemical Society, Boston, MA, October 9-14, 2011.
12. Lidan Xing, Jenel Vatamanu, Oleg Borodin, Grant D Smith "Understanding Electrolyte Stability from DFT Calculations and Double Layer Structure from MD Simulations", Electrochemical Society, Boston, MA, October 9-14, 2011.
13. Xing, L.; Borodin, O.; Smith, G. D.; Li, W. "A Density Function Theory Study of the Role of Anions on the Oxidative Decomposition Reaction of Propylene Carbonate" J. Phys. Chem. A (published on the web)
14. Vatamanu, J.; Cao, L.; Borodin, O.; Bedrov, D.; Smith, G. D."On the Influence of Surface Topography on the Electric Double Layer Structure and Differential Capacitance of Graphite/ionic Liquid Interfaces" J. Phys. Chem. Lett. 2011, 2, 2267-2272.
15. Vatamanu, J.; Borodin, O.; Smith, G.D. "Molecular Dynamics Simulation Studies of the Structure of a Mixed Carbonate/$LiPF_6$ Electrolyte as a Function of Electrode Potential", J. Phys. Chem. C, submitted
16. Bedrov, D.; Smith, G.D.; van Duin, A.C.T.; Reactions of Singly-Reduced Ethylene Carbonate in Lithium Battery Electrolytes. A Molecular Dynamics Simulation Study", J. Phys. Chem. A, submitted

V.D.4 Bi-functional Electrolytes for Lithium-ion Batteries (CWRU)

Daniel Scherson and John Protasiewicz
Case Western Reserve University
Department of Chemistry
Cleveland, OH 44106
Phone: (216) 368-5186
E-mail: dxs16@po.cwru.edu

Start Date: October 1, 2009
Projected End Date: September 30, 2013

Objectives

- Design, synthesize, and characterize the physical and electrochemical properties of functionalized Li salt anions containing phosphorous and boron moieties, Such chemical functionalities are known to impart materials with flame retardant properties (Flame Retardant Ions or FRIons) and as such are expected to improve device safety.
- Gain insight into the overall chemical and electrochemical behavior of these novel bifunctional electrolytes toward charged Li and Li-ion anodes using a combination of electrochemical and *in situ* spectroscopic techniques.
- Develop structure-function relationships that will guide further search of optimized FRIons and other species that contribute to enhanced abuse tolerance.

Technical Barriers

This project addresses the abuse tolerance barriers from the BATT program.

Technical Targets

- Demonstrate superior abuse characteristics compared to a baseline cell: Conoco Philips CPG-8 Graphite/1 M $LiPF_6$+EC:DEC (1:2)/Toda High-energy layered (NMC)

Accomplishments

- Two new classes of FRIons were developed and certain aspects of their flammability characteristics examined with state of the art combustion methods.
- The second generation of FRIons revealed a substantial increase in the cycling performance of 2032 coin cells when incorporated as additives to conventional solvent formulations.
- The cell initially designed to perform *in situ* ATR-FTIR measurements was successfully modified to allow spectra to be recorded in the external reflection mode (IRAS).

Introduction

The main objectives of this project are to develop rational guidelines for the design and synthesis of new classes of Li-based salts endowed with flame retardant properties. In addition, such *bifunctional electrolytes* should be weakly coordinating and of low molecular weight, exhibit low toxicity, promote formation of low impedance solid electrolyte interfaces (SEI) and from an economic viewpoint be relatively inexpensive.

Approach

The tactic being implemented in our research group seeks to impart lithium ion batteries with enhanced safety features by incorporating flame retardant and overcharge protection chemical groups to anionic species that display good transport properties and optimum SEI properties. These new materials are expected to either substitute for currently used electrolyte salts or be introduced as additives in conventional formulations. Systematic studies of compounds of this type will provide guidelines for the search of materials displaying optimized characteristics. Also to be thoroughly investigated is the structure of the SEIs formed in these new media via a combination of electrochemical and *in situ* ATR-FTIR and *in situ* external reflection FTIR (IRAS). To this end a cell was optimally designed to avoid problems associated with impurities was constructed with an interchangeable window, either diamond for ATR or CaF_2 for IRAS.

Results

Synthesis. In the previous annual report we introduced two new FRIons, LiBOBPHO-Ph and LiBOBPHO-Ar. These compounds were synthesized by the dehydration of boric acid in the presence of oxalic acid, lithium hydroxide and the corresponding di-substituted phosphinic acid (Figure V - 144). Unfortunately, we experienced severe problems with isolation of these materials, forcing us to shift attention momentarily toward the synthesis of two completely new classes of FRions.

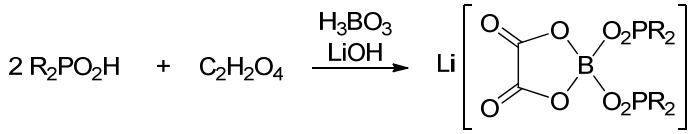

Figure V - 144: Synthesis of LiBOBPHO-R (R = Ph, 2-MePh).

The first class, lithium cyclic triol borates (CTB), was readily synthesized by a dehydration reaction between an organic triol, a substituted boronic acid, and lithium hydroxide (Figure V - 145). An interesting class of compounds was prepared by replacing the substituted boronic acid with boric acid, resulting in R' = OH. This strategy may afford a very promising avenue toward the synthesis of more advanced materials.

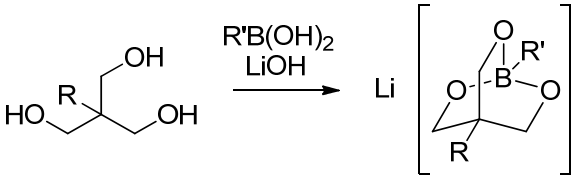

Figure V - 145: Synthesis of lithium CTB (R = Me, Et; R' = Ph, 4-MePh, 4-MeOPh, Me, Bu, Cy, OH).

The second class of compounds we prepared was based on a tris(hydroxymethyl)phosphine oxide, a phosphorus analog to the organic triols (Figure V - 146).

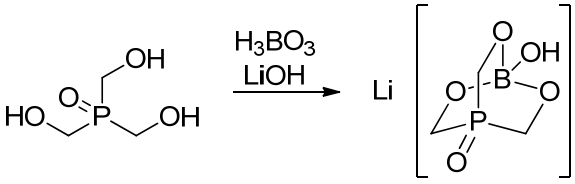

Figure V - 146: Synthesis of lithium CBPO

Characterization of these materials (Figure V - 147) using pyrolysis combustion flow calorimetry (PCFC), was performed by our collaborator, Dr. Alexander Morgan at the University of Dayton Research Institute. This specific technique monitors the instantaneous heat of combustion by oxygen consumption calorimetry. The first generation of FRIons displayed an increased delay time to ignition than the control, lithium *bis*(oxalatoborate), LiBOB, as well as significant char yield (Table V - 3), whereas the lithium cyclic triol borates displayed an increase in char yield as well as a slight decrease in the total heat released.

Table V - 3: Heat Release Data

Compound	Generation	Char Yield (%)	Total HR[a] (kJ/g)
LiBOB		19(5)	3.0(0.1)
LiBOBPHO-Ph	1st	23.6(0.4)	20.5(0.5)
LiBOBPHO-Ar		20.1(0.6)	24.7(0.2)
$LiC_{Me}B_{Me}$	2nd	34(11)	18.1(0.2)
$LiC_{me}B_{Ph}$		31(1)	21.1(0.2)
$LiC_{Et}B_{Ph}$		32(1)	19.6(0.4)

Values in parentheses represent standard deviation

[a]HR: total heat released.

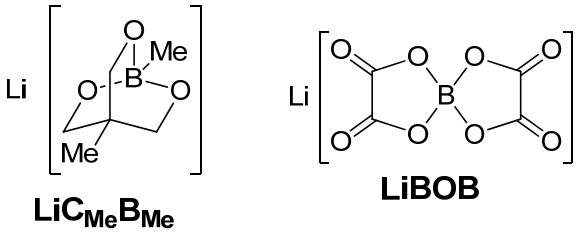

$LiC_{Me}B_{Me}$

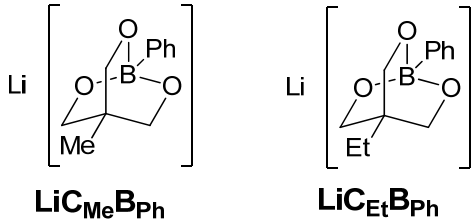

$LiC_{Me}B_{Ph}$ **$LiC_{Et}B_{Ph}$**

Figure V - 147: Molecular structure of the compounds in Table V - 3.

Thermogravimetric analysis of the first generation of FRIons displayed a first thermal event at a temperature lower than that observed for LiBOB (see Figure V - 148); however, this event was caused by desolvation of the FRIons, not decomposition which occurred around 290°C for both FRIons. These results were confirmed by TGA-MS measurements performed by our collaborator, Dr. Robert Latimer at the Lubrizol Corporation. Analysis of these specific measurements revealed several plausible m/z fragments for LiBOBPHO-Ph and LiBOB. The second generation of FRIONs underwent decomposition between 218-230°C, displaying similar stability to the first generation with little regard to the obvious structural differences.

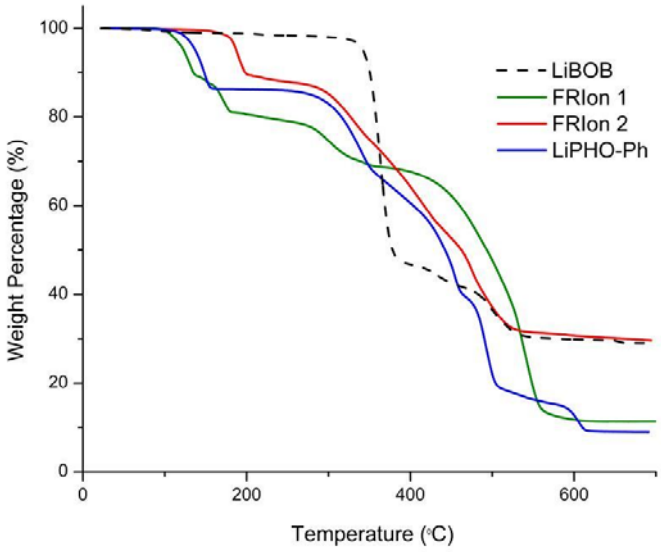

Figure V - 148: TGA of the first generation FRIons.

To demonstrate the feasibility of the FRIons acting as a bifunctional electrolyte, our collaborators at Novolyte Technologies incorporated two of our salts, as additives a the 2% level, into 2325 coin cells with a graphite anode and a $LiCoO_2$ cathode. The cell was cycled at 1 mA between 4.2 and 2.5 V in 1M $LiPF_6$ in EC/EMC (3:7 by vol) + 1.5% VC (Figure V - 149). As indicated, $LiC_{Me}B_{Ph}$ displayed improved performance over the baseline for long term cycling.

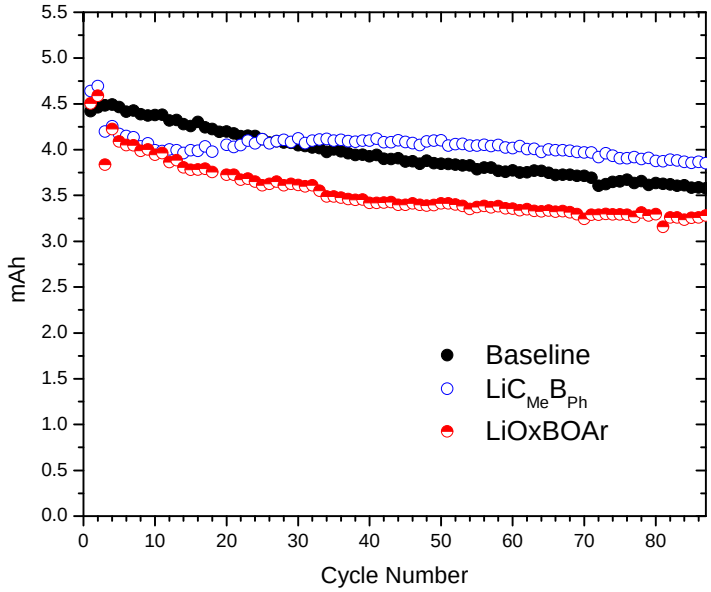

Figure V - 149: Capacity versus cycle number for the specified electrolyte formulations.

Spectroscopic Studies.

External reflection FTIR. The ATR-FTIR cell was modified to perform measurements in the external reflection mode (IRAS) using a CaF_2 window and p-polarized light to enhance surface spectral contributions. IRAS data were collected in 1M $LiPF_6$ in EC/EMC (3:7 by vol) with the Ni electrode pressed against the window while scanning the potential from the open circuit value (OCP ca. 2.2 V) down to 0.05 V vs Li/Li^+. Representative results are shown in Fig. 4 as $\Delta R/R = (R_{OCP} - R_{samp})/R_{OCP}$, where R is the single beam spectrum and *samp* refers to the potential at which the specific spectrum was recorded. The arrows in Figure V - 150 point to the peaks associated with solvated PF_6^- the intensity of which decreases for decreasing potentials due to migration in and out of the trapped electrolyte

layer, an effect resulting from the adsorption/reaction of underpotential deposited Li.

Conclusions and Future Direcitons

Three generations of FRIons have been designed and synthesized, of which the most promising has been the second generation. However, it is important to note that the third generation has only recently been isolated in substantial amount for further analysis. One of the most interesting goals will be to determine any structure-function relationships the series of compounds display as well as optimizing battery cell conditions. Furthermore, the positive results from preliminary coin cell testing will be repeated in prismatic cells to verify the observed behavior. Most importantly, we need to continue efforts to create materials with enhanced solubility properties. Specifically, we are preparing materials having solubilizing groups (such as longer chain alkyls or alkyloxy groups). Our efforts to systematically vary R groups on these materials will also aid in this search for compounds with enhanced solubility. In conjunction with these efforts, we are also investigating new methods for the synthesis of these materials that yield larger amounts of products (methods such as solid state reactions).

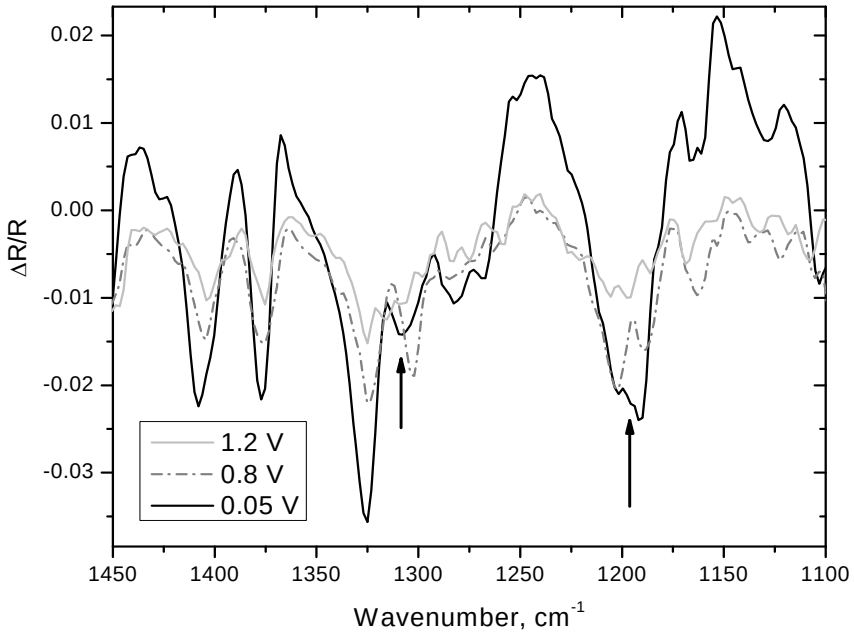

Figure V - 150: In situ ΔR/R vs wavenumber for various sampling potentials, samp, as specified. See text for details

The newly constructed cell for *in situ* external reflection-FTIR (IRAS) measurements will be extensively used to characterize SEI layers in various electrolytes incorporating FRIons synthesized under this program.

FY 2011 Publications/Presentations

Publications

1. Shaffer, A. R., Deligonul, N., Scherson, D. A., and Protasiewicz. J. D. **A Hybrid Lithium Oxalate-Phosphinate Salt**. *Inorg. Chem.* **(2010)** *49*, 10756-10758

Presentations

1. FRIONs: Flame Retardant Ions for Safer Lithium Ion Batteries, 241st ACS National Meeting, Anaheim CA.
2. Hybrid Lithium Oxalate-Phosphinate Salts, 2011 Meeting in Miniature, Pepper Pike, OH.
3. A Hybrid Lithium Oxalate-Phosphinate Salt, 219th ECS Meeting, Montreal, QC.

V.D.5 Advanced Electrolyte and Electrolyte Additives (ANL)

Khalil Amine (Project Manager)
Argonne National Laboratory
Chemical Sciences and Engineering Division
Argonne, IL 60439
Phone: (630) 252-3838; Fax: (630) 252-4672
E-mail: amine@anl.gov

Start Date: Jan 1, 2010
Projected End Date: Dec. 30, 2014

Objectives

- Use our advanced quantum chemical model to predict functional additives that form stable Solid Electrolyte Interphases (SEI) on electrodes and for overcharge protection.
- Use the model to predict how additives interact with the surface of anode and cathode to form good protective films.
- Synthesize suitable additives predicted by the modeling, characterize them and carry out extensive cycle and calendar life test.

Technical Barriers

This project addresses the following technical barriers in lithium ion battery technology

(a) Cycle/calendar life

(b) Abuse tolerance

Technical Targets

- New additives that form stable film formation on anodes and cathodes
- Increased cycle life
- Improved safety

Accomplishments

- We have used our improved quantum chemical model for screening of reduction and oxidation potentials of over 300 additive molecules and shuttle molecules.
- Further screening has identified about 75 candidates with favorable reaction pathways for decomposition including oxalates, carbonates, anhydrides., and allyl substituted compounds.
- Tetrafluoro(oxalate) phosphate and lithium difluoro[oxalato] borate were found to be effective electrolyte additives to significantly improve both the life and safety of Li-ion batteries. Density functional calculations have shown how the fluorine groups promote a good SEI layer.
- A computational study of the reaction pathways involving one and two-electron transfer for decomposition of ethylene carbonate has provided evidence for possible products important in forming an effective SEI.
- Among promising additive candidates predicted by density functional theory is 1,3,5-triallyl-[1,3,5]triazinane-2,4,6-trione (TTT). This has been found to be effective as an SEI additive in experimental testing.

Introduction

The development of advanced electrolytes with functional additives that provide for stabilization of the interface of lithium ion batteries to prevent detrimental decomposition is important for enhancing the cycle life and safety of lithium ion batteries. In addition, electrolyte additives can provide protection against overcharge. We are using high level quantum chemical methods to screen for electrolyte additives that can be added to the electrolyte and form a protective SEI during the initial charging to prevent any conventional passivation film from taking place first. These additives must form a thin and a uniform film that protects the electrode. We are also investigating new additives for overcharge protection.

Approach

We are using a joint theoretical/experimental approach for design and discovery of new electrolytic additives that react in a preferential manner to prevent detrimental decomposition of cell components. We use quantum chemical screening to predict oxidation and reduction potentials and decomposition pathways that form desirable coatings and to find stable additives for overcharge protection. Synthesis of the new additives and testing of them is done to determine the cycle life of the batteries. Investigation of the SEI is done to determine structure and formation with both experiment and theory.

Results

Screening of electrolyte additives. Over 300 candidate additives have been screened for their reduction

and oxidation potentials using our quantum chemical model. In addition, the candidates are further down selected on the basis of reaction pathways for decomposition. These calculations are being used to suggest additives for protective film formation on anodes and cathodes as well as for redox shuttles for overcharge protection.

Lithium tetrafluoro(oxalate) phosphate additive. Among the promising candidates based on reduction potential screening are lithium tetrafluoro(oxalate) phosphate (LTFOP) and lithium tris(oxalato) phosphate (LTOP). These two compounds were investigated as additives for MCMB/$Li_{1.1}[Ni1_{/3}Co_{1/3}Mn_{1/3}]_{0.9}O_2$ (NCM) cells. The reduction potentials were determined by charging a Li/MCMB half cell. Reduction peaks shown in Figure V - 151 at 1.7V and 2.1V are observed for LiTFOP and LTOP, respectively, indicating a new SEI formation prior to EC decomposition. The measured reduction peaks are in good agreement with those predicted from our quantum chemical model of 1.52 and 1.88 eV, for LTFOP and LTOP, respectively. Based on cell testing including cycling performance and impedance measurements, the LTFOP additive is found to perform significantly better than LTOP. Our density functional calculations suggest that the presence of the fluorines promotes 2-dimensional SEI film growth as opposed to 3-dimensional structures for LiTOP as an additive.

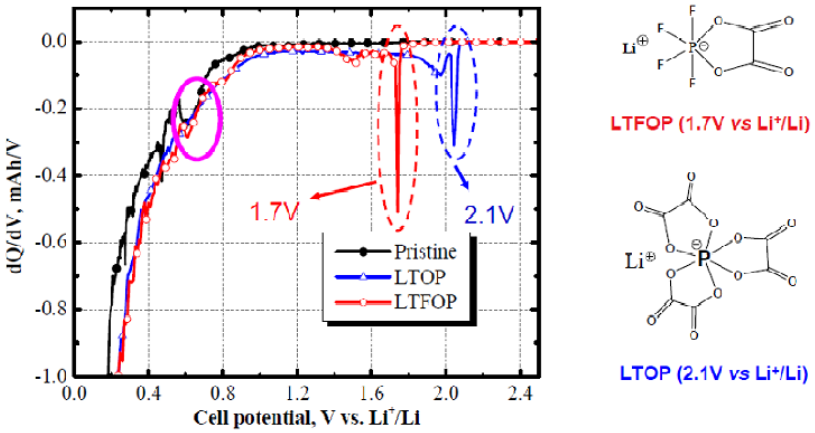

Figure V - 151: Differential capacity profiles of Li/MCMB with 1.2M $LiPF_6$ EC/EMC 3/7+2% additive.

Reaction pathways for ethylene carbonate decomposition. A computational study of the reaction pathways involving one and two-electron transfer for decomposition of ethylene carbonate upon reduction has been carried out to provide evidence for possible products that may be important in forming an effective SEI needed for good performance of Li ion batteries. Understanding the electrolyte reaction mechanisms for SEI components is necessary for our screening of new electrolyte additives. In addition, the knowledge will be used in development of potentials for simulations of the growth of the SEI layer by our collaborator, Grant Smith of the University of Utah

We carried out a density functional study of the different possible reaction mechanisms that will result in the two alkyl carbonates mentioned above. In this study we have considered the effect of spin curve crossing in the reaction pathways for the first time because of the possibility of radical reactions. Consideration of this effect is necessary to obtain accurate information on the pathways. Five distinct pathways were investigated. Of these five reactions, the only viable path to lithium ethylene dicarbonate involves two electron reduction. The other pathways are found to be not favorable due to large activation barriers. These calculations provide a reaction pathway for formation of the lithium ethylene dicarbonate consistent with experimental observation.

1,3,5-triallyl-[1,3,5]triazinane-2,4,6-trione additive. We have used density functional theory to investigate 1,3,5-triallyl-[1,3,5]triazinane-2,4,6-trione (TTT) as an SEI additive. The results show that when this molecule is reduced, an allyl radical detaches as shown in Figure V - 152 without a barrier via an apparent charge-spin segregation mechanism. This allyl radical can react with other species in solution to form an SEI layer. The pores of this SEI layer are likely to be large enough to allow Li^+ transport.

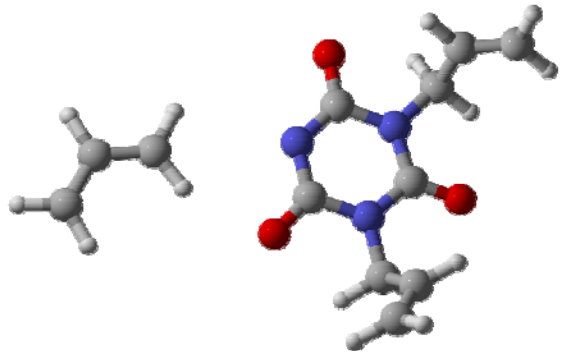

Figure V - 152: Illustration of the dissociation of the ally group from a 1,3,5-triallyl-[1,3,5]triazinane-2,4,6-trione molecule.

The 1,3,5-triallyl-[1,3,5]triazinane-2,4,6-trione was tested as an SEI additive for Li ion batteries. With 0.2 w% additive, the cell showed dramatic improvements in capacity retention as shown in Figure V - 153. X-ray photoelectron spectroscopy (XPS) was used to analyze the SEI. The XPS results confirm that the additive does decompose and participates in the SEI formation process on the anode surface as predicted by theory

Conclusions and Future Directions

Stabilization of the interfaces of lithium ion batteries is needed to prevent detrimental decomposition of the electrodes. We have screened over 300 candidate materials for reduction potentials and selected decomposition pathways. The results of these calculations have been used to help find new additives described in this report and to understand the mechanism by which the protective film is formed. We will continue to screen further candidates based on experimental feedback. In future work we will also be using density functional calculations to help understand the properties of shuttle molecules for overcharge protection that are being studied experimentally and the using this information to help design new shuttle molecules.

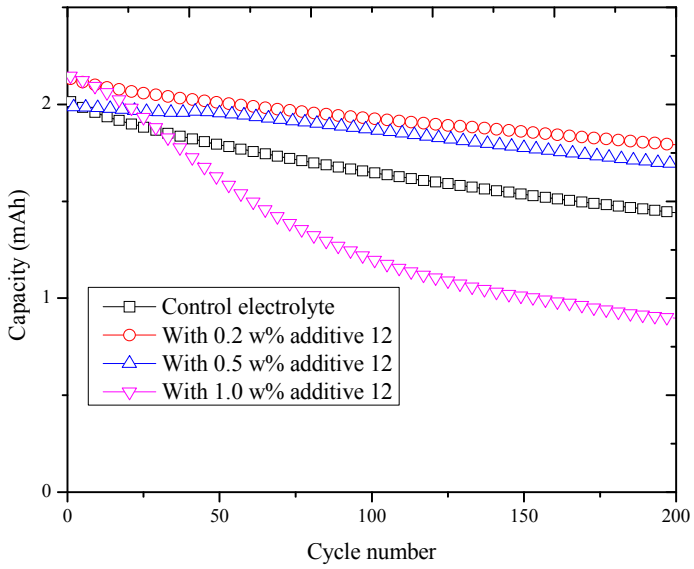

Figure V - 153: Capacity retention of MCMB/NCM cells cycled between 3 and 4.0V at 55 ◦C in electrolyte of 1.2M $LiPF_6$ EC/EMC 3/7 with no and various amount of the TTT additive.

Publications/Presentations

1. Y. Qin, Z. Chen, J. Liu and K. Amine, Lithium Tetrafluoro Oxalato Phosphate as Electrolyte Additive for Lithium-Ion Cells, *Electrochem. Solid-State Lett.*, 13(2) A11-A14, (2010)
2. Patent: ANL-IN-10-039 "Non-aqueous electrolyte for lithium-ion batteries"
3. Y. K. Sun, Z. Chen, Z. Zhang, P. Redfern, L. A. Curtiss, K. Amine, "Mechanism and Mitigation of Capacity Fade of Li1.1[Mn1/3Ni1/3Co1/3]0.9O2 Based Lithium-Ion Batteries,", Journal of Materials Chemistry, **21**, 17754, (2011)
4. G. Ferguson, P. Redfern, L. Cheng, D. Bedrov, G. Smith and L. A. Curtiss, "A Theoretical Study of the Reaction of Reduced Ethylene Carbonates in Lithium-Ion Batteries", to be submitted.
5. 2011 DOE Annual Peer Review Meeting Presentation

.

V.D.6 Inexpensive, Nonfluorinated (or Partially Fluorinated) Anions for Lithium Salts and Ionic Liquids for Lithium Battery Electrolytes (NCSU)

Wesley Henderson

North Carolina State University
Ionic Liquids & Electrolytes for Energy Technologies (ILEET) Laboratory
Department of Chemical & Biomolecular Engineering
911 Partners Way, Campus Box 7905
Raleigh, NC 27695
Phone: (919) 513-2917; Fax: (919) 515-3465
E-mail: wesley_henderson@ncsu.edu

Collaborators: Michel Armand, Peter Fedkiw (co-PIs)

Start Date: April 1, 2009
Projected End Date: March 31, 2012

Objectives

- Develop new anions as replacements for PF_6^- or as additives for electrolytes
- Establish characterization methods for electrolyte solvent-lithium salt and ionic liquid-lithium salt mixtures to aid in understanding structure-property relationships and optimization of cell performance

Technical Barriers

This project addresses the following technical barriers from the VT Research & Development plan regarding electrolytes:

- Improved cell performance, calendar life and abuse tolerance
- Improved low temperature performance
- Reduced cost

Technical Targets

- Obtain electrolyte salt materials that can operate in the potential range (4-5 V vs. Li/Li^+) enabling the use of high-voltage cathode materials
- Develop electrolyte materials which enable cell operation in the temperature range -30 to 55°C or higher
- Improve cycle life and safety

Accomplishments

- Synthesized several new anions and dianions which contain nitrile functional groups and/or are partially fluorinated
- Characterized the phase behavior LiFSI mixtures with nitrile solvents
- Characterized the phase behavior and solvate structures of LiDFOB mixtures with nitrile and dinitrile solvents
- Ionic liquids (ILs) have been synthesized with the $DFOB^-$ anion—these are found to effectively inhibit the corrosion of the Al current collector
- Concentrated IL-LiTFSI-solvent electrolytes with high lithium salt and low solvent content have been demonstrated to have excellent electrolyte properties

✧ ✧ ✧ ✧ ✧

Introduction

Electrolyte materials are a key component in terms of both the cost and performance (power, safety, lifetime) of a battery. The properties of salts (either lithium salts or ionic liquids) containing new anions are being explored to determine their utility for lithium battery applications.

Approach

To explore new anions for alternative salts to $LiPF_6$, ionic liquids and electrolyte additives, two classes of nonfluorinated (or partially fluorinated) anions were synthesized and characterized: 1) chelated and non-chelated organoborate anions (related to bis(oxalate) borate or BOB^-), and 2) Hückle-type anions in which the charge is stabilized on a 5-member azole ring and noncyclic cyanocarbanions. The physical properties of these new anions, incorporated in both lithium salts and ionic liquids, are being examined including the thermal phase behavior (phase diagrams); thermal, chemical and electrochemical stability; transport properties; interfacial properties; molecular interactions and cell performance. These salts will be compared with current salts of interest such as $LiBF_4$, $LiPF_6$ and LiBOB and ionic liquids based upon the bis(trifluoromethanesulfonyl)imide anion.

Results

Anion Synthesis. Several new anions have been synthesized. Examples of these are shown in Figure V - 154. Synthesis procedures are now being optimized for scaled-up production of the salts. The DCP^- and TCP^{2-} anions are initially prepared as potassium salts. Ion-exchange and purification of the resulting lithium salts to electrochemical-grade materials is now underway. The anions containing nitrile groups are found to polymerize during thermal degradation (Figure V - 155)—a feature which may provide a shut-down mechanism for a battery during thermal abuse. Unfortunately, the TCP^{2-} salts have been found to have very poor solubility in aprotic solvents. Crystal structures for pure LiETAC (Figure V - 156) and a $(THF)_1$:LiETAC solvate have been determined to gain insight into how this anion coordinates Li^+ cations. The electrochemical properties of the salts in aprotic solvent mixtures are currently being determined.

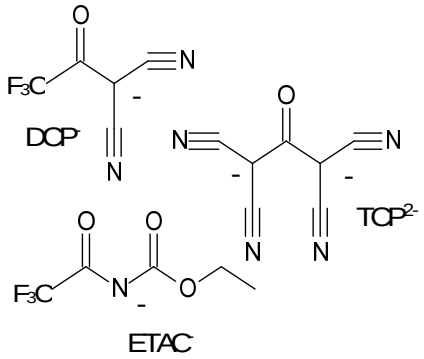

Figure V - 154: Examples of anions synthesized.

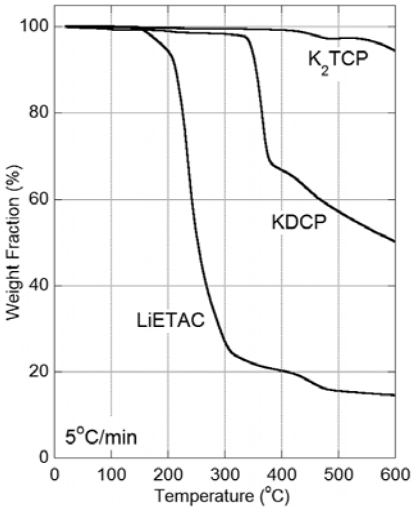

Figure V - 155: TGA heating traces of the salts.

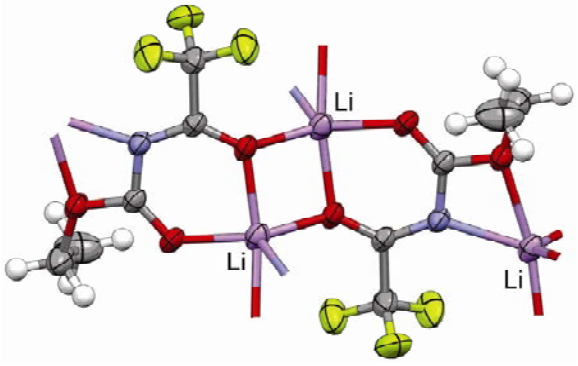

Figure V - 156: Ion coordination in the crystal structure of LiETAC (Li-purple, O-red, N-blue, F-green).

Characterization of Solvent-LiFSI Mixtures. Lithium bis(fluorosulfonyl)imide is a promising salt for electrolyte applications due to the very high conductivity of LiFSI mixtures with aprotic solvents (comparable to $LiPF_6$). Little is known about this salt at present. Some work has been conducted to gain insight into why the FSI^- anion results in exceptional electrolyte properties. In addition, nitrile and dinitrile solvents may be of interest for electrolytes suitable for use with high-voltage (> 4.3 V) electrodes and/or low-temperature applications. A phase diagram for acetonitrile $(AN)_n$-LiFSI mixtures has therefore been prepared (Figure V - 157). Both 6/1 and 4/1 crystalline solvate phases form which melt at low temperature, in common with $(AN)_n$-LiTFSI mixtures. In contrast, $(AN)_n$-$LiPF_6$ mixtures form a high melting 5/1 phase which consists of Li^+ cations tetrahedrally coordinated to four AN molecules, one uncoordinated AN molecule and uncoordinated PF_6^- anions. Certain compositions of the $(AN)_n$-LiFSI mixtures, in fact, form crystallinity gaps in which the samples cannot be crystallized. The data suggests that binary solvent-LiFSI electrolytes may be of practical utility due to the low T_m of the solvates, whereas mixed solvents are generally required with $LiPF_6$ electrolytes due to the high T_m of the corresponding solvates.

Characterization of Solvent-BF_4 and LiDFOB (or BF_2Ox) Mixtures. Phase diagrams for $(AN)_n$-LiDFOB and adiponitrile $(ADN)_n$-LiDCTA mixtures have been prepared (Figure V - 158). Crystal structures for $(AN)_3$:LiDCTA, $(AN)_1$:LiDCTA and $(ADN)_1$:LiDCTA solvates have been determined (Figure V - 159 and Figure V - 160) to provide insight into the molecular interactions of these solvents with the Li^+ cations and $DCTA^-$ anions.

Ionic Liquid (IL) Synthesis. ILs with *N*-alkyl-*N*-methylpyrrolidinium cations and the difluoro(oxalato)-borate anion ($PY_{1R}DFOB$ where R is the alkyl chain length) have been synthesized and characterized. Despite utilizing various synthesis and purification procedures, the ILs always contain small amounts of BF_4^- and bis(oxalato)-borate (LiBOB) impurities. It is

believed that this is due to an equilibrium which exists between these three anions. Electrolytes consisting of EC/DMC or EC/EMC with either LiTFSI or LiFSI are found to readily corrode Al, whereas those with $LiPF_6$ or LiDFOB do not. In contrast, neither $PY_{14}TFSI$ nor $PY_{14}DFOB$ mixtures with LiTFSI corrode Al at high potentials. Negligible current is observed for the IL-based electrolytes and no pitting corrosion of the electrode surfaces is noted.

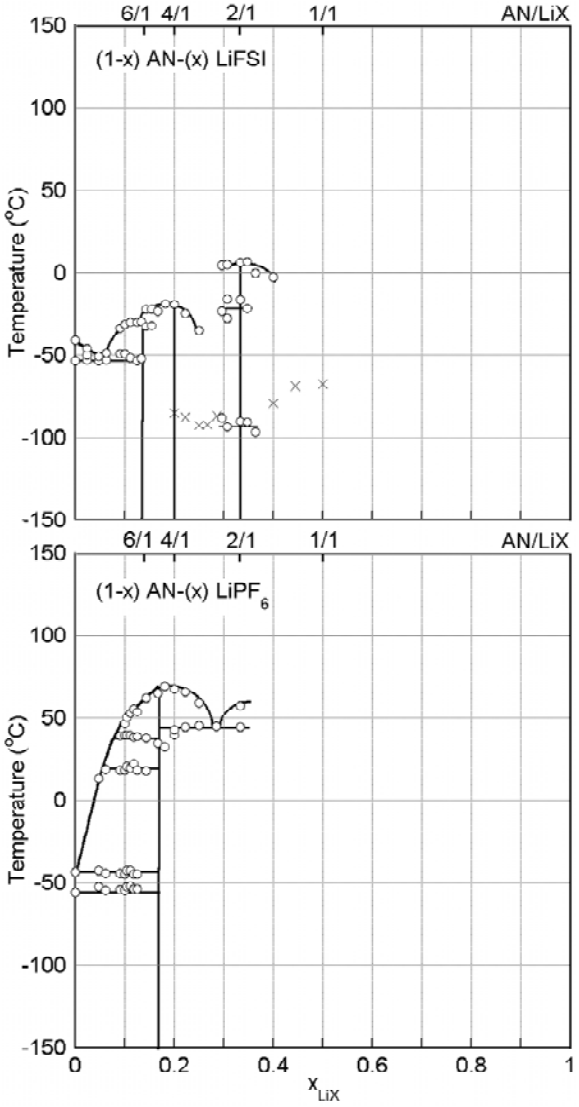

Figure V - 157: Phase diagrams for (AN)n-LiFSI and (AN)n-LiPF6 mixtures.

Concentrated IL-Based Electrolytes. Recent work has demonstrated that highly concentrated IL-LiTFSI-solvent mixtures in which 50 mol% of the salt is LiTFSI can be prepared with select amounts of solvent so that little or no bulk (uncoordinated) solvent is present in the electrolytes. These mixtures have very promising properties including low solvent volatility, low flammability, wide liquid temperature range, high conductivity, etc. These mixtures are now being tested as electrolytes with various electrode materials.

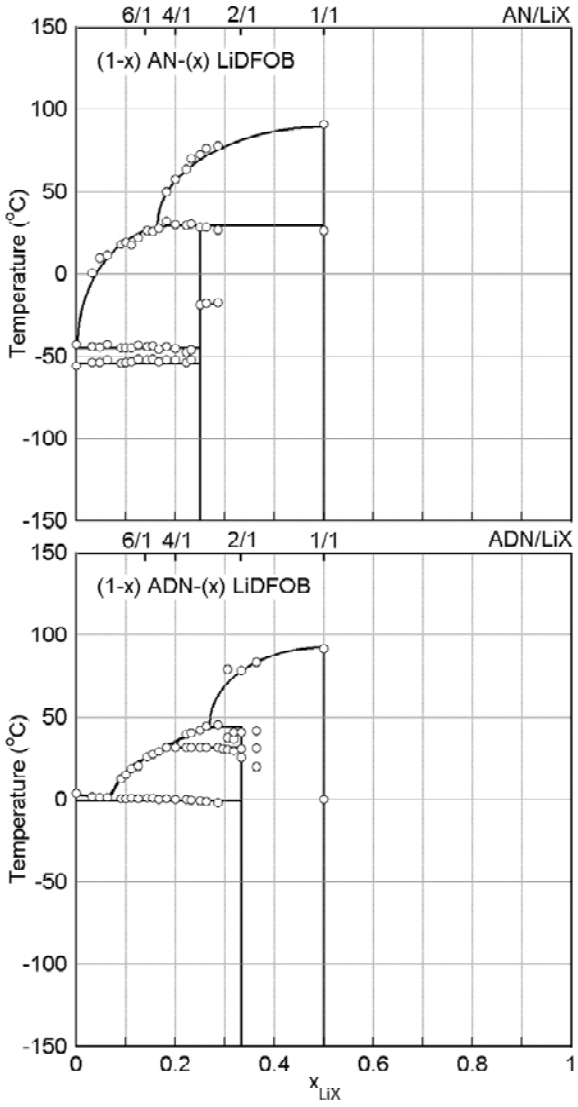

Figure V - 158: Phase diagrams for (AN)n-LiDFOB and (ADN)n-LiDFOB mixtures.

Conclusions and Future Directions

Several new anions have been synthesized and are now being characterized. Phase diagrams and solvate crystal structures have been used to gain insight into the differences in solvation interactions of different salts including LiFSI and LiDFOB. This information is being correlated with electrolyte properties to aid in understanding the link between salt structure-property relationships and how this influence cell performance.

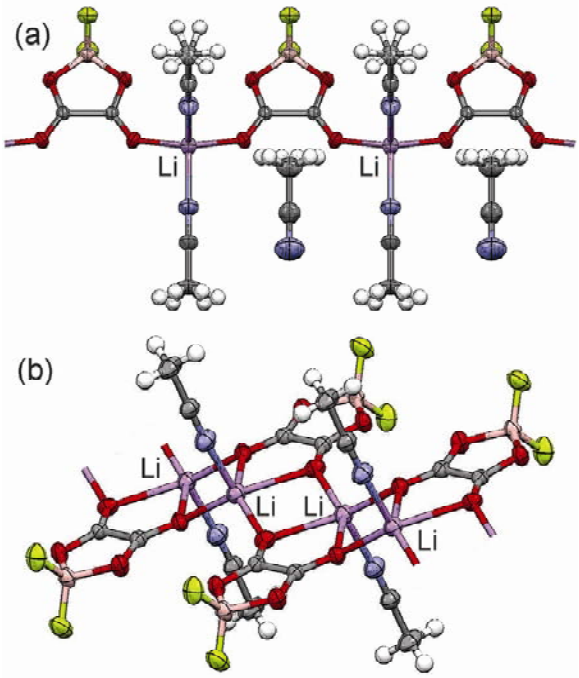

Figure V - 159: Ion coordination in the crystal structures of (AN)3:LiDFOB and (AN)1:LiDFOB (Li-purple, O-red, N-blue, B-tan, F-green).

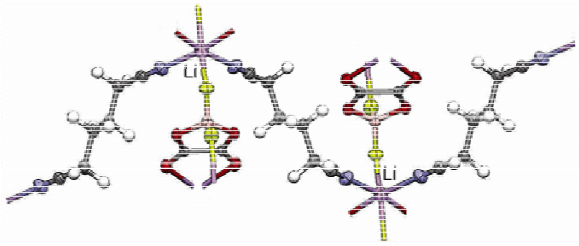

Figure V - 160: Ion coordination in the crystal structures of (ADN):LiDFOB (Li-purple, O-red, N-blue, B-tan, F-green).

FY 2011 Publications/Presentations

1. Allen. J. L.; Boyle, P. D.; Henderson, W. A. "Lithium difluoro(oxalato)borate tetramethylene sulfone disolvate" Acta Crystallogr. 2011, E67, m533.
2. Allen, J. L.; Boyle, P. D.; Henderson, W. A. "Poly[diacetonitrile[μ_3-difluoro-(oxalato)borato]-sodium" Acta Crystallogr. 2011, E67, m678.
3. Allen, J. L.; Han, S.-D.; Boyle, P. D.; Henderson, W. A. "Crystal structure and physical properties of lithium difluoro(oxalato)borate (LiDFOB or $LiBF_2Ox$)" J. Power Sources 2011, 196, 9737.
4. MIT, Boston, MA, Oct 14, 2011—Molecular Insight into the Electrolyte Heart that Beats Life into Lithium Batteries—Tuning Stability, Conductivity, Crystallization…and Other Vitals.
5. 5th International Conference on Polymer Batteries and Fuel Cells (ICPB-5), Argonne National Laboratory, Chicago, IL, Aug 1-5, 2011—Scrutinizing Liquid and Solid Polymer Electrolyte Solvation via Phase Diagrams and Crystalline Solvate Structures.
6. ACS/MARM-2011—New Technologies for Ion Lithium Batteries II, College Park, MD, May 23, 2011—Ionic Liquid-Based Electrolytes for Lithium Batteries: Linking Structure with Physical Properties
7. DOE Annual Merit Review & Evaluation Meeting—Hydrogen Program and Vehicle Technologies Program, Crystal City, VA, May 9-12, 2011—Inexpensive, Nonfluorinated (or Partially Fluorinated) Anions for Lithium Salts and Ionic Liquids for Lithium Battery Electrolytes.
8. Symposium on Scalable Energy Storage Beyond Li-Ion: Materials Perspectives, Oak Ridge National Laboratory, Oak Ridge, TN, Oct 7-8, 2010—Ionic Liquids, Lithium Salts, Solvents and Water: Phase Behavior and Molecular Interactions.

V.D.7 Development of Electrolytes for Lithium-ion Batteries (URI)

Brett L. Lucht (Project Manager)
University of Rhode Island
Department of Chemistry
51 Lower College Rd., Pastore
Phone: (401) 874-5071; Fax: (401) 874-5072
E-mail: blucht@chm.uri.edu

Start Date: April 1, 2009
Projected End Date: March 31, 2014

Objectives

- Investigate cathode film forming additives for high voltage (> 4.5 V) cathode materials.
- Investigate properties of $LiPF_4C_2O_4$/carbonate electrolytes at low temperature after accelerated aging.
- Investigate incorporation of electrolyte solid electrolyte interphase (SEI) forming additives for Si-based anodes.
- Investigate the surface of cathodes and anodes cycled with novel electrolytes, with or without additives, to develop a mechanistic understanding of interface formation and degradation.

Technical Barriers

This project addresses the following technical barriers from the Batteries for Advanced Transportation Technologies Research, Development Plan regarding electrolytes.

- Improve cell performance, life and cost
- Improve calendar Life
- Expand survival temperature range

Technical Targets

- Cell performance, life, cost: Calendar life: 40°C, 15 yrs
- Survival Temp Range: -46 to +66°C
- Unassisted Operating & Charging Temperature Range, -30 to + 52°C.

Accomplishments

- Development of cathode film forming additives that improve the performance of high voltage cathodes.
- Development of a thorough understanding of the source of poor first cycle efficiency for $LiPF_4(C_2O_4)$ electrolytes on graphite anodes.
- Investigation of the low temperature performance of $LiPF_4(C_2O_4)$/PC electrolytes after accelerated aging.
- Investigation of novel electrolytes additives to improve performance of Si-based anodes.

Introduction

While commercial lithium-ion batteries (LIBs) perform well for most home electronic applications, currently available LIB technology does not satisfy some of the performance goals for Plug-in Hybrid Electric Vehicles (PHEV). In particular, currently available LIB technology does not meet the 15 year calendar life requirement set by the United States Advanced Battery Consortium (USABC).

The most extensively used LIB electrolytes are composed of $LiPF_6$ dissolved in organic carbonates. However, $LiPF_6$ based electrolytes have poor thermal stability and performance when cycled to high voltage (> 4.5 V vs Li). Significant energy fading occurs after several years at room temperature and over only a few months at the moderately elevated survival temperature of 66°C required by the USABC. While there are several different factors that limit the thermal stability, calendar life and voltage window of LIBs, the reactions of the electrolyte with the surface of the electrode materials are frequently reported to be the most important.

Approach

Test cells were constructed with novel electrolyte formulations and *ex situ* analysis of the surfaces of cathodes and anodes was conducted to develop a mechanistic understanding of interface formation and degradation. Cathode film forming additives for high voltage (> 4.5 V) cathode materials were studied to improve cycling performance at high potential. An investigation of the properties of the thermally stable highly conductive salt, $LiPF_4C_2O_4$, in carbonate solvents was conducted to better understand the novel salt. The electrode surface films for cells cycled with $LiPF_4(C_2O_4)$ electrolyte were investigated to determine source of performance differences compared to $LiPF_6$. Incorporation of electrolyte SEI forming additives was studied to improve the performance of Si-based Alloy anodes.

Results

Development of Cathode Film Forming Additives. An investigation of the reactions of electrolyte with the surface of $LiNi_{0.5}Mn_{1.5}O_4$ cathode materials cycled to 4.9 V vs Li or stored at elevated temperature (55°C for two weeks) has been conducted to develop a better understanding of the sources of performance fade. In order to investigate the difference in electrolyte oxidation on $LiNi_{0.5}Mn_{1.5}O_4$ vs Pt, electrodes were stored at 4.75 and 5.30 V vs Li for several days. After subtraction of the current associated with lithium extraction from $LiNi_{0.5}Mn_{1.5}O_4$ the residual currents are very similar suggesting that the oxidation reactions are similar for $LiNi_{0.5}Mn_{1.5}O_4$ and Pt (Figure V - 161). Surface analysis suggests that the surface species on $LiNi_{0.5}Mn_{1.5}O_4$ and Pt are very similar. Thus, electrolyte oxidation reactions apper to be largely independent of the electrode structure. Elevated temperature storage experuiments suggest that the electrolyte reacts with the cathode surface and Mn dissolution is a problem for $LiPF_6$ electrolytes.

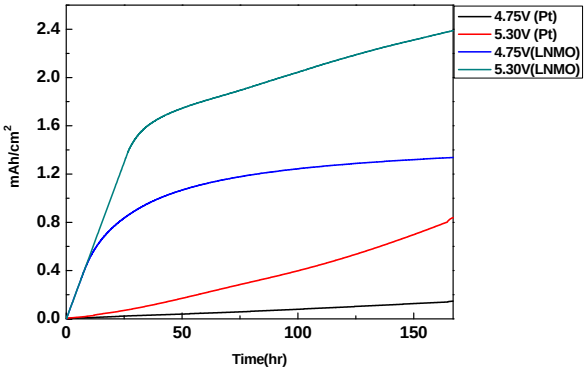

Figure V - 161: C/20 charging to 4.75 & 5.30V and hold at same V, $LNi_{0.5}Mn_{1.5}O_4$; Scan (5mV/S) and hold (4.75 & 5.30V) on Pt; $LiPF_6$/EC/EMC.

Investigations of cathode film forming additives with $LiNi_{0.5}Mn_{1.5}O_4$/Li cells cycled to 4.9 V vs Li have been conducted. The discharge capacities are provided in Figure V - 162. Cells containing baseline electrolyte showed higher discharge capacity after the first cycle but gradual capacity fade was observed after subsequent cycling. Cells containing LiBOB showed lower discharge capacity after the first cycle but capacity retention was improved in following cycles. Cells containing LiBOB retained 93% of the initial discharge capacity as compared to 71% capacity retention from baseline electrolyte cells. The cell efficiency was also improved from 95 % for the STD to above 99 % for cells containing 0.25 LiBOB (Figure V - 162). The electrochemical impedance of the cells indicate lower impedance for cells containing LiBOB than the cells containing baseline electrolyte. The increased capacity retention and efficiency suggest that the presence of LiBOB is decreasing the detrimental reactions of the electrolyte with $LiNi_{0.5}Mn_{1.5}O_4$ cathode materials while the smaller impedance suggests thinner surface films. Related investigations are also being conducted on novel Lewis basic additives to inhibit Mn leaching form the cathode and provide similar performance improvements.

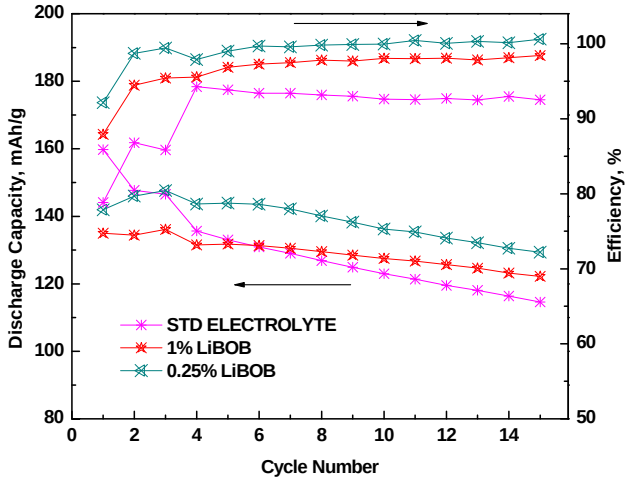

Figure V - 162: Specific capacity of $LiNi_{0.5}Mn_{1.5}O_4$ cells containing standard electrolyte and added LiBOB.

The XPS spectra of fresh and cycled cathodes were acquired. The C1s element spectra are very similar and support the presence of polyethylene carbonate (PEC) while the F1s spectra of the cathodes extracted from cells containing LiBOB have a slightly higher concentration of LiF at 685 eV than the cells cycled with standard electrolyte. The O1s element spectra contain higher concentration of the lithium metal oxide at 529.5 eV for the cell cycled with electrolyte containing LiBOB than for the standard electrolyte. The greater relative concentration of metal oxide on the surface supports a thinner cathode surface film, or less Mn dissolution from the surface, and suggests that the presence of LiBOB is inhibiting the reaction of the electrolyte with the surface of the cathodes.

Development an understanding of poor first cycle efficiency for $LiPF_4(C_2O_4)$. The reversible capacity observed on the formation cycles of cells (MCMB/$LiNi_{0.8}Co_{0.2}O_2$) containing $LiPF_4(C_2O_4)$ electrolytes is 62 % compared to 84 % for $LiPF_6$ electrolytes. The differences were suspected to be due to lithium oxalate impurities in the $LiPF_4(C_2O_4)$. Extensive purification of $LiPF_4(C_2O_4)$ followed by cycling of the electrolyte in cells suggests that the lithium oxalate impurities contribute to the irreversible capacity, but efficiencies in excess of 65 % could not be obtained via $LiPF_4(C_2O_4)$ purification.

However, formation cycle efficiencies vary significantly as a function of the electrode materials. Investigation of $LiPF_4(C_2O_4)$ electrolytes in natural graphite (NG)/$LiNi_{0.8}Co_{0.2}O_2$ cells provided nearly identical reversible capacity (89 %) to $LiPF_6$ electrolytes upon formation (Figure V - 163). In addition, the cell capacity

during the first 50 cycles is slightly better for $LiPF_4(C_2O_4)$ than $LiPF_6$. Related NG/$LiFePO_4$ cells and MCMB/$LiFePO_4$ cells were prepared and cycled confirming the source of the efficiency difference as the anode material.

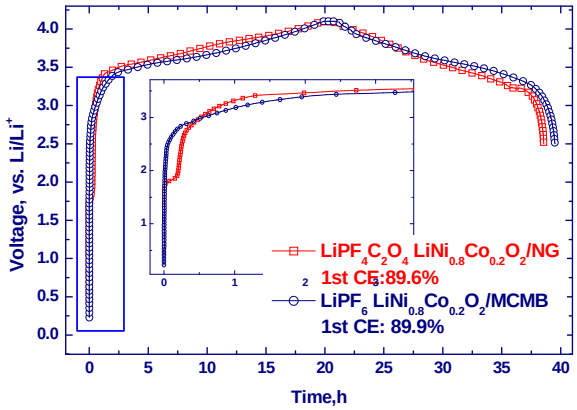

Figure V - 163: First charge-discharge curve for LiPF4(C2O4) and $LiPF_6$ electrolytes.

Surface analysis of the anodes after cycling support the presence of very similar species on MCMB and NG (Figure V - 164), but thicker furface films on MCMB.

Investigation of the performance of $LiPF_4(C_2O_4)$/PC electrolytes after accelerated aging. Investigations of $LiPF_4(C_2O_4)$ in PC based electrolytes, cell cycling and post-mortem analysis of the electrodes was conducted. Cells containing $LiPF_4(C_2O_4)$ in PC/EMC have similar cycling performance at RT to cells containing $LiPF_6$ in EC/EMC or $LiPF_4(C_2O_4)$ in EC/EMC (Figure V - 165). The initial cycling performance at low temperature (-10°C, charge and discharge) is better for the $LiPF_4(C_2O_4)$ electrolytes than the $LiPF_6$ electrolyte. The cells were then stored at 55°C for two weeks to simulate accelerated aging where cells containing $LiPF_6$ electrolytes surprisingly out performed cells containing $LiPF_4(C_2O_4)$ electrolytes. Further investigations of $LiPF_4(C_2O_4)$ electrolytes containing methyl buterate (MB) with superior low temperature performance and good thermal stability will be conducted in FY12.

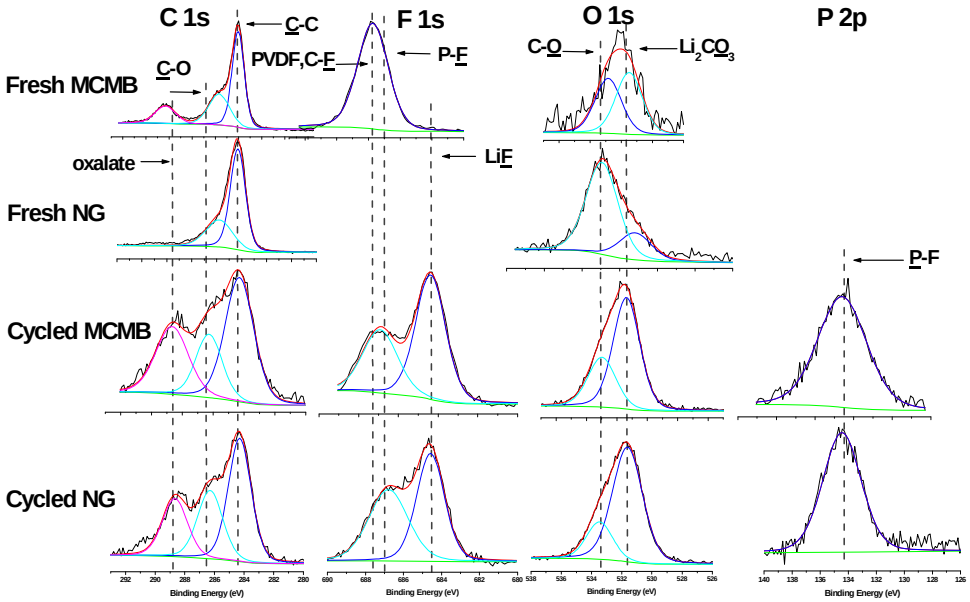

Figure V - 164: XPS analysis of graphite/$LiFePO_4$ cells.

Investigaton of novel electrolytes additives to improve performance of Si-based anodes. Si anodes were cycled with $LiPF_6$/carbonate electrolytes with various additives and post-mortem analysis was conducted (Figure V - 166). Several of the additive electrolyte combinations provide superior cycling performance. The best additives include VC, MEC, and $LiBF_2(C_2O_4)$. Surprisingly, cells containing FEC did not perform as well as other electrolytes. *Ex situ* surface analysis suggests the cycling performance differences are due to differences in the structure of the Si anode SEI.

Conclusions and Future Directions

Detailed investigations of the cycling performance and electrode surface film structure of novel electrolyte formulations in lithium ion cells were conducted. Cathode film forming additives have been developed which improve performance of high voltage $LiNi_{0.5}Mn_{1.5}O_4$ cathodes. An understanding of the source of the poor first cycle efficiency for $LiPF_4(C_2O_4)$ electrolytes on graphite anodes was determined. The low temperature performance of $LiPF_4(C_2O_4)$/PC electrolytes after accelerated aging was

investigated. Novel electrolytes were investigated to improve performance of Si-based anodes.

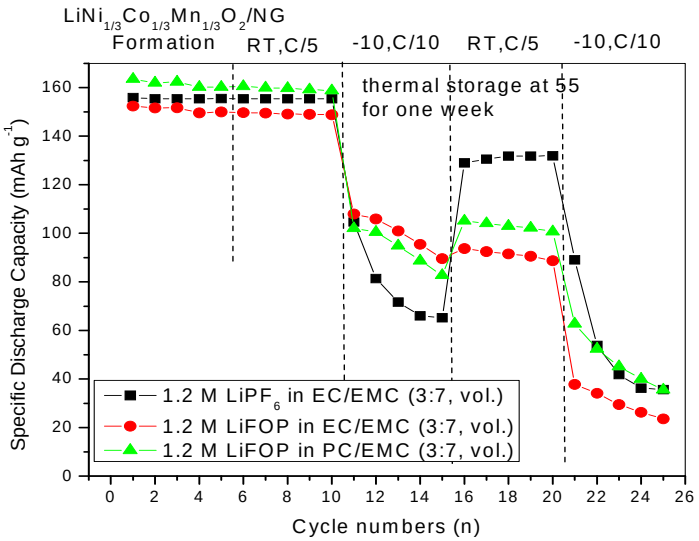

Figure V - 165: Cycling performance of graphite /$LiNi_{1/3}Co_{1/3}Mn_{1/3}O_2$ cells with different electrolytes.

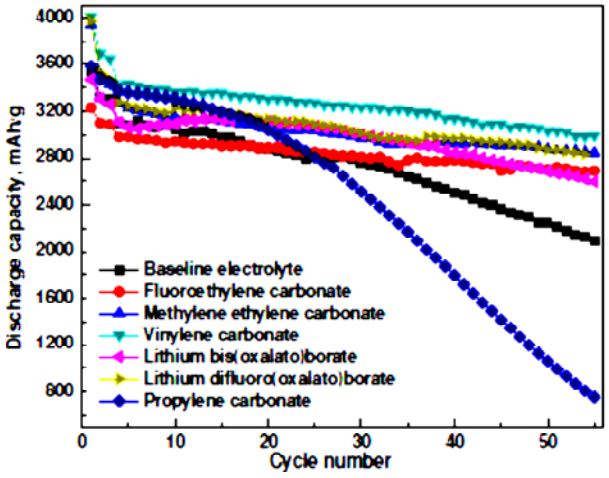

Figure V - 166: Cycling performance of Si/Li half cells containing various electrolytes.

Our future work will include the development of an $LiPF_4(C_2O_4)$ electrolyte with optimized performance at low temperature after accelerated aging. A better understanding of the role of electrolytes in the poor cycling efficiency and capacity fade of $LiNi_{0.5}Mn_{1.5}O_4$ cathodes will be developed. Finally, we will develop electrolyte formulations which optimize the performance of $LiNi_{0.5}Mn_{1.5}O_4$ cathodes cycled to high voltage (4.9 V vs Li).

FY 2011 Publications/Presentations

1. Experimental and Theoretical Investigations on Dimethyl Vinylene Carbonate as Solid Electrolyte Interface Forming Additive for Lithium-ion Batteries, Mengqing Xu, Liu Zhou, Lidan Xing, Weishan Li, and Brett L. Lucht Electrochim. Acta, **2010**, 55, 6743-6748.
2. Inorganic Additives for Passivation of High Voltage Cathode Materials, Li Yang, Tippawan Markmaitree, and Brett L. Lucht J. Power Sources **2011**, 196, 2251-2254.
3. Effects of Different Electrode Materials on the Performance of Lithium Tetrafluorooxalatophosphate (LiFOP) Electrolyte, Liu Zhou, Swapnil Dalavi, Mengqing Xu, and Brett L. Lucht J. Power Sources **2011**, 196, 8073-8084.
4. Investigation of the Solid Electrolyte Interphase on MCMB and NG Electrodes in Lithium Tetrafluorooxalatophosphate [$LiPF_4C_2O_4$] Based Electrolyte Mengqing Xu, Liu Zhou, Dinesh Chalasani, Swapnil Dalavi, and Brett L. Lucht J. Electrochem. Soc. 2011, 158, A1202-A1206.
5. Cathode Solid Electrolyte Interphase Generation in Lithium Ion Batteries with Electrolyte Additives, Meeting of the Electrochemical Society, Las Vegas, October 2010.
6. Investigation of Lithum Tetrafluorooxalatophosphate ($LiPF_4C_2O_4$) Based Electrolytes, Meeting of the Electrochemical Society, Las Vegas, October 2010.
7. Development of Electrolytes for Lithium Ion Batteries, DOE Annual Merit Review, Washington, DC, May 2011.
8. Investigation of Lithum Tetrafluorooxalatophosphate ($LiPF_4C_2O_4$) Based Electrolytes, 4th Symposium on Energy Storage: Beyond Lithium Ion, Pacific

Northwest National Laboratory, Richland, WA, June 2011.
9. Development of Electrolytes for High Voltage Lithium Ion Batteries, 5th Polymer Batteries and Fuel Cells Conference, Argonne, IL, August 2011.

V.D.8 Sulfones with Additives as Electrolytes (ASU)

Austen Angell (Project Manager)
Arizona State University
Department of Chemistry and Biochemistry
PO Box 871604
Tempe, AZ 85287-1604
Phone: (480) 965-7217; Fax: (480) 965-2747
E-mail: caa@asu.edu

Subcontractor: None

Start Date: March 2009
Projected End Date: December 2012

Objectives

- **Primary:**To evaluate the possibility of enhancing the ionic conductivity of sulfone solvents that are known for their high resistance to oxidating and reducing conditions, by fluorination, or mixed solvent methods.
- **Secondary:** (a) to develop a novel type of nanoporous framework support for high voltage stable electrolyte systems, (b) to explore possible alternative glassy and composite solid ionic conductor systems that avail themselves of structure-uncoupled conductivity mechanisms that permit conductivities comparable to those of liquid electrolytes but with fewer complications from side reactions.

Technical Barriers

1. Electrolyte solvents

(a) Synthetic obstacles to fluorination of organic sulfones

(b) Lack of knowledge of mixing rules for sulfones with low viscosity cosolvents

(c) unknown ability to form SEIs at lithium or graphite surfaces

(d) Unknown stability at high voltage cathode surface

2. Nanoporous nets as electrolyte supports

(a) mechanism of formation of nets

(b) manner of forming continuous films as opposed to insoluble amorphous powders

(c.) manner of incorporating ionically conducting solutions or other ionic phases within nets

(d) lack of knowledge about mobility of ions in the nanoporous environments

3. Decoupled conducting carrier solid state glassy or microcrystalline Li conductors as liquid electrolyte substitutes

(a) lack of knowledge about decoupling mechanisms

(b) lack of knowledge about conditions for amorphization of highly decoupled conducting systems

Technical Targets

- Develop synthetic methods for new fluorinated materials.
- Develop alternative solvents-cosolvent systems and examine performance
- See remaining barriers

Accomplishments

- Demonstrated high conductivity in solvent with 5.5 volt stability windows.
- Developed graphical representations of measured quantities that differentiate mobility from ionic concentration and clarify efficacy of different solvents systems (Walden plot approach).
- Demonstrated reversible Li intercalation at Gr anodes.
- Developed procedures forming nanoporous framework membranes of variable pore dimensions.

✧ ✧ ✧ ✧ ✧

Introduction

The end of the first full year of support of this project comes with a mixture of success and uncertainty. We have succeeded in synthesizing a group of fluorinated sulfone solvents, and their electrochemical windows have been found, in some cases, to be as wide as those of their unfluorinated progenitors. However there has been disappointment in the conductivities of the solutions they have formed with $LiPF_6$ as preferred salt. On the other hand, concern about the conductivity performance should be weighed against the findings from recent studies (reported at a Japanese battery workshop this past August) that the sulfones prove to be much ***safer*** electrolyte solvents than the carbonate solvents of common usage because of the thermal balance factors that determine whether or not thermal runaway occurs on failure. The well-known cyclic sulfone, tetramethylene sulfone (commonly known as sulfolane) was the solvent used in the Japanese study, because of its low melting point. Indeed sulfolane has been a component in many of the solutions of the present study, serving as a known starting point and reference case as will be seen below. A number

of features of its behavior, including its unusually high efficiency in usage of the solute ions for charge transport, will be documented below.

This report is divided into sections on synthetic targets, electrochemical characterization of synthesis products and mixed solvent systems, testing of anode half cells (lithium in graphite intercalation), testing of cathode half cells (stability to $LiNi_{0.5}Mn_{1.5}O_4$), and finally the recently successful realization of a nanoscopic tetrahedral mesh supporting medium for liquid electrolytes.

Approach

All technical problems are approached with the same strategies. A sequence of rational steps and best ideas are taken until an objective has been reached, and the sample has been made, purified, and tested, or alternatively is proven impossible, or too difficult, to make by available methods.

Characterizations of successful preparations are carried out with standard methods.

Results

1. Electrolyte Development.

(a) Fluorinated sulfone syntheses. In the first quarter, a second fluorinated sulfone, $CF_3CH_2OCH_2SO_2CH_3$, designated FEOMMS, was developed which is a 1,1,1 perfluoromethylated version of one of the ethersulfones described in papers preceding this grant (and forming part of the original proposal). Similar to the 3F-sulfolane synthesized in the previous year, it has a pleasingly low melting point, but its conductivity, shown in Figure V - 167, is a factor of two lower than that of sulfolane and little better than that of 3F-sulfolane. Its purification was therefore not pursued, and its electrochemical window was not evaluated.

Contrary to prior indications, no advantage in terms of solution conductivity has been found for the fluorinated solvents over hydrogenated equivalents, unless molecular size is simultaneously reduced. Small molecule fluorinated sulfones were either purchased or synthesized. Perfluoro methyl methyl sulfone was found to have such acid protons that bubbles of hydrogen were released in the presence of lithium metal. 1,1,1trifluoroethylmethyl sulfone had been prepared in an earlier study and was known to be an excellent solvent with high conductivity, but also with methyl hydrogens too active to be acceptable. Finally, fluoromethyl sulfone FMS, available commercially, was found to be very fluid, as expected from its boiling point, and also found to be very stable electrochemically, hence would seem interesting.

However, it is such a poor solvent that only LiTFSI, not $LiPF_6$. can be dissolved, and the LiTFSI solution proves to be a poor conductor despite the high fluidity. Clearly, due to low polarity, ion dissociation is a major problem with this solvent (see also Figure V - 169, lowest curve). However FMS has potential as a fluidity-enhancing cosolvent, and has been studied in this role in successful experiments reported below.

(b) Mixed solvent evaluations. For comparison, sulfolane-DMC solutions were studied over a wide range of compositions to find the range over which the electrochemical stabilization of co-solvents reported previously could be exploited, in high voltage cell applications. In a revealing study, conductivities and viscosities were both determined at each composition, and a Walden plot, not used previously in non-aqueous solution analysis, was constructed.

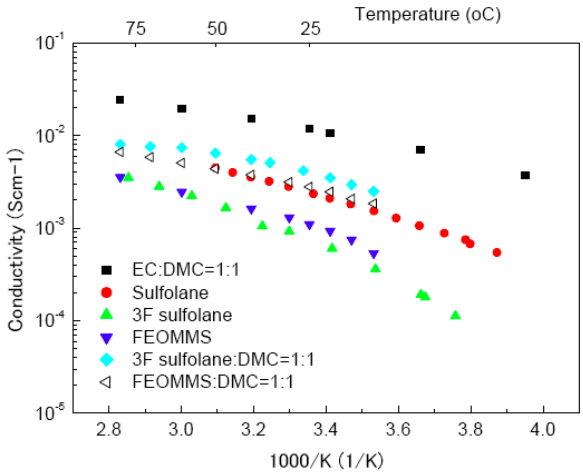

Figure V - 167: Arrhenius plot comparison of conductivities of 1M $LiPF_6$ in 1:1 EC-DMC, commercial sulfolane solvents with those in the newly synthesized solvents and their mixtures in DMC.

Figure V - 168 shows the variation of conductivity with DMC content in wt% while the Figure V - 169 shows the corresponding viscosity data. The densities were measured in order that the equivalent conductivity needed for the Walden plot could be derived. The equivalent conductivity monitors the ionic mobilities (sum of all) and, according to Walden, is controlled by the liquid fluidity. Thus, to first approximation, the failure of experimental points to lie on the ideal unit slope line (calibrated with dilute aqueous KCl), gives information on the failure to dissociate into ions. It is notable that in pure sulfolane as solvent, the Walden rule is obeyed, but then there is a systematic fall-off as the low dielectric constant component is added. It is notable that the standard electrolyte, $LiPF_6$ in EC:DMC 1:1 marked as red solid circle, is conductimetrically inefficient with respect to utilizing the intrinsic mobility of its ions to the extent of almost an order of magnitude.

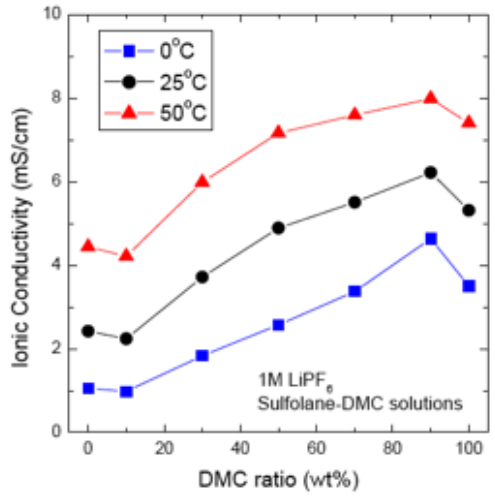

Figure V - 168: Conductivities of sulfolane-DMC mixtures

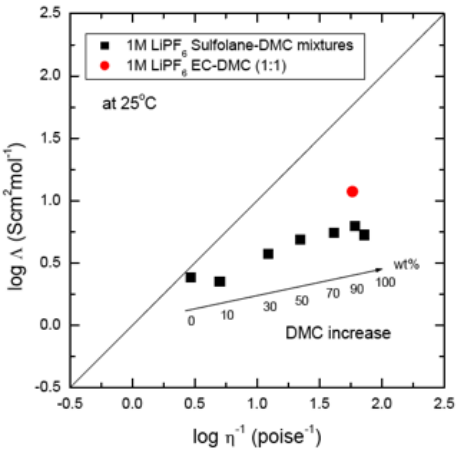

Figure V - 169: Walden plot for assessing ionicities.

Conversely, and keeping in mind that it enhances cell safety, it should be recognized that although sulfolane is more than an order of magnitude more viscous than EC:DMC, it only gives up a factor of two or so in conductivity. At the same time the solution gains in electrochemical stability. The gain should be even greater for the acyclic sulfone EMS, the "window" of which is the widest on record. It should be noted that sulfolane as solvent has already passed tests of stability against the LNMO high voltage cathode in the 1,000 cycle tests reported by Amine and colleagues, at ANL.

To consider solutions based on EMS, data are presented in Figure V - 170. It is seen that the mixture of EMS and FMS has a very favorable temperature dependence such that at 70ºC it has a conductivity not only as high as the EMS-DMC solvent, but almost as high as that of EC:DMC in Figure V - 167. Figure V - 171 shows that the electro-chemical stability is above 5.5 volts, and Figure V - 172 shows that a graphite anode half cell quickly establishes a stable SEI and then intercalates lithium reversibly. This is impressive in view of the immediate exfoliation that occurs when EMS is used alone as solvent. We note that the fluorosulfonyl group is also implicated in the efficacy of the bis-fluorosulfonylimide anion as an SEI-forming agent (observed in Japanese laboratories).

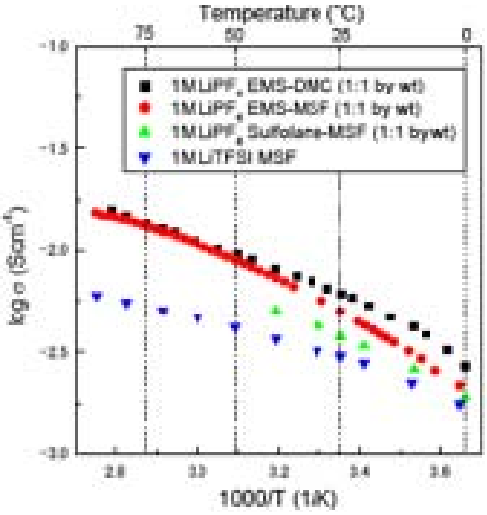

Figure V - 170: Conductivities with EMS and FMS co-solvents

EMS with FMS co-solvent also supports cycling at the graphite anode, though the SEI does not form as rapidly and efficiently as with sulfolane.

Turning to the cathode half cell, less success has been had, but the preparation of the cathode is more complex and there has been no access to proper cathode preparation facilities (spin-coaters etc). The results are shown in Figure V - 173, and it is found, in follow-up experiments, that the electrodes prepared in the ASU lab cannot be charged beyond 4.7 V before some irreversibility is encountered. In view of the success reported by the Amine lab, we will not consider the EMS-FMS solvent based electrolyte a failure until tests on more satisfactory cathodes can be carried out. Dr. Ueno, now back in Japan, has offered to use sophisticated electrode fabrication tools available in his current laboratory to prepare more reliable cathodes and thereby to establish the true efficacy of the sulfone-based electrolytes for high voltage cells of the LNMO type.

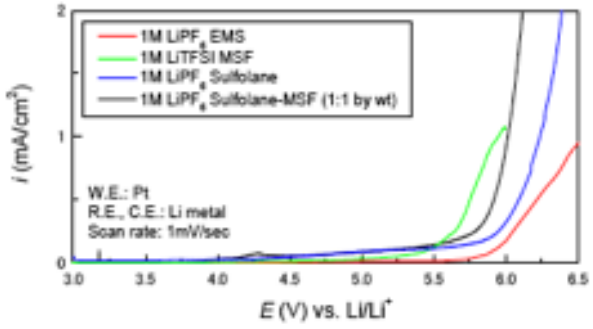

Figure V - 171: Oxidative stabilities of EMS and FMS

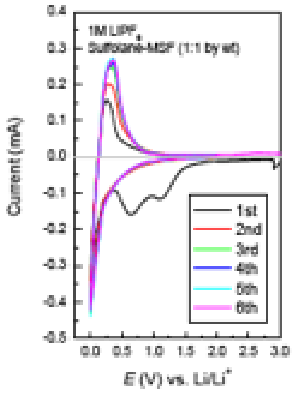

Figure V - 172: Li deposition and stripping at a graphite anode sulfolane:MFS as solvent

2. Nanoporous nets as electrolyte supports. After months of frustrating effort trying to produce reversible H-bonded models of the open nets we had conceived for this projects' electrolyte support, we changed course to tackle directly the covalent net versions that were expected to be irreversible. We have immediately been rewarded with success. The flexible solid film seen in Figure V - 174a is a new product for which we show XRD patterns and their conversion to real space distributions in Figure V - 174b. These establish that an open network with ~15-20Å pores has been obtained. We have successfully prepared a second version using struts 3 times as long, which are of extremely low density, and should support both solution and ionic liquid electrolytes up to 200ºC.

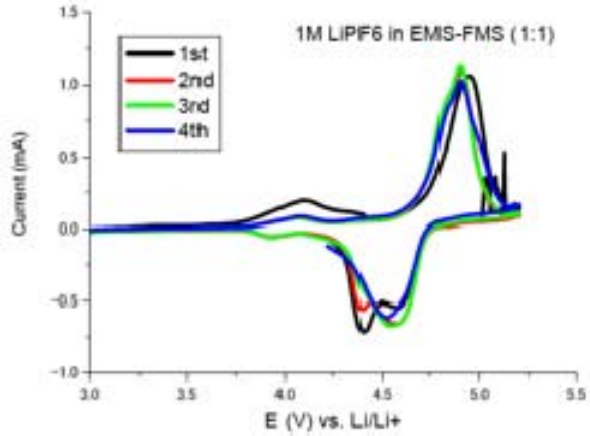

Figure V - 173: CV for 1M $LiPF_6$-EMS-MSF (1:1 by wt) on LNMO cathode. Scan rate 0.2mV/sec. Working electrode: LNMO composite placed on Al substrate, Li ref and counter electrode

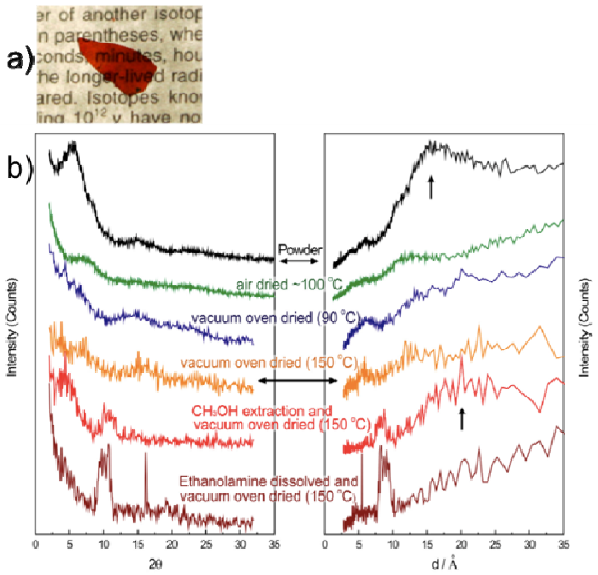

Figure V - 174: Nanoporous film, w/ XRD analysis, showing ~20nm pores in continuous film structure

Future work

Nets and their liquid-filled properties will be explored.

FY 2011 Publications/Presentations

1. 2011 DOE Annual Peer Review Meeting talk
2. Nature Materials (in preparation).

V.D.9 Long-lived Polymer Electrolytes (ORNL)

Chris Janke
Oak Ridge National Laboratory (ORNL)
1 Bethel Valley Rd.
P.O. Box 2008, MS-6053
Oak Ridge, TN 37831-6053
Phone: (865) 574-9247; Fax: (865)-574-8257
E-mail: jankecj@ornl.gov

Collaborators: Xiao-Guang Sun, Art Clemons, Claus Daniel, Cliff Eberle, Louis Mansur (ORNL)

Start Date: January 2010
End Date: June 2011

Objectives

Demonstrate that ion beam irradiation can be used to harden the surface of solid PEO electrolyte and thus significantly improve the lifetime of lithium polymer batteries, and to develop the technology sufficiently to enable its successful and rapid commercialization.

Technical Barriers

Poor battery cycle life and calendar life

Technical Targets

- Develop lithium ion batteries for EV applications with a specific energy of 200Wh/kg and a specific pulse power of 400W/kg.

Accomplishments

- Completed preparation of solid polymer electrolyte films.
- Completed ion-beam irradiation of first set of film specimens.
- Completed ionic conductivity testing of first set of film specimens.
- Completed preparation and ion-beam irradiation of final set of solid polymer electrolyte films and conducted ionic conductivity and dendrite growth testing.

✧ ✧ ✧ ✧ ✧

Introduction

Lithium polymer batteries are of great interest for plug-in hybrid electric vehicles due to their low weight and minimization of inactive material, non-flammability and high voltage stability.[1] However, they are plagued by short lifetimes that have prevented their application in hybrid electric vehicles. The short lifetime results from roughening of the lithium surface with repeated cycling, which eventually leads to catastrophic dendrite growth that shorts the lithium anode to the cathode.[2] Figure V - 175 shows a progressive sequence of dendrite growth and the resultant shorting.[3]

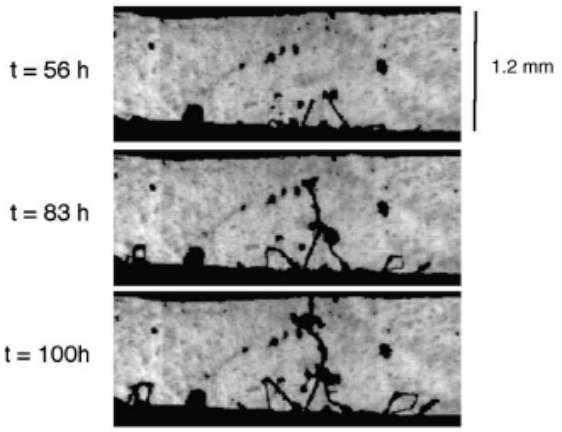

Figure V - 175: Dendrite growth sequence (Courtesy Rosso et. al.)

Making the electrolyte hard is a widely proposed solution to dendrite growth and the resultant cathode-anode short in lithium polymer batteries. Due to Newman and Monroe's calculations, an increase of the polymer modulus to ~ 1 GPa is expected to prevent dendrite growth.[4] This hardness is readily achievable in several polymers by ion beam irradiation.

Research at ORNL has indicated that high energy ion beam irradiation can generate hard-surfaced polymers with surface hardness up to ~ 20 GPa. This is much harder than most metals, for example stainless steel at typically 2-3 GPa or even martensitic tool steel with typical hardness ranging from 5-12 GPa. Ion beam irradiation cross-links many polymers to a depth of a few microns with an exceedingly high cross-link density, producing high hardness in the highly cross-linked material.

Approach

Our approach is to use commercial polyethylene oxide (PEO) with different molecular weights to make polymer electrolytes with lithium bis(trifluoromethane sulfonyl)

imide (LiTFSI) at the salt ratio of EO/Li = 10/1 through a solution cast method. The casted and dried self-standing membranes were subjected to oxygen ion beam irradiation with different energies and doses (Figure V - 176 and Figure V - 177). The irradiated membranes were further dried completely and evaluated through ionic conductivity and dendrite growth tests.

Figure V - 176: UES, Inc. Tandetron. The accelerator tank is in the foreground and the specimen target chamber is the disk shaped object partially visible at the end of the beamline.

Figure V - 177: Opened specimen handling target chamber, denoted as a wafer handler. In this photograph several 10 cm specimens for demonstration are shown in specimen positions.

Results

The focus of the project is to use commercial PEO (molecular weight of 900,000) as the polymer matrix and LiTFSI as the doping salt to study the irradiation effects on the dendrite prevention in Li||Li symmetric cells. The self-standing membranes were obtained via solution casting. The membranes were irradiated under different beam energies with varying doses.

In the first set of irradiation experiments, sufficient care was not taken to avoid moisture adsorption during sample mounting, handling and shipping to the irradiation facility, therefore the membranes adsorbed moisture, which we could not easily get rid of by simply drying at lower temperatures under vacuum. To circumvent this problem on the final set of samples, we procured large desiccators to store the dried membranes for transportation to and from the irradiation facility. In addition, in order to avoid moisture adsorption of the samples, we mounted the samples inside an Argon filled glove box and used a plastic glove bag over the sample mounting port located on the ion beam irradiation machine. After irradiation, the membranes were stored in the desiccators and the membrane surfaces remained very dry. As seen in Figure V - 178A, the conductivity of the membrane samples decreased with increasing ion beam dose at fixed ion beam energy of 1 MeV compared with the un-irradiated reference sample. In addition, the conductivity also decreased with increasing ion beam energies at a fixed ion beam dose of 5 x 10^{13} ion/cm^2 (Figure V - 178B). These results indicate that irradiation on both sides of the membrane resulted in a sufficient surface defect that influenced the ionic conductivity of the membrane. We used Swagelok hardware to make symmetric lithium cells. To avoid disturbing the surface effect from irradiation, we conducted the tests at ambient temperature. The cycling sequence is 2 hrs charge, 1 hr rest, 2 hrs discharge and 1 hr rest. Due to the lower ionic conductivity, the currents of 20μA and 10μA all resulted in a voltage exceeding the safety limit of 10V. Therefore, the final cycling current used was 5μA.

Due to the low current, even after 100 cycles (Figure V - 179A) there are no signs of dendrite growth, so it is difficult to judge the surface treatment effect on dendrite growth. It would be much preferred to use a higher current at higher temperatures, however, due to the linear nature of the polymer, which can easily flow under high temperatures, the surface treatment effect is smeared out. Therefore, it would be much better to use a cross-linked polymer, which cannot flow under high temperature, then subject the polymer to the same ion implantation process and evaluate for dendrite prevention.

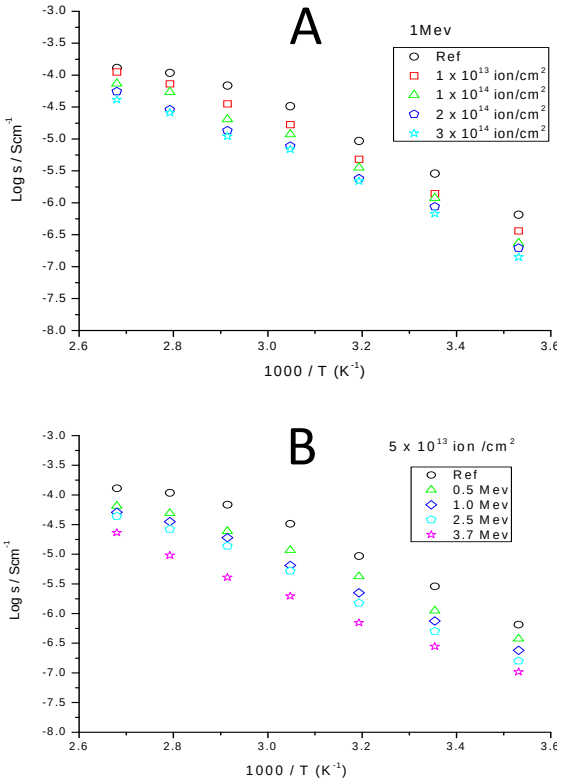

Figure V - 178: The temperature dependence of the ionic conductivities of the membranes after irradiation at a fixed ion beam energy of 1 MeV and at different doses (A); and under different ion beam energies at a fixed ion beam dose of $5x10^{13}$ ion/cm^2 (B).

Conclusions and Future Directions

As shown in the results, it is difficult to evaluate the effect of the surface treatment on the prevention of dendrite formation at room temperature using linear PEO. However, if evaluated at higher temperature, the surface effect will be disturbed due to the linear structure of PEO. In the future, we would like to make a series of cross-linked membranes with short PEO side chains, such as those based on polyethylene glycol dimethacrylate. Once cross-linked these membranes cannot flow at higher temperature so that they can be further surface treated using the same ion beam irradiation technique, followed by cycling evaluation at medium temperatures under high current to check the dendrite prevention effect.

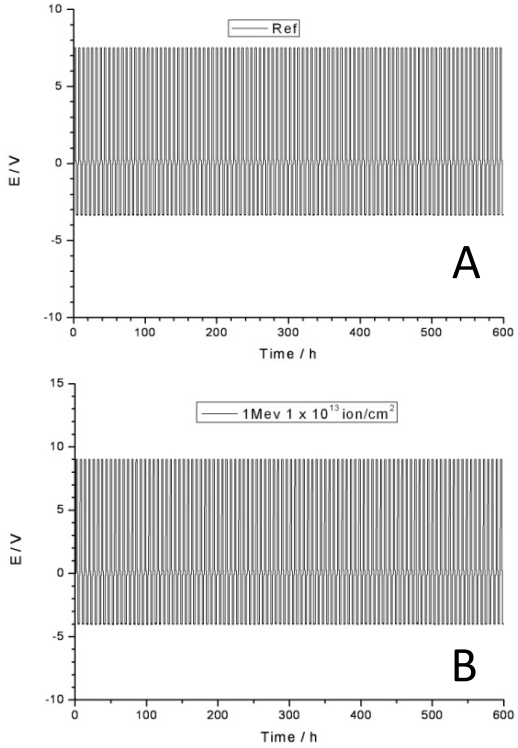

Figure V - 179: The typical cycling profile of (A) reference and (B) the sample irradiated at the beam energy of 1Mev and dose of $1x10^{13}$ ion/cm^2 under the cycling sequence of 2 hour charge, 1 hour rest, 2 hour discharge and 1 hour rest.

Acknowledgment

Ion beam irradiations were conducted at UES, Inc. in Dayton, OH.

References

1. Patil et al., Mater. Res. Bull. 2008, 43, 1913.
2. D. Howell, VT Program, Office of EERE, U.S. DOE, Washington, DC, 2008.
3. M. Rosso et. al., Electrochimica Acta 2006, 51, 5334.
4. C.W. Monroe and J. Newman, Journal of the Electrochemical Society 2005, 152:2, A396.

V.E Cell Analysis, Modeling, and Fabrication

V.E.1 Electrode Fabrication and Failure Analysis (LBNL)

Vincent Battaglia (Principal Investigator)
Lawrence Berkeley Nationl Laboratory
1 Cyclotron Road
M.S.70R0108B
Berkeley, CA 94720
Phone: (510) 486-7172; Fax: (510) 486-4260
E-mail: vsbattaglia@lbl.gov

Start Date: October 1, 2009
Projected End Date: September 31, 2013

Objectives

- Develop fundamental understanding of the effect of electrode fabrication procedures on cell performance.
- Develop techniques for evaluating cell failure.
- Provide full- and half-cell evaluations of materials with the potential to improve energy density or life over the baseline.

Technical Barriers

Electrode performance as a function of electrode fabrication is poorly understood. Measuring the cycle life of a new material can be confounded with poor electrode fabrication.

All Li-ion cells fail with time. Much of the failure is a result of side reactions in the anode and/or the cathode; although, the rate of cell failure is only a fraction of the rate of the side reactions. Understanding the underlying source of cell failure is critical to solving the problem.

For FY2011, the BATT Program decided to put more emphasis on higher voltage systems as this is a path to higher energy density cells. The Program selected the high-voltage $LiNi_{1/2}Mn_{3/2}O_4$ spinel material as a baseline for the studies. Understanding how this material fails against different counter electrodes may provide clues to its failure mechanism/s.

Technical Targets

- Develop electrode fabrication capabilities that allow for the cycling of materials to > 1000 cycles.
- Assess the rate of capacity fade of $LiNi_{1/2}Mn_{3/2}O_4$ against the PHEV and EV life targets.

Accomplishments

- Measured the rate of side reactions on graphite and NCM when each is cycled against Li and when cycled against each other.
- Determined the upper cut-off voltage limit when cycling $LiNi_{1/2}Mn_{3/2}O_4$ against Li and against graphite.
- Measured the rate of capacity fade of the $LiNi_{1/2}Mn_{3/2}O_4$ cell and showed that the side reactions are 4 times greater than the rate of capacity fade.
- Measured the amount of dissolution of fresh electrodes of $LiNi_{1/2}Mn_{3/2}O_4$ in electrolyte.

✧ ✧ ✧ ✧ ✧

Introduction

Cell manufacturing in the US is improving. Cells are now seen to last 1000 cycles, but not 5000 cycles as is required for PHEVs. This group's cell manufacturing capabilities have kept pace. Our goal is to test good materials in cells and identify main sources of fade, in the face of limited capcity fade. Since most cells appear to die as a result of deleterious side reactions, we will pay special attention to the rate of these reactions and attempt to identify those that are benign and those that contribute to failure. We will develop new electrochemical methods where necessary.

If the challenging energy density targets of EVs and PHEVs are to be realized, materials capable of cycling larger quatities of lithium and at higher voltages are required. To begin developing high-voltage electrolytes, high-voltage cathodes are required. $LiNi_{1/2}Mn_{3/2}O_4$ intercalates lithium with a flat potential at 4.7 V. This material will be evaluated for its performance and cycleability against different counter electrodes.

Approach

The BATT Program has identified the high-voltage Ni-spinel material as part of a system of interest. Our role is to identify a baseline cell chemistry. This chemistry must have reasonably good cycleability. Once established, our role is to quatify the sources of fade, whether it is power or energy. We accomplish this through particle analysis, electrode analysis, half-cell analysis, and full cell

analysis. Theories of energy or power fade are shared with Diagnostocs and Modeling teams and follow-on experiments are designed. Materials with purported advancements are also examined rigorously and correlations of physical properties with performance are sought. Results are shared with the suppliers.

Results

Side reactions of full-cells *versus* half-cells. During the first quarter, we investigated the rate of side reactions in full-cells *versus* half-cells. Through careful cell design and analysis of the charge and discharge curves, one can measure the rate of side reactions occuring in both electrodes of a cell, although not the rate on lithium. The process is more expeditious for full cells through the introduction of a reference electrode, and meaningful if the introduction does not contribute to cell leakage. Figure V - 180 shows the fraction of integrated current that goes toward the side reaction for NCM (from ANL) when tested against Li, for graphite (Conoco Phillips) when tested against Li, and for graphite when tested against NCM.

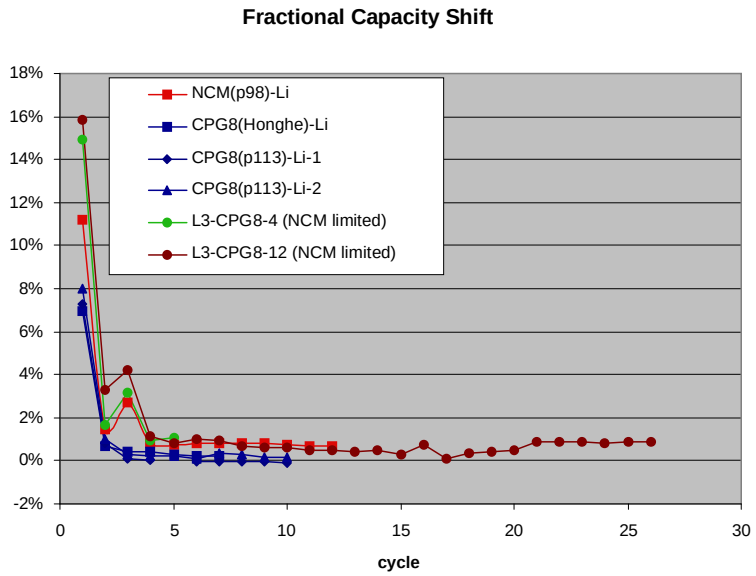

Figure V - 180: Fraction of capacity shift per cycle as a result of side reactions.

One sees that the side reaction on graphite when Li is the counter electrode is about three times less than when NCM is the counter electrode. We also see that the rate of the side reaction on NCM is the same whether graphite or Li is the ecountre electrode. This suggests that the side reaction is a result of a "natural" shuttle in the cell that is formed from the products of either the electrolyte oxidation or reduction. It also suggests that the coulombic efficiency is not a good indicator of cell life if the side reactions are mostly benign.

Characterizing $LiNi_{1/2}Mn_{3/2}O_4$. Through ABR Program resources, a high-voltage spinel material was identified. From there, we wanted to investigate its cycleability. Through half cell experiments it was determined that this material will not cycle well when the upper cut-off voltage exceeds 4.88 V at C/10. However, when cycling such a cell with a Li counter electrode, instabilities appear as reflected in the voltage curve, see Figure V - 181.

While cycling full cells with a graphite anode, it was discovered that these voltage instabilities stopped and that the upper-cutoff voltage is no longer 4.88 V but 5.3 V.

The present inductive reasoning is that the istabilites found in half cells are a result of oxidation products that are either gases or form gases upon migration to the lithium counter electrode. We intend to follow up on this speculation with some experiments that might capture any gases that are being formed.

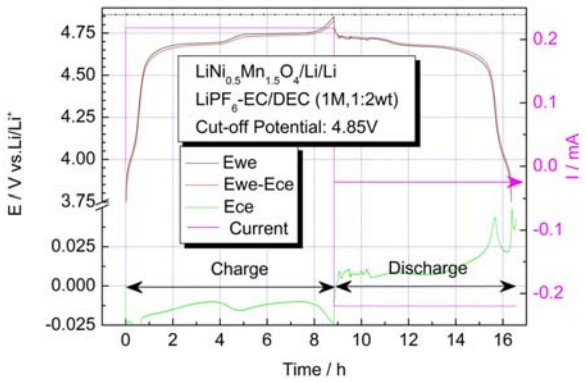

Figure V - 181: Cycling results of a Li/$LiNi_{1/2}Mn_{3/2}O_4$ cell.

The long-term cycling stability of the high-voltage electrode *versus* a graphite was also investigated, results of which are provided in our Annual Report for the ABR program. In that report, 250 cycles with very little capacity fade are shown. This cell continued to cycle for another 800 cycles with a loss of 20% of its capacity. A closer investigation of that data indicated that we could plot the rate of side reaction of the anode and the cathode, as provided in Figure V - 182.

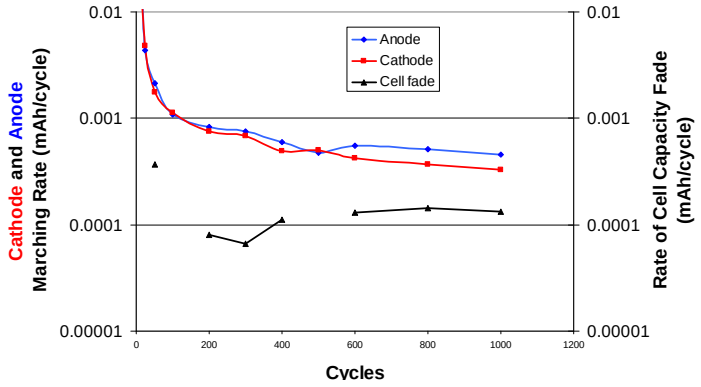

Figure V - 182: Cathode and anode capacity shift per cycle and the difference between the two, which is equivalent to the cell capacity fade.

The difference between these two is equal to the amount of capacity loss per cycle. One sees that the rate of capacity loss is a fraction of the rate of the side reactions at either electrode, again suggesting a benign side reaction like a shuttle.

As with most cathode materials, transition metals are lost from the cathode and found in the anode. This transfer of transion metals appears to have an accentuating effect on the 1st cycle irreversible capacity loss of the anode and on the rate of the side reactions during subsequent cycles. Figure V - 183 is of the fraction of transition metals found in the electrolyte after 1, 4, and 9 weeks at 55°C.

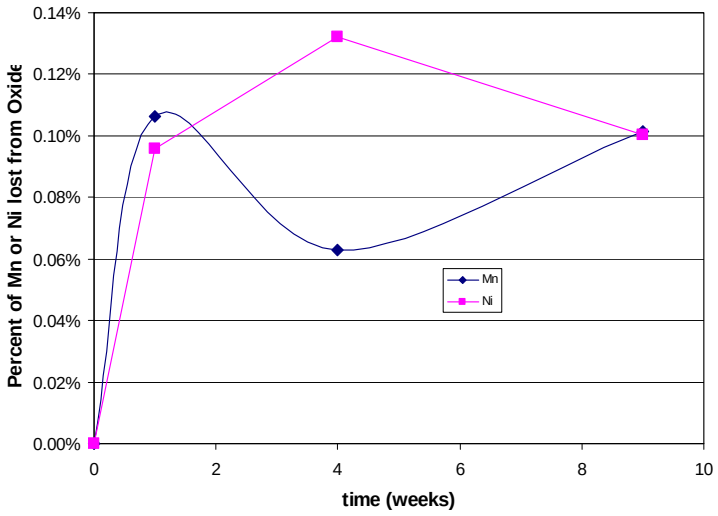

Figure V - 183: Fraction of transition metals lost from a sample of fresh $LiNi_{1/2}Mn_{3/2}O_4$ when immersed in electrolyte for 1, 4, and 9 weeks.

These results show that, for fresh powders, the dissolution is completed after the first week and is equivalent to just 0.1 % of the transition metals. It is possible that these results are measuring the amount of dissoluable impurity species in the cathode. These experiments will be followed-up by similar experiments with the electrode charged to differend states-of-charge.

Conclusions and Future Directions

Previous work, either performed in our lab or published in the literature, has indicated that side reactions play a critical role in cell capacity fade, especially for those materials where cycleability beyond 1000 cycles is possible. We have found that not all of the side reactions are detrimental and thus may be the result of a shuttle that is formed during the first charge. We are attempting to measure the rates of these reactions and to isolate the shuttle.

LBNL has initiated a focus group on high-voltage electrodes/electrolyte. The baseline materials are $LiNi_{1/2}Mn_{3/2}O_4$ from NEI and 1 M $LiPF_6$ in EC:DEC 1:2. Cycling has been performed with lithium and graphite as the counterelectrode. The upper cutoff limit when cycling against Li at C/10 is 4.88 V and against graphite is 5.3 V. Cells cycled against graphite have side reactions that are 4 times the rate of capacity fade and suggest a shuttle is active in the cell. Dissolution experiments reveal that the fresh powder losses about 0.1 % of the transition metals after 1 week at 55°C.

Future efforts will be dedicated to understanding the source of the shuttle, the composition of expected gasses, and the source of the gasses. We are also looking to test advanced electrolytes and cathodes from other suppliers to determine the uniqueness of each.

We also expect to take up a study of electrode fabrication procedures in identifying those sources that make for the largest contributions to cell-to-cell variability.

FY 2011 Publications/Presentations

1. 2011 DOE Annual Peer Review Meeting Presentation.

V.E.2 Modeling-Thermo-electrochemistry, Capacity Degradation and Mechanics with SEI Layer (UM)

Ann Marie Sastry
University of Michigan
2350 Hayward St.
Ann Arbor, MI 48109
Phone: (734) 998-0006; Fax: (734) 998-0028
E-mail: amsastry@umich.edu

Start Date: October 1, 2008
Projected End Date: September 30, 2011

Objectives

- Create a multiscale finite element (FE) model that considers self-assembled structure in order to evaluate the effective electrochemical properties of the aggregated particles
- Perform numerical studies of capacity fade due to the SEI layer and stress analysis/mechanical stability of the SEI layer in anode particles
- Characterize the SEI layer and investigate the effect of different environmental conditions on SEI layer formation through experimental techniques

Technical Barriers

Inadequate power and life in PHEV systems

Technical Targets

- Available energy: 56 Wh/kg (10 mile) and 96 Wh/kg (40 mile)
- 10 s discharge power: 750 W/kg (10 mile) and 316 W/kg (40 mile)
- Cycle life: 5,000 cycles
- Calendar life: 15 years

Accomplishments

- Development of a multiscale FE model including particle aggregation of active and additive materials in order to determine the effective electrochemical properties of the electrode material
- Demonstration of capacity fade due to the SEI layer via a multiphysics model that considers film resistance and the double-layer charging current
- Demonstration of the stress evolution in both the active particle and SEI layer by considering a misfit between the two phases
- Measurement of EIS and XPS for the resistance variation due to the SEI layer and the concentration change of elements in the surface of the SEI layer

Introduction

In order for battery performance to improve, the failure mechanisms of Li-ion batteries, which involve many mechanisms such as active material dissolution, SEI layer evolution, mechanical instabilities, and thermal failure, have to be understood and minimized. As an extension of multiscale thermo-electrochemistry modeling in FY2010, this model was refined based on the findings from simulated performances and experimental observations. The improved model enabled us to investigate such key battery performance-determining parameters as multi-phase particle structure and SEI layer structure. SEI formation in composite electrode microstructures and its effect on battery kinetics were investigated via both experimental and numerical tools. Improved prediction of lifetime in Li-ion battery cells will be informed by exploring capacity degradation in composite multi-phase electrodes in the context of both multiple scales and multiphysics that considers electrochemical kinetics

Approach

Aggregation between additive particles and active particles in the electrode material of batteries strongly affects their interfacial impedance and power performance. A three dimensional model that simulates the aggregation process of carbon black and $LiMn_2O_4$ active material particles within a liquid medium (PVDF polymer dissolved in NMP solvent) was developed. A Brownian dynamics was employed in the simulation and the resulting aggregates are exported to multiphysics finite element models. This model was then used to evaluate effective material properties by applying a volume averaging theory. A mathematical model that includes film resistance and the double-layer charging current was developed, and this model was coupled with a frequency responses analysis in order to characterize capacity fade due to SEI layer formation. Also calculated were the stress evolutions

inside the active particle as well as the SEI layer, in the latter case by considering a misfit due to the difference in volume expansion between the two phases. For this experimental study, the interfacial impedance change as a function of cycling number and storage at various conditions is measured via the EIS technique. The composition change and thickness of the surface layer were then examined via X-ray Photoelectron Spectroscopy.

Results

Multiphysics FE model – The microstructure of percolated particle aggregates has been generated using a Brownian dynamics simulation as shown in Figure V - 184a. (blue: active materials, red: inert materials). This microstructure of particle aggregates has been modeled for finite element analysis as shown in Figure V - 184b and Figure V - 184c. At the middle of the cathode, the temporal variation of reaction current density from the pseudo-2D thermo-electrochemical model and 3D microscopic model is compared in Figure V - 185, which reveals a 14% difference.

In Table V - 4, the calculated effective diffusivity and conductivity are compared with the approach of Bruggeman's equation.

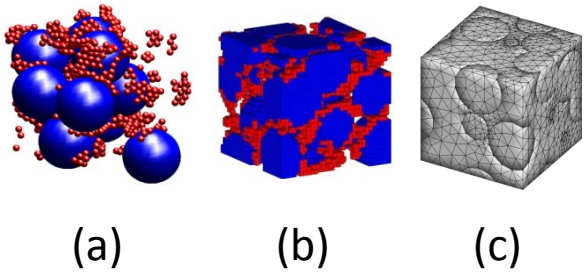

Figure V - 184: (a) aggregated structure (b) voxel mesh (c) tetrahedral mesh

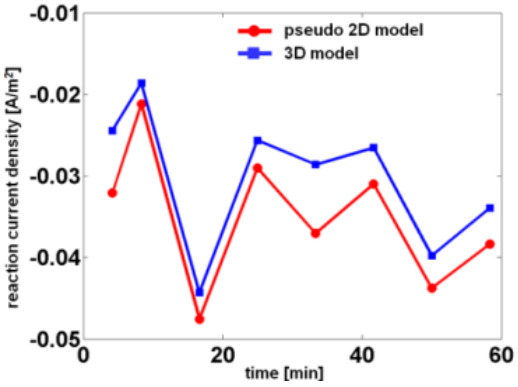

Figure V - 185: reaction current density

Table V - 4: Change in surface atomic concentration of each element

	Volume fraction	Bruggeman	3D microstructure
$D^{eff}_{active}/D_{active}$	0.49	0.34	0.346
$D^{eff}_{elyte}/D_{elyte}$	0.51	0.37	0.378
$\sigma^{eff}_{solid}/\sigma_{solid}$	0.49	0.34	0.300

Capacity fade due to SEI layer formation - The developed model enabled us to overcome the limitation of a conventional approach that assumes a steady state (at low frequencies the system may vary due to the long duration of measurement). Also, this numerical approach can facilitate the experimental studies on capacity fade due to SEI layer formation because capacity fade in Li-ion batteries comes from complex processes. The simulation demonstrated that capacity fade was accelerated as the film resistance increases, as shown in Figure V - 186a. It also demonstrated that impedance characteristics and frequency responses were changed depending on film resistance, as shown in Figure V - 186b.

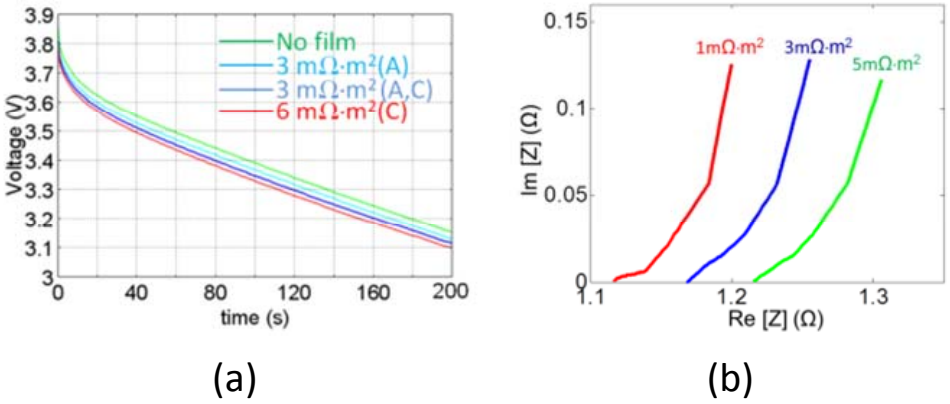

Figure V - 186: (a) capacity change (b) frequency response function

Anode particles near the separator underwent high stress due to (de)intercalation, which resulted in structural degradation of the active particles as shown in Figure V - 187a. When the SEI layer was formed at the surface of the anode particle, this layer changed the stress evolution inside the particle due to the mismatch of the partial molar volume as shown in Figure V - 187b. Also, this SEI layer itself underwent high stress due to the expansion of the active

material inside as shown Figure V - 187c. This high stress may cause cracking and instability of the SEI layer that may reduce battery performance.

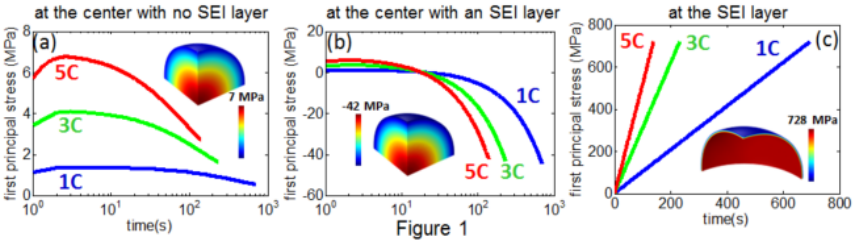

Figure V - 187: Stress (a) without SEI (b) with SEI (c) stress at SEI layer

Measurement of SEI Properties – Figure V - 188 shows the interfacial resistance change as a function of cycle number while the voltage is fixed at 4.1V. Both film resistance and charge transfer resistance are increased as the cycle number increases. The main contribution to the increase in film resistance may come from the increase of the cathode film resistance, which means that film formation in the cathode material has a significant effect on capacity fade for long-term cycling.

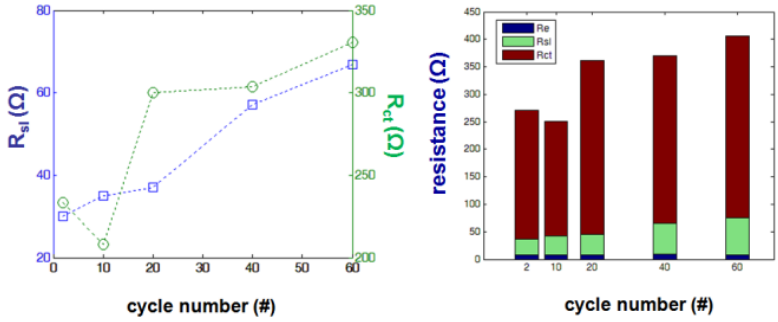

Figure V - 188: Resistance change

Figure V - 189 shows the XPS peak assignments in each element spectra in the cycled sample. The examination of peak positions indicates that the surface layer species formed in the cycled sample are similar to those in the stored sample. In addition, initial relative amounts of the elements in the surface layer are not much different in the two samples as shown in Table V - 1. Upon sputtering with Ar ions, the atomic concentration of F and P decreases, while Mn, O, and C increase. Significantly, the Mn concentration is largely increased in the cycled sample after 5 min of sputtering, showing that the Mn/O ratio is 1:2, which is consistent with the presence of pristine LMO electrode. It is suspected that the surface layer of the cycled sample is thinner or more easily removed via sputtering than those of the stored sample.

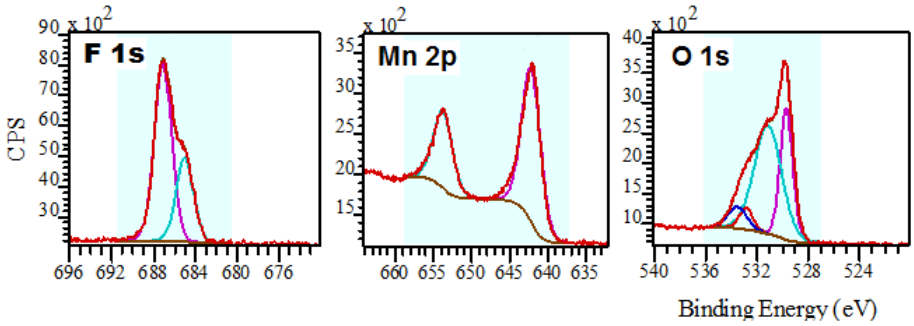

Figure V - 189: XPS spectra for the cycled sample

Table V - 5: Change in surface atomic concentration of each element

Elements	LMO electrode, 100 cycles, C/2.5		LMO electrode, stored for 21 days	
	Surface (Atom %)	5min sputtering (Atom %)	Surface (Atom %)	5min sputtering (Atom %)
F 1s	24.13	17.10	22.92	16.77
Mn 2p	4.26	9.70	4.24	4.84
O 1s	15.32	17.57	16.52	19.27
C 1s	54.74	54.87	53.93	57.27
P 2p	1.56	0.76	2.40	1.85

Table V - 6 shows changes in element quantities for different temperatures resulting from XPS measurements. The quantity of phosphorus was significantly increased as the temperature increased. This was due to higher decomposition of the $LiPF_6$ at high temperatures. Also, a relatively large amount of oxygen and lithium was observed at high temperatures, indicating that more SEI layer components such as lithium alkyl carbonate, Li_2CO_3, and LiF formed at high temperatures.

Table V - 6: SEI element quantity change

Temperatures	Oxygen	Lithium	Phosphorus
0 °C	4.4 % increase	34.7% increase	20.4% increase
25 °C	19.4% increase	5.84% increase	109.2% increase
60 °C			

Conclusions and Future Directions

A multiphysics model of thermo-electrochemistry using self-assembled structure has demonstrated the differences in predicted reaction current density from the pseudo-2D model. Also, volume-averaging theory was applied for the fluxes and perturbations to the micro simulations in order to calculate effective diffusivities and conductivities of the aggregated system. The developed model will be extended to the linking of macro and micro-scale simulation. Capacity and power fade due to the SEI layer have been modeled by considering film resistance and the double-layer charging current. The simulation has revealed that capacity fade is accelerated as film resistance increases. Also, the stress evolution due to misfit between the phases inside the particle and SEI layer has been demonstrated. This result will be used to evaluate the mechanical stability of the SEI layer and capacity fade due to mechanical failure. Several experimental techniques (*ex situ* and/or *in situ*) were applied to validate the SEI layer formation model and characterize the SEI layer; these included film resistance change due to the SEI layer and SEI layer component change. These experimental techniques will in the future be applied with new techniques such as AFM-based nanoindentation to measure Young's modulus of the surface layer.

FY 2011 Publications/Presentations

1. 2011 DOE Annual Peer Review Meeting Presentation.
2. Gupta, A., Seo, J.H., Zhang, X., Du, W., and Sastry, A.M., 2011, "Effective transport properties of LiMn2O4 electrode via particle-scale modeling," Journal of the Electrochemical Society, v. 158 (5), pp. A487-497.
3. Seo, J.H., Chung, M.D., Park, M., Han, S.W., Zhang, X., and Sastry, A.M., 2011, "Generation of realistic particle structures and simulations of internal stress: a numerical/AFM study of LiMn2O4 particles," Journal of the Electrochemical Society, v. 158 (4), pp. A434-442.
4. Chung, M.D., Seo, J.H., Zhang, X., and Sastry, A.M., 2011, "Implementing realistic geometry and measured diffusion coefficients into single particle electrode modeling based on experiments with single LiMn2O4 spinel particles," Journal of the Electrochemical Society, v. 158 (4), pp. A371-378.
5. Park, J., Seo, J.H., Plett, G., Lu, W., and Sastry, A.M., 2011, "Numerical simulation of the effect of the dissolution of LiMn2O4 particles on Li-ion battery performance," Electrochemical and Solid-State Letters, v. 14 (2), pp. A14-18.
6. Park, J., Lu, W., and Sastry, A.M., 2011, "Numerical simulation of stress evolution in lithium manganese dioxide particles due to coupled phase transition and intercalation," Journal of the Electrochemical Society, v. 158 (2), pp. A201-206.
7. M. Zhu, J. Park, and , “Particle Interaction and Aggregation in Cathode Material of Li-Ion Batteries: A Numerical Study”, 2011, J. Electrochem. Soc. 158 A1155.

V.E.3 Intercalation Kinetics and Ion Mobility in Electrode Materials (ORNL)

Claus Daniel

Oak Ridge National Laboratory
One Bethel Valley Road
P.O. Box 2008, MS-6472
Oak Ridge, TN 37831-6472
Phone: (865) 241-9521; Fax: (865) 241-5531
E-mail: danielc@ornl.gov

Collaborators: Sergei Kalinin, Nina Balke, Nancy Dudney, Hongbin Bei, ORNL
Ann Marie Sastry, University of Michigan

Start Date: September 2009
Projected End Date: September 2011

Objectives

- Develop fundamental understanding of deformation processes and stress generation during lithium (Li) intercalation (and deintercalation).
- Understand the role of crystal orientation and deformation damage in Li ion kinetics in intercalation compounds.

Technical Targets

- Apply Electrochemical Strain Microscopy (ESM) to focused ion beam (FIB) micromachined samples of lithium intercalation electrode materials.
- Develop and validate a coupled kinetic, thermal, and mechanical model based on the experimental results.
- Investigate Li ion kinetics as a function of state of charge.

Accomplishments

- Validated coupled kinetic, thermal, and mechanical model based on the experimental results from AFM and ESM
- Correlated crystal orientation and deformation damage in Li ion kinetics in intercalation compounds with ion mobility.

✧ ✧ ✧ ✧ ✧

Introduction

It is commonly accepted that Li-ion battery life is limited due to the process of degradation of electrode materials with repeated charging/discharging. One of the degradation mechanisms is related to development of internal stresses in electrode particles due to repeated lithium insertion and removal, which ultimately leads to cracking and fracture of particles. This project targeted the fundamental understanding, description through mathematical modeling, and controlled experimental validation of internal stress generation and morphology change of electrode particles in a Li-ion battery. While the intercalation/deintercalation process induces displacements changing the overall dimension of the specimen, the Li diffusion should be investigated on the single grain level. The second integral part of the project looks into the local lithium ion mobility, which is the underlying process for diffusion-strain coupling.

This project was heavily leveraged by our collaborators, the Kalinin group at the Center for Nanophase Materials Science funded by the Office of Science, Basic Energy Sciences Program and Nina Balke's Presidential Early Career Award for Scientists and Engineers.

Approach

Thin films, produced by radio frequency (RF) magnetron sputtering, as well as single grains of cathode material embedded in the current collector were investigated for Li ion mobility using the Electrochemical Strain Microscopy (ESM) technique at ORNL. This technique, based on strain-bias coupling, was recently developed at CNMS and allows for studying Li ion kinetics at the nanometer scale. A high frequency low voltage pulse was applied via the AFM tip, which re-distributed lithium in the tip vicinity causing local displacements in the grains. A dense population of microcracks and slip lines can be introduced by nano-indentation of the thin film cathode, in which case the severity of damage is controllable via indenter penetration depth.

Investigation of diffusion-stress coupling on the micro-scale was performed on samples of pre-defined simple geometry. The goal was to quantify the intercalation induced strains in the representative micro-sample of cathode material, analogously to the mechanical behavior studies on the macroscopic samples. Samples of cylindrical shape with micrometer dimensions were fabricated from the thin films of cathode material. The

changes in the sample dimensions upon charging where measured *in situ* by AFM in tapping mode. The results were used to validate the model predictions for the intercalation induced strains.

Results

***In situ* Electrochemical Strain Microscopy (ESM) investigation of Li ion kinetics on the nano-scale.** As a model system, we have chosen $LiCoO_2$ which is widely used as a cathode material in small format Li-ion batteries. Thin film samples were prepared by RF magnetron sputtering of a cold pressed and sintered $LiCoO_2$ target. The substrate was polished 99.6% Alumina and a 300 nm thick film of gold was deposited on the substrate prior to $LiCoO_2$ deposition. In order to improve adhesion of Au to the substrate, a 20 nm thin layer of Ni was deposited first. The samples were annealed at 800°C. The thickness of the $LiCoO_2$ film was maintained at 1 µm. X-ray analysis conducted on the samples shows preferential (101) orientation of the grains. Comparison of relative peak intensities obtained from the samples shows that as much as 77% of grains in the thin film sample are oriented with (101) plane being parallel to the substrate while 15% of the grains are (104) oriented. The SEM image of the thin film is shown in Figure V - 190.

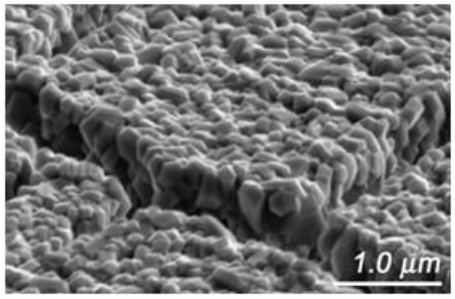

Figure V - 190: Thin film of $LiCoO_2$

Three Band Excitation (BE) techniques were applied: BE-line, BE-loop measurement, and BE-relaxation measurement. All of the ESM experiments were performed in ambient air. The effect of mechanical damage on Li ion kinetics was assessed on a thin film sample indented by a large spherical indenter.

The results show anisotropy of the material with respect to Li ion mobility (Figure V - 191). Evidence of the "hot spots", i.e. locations of the strain maxima, can be seen. There is a clear difference between out-of plane (OP) and in-plane (IP) signal, which can be in part attributed to the texture of the film.

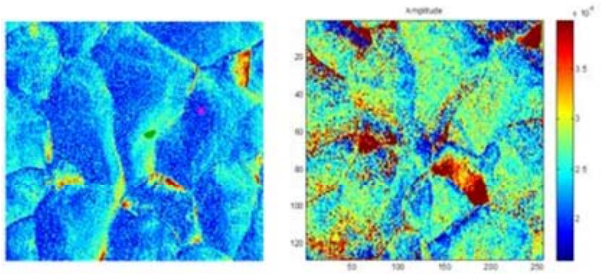

Figure V - 191: In-plane (a) and out-of-plane (b) ES amplitudes measured on $LiCoO_2$ thin film

The ESM technique was applied to $LiCoO_2$ thin film (500 nm thick) samples in order to map the strain, induced by Li concentration gradients, as a function of temperature. The experiments were performed using the *in situ* hot stage AFM at two levels of temperature: room temperature (RT) and 150 ^{0}C. The results (Figure V - 192) show significant dependence of electrochemical activity on the temperature of the sample. Both out-of-plane (OP) and in-plane (IP) strain amplitudes increase with the temperature. Additional voltage spectroscopy ESM measurements were performed in order to study the influence of the temperature on Li ion motion governed by diffusion. In these measurements a DC applied bias is followed by the high frequency AC ESM measurements that track re-distribution of the ions after DC pulse application. A series of such short pulses are applied to form a triangular wave and the amplitude signal collected from these measurements clearly shows hysteretic behavior (Figure V - 192f). It can be seen that the amount of energy lost due to application of reversed bias (the loop area) increases with increase of specimen temperature.

Nano-indentation of the $LiCoO_2$ thin films was performed with two purposes: i) determination of elastic constants of the material (Young's modulus), and ii) evaluation of the effect of mechanical damage on Li ion mobility. For the first purpose two thin-film samples were indented with a Berkovich tip indenter using an MTS Nanoindenter XP. A total of 50 indentations were made. The experimental data of load-displacement complemented with continuous stiffness measurement were analyzed in order to extract elastic modulus. The resulting modulus-depth curves are shown in Figure V - 193. The value of Young's modulus obtained from two samples was consistent (119 and 107 GPa).

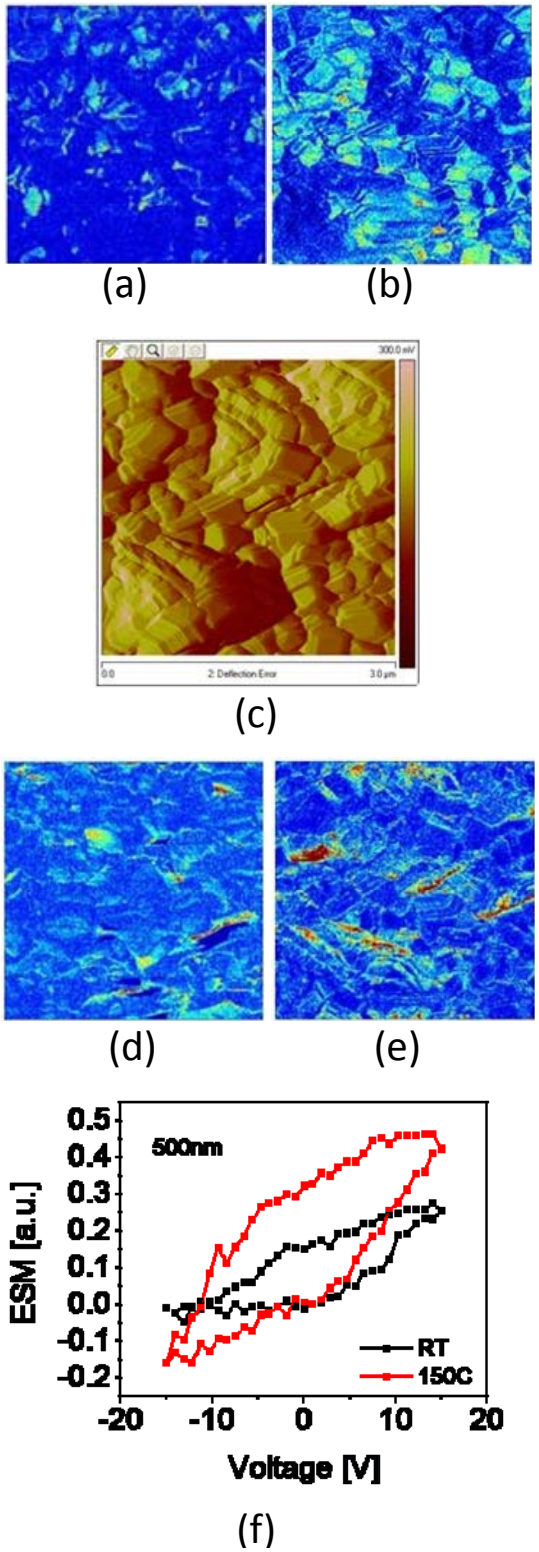

Figure V - 192: ESM of $LiCoO_2$ grains: a) OP at RT; b) OP at 150°C; c) Topography of the sample; d) IP at RT; e) IP at 150°C; f) Hysteresis loops from voltage spectroscopy

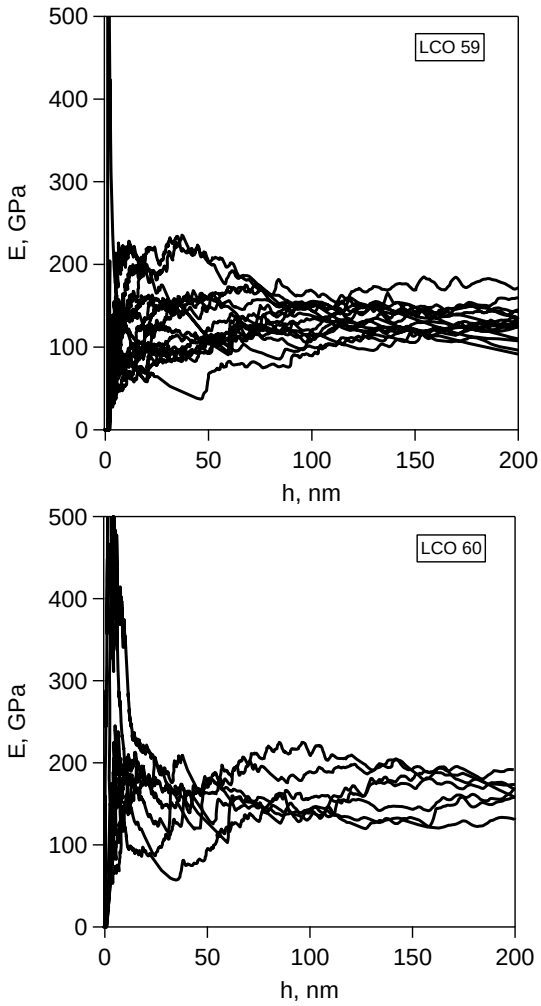

Figure V - 193: Modulus-depth data from the nanoindentation experiments

To investigate the effect of mechanical damage, thin film samples of $LiCoO_2$ were indented by indenter with a large spherical tip. 400 nm deep indents were made on a 1 µm thick film. The results show reduced ESM signal in the indented areas (Figure V - 194). These findings relate to the possible damage introduced during the calendering step in battery electrode processing.

It should be mentioned that the effect of mechanical damage depends on the damage magnitude. With the shallow (200 nm) indents, the effect is reversed, and the mobility of lithium ions is enhanced (Figure V - 195b). This indicates the possibility of an optimized process for calendering of electrodes, where the electrode performance is enhanced without fracturing the active material.

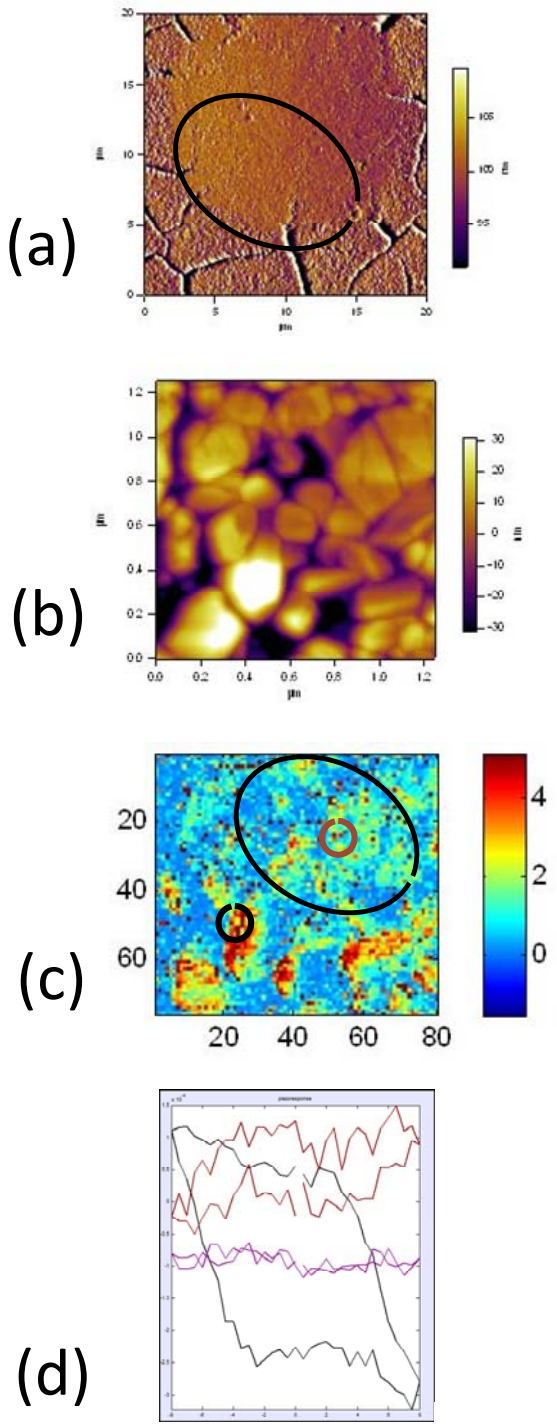

Figure V - 194: ESM study of the indented thin film $LiCoO_2$ cathode: a) indented region; b) analyzed area; c) loop opening; d) corresponding loops

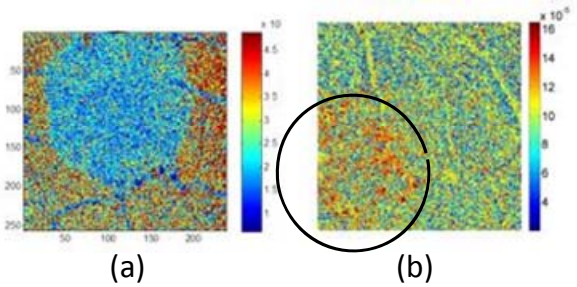

Figure V - 195: Effect of mechanical damage on the ESM activity: a) 400 nm deep indentation; b) 200 nm deep indentation. The indented areas are marked with circles.

Samples with the NCM cathode material ($Li_{1.05}(Ni_{1/3}Co_{1/3}Mn_{1/3})_{0.95}O_2$) were prepared using a new technique for uniformly spreading active material particles over the current collector (as opposed to traditional composite electrode samples made from slurry) which is suitable for ESM studies. The results (Figure V - 196) show significant dependence of electrochemical activity on the crystallographic features of the sample. Bias induced strain amplitude from BE-line measurements is a function of location of pulse application. In addition, the amplitude of normal strain in the direction of the cantilever deflection (out-of-plane) can be very different from that in the in-pane direction (corresponding to cantilever torsion), which is evident in Figure V - 196b and Figure V - 196c. It can be seen that the same area of the material produces either very high or nearly zero strains depending on which of the orthogonal directions is considered. It should be noticed that some of the grain boundaries are highly active while others remain inactive under in-plane measurements (Figure V - 196c).

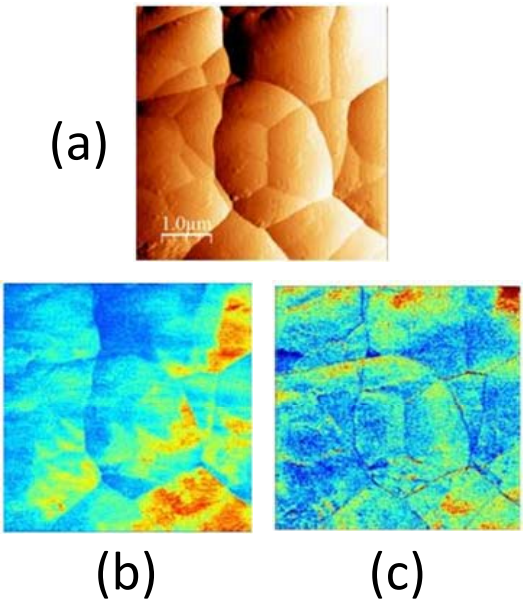

Figure V - 196: ESM of NCM grains: a) deflection; b) out-of-plane amplitude; c) in-plane amplitude

FY 2011 Publications/Presentations

1. Direct mapping of ion diffusion times on LiCoO2 surfaces with nanometer resolution. S. Guo, S. Jesse, S. Kalnaus, N. Balke, C. Daniel, S. Kalinin. *J Electrochem Soc*, (2011) 158(9), pp. 1-9.
2. A study of lithium ion intercalation induced fracture of silicon particles used as anode material in Li-ion battery. S. Kalnaus, K. Rhodes, and C. Daniel. J. Power Sources 196 (2011) 8116-8124.
3. Investigation of the Effect of Mechanical Damage on Li ion Mobility in Lithium-Ion Battery Cathode Material at the Nanoscale. Sergiy Kalnaus, S. Guo, H. Bei, N. Balke, S. Jesse, T. Arruda, N. Dudney, S. Kalinin, C. Daniel – Spring 2011 219th ECS Meeting, Montreal, Canada
4. Uncovering Li-Ion Diffusion near Lithium-Ion Battery Cathode Electrolytes Interface at the Nanoscale. S. Guo , T. Arruda, S. Jesse, N. Balke, S. Kalnaus, C. Daniel, S.V. Kalinin. – Spring 2011 MRS Meeting, San Francisco, CA
5. Lithium ion intercalation induced stress and fracture of active electrode material. S. Kalnaus, K. Rhodes, C. Daniel. - Fall 2010 MRS Meeting, Boston, MA
6. Investigation of lithium insertion/extraction induced morphology changes in micro-machined specimens of Li ion battery cathode material. S. Kalnaus, J. Park, S. Han, Y.K. Lee, G. Less, A.M. Sastry, N. Dudney, C. Daniel – Fall 2010 218th ECS Meeting, Las Vegas, NV.

Acknowledgment

This research at Oak Ridge National Laboratory, managed by UT Battelle, LLC, for the U.S. Department of Energy under contract DE-AC05-00OR22725, and at the University of Michigan was sponsored by the Vehicle Technologies Program for the Office of Energy Efficiency and Renewable Energy. Dual-beam FIB and electron microscopy were performed at the Shared Research Equipment Collaborative Research Center at ORNL, sponsored by the Scientific User Facilities Division, Office of Basic Energy Science.

V.E.4 Modeling – Mathematical Modeling of Next-generation Li-ion Chemistries (LBNL)

Venkat Srinivasan
Lawrence Berkeley National Laboratory
1 Cyclotron Rd. MS 70R0108B
Berkeley, CA 94720
Phone: (510) 495-2679
Fax: (510) 486-4260
E-mail: vsrinivasan@lbl.gov

Start Date: October 1, 2010
Projected End Date: September 30, 2011

Objectives

- Quantify the usefulness of alloy anodes for use in PHEVs.
- Understand the mechanical degradation in electrodes used in EVs and PHEVs.
- Model reaction distribution in battery electrodes.

Technical Barriers

Low energy efficiency; low calendar/cycle life; high cost.

Technical Targets

- Available energy: 56 Wh/kg (10 mile) and 96 Wh/kg (40 mile).
- 10-s discharge power: 750 W/kg (10 mile) and 316 W/kg (40 mile).

Accomplishments

- Quantified the maximum rate capability of thin NMC cathode at the particle scale.
- Estimated qualitatively the diffusion coefficient of lithium inside the NMC particles.
- Extended mechanical degradation model developed for graphite anode to include volume change and pressure diffusion.

✧ ✧ ✧ ✧ ✧

Introduction

Understanding fundamental properties of battery electrodes is crucial in improving battery performance and achieving DOE energy and power goals for vehicular applications. Mathematical modeling is useful for studying electrode processes and determining design parameters that give good battery performance. The primary goal of this project is to develop mathematical models for candidate Li-ion chemistries. High-rate $LiNi_{1/3}Co_{1/3}Mn_{1/3}O_2$ (NMC) and $LiFePO_4$ were selected as baseline cathode materials to study the rate performance associated with the transport limitations in various phases (solid and electrolyte) and the reaction distribution in the porous electrode. The mechanical degradation of battery anodes during cycling was also studied.

Previous continuum models described in the literature have had difficulty in predicting electrode behavior at high rates. In this past year, research has been initiated to ensure that the high-rate behavior of battery electrodes can be captured in continuum models. A single particle model was developed for thin NMC cathodes to study the rate capability when the rate limitation is purely from the transport at the particle scale. The methodology involves starting with a description of solid-phase transport and kinetics and transitioning to thick porous electrodes to describe liquid phase effects and the reaction distribution. Another model was developed to study the effect of particle size in a porous $LiFePO_4$ electrode, which exhibits asymmetric rate behavior and different charge and discharge rate capabilities. Moreover, the degradation of graphite anode was studied. The stress generated in the anode particle and the interaction between the binder and the particle were investigated to understand electrode failure during cycling.

Approach

Transport studies on NMC cathodes. Particle-scale studies were conducted on thin NMC electrodes (~6 µm) in a half-cell configuration with a Li-metal counter electrode. The thin electrodes were charged and discharged at various rates to study the rate behavior of the material. The use of thin electrode eliminates the non-uniform current distribution that is generally present in a porous electrode. For estimating the diffusion properties of the material, the electrodes were set to open circuit after discharging at a rate of 30C to specific states of charge (SOC) in order to isolate diffusion from other electrode processes. The diffusion coefficient of Li in the NMC particles was then estimated by matching the simulated and experimental potentials obtained during open-circuit relaxation.

Particle size study on $LiFePO_4$ cathodes. For studying the effect of particle size distribution in the $LiFePO_4$ system, a porous electrode model that incorporates transport in both the solid and electrolyte phases along with two particles sizes was developed. The $LiFePO_4$ system is characterized by its flat equilibrium potential. The equilibrium potential was obtained by measuring the open-circuit potential after discharging the electrode at a slow rate to a certain SOC. The measured equilibrium potential was applied in the porous electrode model to calculate the electrode potentials during charge and discharge.

Stress studies on graphite anodes. A single particle with a layer of binder was used to study the mechanical degradation of battery anodes. Equations were developed for stress generation in the particle and the interaction of stress in the active material with that in the binder. The model also considers the volume changes in the active material and pressure diffusion. Simulations were conducted to evaluate the stress in the particle and in the binder during delithiation to understand the cause of failure of the battery electrode.

Results

Transport studies on NMC cathodes. The change of electrode potential during passage of current provides an overview of the electrode behavior, such as electrode capacity and rate, and cycle performances. Figure V - 197 shows the charge and discharge curves on a thin NMC electrode measured at various rates. The charge and discharge curves were obtained in separate experiments and plotted together to compare the differences. The electrode capacity measured at the end of charge/discharge at C/25 is *ca.* 160 mAh/g. More than 50% of the capacity was still retained when discharged at rates up to 100C. This capacity retention observed on the thin NMC electrodes is much higher than that reported on the thicker electrodes made of the same material. An even higher rate capability was seen for charge cycles and a clear asymmetry between the charge and discharge was observed.

The high rate capability of the NMC electrode was explored by examining the transport properties of the material at the particle scale. Since the electrodes were made to have approximately one to two layers of NMC particles on the current collector, porous electrode effects are minimized. The NMC particle is assumed to be a nonporous sphere and to be representative of the whole electrode. The diffusion of Li inside the NMC particle is assumed to be the limiting process of the intercalation reaction and is described by Fick's second law. Figure V - 198 shows the estimated Li diffusion coefficients at various states of charge. The diffusion coefficient is strongly dependent on Li concentration. The increasing diffusion coefficient with increasing SOC also explains the asymmetry of electrode utilization between charge and discharge as seen in Figure 2. The strong dependency of Li diffusion coefficient on its concentration suggests that the use of a varying diffusion coefficient is necessary for studying the transport processes in insertion materials and for further application to the macroscopic porous electrode.

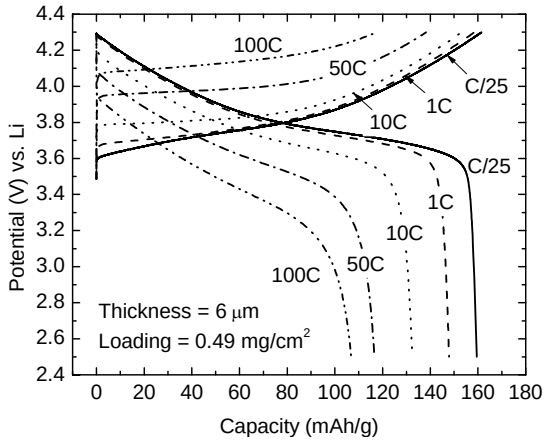

Figure V - 197: Experimental charge and discharge curves on a NMC thin electrode (~6 μm) at various rates. The charge and discharge curves, obtained in separate experiments, are plotted together to compare the differences.

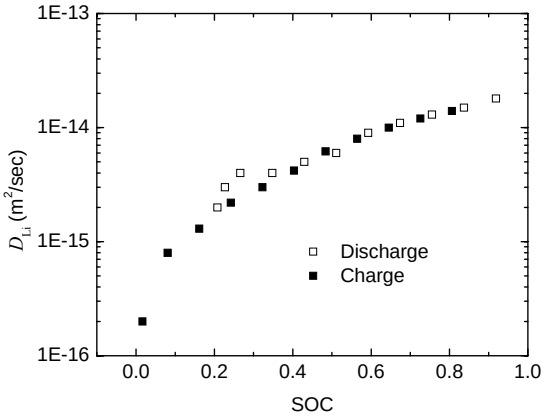

Figure V - 198: Estimated lithium diffusion coefficient as a function of state of charge (SOC). The charge data (■) was obtained by charging the electrode with several current interruptions, and the discharge data (□) was obtained by discharging the electrode with several current interruptions to estimate the diffusion coefficients at various SOC.

Particle size study on $LiFePO_4$ cathodes. During discharge, the smaller particles lithiate at a higher rate than the larger particles. The self-regulating mechanism does not exist in the flat-potential system, and therefore there is a disparity in the level of lithiation between the small and large particles. During charge, on the other hand, the smaller particles delithiate at a higher rate and have smaller Li content. The path dependency on the amount of

Li in particles of different sizes has consequences in the rate behavior of the electrode.

Figure V - 199 shows that the electrode charged from the fully-discharged state has a much higher capacity than the electrode discharged from the fully-charged state. This result provides an explanation for an experimental observation first reported by our group. Model results suggest that the difference in electrode capacity is more pronounced for electrodes where the particle sizes are very different in a bimodal distribution.

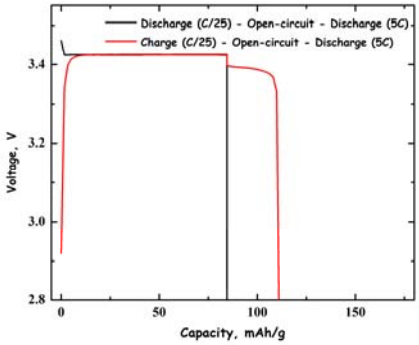

Figure V - 199: Model results that show a difference in rate capability depending on the previous cycling history. The electrode is taken to 50% SOC from either the fully-charged state (black line) or from the fully-discharged state (red line) at a rate of C/25. The electrode is then subjected to open-circuit relaxation, after which a high rate (5C) discharge is conducted.

Stress studies on graphite anodes. Experimental data obtained both at LBNL and by other research groups show that electrode failure is not dominated by particle cracking alone, but is also related to the interaction of binder with the particle. Figure V - 200 shows the calculated stress in the graphite and the binder as a function of discharge rate. The stress in the active material and the binder increases with increasing discharge rate. The graph also marks the strength of the two materials taken from the literature. The simulation shows that the graphite particles are expected to crack when discharging at a rate approaching 2C. However, the strength of binder is exceeded at a comparable rate (3C). The closeness of the rates at failure suggests that both failure of the active material and of the binder needs to be taken into account.

Conclusions and Future Directions

Experimental results obtained from the thin NMC electrodes show that the material is capable of fast charge and discharge, exceeding 100C, and has good capacity retention. The remarkably high rate capability of this chemistry has not been reported previously, and has also not been reported on thicker electrodes. The use of a thin electrode minimized the effect of porous electrode. Therefore, the limitation in the system is attributed only to the transport process inside the particles. The experimental results indicated that the large capacity retention is an inherent characteristic of the material. Therefore, the rate capability of thick electrodes must be associated with the porous structure of the electrodes.

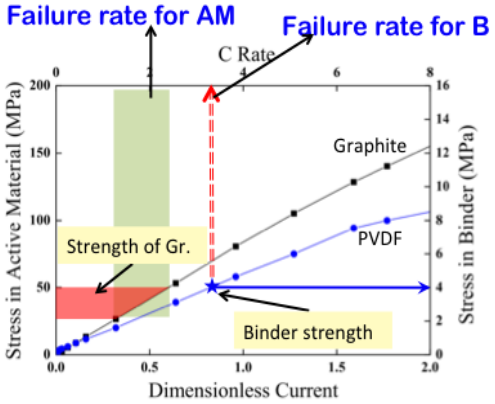

Figure V - 200: Calculated stress in graphite active material (AM) and PVdF binder (B) as a function of discharge current.

Further studies will focus on porous-electrode scale to investigate the transport of Li ions through tortuous pores in the porous electrode. The estimate of the Li diffusion coefficient provides a basic description of the diffusion of Li inside the NMC particles with respect to SOC. This result will then be carried forward to study thick porous electrodes in order to examine the limitations due to the solution phase.

The modeling of electrode behavior in the $LiFePO_4$ system using a two-particle size distribution suggests that there is a path dependency in lithiation and delithiation during charge and discharge. The electrode showed a larger capacity when it was charged from a fully-discharged state. This hysteresis effect has consequences in understanding the rate behavior of all flat-potential systems and will be investigated in detail.

The modeling of battery anode degradation shows that both failure of the binder and of the active material needs to be taken into account. Simulations can be extended to Si anodes to include the effect of mechanical stress and interaction with binder. The effect of different binders on degradation and the debonding from the anode particle surface will also be considered in future studies.

FY 2011 Publications/Presentations

1. S.-L. Wu, W. Zhang, G. Liu, V. Battaglia, and V. Srinivasan, "High Rate Capability of $Li(Ni_{1/3}Co_{1/3}Mn_{1/3})O_2$ Electrode," presented at the 220th Meeting of The Electrochemical Society, Boston, MA, October 9-14, 2011.
2. S.-L. Wu, W. Zhang, X. Song, A.K. Shukla, G. Liu, V. Battaglia, and V. Srinivasan, "High Rate Capability of $Li(Ni_{1/3}Co_{1/3}Mn_{1/3})O_2$ Electrode for Li-Ion Batteries," *J. Electrochem. Soc.*, submitted and under review

V.E.5 Analysis and Simulation of Electrochemical Energy Systems (LBNL)

John Newman
Lawrence Berkeley National Laboratory
306 Gilman Hall
University of California, Berkeley
Berkeley, CA 94720
Phone: (510) 642-4063; Fax: (510) 642-4778
E-mail: newman@newman.cchem.berkeley.edu

Start Date: October 1, 2010
Projected End Date: September 30, 2011

Objectives

- Develop experimental methods for measuring transport, thermodynamic, and kinetic properties.
- Model electrochemical systems to optimize performance, identify limiting factors, and mitigate failure mechanisms.

Technical Barriers

This project addresses the following technical barriers from the USABC:

(A) Capacity and power fade

(B) Safety and overcharge protection

Technical Targets

This project contributes to the USABC Requirements of End of Life Energy Storage Systems for PHEVs and EVs:

- 300,000 shallow discharge cycles
- 15 year calendar life

Accomplishments

- Developed both steady-state and transient methods to characterize the SEI using through-film reduction kinetics of ferrocene
- Expanded ferrocene characterization method from model surface (glassy carbon) to highly-oriented pyrolytic graphite, a more realistic battery material (collaboration with Takeshi Abe, Kyoto University)

✧ ✧ ✧ ✧ ✧

Introduction

Our main project in FY10 was the experimental study of SEI formation reactions and the interaction of the SEI with redox shuttles. Our novel method of SEI characterization contributes to understanding of passivation in nonaqueous electrolytes, which is in turn critical to battery performance and lifetime. While FY09 was spent primarily on the development of reproducible experimental methods, FY10 saw both experimental refinement and the development of theoretical tools for data analysis. Additionally, we began to expand our studies from glassy carbon, a model surface, to highly-oriented pyrolytic graphite (HOPG), which more accurately resembles the carbon found in a lithium-ion battery.

Approach

- Utilize classical electrochemistry experiments to understand the fundamental growth kinetics of the SEI, as well as how it interacts with a redox shuttle.
- Measure shuttle reduction kinetics in the presence and absence of passivating films to determine the relative transport and kinetic inhibitions to reaction.
- Use a rotating-disk electrode (RDE) to measure the steady-state through-film reduction current, and electrochemical impedance spectroscopy (EIS) to measure the frequency response of the ferrocene reaction in the presence and absence of the SEI.

Results

1. Steady-state characterization. Steady-state measurements and model fits are shown in Figure V - 201. The markers show the current measured at 900 rpm after films were built on the electrode for 30 seconds, 6, 30, and 60 minute holds at 0.6 V. Dashed lines are model fits to the passivated current, and the dotted line is the reversible current, which is seen on the clean electrode. Current decreases with passivation time because the electrode has had longer to grow a "thicker" film. The model includes only three adjustable parameters: a transfer coefficient α, an exchange current density i_0, and a through-film ferrocene limiting current i_{lim}, given below.

$$i_{\lim} = \frac{-FD_{O,f}\varepsilon C_O^{bulk}}{L}$$

$$i_0 = k\varepsilon (C_O^{bulk})^{\alpha_c} (C_R^{bulk})^{\alpha_a}$$

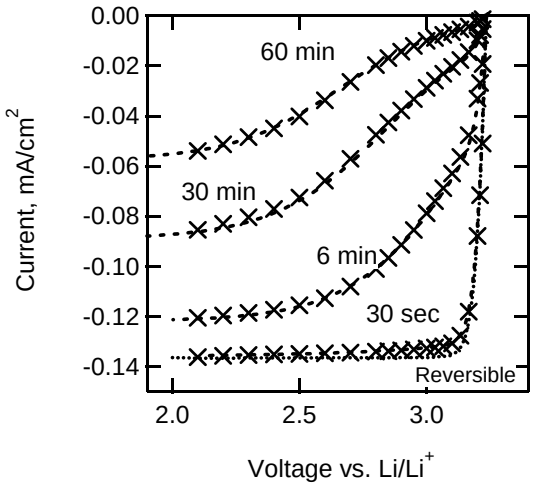

Figure V - 201: Steady-state current vs. voltage after different lengths of passivation holds. Markers are measurements, dashed lines are model fits. Both the exchange current density i_0 and the through-film limiting current i_{lim} decrease. Data is measured at 900 rpm with 1.1 mM ferrocene/ferrocenium hexafluorophosphate.

The shape of the curve between 3.15 and 2.5 V is given by α and i_0. i_{lim} is determined from the limit as the curve approaches very low voltages. Both i_0 and i_{lim} decrease with increased passivation time, and because both expressions contain the porosity ε, a possible explanation may be that longer formation times cause thicker but also less porous films.

2. Impedance characterization. Figure V - 202 shows impedance measurements of the same films as in Fig. 1 at open circuit potential and 900 rpm. Each spectrum exhibits two arcs. The high-frequency arc depends on passivation time, but the low-frequency arc does not. The high-frequency arc width increases with more passivation time. Plotting the imaginary component vs. frequency (Figure V - 203) shows that, similarly, the low-frequency peak is independent of passivation time, but the high-frequency peak decreases with passivation time. The peak frequency corresponds to the reciprocal of the time constant of the system, $\tau = R_{ct}C_{dl}$, where R_{ct} is the charge-transfer resistance and C_{dl} is the double-layer capacitance. As formation time increases, the time constant increases, corresponding to a higher charge-transfer resistance or a slower reaction. These observations agree qualitatively with the steady-state findings.

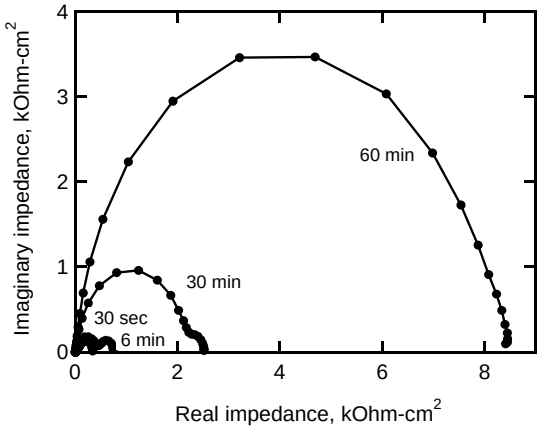

Figure V - 202: Nyquist plot of electrode after different lengths of passivation holds. Longer passivation times cause higher impedance.

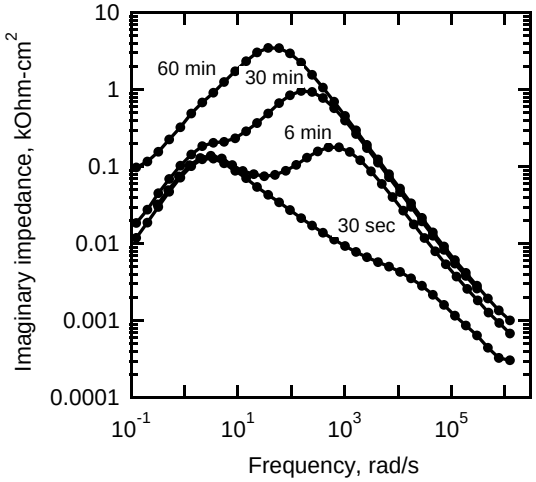

Figure V - 203: Bode plot of electrode after different lengths of passivation holds. The high-frequency peak depends on passivation time, but the low-frequency peak does not.

3. Effect of HOPG orientation. Although comparison of the experimental EIS data with a physics-based model shows that EIS does not provide as unique a fit as the steady-state measurements, the indicators of high-frequency arc width and time constant agree qualitatively with steady-state results. Impedance also has significant experimental advantages over the rotating disk electrode; it is faster, uses less material, and is less subject to variations in temperature and bulk concentration. Most importantly, it permits the use of more materials, including those actually found in lithium-ion batteries. Previous work has found that the SEI formation reactions may differ substantially on the edge and basal planes of graphite; accordingly, the current task is to use the method developed in this work to study how passivation differs with graphite orientation. A preliminary result from this study is shown in Figure V - 204. Two samples of HOPG, one with an edge fraction of 0.06 (primarily the basal surface exposed) and the other with an edge fraction of 0.6 (primarily the edge fraction exposed)

were cycled from 3.7 to 0.1 V vs. Li/Li^+ in a solution of 2 mM ferrocene in 1.0 M $LiPF_6$ in EC:DEC in order to form an SEI. The impedance spectra at open circuit were measured both before and after cycling. Figure V - 204 shows that, before SEI formation, impedance spectra on both samples exhibit a straight line of approximately 45° slope without any high-frequency semicircles (dashed lines). The two dashed lines collapse because the kinetics are fast on both the edge and basal plane. After SEI formation, both samples show an increased impedance, but the impedance on the edge plane is much higher than that on the basal plane, despite higher electronic activity on the edge plane. More work is required to confirm and explain the results shown in Figure V - 204. However, these preliminary results demonstrate the ability of the developed method to characterize materials found in actual batteries.

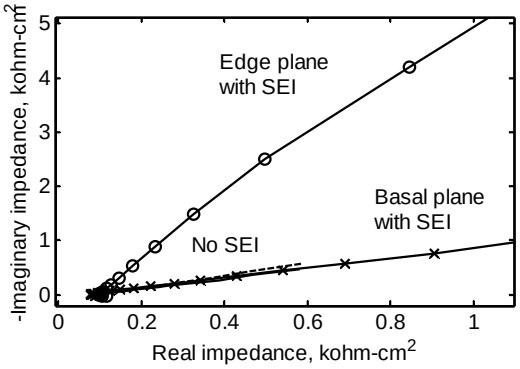

Figure V - 204: Comparison of through-film ferrocene impedance on the edge and basal planes of graphite.

Conclusions and Future Directions

Both RDE and EIS studies on the reduction of ferrocene will continue. The described work has studied the SEI formed at 0.6 V versus lithium; we are currently expanding our studies to the effects of formation voltage and electrode rotation during SEI formation. We also are continuing our work on HOPG to see how the electrochemical behavior of the SEI differs with graphite orientation. The experimental parameters that we are varying include the sweep rate for potentiodynamic formation and the formation voltage. Additionally, preliminary results have shown major differences in behavior with different anions; we plan to investigate this phenomenon further, undertaking non-electrochemical characterization if necessary.

FY 2011 Publications/Presentations

1. M. Tang and J. Newman, *J Electrochem. Soc*. 158 (5) A530-A536, 2011.
2. A. Teran, M. Tang, S. Mullin, N. Balsara, *Solid State Ionics*, in press.
3. M. Tang and J. Newman, *ECS Meeting Abstracts*, 1102 348 (2011).

V.E.6 Investigation of Critical Parameters in Li-ion Battery Electrodes (LBNL)

Jordi Cabana
Lawrence Berkeley National Laboratory
1 Cyclotron Rd. MS62R0203
Berkeley, CA 94720-8168
Phone: (+1) 510-486-7097
Fax: (+1) 510-486-8097
e-mail: jcabana@lbl.gov

Start Date: September 2009
Projected End Date: September 2011

Objectives

- Establish chemistry-structure-properties correlations that aid in the design of better materials active at high voltages (>4.5 V).
- Synthesize materials with controlled crystal-chemistry and microstructure.
- Assess origins of in-cycle and cycling inefficiencies in positive electrode materials reaction at high voltages.
- Develop methods to couple electrode performance and transformations at multiple length scales.

Technical Barriers

- Low energy-density, poor cycle life, safety.

Technical Targets

- PHEV: 96 Wh/kg, 5000 cycles; EV: 200 Wh/kg; 1000 cycles.

Accomplishments

- $LiNi_{0.5}Mn_{1.5}O_4$ was found to crystallize in a variety of schemes with different Ni/Mn ordering. Some samples showing unit cell superstructures were still found to have different levels of Ni/Mn mixing. NMR and neutron diffraction (ND) have been established as the best tools to characterize ordering in this material.
- Mn over-stoichiometry was found in all $LiNi_{0.5}Mn_{1.5}O_4$ samples made, but no evidence of O vacancies. Mn^{3+} observed in the cycling profile is due to a preferential segregation of Ni in a rock salt impurity, which also contains Mn.
- Amounts of impurity and Mn^{3+} increase with synthesis temperature. Impurity is detrimental to performance; needs to be minimized during material preparation.
- Developed a μ-XAS method to evaluate charge distribution with high spatial resolution. Analyzed discharge inefficiency dependence on rate for conversion model system.

✧ ✧ ✧ ✧ ✧

Introduction

Finding Li-ion battery electrode materials that can bring about increases in energy is a critical need if the social impact of their use in electric vehicles is to meet expectations. In order to fulfill this goal, the following strategies can be envisaged: i) raising the voltage of operation of the battery by using electrodes that react at very high and very low potentials, respectively, and/or ii) improving the storage capacity by switching to alternative electrode materials that can exchange a larger amount of electrons/Li^+ ions. Yet these changes cannot come with a penalty in terms of device safety and cycle life of the device, which implies that the mechanisms of their reaction with lithium need to be well understood in order to locate possible sources of failure.

Spinel-type $LiNi_{0.5}Mn_{1.5}O_4$ is a promising candidate for the positive electrode because lithium is extracted at very high potentials (around 4.7 V vs. Li^+/Li^0), concomitant to the oxidation of Ni^{2+} to Ni^{4+}. While very high rate capability has been reported in several cases, it has not been fully ascertained what the role is of the crystal-chemistry of the compound, such as metal ordering and the existence of impurities of Mn^{3+} in the spinel and segregated rocksalt particles. During FY2010, it was determined that nanostructuring is not necessary to get satisfactory performance with this material. During FY2011, we proceeded to investigate the crystal-chemistry-properties correlation.

Some gaps in the knowledge of how batteries operate still remain. One example of these gaps is the difficulty in probing charge distribution within battery electrodes. These electrodes are usually composites of the electrochemically active material with carbon and a polymer binder to form a flexible film that is several tens of microns thick, in which homogeneity and porosity are the key for good electrical contact, electrolyte wetting and mechanical properties. Non-uniformities in the state of charge may impact performance in a variety of ways, including reduced energy and power, underutilization of capacity, localized heat generation, and overcharge or overdischarge. Since reactions at an electrode involve redox phase transformations, the state of charge can easily be correlated to composition. Several models exist that

can simulate or fit macroscopic data to extract current distribution information. However, direct visualization of phase distribution, which could be used to validate them, is hindered by the fact that large areas need to be analyzed to get representative trends, yet inhomogeneities may occur at a very local scale. The thickness of the electrodes also often requires their destruction during the sample preparation process to get measurable signals, resulting in loss of information. Yet such information would have an immediate impact on the application, as it would identify sources of inefficiencies during the electrode manufacturing process. Therefore, the need arises for tools that can probe electrodes directly extracted from cells, covering areas of several tens of microns, even millimeters, at high spatial resolution, in reasonable time. The development as μ-XAS as a tool to probe charge distributions within large electrode (>1 mm) areas was accomplished during FY2011.

Approach

A systematic study of $LiNi_{0.5}Mn_{1.5}O_4$ made from the same precursors, but heat-treated at different temperatures (500-1000°C), was performed. The aim was to understand the correlation between crystal structure, microstructure, composition and electrochemical performance in $LiNi_{1/2}Mn_{3/2}O_4$. The changes were studied by coupling the information of several characterization techniques: TEM, SEM, X-ray absorption spectroscopy, NMR and neutron diffraction. Their electrode performance was evaluated at moderate and high rates. This work was carried out under a Focus Group within BATT devoted to this material.

In order to characterize electrode materials at multiple length scales, tools based on synchrotron radiation were used. In particular, a setup that enables a combination of X-ray absorption spectroscopy and imaging was used to evaluate charge distribution inhomogeneities at micron scales. The ultimate goal is to analyze chemical changes at interfaces, surface and bulk of materials.

Results

A combination of neutron powder diffraction and ^6Li magic angle spinning NMR data indicates that the temperature at which $LiNi_{0.5}Mn_{1.5}O_4$ is made has a critical impact on the location of Ni and Mn in the spinel structure. A two-step disorder-to-order followed by order-to-disorder transition was observed around 700°C (

Table V - 7). Samples made at 100°C above and below 700°C exhibited structures with short range Ni-Mn clustering, whereas the samples made at lower or higher temperatures were largely disordered. However, it was found that even the sample made at 700°C showed some degree of Ni-Mn exchange within the sites of a spinel superstructure.

Table V - 7: Results of the Rietveld refinement of neutron diffraction data combined with transmission electron microscopy.

Sample	Spinel		Rock salt	
	composition	Cell parameter	composition	Cell parameter
OH500	$LiMn_{1.56}Ni_{0.44}O_4$	a=8.1652(1)		
OH600	$LiMn_{1.55}Ni_{0.45}O_4$	a=8.1646(1)		
OH700	$LiMn_{1.53}Ni_{0.47}O_4$	a=8.16439(8) $P4_332$		
OH800	$LiMn_{1.55}Ni_{0.45}O_4$	a=8.1696(1)	$Li_{0.4}Mn_{0.4}Ni_{0.2}$	a=4.151(2)
OH900	$LiMn_{1.57}Ni_{0.43}O_4$	a=8.2006(8)	$Li_{0.4}Mn_{0.4}Ni_{0.2}$	a=4.142(2)
OH1000 *both phases strongly correlated	$LiMn_{1.67}Ni_{0.33}O_4$	a=8.2866(1)	$Li_{0.4}Mn_{0.36}Ni_{0.24}$	a=4.1473(2)

Rietveld refinement of ND patterns revealed the existence of an impurity with a rocksalt structure. This impurity was found to increase with temperature, constituting a significant amount of the sample made at 1000°C. TEM showed that this impurity tends to segregate at the surface of the particles (Figure V - 205) and has a composition close to $(Li_xMn_{0.66}Ni_{0.34})_yO$. Therefore, the Ni/Mn ratio in it is larger than in the original

formulation for $LiNi_{0.5}Mn_{1.5}O_4$. This observation implies that the real composition in the spinel phase is Ni-defficient. Attempts to introduce O vacancies in the refinements to compensate this deficiency were unsuccessful. It is concluded that it is compensated by the partial reduction of Mn^{4+} to Mn^{3+}, in agreement with XAS and electrochemical data.

The electrochemical performance of all samples was evaluated. The best results were obtained for the sample made at 900°C, which shows structural disorder, some Mn^{3+} and large particle size. The worst performance at all rates was obtained for the sample made at 1000°C Figure V - 205). Since this sample contains the largest amount of rocksalt impurity, it is concluded that this phase is not active and very detrimental to electrode performance.

Beamline 10.3.2 at the ALS allows the acquisition of XAS maps of large areas at high spatial resolution (<3 μm). In addition, 10.3.2 is equipped with three different detectors (transmission, fluorescence and electron yield) which are sensitive to different sample depths, thereby providing an easy way of probing electrodes along multiple dimensions. Proof of concept of the power of these tools for the detection of homogeneities in Li-ion battery electrodes is shown for partially reduced NiO (to Ni^0 and Li_2O) electrodes (Figure V - 206). Compositional inhomogeneities were observed at regions of several micrometers along the top of an electrode at 50% discharge at C/20. Comparison of the results from fluorescence and electron yield show that these inhomogeneities also have a depth component, with the electrode being at a more reduced step on the surface. These inhomogeneities are aggravated with rate; a sample discharged at 1C rate showed regions of several microns that were almost intact, next to regions that were close to 100% discharged. These inhomogeneities can be linked to the poor cycle life shown by electrodes based on conversion reactions, which make them technologically unviable.

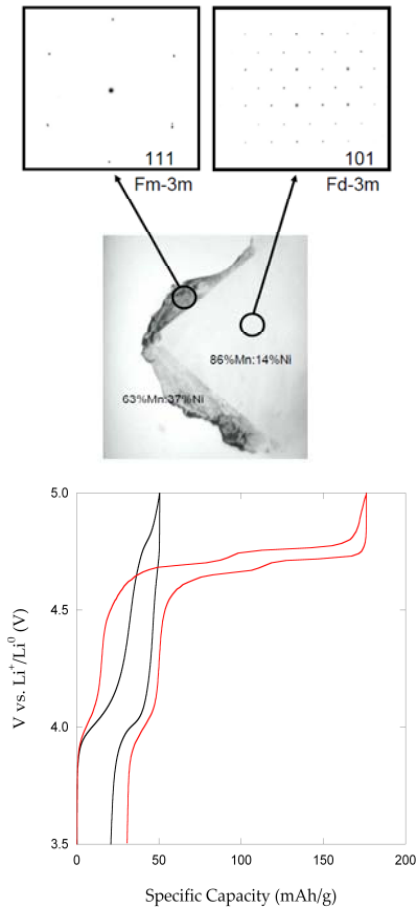

Figure V - 205: (Left bottom) Bright field image of a $LiNi_{0.5}Mn_{1.5}O_4$ particle containing different crystallites. (Left top) Electron diffraction patterns of each crystallite, showing the structure of a rock salt and a spinel phase, respectively. (Right) First cycle of a $LiNi_{0.5}Mn_{1.5}O_4$ made at 900°C (red) and 1000°C (black).

Conclusions and Future Directions

A systematic study of the effect of synthesis temperature on the cation ordering, composition and impurities for $LiNi_{0.5}Mn_{1.5}O_4$ was carried out. The results show that the samples with the best electrochemical performance have large particle sizes combined with structural disorder and the presence of some Mn^{3+}. However, rocksalt impurities should be minimized, as they are inactive and cripple the electrode performance. Therefore, the synthesis temperature should be chosen with this compromise in mind.

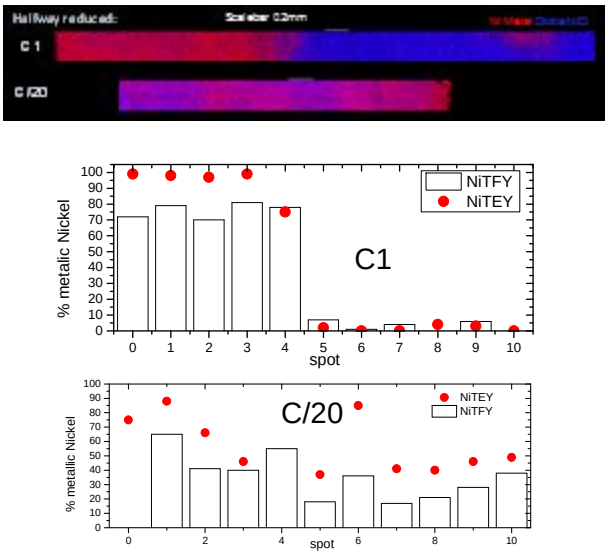

Figure V - 206: (Top) μ-XAS map of NiO electrodes reduced halfway at C/20 and 1C rate. (Bottom) %Ni^0 resulting from the linear combination fit of XANE spectra at different points on the map.

A method based on μ-XAS was developed to evaluate charge distribution in composite electrodes with high spatial resolution. Proof of concept was demonstrated with NiO electrodes that were partially converted to Ni. Severe inhomegeneities were found in all dimensions as the rate of cycling was increased. More broadly, this work proves that the three dimensions of these complex electrode structures can be studied with this methodology. Because XAS is sensitive to the very local changes of oxidation state, its use could be extended to virtually any battery electrode system, including those that undergo amorphization during cycling.

A natural continuation of the work in FY2011 would be to further study samples of $LiNi_{0.5}Mn_{1.5}O_4$ in which crystal-chemistry effects are decoupled from particle size. This goal can be achieved by following different annealing procedures. A plan is in place to use synchrotron-based tools to understand the reactivity of the surfaces of the material toward the electrolyte and identify active species. In parallel, the power of μ-XAS to study battery electrodes will be extended to systems that are relevant to application, such as high voltage cathodes or high capacity alloy-based anodes.

FY 2011 Publications/Presentations

1. 2011 DOE Annual Peer Review Meeting Presentation.
2. J. Cabana, J. Shirakawa, M. Nakayama, M. Wakihara and C. P. Grey. J. Mater. Chem. **2011**, 21, 10012-10020.
3. J. Cabana, H. Zheng, A. K. Shukla, C. Kim, V. S. Battaglia, M. Kunduraci. J. Electrochem. Soc. **2011**, 158, A997–A1004.
4. J. Cabana, L. Monconduit, D. Larcher, and M. R. Palacín. Adv. Mater. **2010**, 22, E170-E192.
5. *Analysis of the mechanism of conversion and the microstructural changes upon cycling of high capacity NiO electrodes*. 2010 MRS Fall Meeting. Boston, MA, Nov. 29th-Dec. 2nd, 2010.
6. *Crystal and Microstructure Characterization of $LiNi_{1/2}Mn_{3/2}O_4$ as a High Voltage Positive Electrode for Li batteries*. 2010 MRS Fall Meeting. Boston, MA, Nov. 29th-Dec. 2nd, 2010.
7. *Understanding how Li-ion Batteries Operate Using in and* ex situ *Synchrotron-based Techniques*. 2010 LCLS/SSRL Users' Meeting. Menlo Park, CA, Oct. 17th-21st, 2010.
8. *Understanding how Li-ion Batteries Operate Using in and* ex situ *Synchrotron-based Techniques*. 2010 LCLS/SSRL Users' Meeting. Menlo Park, CA, Oct. 17th-21st, 2010.
9. *Spectroscopic and imaging study of high capacity Li-ion battery electrodes based on conversion reactions*. 2010 ALS Users' Meeting. Berkeley, CA, Oct. 13th-15th, 2010.
10. *Toward High Energy Density Li-ion Batteries. Understanding the Key Parameters for Performing Electrode Materials*. 2010 TMF and NCEM Users' Meeting. Berkeley, CA, Sept. 30th-Oct. 1st, 2010.

V.E.7 Modeling - Predicting and Understanding New Li-ion Materials Using Ab Initio Atomistic Computational Methods (LBNL)

Kristin Persson (Staff Scientist, LBNL)

Lawrence Berkeley National Laboratory
Advanced Energy Technology
1 Cyclotron Rd, MS 70R0108B
Berkeley, CA 94720
Phone: (510) 486-7218
E-mail: kapersson@lbl.gov

Start Date: September 2008
Projected End Date: September 2010

Objectives

- Predict new chemistries and crystal structures for improved electrodes as defined by the goals of USABC.
- Understand rate-limiting behavior in current electrode materials in order to target and design optimal diffusion properties in new materials.

Technical Barriers

Investigating electrode materials with atomistic modeling require rigorous benchmarking as well as insight into the materials chemistry and its effect on electrode performance. Futhermore, the relevant surfaces of the electrodes are generally not well characterized in terms of chemistry and structure. Both the cathode materials as well as the graphitic anode have solid electrolyte interfaces (SEIs) that depend on the synthesis conditions as well as the electrolyte composition and the conditions under which the battery is operated. Our team systematically benchmarks the calculations and monitors the assumptions under which the modeling is done to make sure that the results are relevant and provide useful information and insights for electrode materials design.

Technical Targets

- Understand the rate limiting bottlenecks in the carbon materials for the negative electrode.
- Investigate the origin of the electrochemical signature of ordered and disordered high-voltage spinel.
- Create an automated high-throughput materials design environment at LBNL.

Accomplishments

- We have evaluated graphite surfaces for Li absorption and found that, while the [0001] surface is the most stable surface facet – it does not absorb Li in its perfectly crystalline defect-free state.
- We have identified the origin of the different electrochemical profiles in ordered and disordered $Li_xNi_{0.5}Mn_{1.5}O_4$ spinel.
- We have successfully launched the first Google-like materials search engine from LBNL/MIT. The web site contains over 15,000 computed compounds for general searches as well as a structure prediction application and a Li-battery electrode materials explorer.

✧ ✧ ✧ ✧ ✧

Introduction

There is increasing evidence that many of the performance limiting processes present in electrode materials are highly complex reactions occurring on the atomic level. The Persson group at LBNL is studying these processes using first-principles density-functional theory (DFT) modeling tools. By understanding the underlying reasons for the electrode materials performance we can suggest improvements or design schemes directed at the root cause of the process.

Last year our group together with the Kostecki group at LBNL showed excellent inherent diffusivity of Li in graphite. However, most carbons exhibit sluggish kinetics, which caused our group to look to the graphite surfaces for the kinetic bottleneck in Li intercalation. We have now found the most stable surface in graphite – the 0001 facet – does not absorb Li in its perfectly crystalline defect-free state. This presents a significant kinetic bottleneck for Li intercalation.

This year we have also joined the BATT focus group on the high-voltage spinel. In this context we have used first-principles calculations and analyses on the high voltage $Li(Ni_{0.5},Mn_{1.5})O_4$ spinel to explain the relationship between cation interactions, ordering and structure and their effect on the materials performance. Our work unravels a complicated coupling between the Li arrangement and the underlying cation lattice, which

results in a different response of the material when synthesized under different conditions.

Approach

The Persson group uses atomistic modeling to study the relevant thermodynamic and kinetic processes. The calculations are performed on the Lawrencium cluster at LBNL and at NERSC. In the case of the high voltage spinel we have used first-principles zero-temperature calculations and a coupled cluster expansion to establish the relationship between the cation order and the electrochemical signature of the materials.

For the investigation on the Li-carbon system we are using a combination of DFT to describe the low temperature characteristics of the material as well as statistical mechanics to calculate the phase diagram and the Li chemical diffusivity and phenomenological models to capture the van der Waals interactions.

Results

$Li_xNi_{0.5}Mn_{1.5}O_4$ Spinel. As part of the high-voltage spinel focus group effort we have investigated the cation ordering influence on the stable ground states as a function of Li content in $Li_x(Ni_{0.5}Mn_{1.5})O_4$. Previous work has shown that the voltage profile is generally much more flat in the spinel where Ni (Mn) sits exclusively at 4b (12d) sites compared to the structure where both sites are occupied randomly by Ni or Mn. Our study unequivocally shows how the preferred Li-Vac arrangement is incommensurate with the cation ordering in the ordered spinel, which results in an absence of intermediate Li concentration ground states. However, for uniformly disordered spinel the cation arrangement accommodates the preferred Li-Vac arrangement, which is exhibited in a strong ground state at half lithiated composition. Figure V - 207 shows the predicted voltage profiles for several cation orderings. The uniformly disordered (blue) corresponds to the highest entropy achievable and exhibits a strong ground state at x = 0.5. A perfectly ordered spinel (red) is expected to exhibit only a combination of the two end states at any Li content, devoid of any intermediate ground state as a function of lithium content.

Li-Carbon. We have concluded our study of Li absorption on graphite surfaces. We have found, in agreement with experimental evidence, that the 0001 surface is the most thermodynamically stable surface. More surprisingly we also found that Li does not absorb on the predominant 0001 surface, if that surface is defect-free.

Furthermore, we have studied the Li absorption and intercalation as a function of increasing number of layers of graphene and Li content. The challenge has been to obtain the correct van der Waals interaction as a function of Li content, especially in the low lithiation regime. We have been exploring the Grimme formulation[24] of the van der Waals potential, which requires tuning to obtain the correct order of magnitude and dissipation, see Figure V - 208.

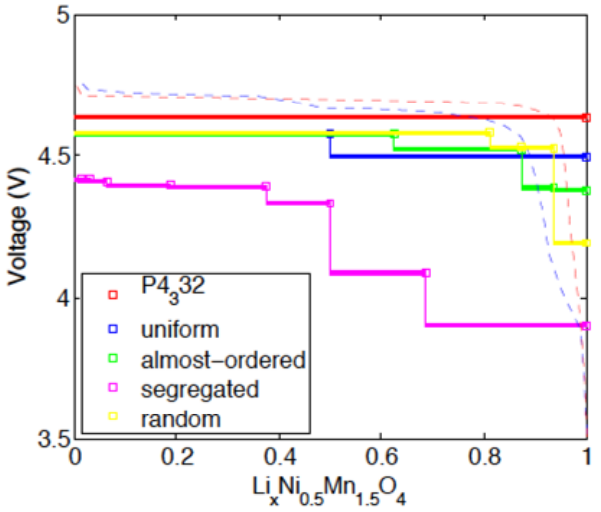

Figure V - 207: The voltage profiles for ordered (red) and 4 different disordered' (yellow, green, blue and magenta) versions of $Lix(Ni_{0.5}Mn_{1.5})O_4$.

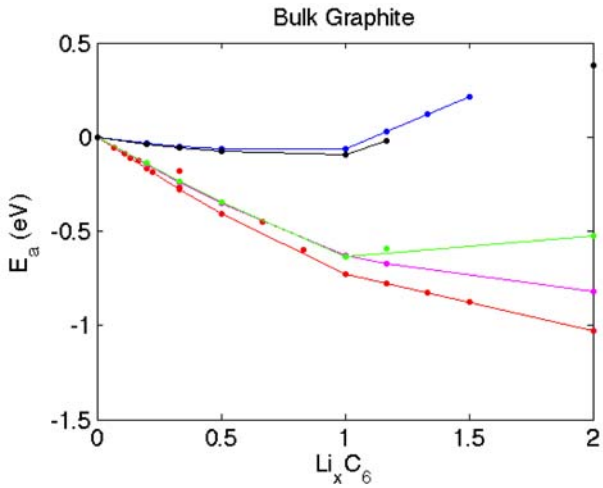

Figure V - 208: Tuning the Li-C absorption energy as a function of Li content using the Grimme vdW formulation.

The Materials Project. To the conclusion of a milestone for 2011, we successfully launched the first Materials Project web site and database. The web site provides free searchable access to general materials properties covering >15,000 inorganic compounds and the number of compounds increases continuously. The site contains tools ('apps') designed to aid in materials design for specific application areas such as Li-ion battery technology. Figure V - 209 shows the announcement featuring many of the possible search capabilities of the web site – among them an example electrode material with its computed voltage profile and oxygen evolution as a

[24] S. Grimme, J. Comp. Chem. 27, 1787 (2006).

function of charge. The Materials Project continues to compute more properties and materials – both known and unknown.

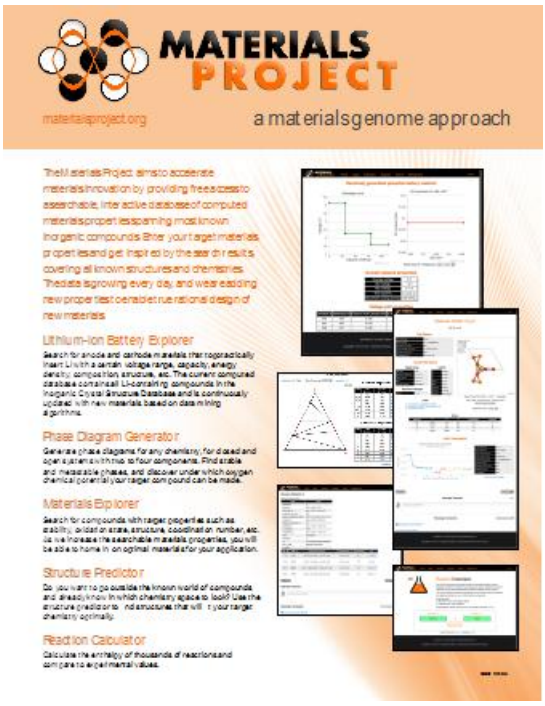

Figure V - 209: Announcement of the Materials Project www.materialsproject.org

Conclusions and Future Directions

For the high voltage spinel system we have quantitatively demonstrated the incommensurateness between the preferred Li/VA configuration and the Ni/Mn configuration in the ordered cation configuration, which explains the observed negligible voltage step at x = 0.5 in the ordered compared to the disordered spinel. For the uniformly disordered cation configuration we predict one strong ground state at x = 0.5 which agrees with experimental observations. Thus, in the case of the high-voltage spinel we find that the cation ordering determines the stable Li orderings, which, in turn, yields the phase transitions as the system undergoes lithiation.

For graphitic carbons we have found that the 0001 surface is the most thermodynamically stable surface. We also found that Li does not absorb on the predominant 0001 surface, if that surface is defect-free. Therefore, to optimize rate performance in graphitic anodes, our findings suggest to increase the fraction of edge-planes, which are exposed to the electrolyte.

For future directions we are investigating surface properties of the spinel systems as well as continueing to study the carbons for Li kinetics.

FY 2011 Publications/Presentations

1. M. Kocher and K. Persson, Li Mobility and the Electronic Structure of $LiMn_{1/3}Ni_{1/3}Co_{1-x}Al_xO_2$ Determined from First-Principles, Submitted to Phys Rev B 2011
2. G. Grimvall, B. Magyari-Kope, V. Ozolins, and K. Persson, Lattice instabilities in metallic elements, Submitted to Reviews of Modern Physics 2011
3. A. Jain, G. Hautier, S. P. Ong, C. J. Moore, C. C. Fischer, K. A Persson and G. Ceder, Formation enthalpies by mixing GGA and GGA plus U calculations, Phys Rev B **84** (4), 045115 (2011).
4. A. Jain, G. Hautier; C. J. Moore, S. P. Ong, C. C. Fischer, T. Mueller, K. A. Persson; G. Ceder, A High-Throughput Infrastructure for Density Functional Theory Calculations, Computational Materials Science, **50** (8), 2295-2310, (2011).
5. K. Persson, Y. Hinuma, Y. S. Meng, A. Van der Ven' and G. Ceder' Thermodynamic and Kinetic Properties of the Li – Graphite System from First-Principles Calculations, Physical Review B **82**, 125416, 2010.
6. 2009 DOE Annual Peer Review Meeting Presentation.
7. Li-ion Battery Electrode Materials Design from First-Principles Calculations, APS in Dallas, 2011 (Invited)
8. First-Principles Calculations for Energy Storage Applications for Transportation, AAAS in Washington, 2011 (Invited)
9. The Li-Graphite System from First-principles, PPSS in Hawaii, 2011 (Invited)
10. First-principles calculations of Li migration in Li battery electrode materials, Gordon Conference 2010 (Contributed)
11. Surfaces of Electrode Materials in Equilibrium with Water from First Principles, ECS in Las Vegas, 2010 (Contributed)
12. First Principles Calculations of Li Migration in Li Battery Electrode Materials, MRS in San Francisco 2010 (Invited)
13. Predicting Solid - Aqueous Equilbria for Materials Design, TMS Hume-Rothery Symposium Seattle 2010 (Invited)
14. Ab Initio Prediction of Nano-Sized Pt Stability in Solution, ECS San Francisco, 2010 (Contributed).

V.E.8 New Electrode Designs for Ultra-high Energy Density (MIT)

Yet-Ming Chiang

Massachusetts Institute of Technology
Department of Materials Science and Engineering
Room 13-4086
77 Massachusetts Avenue
Cambridge, MA 02139
Phone: (617) 253-6471; Fax: (617) 253-6201
E-mail: ychiang@mit.edu

Subcontractor: Antoni P. Tomsia, LBNL, Berkeley, CA

Start Date: May 1, 2010
Projected End Date: April 30, 2012

Objectives

- Develop a scalable high density binder-free low-tortuosity electrode design and fabrication process to enable increased cell-level energy density compared to conventional Li-ion technology for a range of electrode-active materials
- Characterize transport properties in high voltage Ni-Mn spinel.

Technical Barriers

- Low energy density and poor cycle life of EV battery systems

Technical Targets

- EV: 200 Wh/kg; 1000 cycles (80% DoD)

Accomplishments

- Developed a fabrication procedure for low-tortuosity highdensity sintered electrodes, using directional freeze-casting.
- Applied freeze-casting method to two cathode oxides: $LiCoO_2$ and $LiNi_{0.5}Mn_{1.5}O_4$
- Structurally and electrochemically characterized fabricated electrodes
- Conducted transport measurements on sintered $LiNi_{0.5}Mn_{1.5}O_4$

✧ ✧ ✧ ✧ ✧

Introduction

The well-established laminated cell construction and manufacturing paradigm for current lithium-ion batteries has recognized limitations in the mass and volume utilization of active material that is possible. For example, state-of-art 2.9Ah 18650 cells have by volume only 50% active material (positive and negative combined); automotive-grade cells have even lower utilization. The high intrinsic energy density of lithium-ion couples is therefore significantly diluted by inactive materials, limiting lithium-ion battery specific and volumetric energies. While a great deal of past and ongoing research is focused on the discovery of new active materials and cell chemistries as a route to increased energy, there has been proportionally less effort on new cell designs that can leapfrog existing technology by reducing inactive fraction. The objectives of this project are to develop a scalable, high density, binder-free electrode fabrication approach to enable rechargeable lithium batteries of increased active materials utilization.

Approach

The approach used here is based on a sintered electrode architecture into which an additional level of microstructural control is introduced – the introduction of aligned, low-tortuosity porosity. In collaboration with Antoni P. Tomsia of LBNL, a freeze-casting process was developed in which of aqueous suspensions of electrode particles undergo directional solidification. The ice microstructure that is formed creates desired pore morphologies and rejects solid particles from the growth front. Upon lyophilization of the freeze-cast electrodes, the resulting samples are then sintered to produce high-density consolidated electrodes. These electrodes were then structurally characterized and electrochemically tested in lithium half-cells.

This approach was applied to $LiCoO_2$ and $LiNi_{0.5}Mn_{1.5}O_4$. The samples obtained are also amenable to electrochemical titration of Li while simultaneously performing transport measurements

Results

The development of the process to achieve desired sintered densities and pore microstructures involved systematic variations in a number of materials and process variables, including:

- Electrode particle size and solids fraction in the starting suspensions

- Freeze-casting rate
- Surface-tension and viscosity altering additives to the aqueous suspension
- Sintering time and temperature

Examples of freeze-cast and sintered $LiCoO_2$ and $LiNi_{0.5}Mn_{1.5}O_4$ microstructures are shown in Figure V - 210 and Figure V - 211 respectively. It is seen that the directional freeze-drying process produces an oriented microstructure with aligned low-tortuosity porosity, as was desired. A series of experiments were focused towards increasing the degree of pore alignment and controlling/reducing lateral pore spacing while increasing overall sintered density. Previous work in the Tomsia lab on other materials has shown that freezing rate can influence the scale of the microstructures produced. In addition, hygroscopic additives such as sugar, glycerol, ethanol, methanol, and sodium chloride can alter microstructure by changing the morphology of the freezing ice crystals. For $LiCoO_2$, the largest impact on pore alignment and spacing occurred when the freeze-casting rate is decreased from 5 to 1°C/min, with the latter producing highly oriented porosity of ~20 μm scale with relatively few dendrite cross-arms blocking the longitudinal porosity.

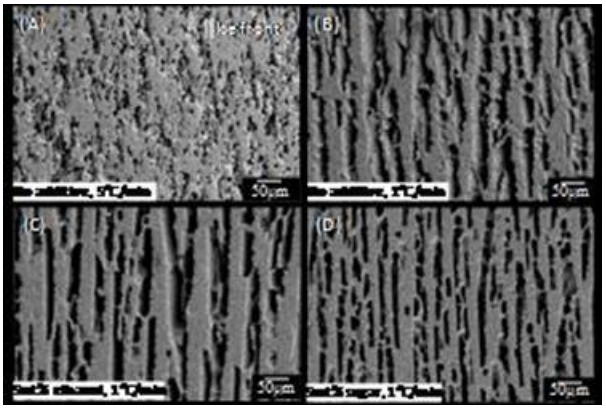

Figure V - 210: Cross-sections of directionally freeze-cast and sintered $LiCoO_2$ electrodes, viewed parallel to the solidifying ice front. The left panels show additive-free samples freeze-dried at 5 and 1°C/min, in which the slower freezing rate is seen to produce greater uniaxial alignment of porosity. The right panels show the effects of 5 wt% ethanol and sugar additive, which respectively produce coarser and finer aligned microstructures.

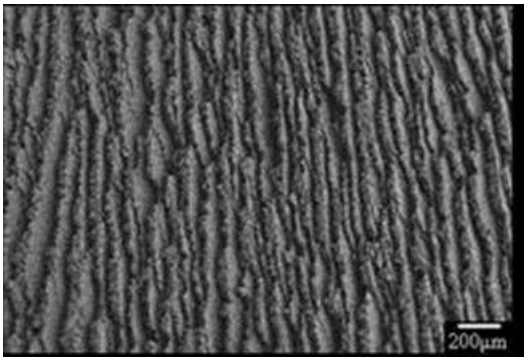

Figure V - 211: Cross-section of directionally freeze-cast and sintered $LiNi_{0.5}Mn_{1.5}O_4$.

An example of results from electrochemical testing of the freeze-cast $LiCoO_2$ samples is shown in Figure V - 212. Here, capacity utilization vs. C-rate of the freeze-cast microstructures is compared with that for sintered electrodes without the aligned low-tortuosity pore features. At low C-rates (C/10) the specific capacity of all samples are similar. With increasing C-rate, however, the results diverge significantly. Comparing at 1C rate, the Gen 1 sample, which has aligned porosity due to freeze-casting (although not as high a degree of alignment as Gen 2), shows significant increase in capacity over both of the sintered samples (at 63% and 74% dense, retaining ~83% (120 mAh/g) of the low-rate capacity. The Gen 2 sample, which has highly aligned pores (and somewhat lower sintered density of 50%), shows further improved capacity retention, with the same capacity retention being achieved at 2C rate. Thus these results validate the approach of introducing low tortuosity porosity to improve rate capability at high electrode densities. Specifically, high capacity at PHEV/BEV rate capabilities is demonstrated.

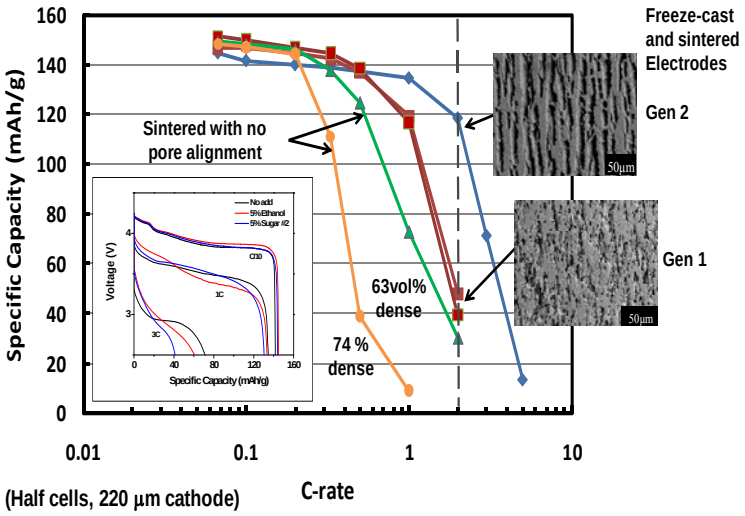

Figure V - 212: Specific capacity vs. C-rate for sintered $LiCoO_2$ electrodes prepared with and without aligned low-tortuosity porosity.

High-density sintered $Li_xNi_{0.5}Mn_{1.5}O_4$ electrodes were also used for transport measurements performed as part of the activities under the new BATT Focus Group on High Voltage Ni-Mn Spinels. The electronic conductivity of undoped $Li_xNi_{0.5}Mn_{1.5}O_4$ in its as-fired condition was measured, for firing temperatures between 735°C and and 950°C. Consistent with trends reported by Kunderaci and Amatucci (J. Electrochem. Soc., 153[7] A1345 (2006)) the conductivity was found to increase with increasing firing temperature at a constant oxygen activity (air). This can be understood as an increase in oxygen nonstoichiometry accommodated by formation of Mn^{3+}. Upon electrochemical delithiation, however, it is expected that the Mn^{3+} is the first transition metal to be oxidized, and furthermore, being low in total concentration compared to the Li deficiency, is not to be the main determinant of electronic conductivity.

The conductivity vs. Li content *x* was then measured using DC current-interrupt measurements of half-cells, the changes in resistance being confirmed by EIS measurements to correspond to changes in the charge-transfer resistance rather than current collector or electrolyte resistance. The changes in the charge-transfer arc were attributed to changes in electronic conductivity. The interpretation of electronic conductivity in $Li_xNi_{0.5}Mn_{1.5}O_4$ is complicated by the existence of three different cubic spinel phases varying in amount with *x*, as well as changes in cation ordering. The heat treatments applied were designed to obtain the cation-disordered state. From multiple measurements, in general it was observed that the electronic conductivity has a maximum value at intermediate SOC, with conductivities at $x \sim 0.5$ being in the range 2×10^{-4} S/cm to 1×10^{-3} S/cm. At both high and low SOC ($x \sim 0$ and $x \sim 1$), the conductivity is lower, being 2×10^{-5} to 1×10^{-4} S/cm. A hysteresis between charge and discharge was also observed, the cause of which remains to be understood.

Conclusions and Future Directions

It has been shown that high density sintered electrodes with aligned low-tortuosity porosity can yield high capacity utilization at practical C-rates for PHEVs and EVs, while having capacities per unit area that are 5-10 times greater than that of conventional Li-ion electrodes. Electrodes of such design may enable higher energy density rechargeable batteries for transportation. It has also been shown that the sintered electrode format permits facile Li titration while simultaneously measuring transport properties, without requiring additional conductive additives or assumptions about particle geometry that can complicate the interpretation of data.

Future directions in this project are as follows:

- The freeze-casting + sintering approach will be applied to other electrode materials, in particular materials of varying electronic conductivity, in order to determine the relative limitations of electronic and ionic transport on utilization
- The tortuosity in sintered electrodes of various microstructures will be characterized and correlated with electrochemical behaviour
- Due to the large capacity per unit area, the pulse power performance of such electrodes may differ from conventional electrodes of much lighter active loading. This behaviour will be characterized, using PHEV and EV specific "drive cycles."
- The sintered electrode format will be used to measure the electronic and ionic transport parameters of materials of interest, and specifically of the high voltage spinel $Li_xNi_{0.5}Mn_{1.5}O_4$.

FY 2011 Publications/Presentations

1. C.-J. Bae, C. Erdonmez, Y.-M. Chiang, and J.W. Halloran, "Influence of Controlled Pore Topology in Sintered Li-ion Battery Cathodes on Electrochemical Performance," Materials Research Society Fall Meeting, Boston, MA, November 2010.
2. Y.-M. Chiang, *Electrical Energy Storage to Enable Clean Transportation and Growth of Renewable Energy*, Dow Distinguished Lectureship in Materials Science and Engineering in Support of Society, University of California at Berkeley, March 31, 2011.
3. Y.-M. Chiang, 2010-2011 Kent R. van Horn Distinguished van Horn Lecturership (3 lectures), CaseWestern Reserve University, Department of Materials Science and Engineering, March 14-16, 2011.

V.E.9 *In Situ* Electron Spectroscopy of Electrical Energy Storage Materials (ORNL)

Raymond R. Unocic
Oak Ridge National Laboratory
Materials Science and Technology Division
One Bethel Valley Rd
PO Box 2008 MS-6064
Oak Ridge, TN 37831-6030
Phone: (865) 574-0096; Fax: (865) 576-5413
E-mail: unocicrr@ornl.gov

Start Date: January 2010
Projected End Date: December 2014

Objectives

- The primary aim of this research is to develop and perform quantitative *in situ* electron microscopy experiments of electrical energy storage materials using an electrochemical cell holder built specifically for *in situ* transmission electron microscopy (TEM) characterization.
- The key benefits include the ability to wholly contain and image through volatile organic electrolytes while performing nanoscale electrochemistry experiments within the high vacuum environment of the TEM column at high spatial and temporal resolution.
- This technique will enable evaluations of critical nm-scaled microstructural and micro-chemical changes as a function of battery test conditions, electrode materials, electrolyte, and electrolyte additives.

Technical Barriers

The technical barrier is the present lack of high-resolution electrochemical characterization techniques, which allow for the direct observations of dynamically evolving electrochemical reactions during charge/discharge cycling.

Technical Targets

- Develop *in situ* characterization technique and methodology to investigate dynamically evolving electrochemical reaction mechanisms.

Accomplishments

- Developed a prototype *in situ* electrochemical cell capable of performing *in situ* mircroscopy experiments
- Studied the formation and growth of the solid electrolyte interphase (SEI) on graphite electrodes in real time and at high spatial resolution.

✧ ✧ ✧ ✧ ✧

Introduction

The accelerated development of materials for utilization in electrical energy storage systems will hinge critically upon our understanding of how interfaces (particularly electrode-electrolyte solid-liquid interfaces) control the physical and electrochemical energy conversion processes. A prime example is found in Li^+ ion-based battery systems, where a passive multiphase layer grows at the electrode/electrolyte interface due to the decomposition of the liquid electrolyte. Once formed, this SEI protects the active electrode materials from degradation and also regulates the transport and intercalation of Li^+ ions during battery charge/discharge cycling. Due to the dynamically evolving nature of this nm scaled interface, it has proven difficult to design experiments that will not only elucidate the fundamental mechanisms controlling SEI nucleation and growth, but will also track microstructural and chemical evolution of the SEI as a function of charge/discharge cycling to be monitored in real time.

Approach

In this program, we have developed an electrochemical fluid cell for *in situ* TEM studies of electrochemical reactions of energy storage materials. The core challenge of preventing the evaporation of high vapor pressure and volatile organic liquid electrolytes has recently been overcome through sealing of the fluid between thin electron transparent viewing membranes. Typically this is accomplished through the use of silicon microchip devices containing a central thin electron transparent silicon nitride (SiN_x) viewing membrane as shown in Figure V - 213. To create the electrochemical cell, two silicon microchips are stacked upon one another and placed within the tip of a precision machined TEM holder.

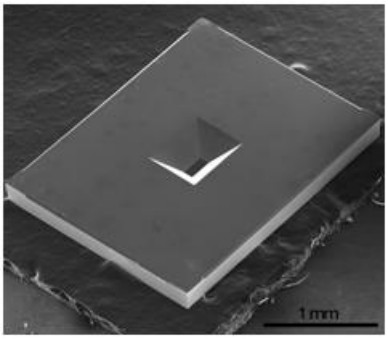

Figure V - 213: SEM micrograph of a MEMS-based silicon microchip used to enclose the liquid electrolyte

Biasing contacts are deposited onto the lower chip/window of the cell, which doubly serves as a platform for attaching battery electrodes and for interfacing with an external potentiostat for electrochemical testing. A 500nm spacer material patterned on the upper chip controls the thickness of the liquid electrolyte layer in the cell.

The cell incorporates a liquid delivery system (microfluidic syringe pump and microfluidic tubing) to flow liquid electrolyte between the SiN_x membranes comprising the cell. This holder was built specifically for the Hitachi HF3300 S/TEM operating at 300kV, which is equipped with TEM and STEM imaging detectors and a Gatan Quantum GIF for EELS and EFTEM. The experimental setup of the *in situ* electrochemical cell TEM holder, microfluidic syringe pump, and potentiostat is shown in Figure V - 214.

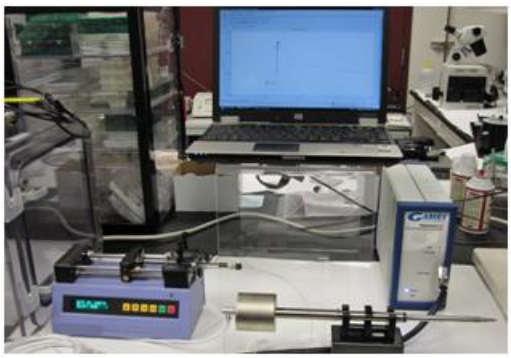

Figure V - 214: Experimental setup of the in situ electrochemical cell TEM holder, microfluidic syringe pump to deliver liquid electrolyte to the cell and potentiostat for electrochemical testing.

Results

This device has been used to dynamically monitor the formation of the SEI on a graphite anode *in situ* within an electrolyte consisting of 1M $LiClO_4$ in EC:DEC. Figure V - 215 shows the biasing chip platform (Figure V - 215a) with a highly oriented pyrolytic graphite (HOPG) anode and $LiCoO_2$ cathode attached using a focus ion beam (FIB) instrument, experimental charging curve Figure V - 215b), and TEM micrographs of the HOPG anode through the silicon nitride viewing window before (Figure V - 215c) and during (Figure V - 215d) an *in situ* electrochemistry experiment. Figure V - 215d clearly shows the formation of the SEI on the graphite anode.

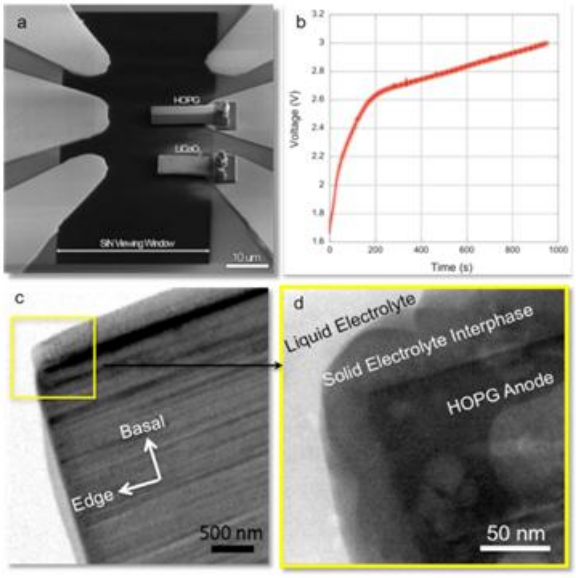

Figure V - 215: a) SEM micrograph of battery electrodes (HOPG anode and $LiCoO_2$ cathode) attached to biasing microchips and across the SiN_x membrane b) charging curve, c) bright-field TEM image of HOPG anode before experiment and d) snapshot acquired during in situ electrochemistry experiment depicting the formation of the SEI on the surface of the graphite anode.

Conclusions and Future Direction

The newly developed *in situ* electrochemical cell TEM holder is is a versatile characterization device that allows for high spatial resolution imaging of dynamically evolving electrochemical reactions during electrochemistry experiments. The future focus of this research will be to quanitify the kinetics of SEI formation, and study the influence of electrolyte and electrolyte additives on SEI stability during electrochemical charge/discharge cycling. This characterization technique will also be used to investigate degradation mechanisms in cathode materials.

FY 2011 Publications/Presentations

1. 2011 DOE Annual Peer Review Meeting Presentation.
2. R.R. Unocic, D.H. Alsem, N.J. Salmon, M. Chi, G.M. Veith, L.A. Adamczyk, N.J. Dudney, and K.L. More, "The Versatility of *In situ* Environmental Fluid Cells for Materials Science Research," MS&T Conference, Columbus, OH, October, 2011. *(Invited)*
3. R.R. Unocic, X. Sun, L.A. Adamczyk, N.J. Dudney, D.H. Alsem, N.J. Salmon, K.L. More, "Development of *in situ* TEM Electrochemical Fluid Cells for Electrical Energy Storage Research," Frontiers in Electron Microscopy in Materials Science, Sonoma, CA, September, 2011.
4. R.R. Unocic, L.A. Adamczyk, N.J. Dudney, D.H. Alsem, N.J. Salmon, K.L. More, "*In situ* TEM Characterization of Electrochemical Processes in Energy Storage Systems," Microscopy and Microanalysis, Nashville, TN, August, 2011.
5. R.R. Unocic, L.A. Adamczyk, N.J. Dudney, D.H. Alsem, N.J. Salmon and K. L. More, "Use of *in situ* TEM Characterization to Probe Electrochemical Processes in Li-ion Batteries," MRS, San Francisco, CA, April, 2011.
6. R.R. Unocic, L.A. Adamczyk, N.J. Dudney and K.L. More, D.H. Alsem and N.J. Salmon, "*In situ* TEM Characterization of the SEI in Li-ion Batteries," Electrochemical Society Meeting, (Oct 2010).

V.F Energy Frontier Research Centers

V.F.1 Energy Frontier Research Center at ANL (ANL)

Michael Thackeray

Argonne National Laboratory
9700 South Cass Avenue
Argonne, IL 60439
Phone : (630) 252-9184 ; Fax : (630) 252-4176
E-mail: thackeray@anl.gov

Collaborators: ANL: S.-H. Kang, J. R. Croy, M. Balasubramanian (APS)
LBNL: V. Battaglia

Start Date: October 1, 2010
Projected End Date: September 30, 2011

Objectives

- Conduct surface studies of electrode materials relevant to the BATT program to complement the research being conducted by the EFRC, Center for *Electrical Energy Storage – Tailored Interfaces* led by Argonne National Laboratory, with Northwestern University and the University of Illinois, Urbana-Champaign as partners.
- Specifically, use x-ray spectroscopic techniques, including *in situ* experiments, at Argonne's Advanced Photon Source and high-resolution electron microscopy to probe and characterize the surface structures of high capacity $xLi_2MnO_3 \bullet (1-x)LiMO_2$ (M=Mn, Ni, Co) materials.

Technical Barriers

- Low energy density
- Poor low temperature operation
- Abuse tolerance limitations

Technical Targets (USABC - End of life)

- 142 Wh/kg, 317 W/kg (PHEV 40 mile requirement)
- Cycle life: 5000 cycles
- Calendar life: 15 years

Accomplishments

- A detailed electrochemical/structural study of lithium-nickel-phosphate-coated $0.5Li_2MnO_3 \bullet 0.5LiCoO_2$ was accomplished.
- One patent application, one paper accepted for publication

✧ ✧ ✧ ✧ ✧

Introduction

Bulk and interfacial electrochemical processes are of fundamental scientific interest as well as of technological importance. The performance of energy storage and power supply systems is largely dependent on these processes, which can occur at an electrode-electrolyte interface or in the bulk of the electrode. In this project, the structural features, ionic transport phenomena and charge-transfer reactions at the electrode/electrolyte interface of lithium battery electrode materials, notably high potential metal oxide cathodes are studied. The electrode materials under investigation are selected specifically from those being investigated in the BATT program and on their potential for making significant advances in electrochemical performance; the studies are complementary to the research being conducted by the Energy Frontier Research Center, *Electrical Energy Storage – Tailored Interfaces* led by Argonne National Laboratory, with Northwestern University and the University of Illinois, Urbana-Champaign as partners.

Of particular importance to this project is Argonne's recent research in the BATT program on electrodes with integrated 'composite' structures, which has highlighted the possibility of designing new, high-potential and high capacity electrodes with Li_2MnO_3 as a stabilizing component. It has been demonstrated, in particular, that it is possible to integrate Li_2MnO_3 with layered $LiMO_2$- or spinel LiM_2O_4 components (e.g., M=Mn, Ni, Co) at the atomic level, and that these composite materials can provide an exceptionally high capacity (240-250 mAh/g), which is significantly higher than the capacity offered by conventional layered $LiCoO_2$, spinel $LiMn_2O_4$ and olivine $LiFePO_4$ electrodes. These lithium- and manganese-rich composite materials have extremely complex structures which are surprisingly stable when delithiated at high potentials (~5 V). Despite the enhanced stability of these electrode materials, it is still necessary to passivate the electrode surface to prevent electrode/electrolyte reactions from occurring, and to improve Li-ion transport at the surface, thereby enhancing the power capability of the cell. In this respect, several coating techniques and passivating agents, such as metal oxides (Al_2O_3, ZrO_2), fluorides (AlF_3) and phosphates ($AlPO_4$) have been shown to

improve surface stability and rate capability of the electrode, but little is known about surface structures, or the mechanisms by which lithium-ion transport occurs at the electrode surface. The knowledge gained from these studies will be used to improve the composition and structure of electrode surfaces and to advance the overall performance of the electrodes to meet DOE's 40-mile PHEV battery requirements.

Approach

Analytical techniques for probing the structure-electrochemical property relationships of lithium battery electrode materials, notably at electrode surfaces, include neutron scattering, x-ray absorption, scattering and photoelectron spectroscopy, nuclear magnetic resonance, Raman spectroscopy, Fourier transform infrared spectroscopy, and electron microscopy. In this project, analytical efforts are focused predominantly on x-ray spectroscopic techniques, including *in situ* experiments, and high-resolution electron microscopy. Major facilities are available at Argonne to conduct these experiments, notably at the Advanced Photon Source (APS) and the Electron Microscopy Center (EMC).

Surface-protected 'coated' cathode materials to be studied include those with integrated 'composite' structures in which the coating contains specific 3d/4d transition metals which are not present in the core structure. Coatings will be applied by various techniques, for example, from solution by standard sol-gel methods or by atomic layer deposition (ALD). *In situ* synchrotron hard x-ray spectroscopic techniques including x-ray absorption spectroscopy (XAS), resonant and non-resonant x-ray emission spectroscopy (XES) and x-ray Raman scattering (XRS) will be used to monitor the interfacial reactions at the electrode-electrolyte interface. The important traits of these spectroscopic techniques, specifically the element specific nature and the sensitivity to dilute constituents, will allow the monitoring of changes in the electronic and atomic structures of the coatings during charge-discharge cycling or during repeated cycling. A comparison of the electrochemical properties of uncoated and coated electrodes will be made. It is envisioned that these studies will provide key information at the molecular level on the structure of the coatings, the mechanism of lithium-transport at the electrode-electrolyte interface and further provide insights into degradation mechanisms during repeated cycling. Another aspect that will be investigated is the effect of the coating on the bulk structure of the composite material itself, particularly on deintercalation at high voltages, for example 4.6 V, during the initial charge. Recent XAS studies of uncoated composite materials (such as those developed under the BATT program) have shown convincing evidence of oxygen loss during first charge at these high voltages. In coated samples, the exact oxygen loss mechanism and the possible condensation of the bulk structure might be significantly different and a detailed understanding of the local structure of the bulk should provide key insights on the structure-property relationship of the coated composites. The knowledge gained from both the bulk and interface using x-ray spectroscopic methods will feed into the design of improved electrodes to meet the 40-mile PHEV goals. In addition to studies of composite cathode structures, studies of well defined electrode surfaces will be undertaken using spectroscopic and microbeam methods. Such studies utilize the property of total external reflection of x-rays at small incident angles, which minimizes the contribution from the bulk of the material and provides interface sensitivity without sacrificing the *in situ* capability of hard x-rays. These spectroscopic investigations will complement the x-ray based scattering approaches which are currently an integral part of Argonne's EFRC, Center for Electrical Energy Storage-*Tailored Interfaces* (CEES) effort.

Results

Lithium-metal-oxides remain the most promising cathode materials for high-energy-density lithium-ion batteries for plug-in hybrid electric vehicles (PHEV) and all-electric vehicles (EVs). To this end, much effort has been invested to advance these materials. However, a significant challenge that remains is the mitigation of irreversible surface damage at high potentials, which occurs with adverse consequences to the power delivery of the cathodes (i.e., rate capability). To date, several surface passivation techniques have been studied with the goal of addressing this issue in a variety of cathodes by way of 1) enhancing the conductive properties of the surface, 2) modifying the electrode surface chemistry to improve performance, and 3) providing a physical barrier which impedes reactions of the surface with the electrolyte.

For this project, a dilute (5 mol%) surface treatment of lithium-nickel-phosphate (Li:Ni:PO_4 ratio = 1:1:1) was deposited on a $0.5Li_2MnO_3 \bullet 0.5LiCoO_2$ ($Li_{1.2}Mn_{0.4}Co_{0.4}O_2$) cathode material, referred to as LNP-coated LCMO. Similar treatments have previously been reported by Kang and Thackeray to enhance electrochemical performance. However, exact structural determinations could not be made regarding the outcome of the surface treatment because the host material was itself a nickel-containing oxide, $0.5Li_2MnO_3 \bullet 0.5LiNi_{0.44}Co_{0.25}Mn_{0.31}O_2$, alternatively, ($Li_{1.2}Mn_{0.52}Ni_{0.18}Co_{0.1}O_2$). In the present case, the host material was chosen to be free of nickel ($0.5Li_2MnO_3 \bullet 0.5LiCoO_2$) and, therefore, structural and chemical information obtained from XAS measurements provide direct information about electrochemical enhancements due to the Li-Ni-PO_4 treatment itself relative to untreated electrodes. The results have exciting implications for tailoring the structures and/or surfaces of high-capacity composite electrodes derived from a

Li_2MnO_3 precursor, and improving their structural stability over long-term cycling.

Figure V - 216 shows the first charge/discharge curve between 4.6 and 2.0 V (15 mA/g) for a LNP-treated LCMO electrode. The numbered points along the curves indicate predetermined states of charge at which cells were prepared for the XAS measurements. Point 1 represents the fresh, uncharged electrode, point 2 (at ~4.3 V) corresponds to the extraction of ~90 mAh/g capacity, and point 3 represents a fully charged electrode at 4.6 V corresponding to the full ~280 mAh/g practical capacity of the electrode. Point 4 represents a fully discharged electrode at 2.0 V after one complete cycle.

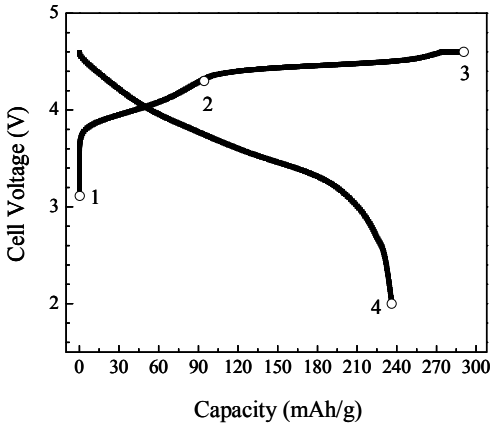

Figure V - 216: Charge/discharge curve between 4.6 and 2.0 V (15 mA/g) for LNP-treated LCMO electrodes. Numbered points indicate predetermined states of charge at which cells were prepared for XAS measurements.

In general, the results obtained at all points of charge for the Mn (not shown) and Co K-edges agree well with those reported elsewhere for manganese and cobalt in similar systems. Attention was focused on the dilute element of interest, namely nickel, as introduced by way of surface treatment on LCMO. However, several observations are worth noting. For example, from the XANES data in Figure V - 217a, it can be observed that the cobalt environment in the parent LNP-treated LCMO electrode (point 1, Figure V - 216) is identical to the Co environment in the untreated LCMO sample; both spectra overlap and are similar to Co^{3+} in $LiCoO_2$, again revealing the composite nature of the material. This observation reveals that the LNP treatment has little effect on the Co-rich regions of the composite material.

However, from the Fourier transformed Mn K-edge data in Figure V - 217b, in which Li_2MnO_3 is used as a reference, it can be seen that the local environment of manganese in the LNP-treated LCMO has undergone slight modifications with respect to that of manganese in the parent LCMO. Both LCMO and LNP-treated LCMO samples show increased amplitudes in the second-shell Mn-M correlations at ~2.5 Å with respect to pure Li_2MnO_3. For LCMO, this is attributed to contact between the boundaries of the $LiCoO_2$- and Li_2MnO_3-like domains, in agreement with Bareno et al. For LNP-treated LCMO, even higher amplitudes for the Mn-M correlation are observed. This result is attributed to the insertion of nickel into the transition metal layers of the Li_2MnO_3-like domains in the $0.5Li_2MnO_3 \bullet 0.5LiCoO_2$ composite structure as described in more detail below.

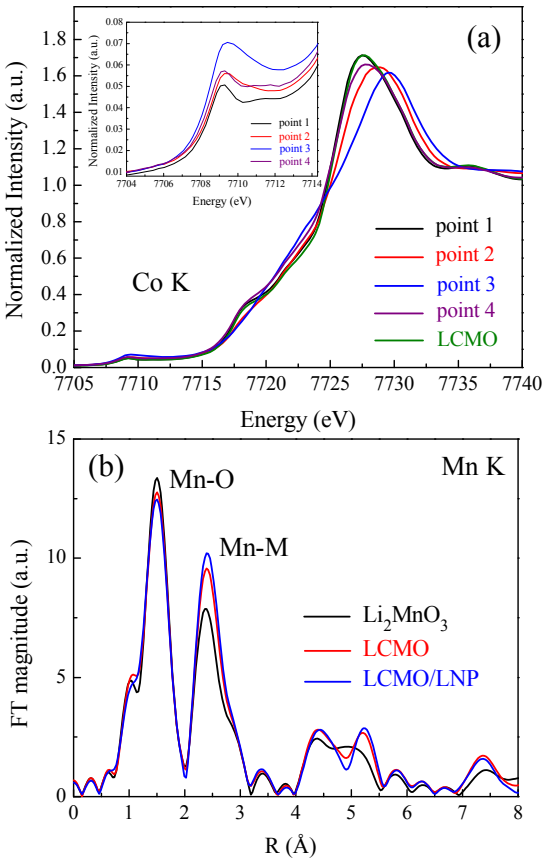

Figure V - 217: (a) Co K-edge XANES showing LNP-treated LCMO at all points of charge in Figure V - 216 and untreated LCMO. The inset in (a) shows a magnified view of the Co K pre-edge region for all points of charge. (b) Magnitude of the Fourier transformed Mn K-edge data for LNP-treated LCMO, untreated LCMO, and a Li_2MnO_3 reference.

Figure V - 218a shows the Ni K-edge XANES data of the LNP-treated LCMO electrode at points 1 and 4 in the electrochemical data (Figure V - 216) relative to a Ni^{2+} reference, $0.5Li_2MnO_3 \bullet 0.5LiMn_{0.5}Ni_{0.5}O_2$ (alternatively, $Li_{1.2}Mn_{0.6}Ni_{0.2}O_2$). The excellent overlap of all three spectra indicates that the nickel ions are predominantly divalent in the uncharged electrode as well as after one complete cycle. Figure V - 218b shows the Ni K-edge XANES data of the LNP-treated LCMO electrodes at points 1, 2 and 3 of Figure V - 216 relative to Ni^{3+} ($LiNi_{0.8}Co_{0.2}O_2$) and Ni^{4+} ($LiNi_{0.8}Co_{0.2}O_2$ charged to 5.2 V) references. At a relatively early stage of charge, point 2 (4.3 V), the nickel ions reach an oxidation state of ~3+. This finding is significant because it would be expected that a lithium-

nickel-phosphate such as olivine $LiNiPO_4$ ($Li:Ni:PO_4$=1:1:1) should be electrochemically inactive to 5.0 V; the result therefore reveals that the nickel ions partake in the electrochemical reaction. Further charging to point 3 (4.6 V, Figure V - 216), when the cell is fully charged, apparently does not increase the oxidation of the nickel ions much further, indicating that the average oxidation is still significantly below 4+. This is an intriguing result, because the bulk oxidation process in other layered nickel oxide electrodes often involves the oxidation of nickel to the tetravalent state during high states of charge.

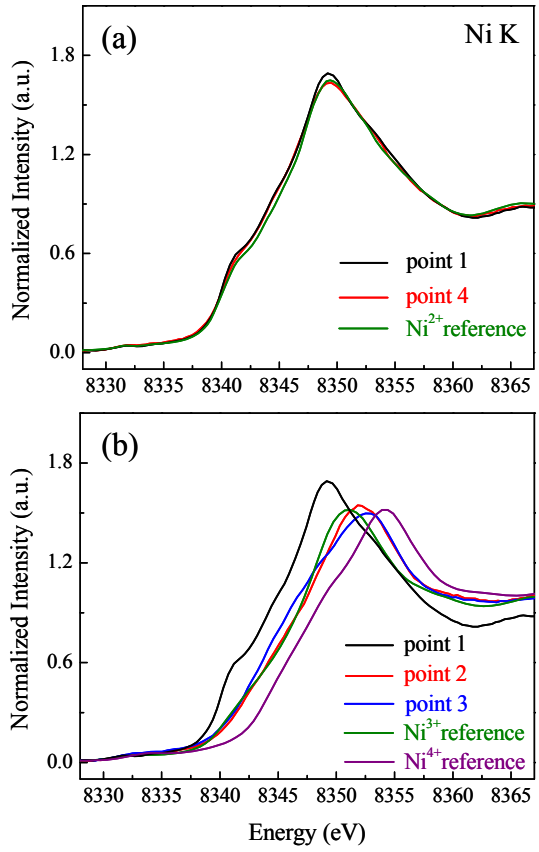

Figure V - 218: (a) Ni K-edge XANES of LNP-treated LCMO electrodes at charge points 1 and 4 in Figure V - 216, and a Ni^{2+} reference. (b) Ni K-edge XANES at points 1, 2 and 3, and Ni^{3+} and Ni^{4+} references.

Conclusions and Future Directions

Conclusions

The element specific nature of X-ray absorption spectroscopy was used to elucidate the chemical and structural details of a surface treatment intended for the protection of high-capacity cathode materials. Electrochemical data showed that surface treatments of $0.5Li_2MnO_3•0.5LiCoO_2$ ($Li_{1.2}Mn_{0.4}Co_{0.4}O_2$) cathodes with an acidic solution of lithium-nickel-phosphate significantly improved their capacity, rate, and cycling stability. XAS data revealed that the surface treatment resulted in a modification of the composite structure itself, where Ni^{2+} cations, intended to be present in a lithium-nickel-phosphate coating, instead displaced lithium in the transition metal layers of Li_2MnO_3-like domains within the $0.5Li_2MnO_3•0.5LiCoO_2$ structure. X-ray diffraction data show the presence of Li_3PO_4, suggesting that phosphate ions from the acidic solution are responsible for lithium extraction and nickel insertion with the formation of vacancies and/or manganese reduction for charge compensation. The results of this study are consistent with a novel approach to synthesize high-capacity cathode materials using a Li_2MnO_3 template.

Future Work

- This project has revealed valuable insights into the complex electrochemical phenomena occurring at the electrode/electrolyte interface of high capacity composite electrode materials. From a practical standpoint, further work is required to stabilize the surfaces to achieve optimum electrochemical performance and cycle life of practical systems. These studies will be continued on materials of relevance to the BATT program using other surface protection agents, e.g. oxides and fluorides.
- Interactions with DOE's energy storage centers (EFRCs) will be continued.

FY 2011 Publications/Patents/Presentations

Publications

1. J. R. Croy, S.-H. Kang, M. Balasubramanian and M. M. Thackeray, *A New Approach to Fabricating Li_2MnO_3-based Composite Cathode Structures for Lithium Batteries*, Electrochem. Comm., **13**, 1063-1066 (2011).
2. J. R. Croy, S.-H. Kang, M. Balasubramanian and M. M. Thackeray, *Designing High-Capacity, Lithium-Ion Cathodes Using X-ray Absorption Spectroscopy*, Chem. Mater., accepted (2011).

Patents

1. M. M. Thackeray, S.-H. Kang, M. Balasubramaian and J. R. Croy, *Electrode Structures and Surfaces for Li Batteries*, US Patent Application, Serial No. 13/044038 (9 March 2011).

Presentations

1. J. R. Croy, S.-H. Kang, M. Balasubramanian and M. M. Thackeray, *Advances in Li_2MnO_3-based Electrodes for Lithium Batteries*, 5th International Conference on Polymer Batteries and Fuel Cells,

(PBFC-5), Argonne National Laboratory, Illinois, 1-5 August (2011).

V.F.2 Novel *In Situ* Diagnostics Tools for Li-ion Battery Electrodes (LBNL)

Jordi Cabana, Robert Kostecki
Lawrence Berkeley National Laboratory
1 Cyclotron Rd. MS62R0203
Berkeley, CA 94720-8168
e-mail: jcabana@lbl.gov
Phone: (+1) 510-486-7097
Fax: (+1) 510-486-8097

Start Date: September 2009
Projected End Date: September 2011

Objectives

- Develop synchrotron-based Transmission X-ray Microscopy (TXM) and X-ray Raman Spectroscopy (XRS) for the production of unprecedented insight into Li-ion battery electrode operation.
- Develop setups that allow the collection of data during the electrochemical reaction.

Technical Barriers

Better understanding of the fundamental processes that occur in Li-ion batteries at different levels is essential for progress toward better performance. There is a need for new diagnostics techniques with high sensitivity and that cover wide time and dimension scales to probe phenomena at surfaces and interfaces, and the evolution of the phase transitions and boundaries upon electrode operation. Given the importance of kinetics and transient phenomena that occur in batteries, the development of these new techniques must run concurrent to the development of setups that enable the performance of experiments in real time.

Technical Targets

- Understand impact of materials and electrode design on performance and the underlying mechanisms of reaction.
- Develop synchrotron-based tools for the study of fundamental processes in battery materials.
- Streamline the use of these tools to answer questions that span from fundamental to close-to-application problems, with potential impact in other DOE programs such as BATT or ABR.
- Obtain 2D and 3D maps with chemical resolution of battery electrodes reacting through intercalation and conversion mechanisms.
- Reveal the nature of chemical bonding between Li and host lattice in intercalation materials.

Accomplishments

- 2D and 3D Fe K edge XANES tomography images of partially delithiated $LiFePO_4$ have been collected.
- XRS data on graphite and its lithiated compounds has revealed the changes in electronic structure and bonding occurring in the material.
- *In operando* setups for XRS and TXM have been designed and demonstrated.

✧ ✧ ✧ ✧ ✧

Introduction

In order to fulfill the energy density and life requirements for batteries in emerging applications such as transportation or grid storage, new electrode materials have to be developed and the performance of existing materials maximized. Because Li-extraction/insertion is a diffusion-controlled process that depends on both electron and ion conduction, the design of architectures that optimize these parameters is critical to achieve ultimate performance. Fundamental understanding of how the number of points of contact for transport of electrons from the current collector and ions from the electrolyte into the active material particles affects the utilization of the material is needed to approach these limits. Nevertheless, this picture still ignores the fact that Li extraction in a variety of candidate materials is further complicated by the fact that it involves multiple consecutive (even simultaneous) phases, in which the movement of interfaces is key to the progress of the reaction. Therefore, insight into how individual particles electrochemically transform depending on conditions such as particle size/shape, carbon coating or rate at which the material is operated, could provide vital information that could be integrated into the process of electrode design to result in architectures with close-to-theoretical utilization.

On the other hand, diffusion within the active material particle will determine how large this particle can be to perform satisfactorily at desired rates of operation. This diffusion is determined by the interaction of the charge carrier with its environment. Therefore, understanding of the nature of chemical bonding between ions and the lattice can provide valuable information about the bottlenecks that exist for their mobility. Removing these barriers through materials design could enable the use of larger particles which, in turn, increase the density of the

material because they can be packed more easily. The result would be electrodes with higher energy density.

Advanced synchrotron-based techniques will enable the probing of processes occurring on increasingly shorter timescales and, through their enhanced sensitivity, to study increasingly more subtle changes. The high energy of the beam allows collection of data from whole battery ensembles. The purpose of this effort is to continue to expand our diagnostic capabilities by leveraging the two synchrotron user facilities in the Bay Area. The goal is to offer new insight into processes that determine phase transformations and the interaction of Li with its host lattice in battery materials.

Approach

This effort is currently centered on the use of transmission X-ray microscopy (TXM) and X-ray Raman spectroscopy (XRS). The measurements were performed at the wiggler beamline 6-2 at Stanford synchrotron radiation lightsource (SSRL).

TXM is an imaging tool that provides information on the microstructure of materials. The spatial resolution is generally poorer than that for TEM, but recent advances make it possible to achieve a resolution of 20 nm, a length scale that is relevant to many battery features. TXM does not require elaborate sample preparation or exposure to high vacuum, and X-rays are less damaging to the sample than an electron beam. Both 2D and 3D images can be collected by turning the sample with respect to the beam, so that tomographic reconstructions are generated. In addition, TXM can be coupled with XAS to obtain spatially resolved chemical speciation. XRS also employs hard X-rays and provides information on the bulk electronic structure of a given element, even light ones such as Li or C, at long penetration lengths without the need of ultrahigh vacuum. XRS allows access to the same information as soft X-ray absorption spectroscopy (XAS), but uses penetrating radiation.

Because these techniques do not require ultrahigh vacuum, it is possible to design a setup with liquid electrodes for *in situ* analysis of operating cells. Examples of proposed experiments include measurements of structural changes in carbonaceous materials upon cation and anion intercalation, and monitoring changes in species distribution within a particle in electrochemical reactions.

Results

2D XANES TXM images of partially delithiated $LiFePO_4$ hexagonal crystals (200x2000x4000 nm) were collected at the Fe K-edge, with spatial resolution of about 25nm. The chemical resolution allows to distinguish clearly between Fe^{3+} and Fe^{2+} species distributed within a partially delithiated crystal. Figure V - 219a and Figure V - 219b show the single field of view images obtained below and above the edge respectively. To distinguish between species at different oxidation states, images were obtained at selected energies. For each pixel, a XANES scan was thus approximated. Figure V - 219c shows the phase map that was obtained by fitting each XANES spectra for each pixel by a linear combination of $FePO_4$ and $LiFePO_4$.

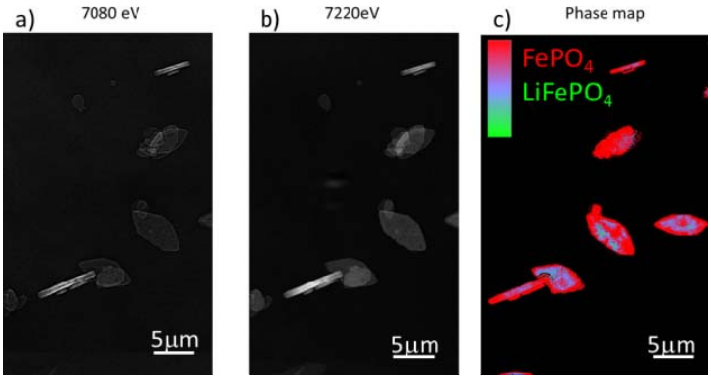

Figure V - 219: Partially delithiated $LiFePO_4$ below (a) and above (b) the Fe K-edge and the corresponding phasemap (c) with the distribution of phases within the crystals.

Some hurdles were found during these measurements. The crystals measured along the shortest dimension (200nm, i.e., lying flat) are thin enough that about 95% of the beam is transmitted above the Fe-K-edge, which leads to serious contrast issues and high signal to noise ratio. The result is an increase in the measurement time and uncertain data reliability. To circumvent this issue, even larger crystals (10x10x40 µm) were analyzed. With these crystals, the method could be extended by repeating the procedure at different rotation angles along a vertical axis, leading to 3D spectroscopic imaging. The data are currently being analyzed and conclusions are expected during FY2012.

During this past year, a setup to perform *in operando* TXM with XANES in 2D was developed. Proof of concept was shown with the conversion reaction of NiO. The selected images at different stages of the battery

discharge/charge illustrate the massive changes in the morphology that occur when Li reacts with NiO. The impact and changes of morphology are shown in Figure V - 220. The conversion reaction leads to a drastic volume expansion which swells the particle and leads to its collapse and the formation of nanoparticles. During the experiment, spectroscopic information was obtained to track the distribution of metallic Ni and NiO during the reaction.

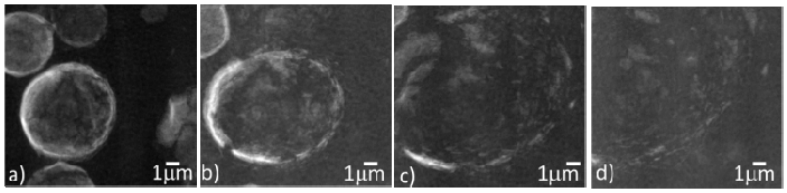

Figure V - 220: Morphology changes in a NiO particle during electrochemical cycling.

XRS data at the Li and C K edges was collected for a sample of highly oriented pyrolytic graphite (HOPG) before and after lithiation. The results at the C K edge (Figure V - 221) show a remarkable decrease in the π^* signal, which is related to the filling of unoccupied bands above the Fermi level. This filling is at the origin of the metallic character of lithiated graphite. A shift in the σ^* signal toward lower energies was also observed, which is related to a stiffening of the C-C bonds upon lithiation. The Li K edge data show that Li is far from being completely ionized within the structure of the material, contrary to previous studies.

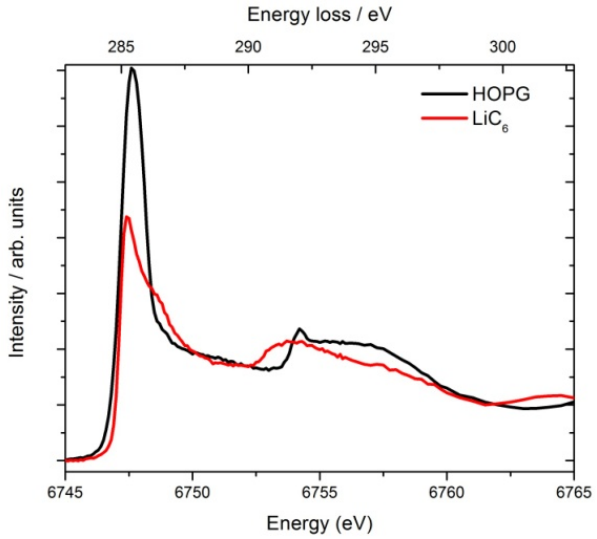

Figure V - 221: XRS data at the C K edge for pristine and lithiated HOPG.

A setup for *in operando* XRS was also designed and successfully tested in the laboratory. Preliminary experiments show that the setup is very well suited for the collection of XRS simultaneous to the lithiation of graphite. Results are expected during FY2012.

Conclusions and Future Directions

Chemical maps of the species involved in the Li deintercalation mechanism in $LiFePO_4$ were produced in both 2D and 3D for particles of different sizes. The distribution of phases within a crystal was uncovered. In parallel, a setup designed for *in operando* data collection was built and successfully used at the beamline. Further experiments will leverage this new capability to follow the chemical phase transformations front during electrochemical reactions in different battery electrodes. Attempts will be made to collect data in both 2D and 3D.

Data at the Li and C K edge were collected for samples of graphite at different lithiation states. The data reveal the complex bonding nature of the material, with a covalent Li-C interaction leading to a material with metallic character. *In operando* measurements have also been demonstrated. Further work during FY2012 will be directed at the full leveraging of this capability to follow the chemical interactions between Li and the graphite during intercalation reactions.

FY 2011 Publications/Presentations

1. Contributed to the EERE communication in the EFRC and DOE Research and Networking Poster Reception at the EFRC Summit & Forum.
2. F. Meirer, J. Cabana, Y. Liu, A. Mehta, J. C. Andrews, P. Pianetta. J. Synch. Rad. **2011**, 18, 773-781.
3. *Analysis of the mechanism of conversion and the microstructural changes upon cycling of high capacity NiO electrodes*. 2010 MRS Fall Meeting. Boston, MA, Nov. 29th-Dec. 2nd, 2010.
4. *Understanding how Li-ion Batteries Operate Using in and* ex situ *Synchrotron-based Techniques*. 2010 LCLS/SSRL Users' Meeting. Menlo Park, CA, Oct. 17th-21st, 2010.
5. *Spectroscopic and imaging study of high capacity Li-ion battery electrodes based on conversion reactions*. 2010 ALS Users' Meeting. Berkeley, CA, Oct. 13th-15th, 2010.
6. *Toward High Energy Density Li-ion Batteries. Understanding the Key Parameters for Performing Electrode Materials*. 2010 TMF and NCEM Users' Meeting. Berkeley, CA, Sept. 30th-Oct. 1st, 2010.

V.G Integrated Lab-Industry Research Program (LBNL, ANL)

Jordi Cabana[1], John T. Vaughey[2], Jeff Chamberlain[2], Michel Foure[1], Venkat Srinivasan[1]

[1]Environmental Energy Technologies Division
Lawrence Berkeley National Laboratory
1 Cyclotron Rd. MS62R0203
Berkeley, CA 94720-8168
E-mail: jcabana@lbl.gov

[2]Chemical Sciences and Engineering Division
9700 S Cass Ave
Argonne National Laboratory
Lemont, IL 60439
E-mail: vaughey@anl.gov

Participants:
Brian Ingram, Guoying Chen, Tom Richardson, Robert Kostecki, Marca Doeff, Gao Liu, John Zhang, John Kerr, Vince Battaglia, D. Schroeder (NIU)

Start Date: August 2010
Projected End Date: September 2015

Objectives

- Design, synthesize and characterize solid lithium ion conductors that enhance the cycle life of lithium metal based anodes in a lithium battery.
- Develop characterization tools that give a better understanding of how the coatings and lithium metal interact and how they interact in an electrochemical cell environment.
- Design, synthesize and characterize organic lithium ion conducting materials that enhance the cycle life of lithium metal based anodes in a lithium battery.

Technical Barriers

This project addresses the following technical barriers from the Energy Storage section of the DOE Vehicle Technologies Program Multi-Year Research, Development and Demonstration Plan:

(A) 40 mile range for PHEVs

(B) Abuse tolerance

(C) Cell life

Technical Targets

- Design polymer-based single ion conductor electrolytes with low bulk resistance and interfacial impedance.
- Synthesize, design and characterize ceramic and composite ceramic electrolytes with suitable mechanical, electrical and chemical properties.
- Use microscopy and spectroscopy to study and evaluate changes on lithium metal anode surfaces in the presence of different surface modifications.
- Evaluate Li^+ diffusion at the heterogeneous interface between a liquid and a solid electrolyte.

Accomplishments

- Developed low temperature synthetic methods for $Li_x(Ti,Al)_2(PO_4)_3$ (LATP), the most widely used solid lithium ion conductor, $(Li,La)TiO_3$ (LLTO) and $Li_7La_3Zr_2O_{12}$ (LLZ) Method allows for better control of particle size and morphology.
- Carried out detailed MAS-NMR and TGA-MS studies to determine relationship between annealing temperature, phase formation, and cation ordering in LATP.
- Determined the phase relationships in the Li_2O-P_2O_5-SiO_2 phase diagram and optimized compositions for high Li-ion conductivity and stability. Investigated role of lithium borate in enhancing grain boundary conductivity and sintering for glasses and LATP ceramics.
- Developed a series of nanoscale coatings based on the surface chemistry of lithium metal. Determined how coatings enhance cycle life and how they interact in the cell environment. Initiated ellipsometry studies to examine how the coating changes as a function of cycling.
- Single ion conductor polymer gels based on polysulfones that show very low interfacial impedance have been prepared.
- The integrity of siloxane coatings on lithium was evaluated by both Raman and FTIR spectroscopy.

Introduction

Achieving the DOE 40 mile range target for PHEVs will require significant advancements in energy storage technology. The main focus of this project will be to devise new methods to understand and stabilize lithium metal anodes in a lithium battery. Previous literature work has focused on the electrolyte reactivity and electrodeposition problems and the effects of these issues on long term cycling stability. We have initiated

a project to utilize recent advances in ceramic electrolyte materials, polymer science, and materials characterization to stabilize the interface of lithium metal in an electrochemical cell. With advantages for lithium metal including significant increases in anode capacity versus most alternatives, increased options for cathode materials, and a factor of 4 reductions in coating volume, new approaches to stabilizing this class of anodes would be a benefit to researchers seeking next generation energy storage systems.

After consultation with interested industrial concerns, the program was divided into two main technological focuses – (1) developing a ceramic membrane capable of working with lithium metal, and (2) developing a stable organic-based coating stable against lithium. The ceramic section has taken a two-pronged approach with one effort working on non-reducible glassy phases and the other early transition metal crystalline phases. Each approach has advantages and disadvantages that will be explored and evaluated with regard to end-user requirements. The organic effort has focused on two approaches as well – one utilizing a new technique to functionalize the surface of lithium metal to establish a platform for further functionalization, and the other focused on the formation of a stable lithium-ion conducting polymer.

Approach

The work under this program leverages the unique expertise of the groups at ANL and LBNL to address the challenge of developing a lithium metal electrode for an electrochemical cell. To evaluate the surface of the electrode, vibrational and scanning probe microscopies will be employed to study and evaluate changes on lithium metal anode surface with different modifications. These will include stabilizing the metal interfaces using silane coatings or via development of polymeric single ion conductor electrolytes with new attached anions that reduce the interfacial impedance at lithium metal. With this aim, cells that that are suitable for experiments with simultaneous cycling and probing have been designed.

Solid state lithium ion conductors based on either transition metal-free ceramic phases with high chemical stability, or higher conducting transition metal based framework structures will be synthesized and evaluated. This effort will be gradually combined with the polymeric effort to develop composite type ionically conducting membranes. In addition, the study type and rate of ion transport occurring at the interface between a liquid electrolyte and a ceramic protective coating was initiated.

Results

Ceramics. Initial work on transition metal containing lithium ion conducting ceramics was focused on LATP. The choice of material was based on commercial interest and its high lithium ion conductivity at room temperature. Discussions with industrial partners had identified several research problems in need of resolution, including ceramic stability to lithium, and ability to tape-cast the powder to form plates.

Initial tape casting efforts highlighted the need for a preparation that allowed better control of particle size and morphology. A new synthetic route based on the common solubility of a series of precursors in water was developed and used in subsequent studies. Phase formation was studied using a combined XRD-NMR-TGA annealing study to define points where phases were first isolated and where cation shifts within the phase could be identified and related to other variables (Figure V - 222). In this process, the new route was successful in lowering the temperature of formation by 100°C while achieving literature values of ionic conductivity.

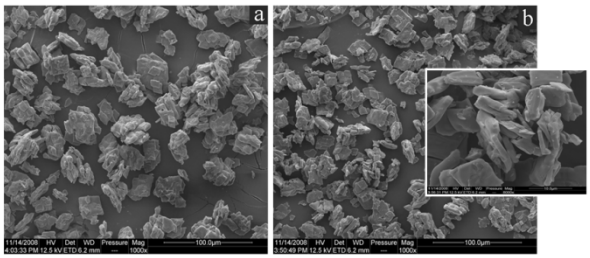

Figure V - 222: SEM image of the a-TiO_2 particles (20-25 µm) used for the synthesis.

Further solid state NMR diagnostic work on the sintering process was able to identify an unreported phase transition. This transition is at a temperature that makes it appear to be related to the difficulty in sintering LATP. Figure V - 223 shows the MAS-NMR spectrum of the LATP formation process.

Combining the data from the NMR, TGA, XRD, and synthesis studies several attempts were made to produce denser LATP plates. Figure V - 224 highlights the type of plates formed during the processing.

Exploration of crystalline phases in the Li2O-SiO2-P2O5 identified $0.6Li_3PO_4 \cdot 0.4Li_4SiO_4$ as the phase with the highest conductivity, 4.6x10-6 S/cm, at room temperature. This conductivity is the same as that of LiPON, a well-known Li battery electrolyte. A significant lowering of the sintering temperature from 850 to 700°C was achieved by adding small amounts of B2O3, making their processing simpler. These

materials were shown to be completely stable to cycling in direct contact with lithium, as shown in Figure V - 225.

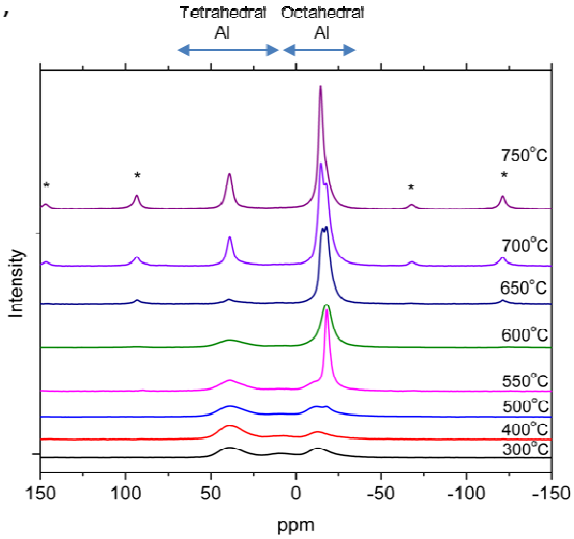

Figure V - 223: MAS-NMR spectra of LATP sintering as a function of temperature.

Both electrochemical and spectroscopic experiments to diagnose lithium surface response to electrochemical manipulation were initiated. During FY2011, the integrity of siloxane coatings was evaluated by both Raman and FTIR spectroscopy to determine how lithium is functionalized and to what extent. Lithium was evaporated onto silicon/silicon oxide to ensure a smooth uniform lithium surface for AFM studies. In parallel, ion transport through the liquid-ceramic interface was studied with a two compartment Devanathan-Stachurski type cell. Figure V - 226 illustrates the complicated impedance spectrum of solid/liquid interphases, frequency range (1Mhz - 100mHz). The semicircle in the high frequency range 250kHz is attributed to the bulk resistance(R2) and the small semicircle at 11kHz can be attributed the the grain boundary resistance(R3). The resistance at 700Hz maybe attributed to the resistance of lithium ion transfer through the solid inorganic electrolyte. This preliminary information is pertinent to the development of these dual systems and protection of lithium.

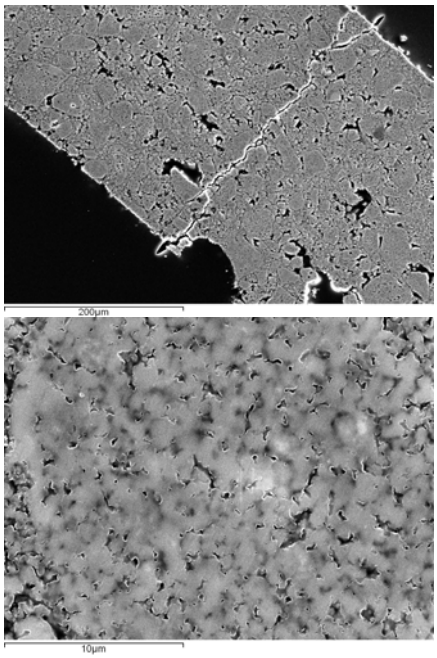

Figure V - 224: (top) Sintered LATP plate, (b) close-up of sintered plate morphology.

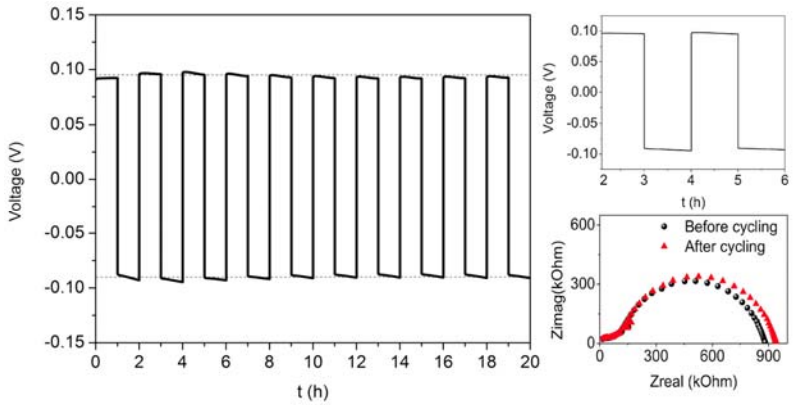

Figure V - 225: Cycling of a lithium-lithium symmetrical cell using $0.6Li_3PO_4 \cdot 0.4Li_4SiO_4$ with boron-based sintering as solid electrolyte. The lower inset shows a Nyquist plot of the cell before and after cycling.

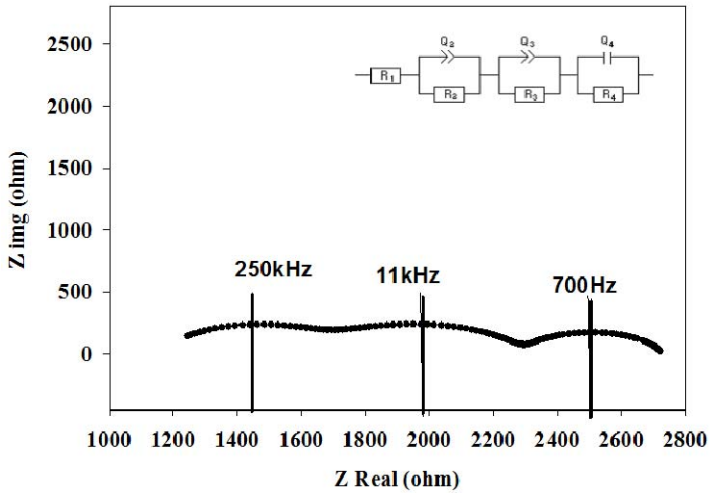

Figure V - 226: Nyquist plot of a 4 electrode Devanathan-Stachurski cell. All four electrodes were lithium. The electrolyte chosen was 1 M$LiPF_6$ EC:DEC. Frequency range (1Mhz - 100mHz).

Organics. Single ion conductor polymer gels have been prepared with polysulfone polymers with attached fluoroalkylsulfonylimide anions (TFSI). These have excellent conductivities as gels and the interfacial impedances are excellent as shown in Figure V - 227. Even at 25°C the impedance is only 300 ohm.cm^2. These values are an order of magnitude better than similar PEO-based polyelectrolytes. The better performance is postulated to be due to phase separation of the backbone from the anions to provide conducting liquid-like channels. The polymer backbone also provides considerable mechanical strength of the electrolyte. The high strength and low interfacial impedance of the polyelectrolyte in combination with the lack of concentration polarization leads to very good cycling of lithium metal with no sign of dendrite initiation.

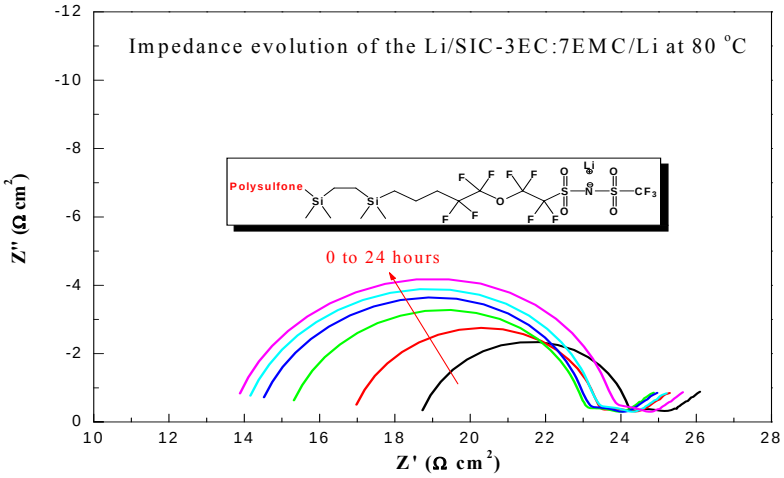

Figure V - 227: Nyquist plot of Li/Li cell with a Polysulfone-TFSI polyelectrolyte used as a gel with EC/EMC solvent.

Another approach under investigation is dedicated to developing methods to functionalize the surface of lithium metal. Initial efforts have focused on the use of silane-based chemistry that has been shown to produce a single monolayer on the surface of lithium stabilized by a silicon-oxygen bond. Impedance (EIS) studies have shown that the addition of this 1-2 nm layer (determined by XPS) appears to have a significant influence on the cycling ability of the underlying lithium metal anode. Figure V - 228 highlights the difference between the uncoated electrode over 50 cycles and an electrode coated with trimethylsilane (TMS) over the same window.

In a lithium-anode based electrochemical cell, the effect of the coating can be seen by the 2-3 fold enhancement of cycle life before cell failure. At the present time, the modeling effort is investigating various ideas of how the electrode surface appears to be

stabilized by this coating for extended time. Figure V - 229 highlights the change in cycling lifetimes.

Conclusions and Future Directions

The design of materials that can act as single ion solid electrolytes was shown to move forward. Polysulfone-based structures were prepared and showed to have both suitable ionic conductivity and low interfacial impedance in contact with metallic lithium. Transition metal-free ceramic electrolytes that are stable to cycling against lithium and conductivities comparable to LiPON were described. Their processing conditions were improved with the addition of B_2O_3 as sintering aid. Transition metal based solid electrolytes were optimized for plate sintering and found to have underlying structural reasons for the reported difficulties. A study of the physical phenomena related to the lithium electrode both bare and in the presence of surface modifications was initiated. In parallel, the character of the liquid-solid interface in dual phase electrolytes was evaluated.

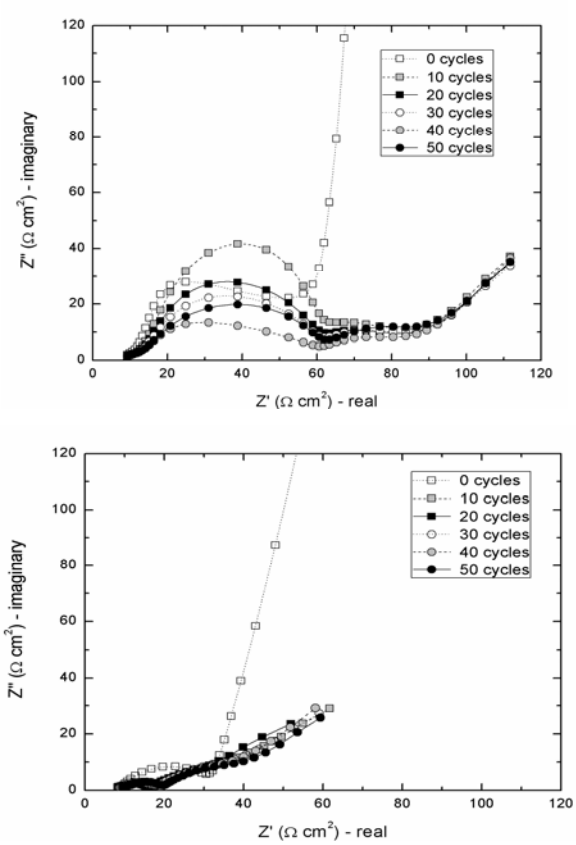

Figure V - 228: Nyquist plot of Li/LTO cells with (top) no coating on the lithium anode over 50 cycles, and (b) a TMS-based coating on the lithium metal surface.

During FY2012, the diagnostics studies will continue and be expanded with the use of scanning probe microscopy to study silane and siloxane-coated lithium. This tool enables the examination of the local conductivity through the application of a bias between an AFM tip and counter electrode. Composite ceramic layers will be designed with the deposition of thin layers of the ion conductors identified in FY2011 onto mechanically stable porous substrates. The aim will be to enable the use of stable phases that show moderate bulk conductivity.

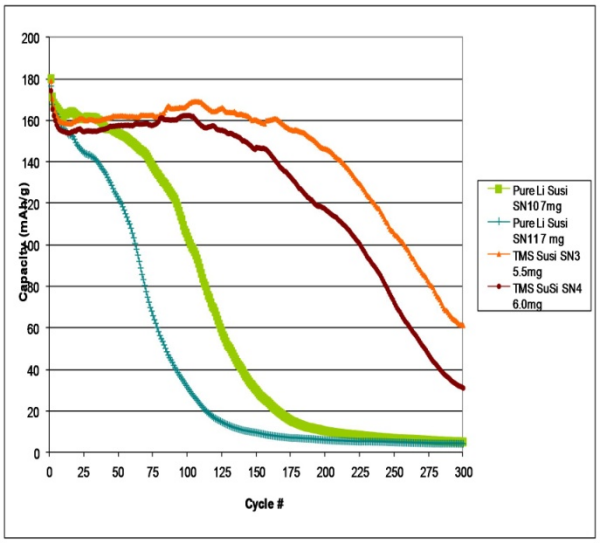

Figure V - 229: Cycling plots of Li/LTO cells comparing two different cells with no coating on the lithium anode, and (b) two cells with a TMS-based coating on the lithium metal surface.

FY2011 Publications/Patents/ Presentations

1. Rebecca Thompson, David J. Schroeder, Carmen M. Lopez, Susanna Neuhold, J. T. Vaughey "Stabilization of Lithium Metal Anodes using Silane-based Coatings" *Electrochem. Comm*., in press, (2011).
2. C.M. Lopez, J. T. Vaughey, D. W. Dees "The Role of Interfacial Morphology on the Electrochemical Properties of Metallic Lithium Electrodes". *J Physical Chem C*, submitted, (2011).
3. B. Key, D. Schroeder, B. Ingram, J. Vaughey "Solution-based Synthesis and Characterization of Lithium-ion Conducting Phosphate Ceramics for Lithium-Metal Batteries" *Chem. Mater.,* in press, (2011).
4. J. T. Vaughey, C. M. Lopez, D. W. Dees "Morphological Evolution of Lithium Metal Anodes on Cycling" NEDO-Argonne Meeting on Lithium-Ion Batteries, Argonne, IL, October, 2010.
5. J. Cabana, L. Zhang, T. Richardson, M. Doeff, G. Chen "ILIRP: Lithium Metal Anodes" DOE Hydrogen Program and Vehicle Technologies Program Annual Merit Review, Washington, DC, May, 2011.
6. J. Cabana, L. Zhang, T. Richardson, M. Doeff, G. Chen "The Li_4SiO_4-Li_3PO_4System as a Protective Layer in Li-metal Batteries" 4th Symposium on Energy Storage: Beyond Lithium Ion. Richland, WA Jun.7-9, 2011.
7. J. Vaughey, C. M. Lopez, D. Dees "Morphological Changes on Cycling for the Lithium Metal Anode" Argonne-PNNL Joint Workshop on Energy Storage, Argonne National Laboratory, November, 2010.
8. D. Schroeder, J. Vaughey, B. Key "Ceramic Electrolytes: Synthesis and Characterization" Joint ANL-LBNL ILIRP Meeting, March, Berkeley, CA, 2011.
9. J. Vaughey, D. Schroeder, J. Zhang, S Neuhold "Organic Coatings for Lithium Metal: Synthesis and Characterization" Joint ANL-LBNL ILIRP Meeting, Berkeley, CA, March, 2011.
10. J. T. Vaughey, D. J. Schroeder, B. Key, S. Neuhold "ILIRP: Lithium Metal Anodes" DOE Hydrogen Program and Vehicle Technologies Program Annual Merit Review, Washington, DC, May, 2011.
11. J. T. Vaughey, D. J. Schroeder, S. Neuhold, C. M. Lopez "Lithium Metal Anodes" Polymer Batteries and Fuel Cells-5 (PBFC5), Argonne, IL, July, 2011.
12. J. T. Vaughey, D. J. Schroeder, S. Neuhold, C. M. Lopez "ILIRP: A New Program to Study Lithium Metal Anodes" POD Seminar Series, Office of Basic Energy Sciences, Germantown, MD, July, 2011.
13. B. Ingram, D. Schroeder, J. Vaughey, B. Key "Ceramic Electrolytes: Synthesis and Characterization" Joint ANL-LBNL ILIRP Meeting, Berkeley, CA, October, 2011.
14. S. Neuhold, J. Vaughey, D. Schroeder "Organic Coatings for Lithium Metal: Synthesis and Characterization" Joint ANL-LBNL ILIRP Meeting, Berkeley, CA, October, 2011.
15. Baris Key, David J. Schroeder, Brian Ingram, John Vaughey "Synthesis and Characterization of Lithium-ion Conducting Ceramics for Lithium Metal Batteries" 219th Meeting of the Electrochemical Society, Boston, MA, October, 2011.